PRION PATHOLOGY IN THE BRAINSTEM: CLINICAL TARGET AREAS IN PRION DISEASE

A thesis submitted in partial fulfilment for the degree of Doctor of Philosophy to the University College London

by

Ilaria Mirabile

MRC Prion Unit

Institute of Neurology

University College London

Declaration

I, Ilaria Mirabile, confirm that the work presented in this thesis is my own. Where information has been derived from other sources, I confirm that this has been indicated in the thesis

List of contributions

All the procedures described in this thesis were performed by the candidate, with the following exceptions:

In vivo procedures

Mice breeding, colony maintenance, ear biopsies, prion inoculation, prion symptoms monitoring, mice culling and brain sampling were performed by designated staff at the Prion Unit animal house facility.

Prion inocula were prepared by Dr Jonathan Wadsworth.

Immunohistochemistry

Paraffin embedding and microtome slicing were performed by designated staff in the MRC Prion Unit histology support group.

Molecular biology

DNA sequencing was performed by Gary Adamson.

Cell culture

Flow cytometry was performed by Dr Annika Alexopoulou, Dr Sara Monteiro, and Melania Tangari.

Acknowledgments

I am extremely grateful to all the members of the MRC Prion Unit for their intellectual, practical and moral support. Firstly, I would like to thank my supervisors, Prof. Parmjit Jat, Prof. John Collinge and Prof. Sebastian Brandner for their guidance. I am particularly grateful to Jackie Linehan, Catherine O'Malley, Caroline Powell and Lorrain Spence in the Histology Core Facility, and to the Prion Unit Animal Facility, for their tremendous hard work. A big thank goes to the members of Prof Parmjit Jat's laboratory who welcome me as a second family, to Prof. Giovanna Mallucci, my supervisor when I first joined the Prion Unit, and to Dr Emanuel Asante for his help on planning experiments once Prof. Mallucci left.

I am in debt with the wonderful people at the Education Unit, Dr Caroline Selai and Miss Daniela Warr Schori for their support through these years at the Institue of Neurology.

A special thank goes to Michael, who has always been there for me during this sometime not easy journey, and all the other friends I met in the Unit who lifted my mood up, and put things in prospective: Nathalie, Inma, Kat, Savroop, Pela, Hazel, Pedro, Andy, Olivia, Aarti, Jeremy, Kevin, Sabeena, Melania, Sara, Sarah, Steph, Andrew, Annika, Emilie, Samira, Jess, Gary, Chris C, Adrian, Chris M, Mar, Julie, Mike B, Aaron …I am really grateful I could count on your support throughout these years!

Enormous thanks to past and present flat mates, Lucy, Sunny, Oy, Kim, Aaren, Kate for tolerating my mood swings and thesis-writing drama. Huge thank you to my friends back home, Alessandra, Maria, Feliciana, and Simona, for their unconditional love and support.

My major thanks to my wonderful family, mum, dad and Manuela. Thanks for being my source of inspiration, my rock and my home. Without you I would have probably given up when things got "messy"…

Dulcis in fundo, an immense thank you to Salim, for his enthusiasm, positive thinking, and faith in me… and, of course, for introducing me to the "Pomodoro technique"!

To my family

Abstract

Prion diseases are fatal transmissible neurodegenerative disorders characterized by spongiform changes, neuronal loss, reactive astrocytosis, and deposition of disease associated prion protein (PrP).

Our aim was to investigate "clinical target areas" for prion disease, responsible for disease onset, progression, and the clinical phenotype, using PrP overexpressing M*lox*P and PrP depleted NFH-Cre/M*lox*P transgenic mouse lines.

Upon infection with different prion strains NFH-Cre/M*lox*P mice have significantly longer survival than M*lox*P mice (first set of experiments: Me7, ~29 weeks vs. ~17 weeks; Mouse-adapted BSE , ~33 weeks vs. ~20 weeks; second set of experiments: RML, ~35 weeks vs.12 weeks; Me7 ~29 weeks, vs. ~17 weeks; MRC2 ~31 weeks vs. ~22 week.

As we found that the first pathological changes in the brains of Me7 and Mouse–adapted BSE infected mice are localized in the brainstem, and clinical signs of prion disease point to brainstem failure, we quantitatively scored spongiosis, abnormal PrP accumulation and astrogliosis at early and late stage of disease in specific brainstem nuclei of RML and Me7 infected M*lox*P and NFH-Cre/M*lox*P mice. The first target areas showing abnormal PrP accumulation and gliosis in both prion infections are the locus coeruleus (LC), the nucleus of the solitary tract (NTS) and the pre-Bötzinger complex (PBC).

We then studied the pathology progression, scoring prion pathology in these and other brainstem nuclei of infected M*lox*P and NFH-Cre/M*lox*P mice in the course of the disease. We show that neural degeneration in the LC, NTS, and PBC correlate with clinical signs characteristic of terminally ill mice. We therefore propose that these areas are potential clinical target areas of prion disease.

We also studied the spatial and temporal characteristics of Cre-mediated recombination. With immunohistochemistry in reporter mice, we estimated that in the LC, NTS, and PBC, Cre-mediated recombination is 60% or lower, and this can explain why mice proceed to terminal stage of the disease. In NFH-Cre/M*lox*P mice we found

that recombination is a progressive event and in the hippocampus it is complete by 5 weeks post-natally, differently from previous data.

Finally, we produced anti PrP RNAi –encoding lentivirus which could be used as focal therapy in the clinical target areas we propose.

Table of contents

List of figures and tables

Abbreviations

All amino acid abbreviations as standard

°C degrees Celsius

10 N nucleus of the X (vagus) nerve

12 N nucleus of the XII (hypoglossal) nerve

4 V forth ventricle;

5 nucleus of the V (trigeminal) nerve

6-FAM 6 - Carboxyfluorescein

7n VII (facial nerve)

AD Alzheimer's disease

ALS Amyotrophic lateral sclerosis

Amb nucleus ambiguous

bp base pair

BSE bovine spongiform encephalopathy

CaN Calcineurin

cb cerebellum

cd caudate nucleus

CJD Creutzfeldt-Jakob disease

CNS central nervous system

CSF Cerebrospinal fluid

cVRG caudal ventral respiratory group

CWD chronic wasting disease

cx cortex

DBH dopamine-beta-hydroxylase

dNTPs Deoxynucleotide Triphosphates

Dpl Doppel gene (mouse)

DS Down syndrome

dsRNA double strand RNA

DY drowsy prion strain (hamster)

EDTA ethylene diamine tetra-acetic acid

EEG electroencephalogram

ER endoplasmic reticulum

FACS fluorescent-activated cell sorting

fCJD familiar Creutzfeldt-Jakob disease

FCS foetal calf serum

FFI fatal familial insomnia

FTIR Fourier Transform Infrared Spectroscopy

g gravity (acceleration due to)

GAPDH glyceraldehyde-3-phosphate dehydrogenase

GFAP glial fibrillary acidic protein

GFP green fluorescent protein

GPI glycosyl phosphatidyl inositol

GSS Gerstmann-Sträussler-Scheinker disease

H&E haematoxylin and eosin

hc hippocampus

HY hyper hamster prion strain

i.c. intracerebrally

i.p. intraperitoneally

i.s. intraspinally

iCJD iatrogenic Creutzfeldt-Jakob disease

Ig immunoglobulin

iNOS inducible Nitric Oxide Synthase

kDa kilodalton

KF Kolliker-Fuse nucleus

LB Luria Broth

LC locus coeruleus

LD_{50} median lethal dose, to kill half of the experimental population

LPB lateral parabrachial nucleus

MBM meat and bone meal
MGB minor groove binding
miRNAs micro RNAs
MPB medial parabrachial nucleus
MRI magnetic resonance imaging
mRNA messenger ribonucleic acid
MSA multiple system atrophy
NA Noradrenalin
NE Norepinephrine
NET noradrenalin (or norepinephrine) transporter
NFH neurofilament heavy chain gene
NK1 neurokinin
nNOS neuronal nitric oxide synthase
nt nucleotide
NTS nucleus of the solitary tract
ob olfactory bulb
OPRI octapeptide repeat inserts
ORF open reading frame
p pons
PBC pre-Bötzinger complex
PBN parabrachial nuclei
PCR polymerase chain reaction
PD Parkinson's disease
PFA paraformaldehyde
PMCA protein misfolding cyclical amplification
PR N prepositus nucleus
PRG pontine respiratory group
PRNP prion protein gene (human)
Prnp prion protein gene (mouse)
PrP prion protein
PrP^C normal isoform of the prion protein
m medulla
qPCR quantitative PCR
RISC RNA-induced silencing complex
RML Rocky Mountain Laboratory (mouse adapted scrapie strain)
RNA ribonucleic acid
RNAi RNA interference
ROb raphe obscurus
ROS Reactive oxygen species
RTN retrotrapezoid nucleus
RVLM rostral ventro-lateral medulla
scFv single chain variable fragment
sCJD sporadic Creutzfeldt-Jakob disease
scp superior cerebellar peduncle
SDS sodium dodecyl sulphate
shRNA short hairpin RNA
SIDS sudden infant death syndrome
SO superior olive
Sp5 spinal nucleus of the V nerve;
TAE Tris-acetate-EDTA buffer
TE Tris-EDTA
tg transgenic
th thalamus;
TH tyrosine hydroxylase
TME transmissible mink encephalopathy
TN tegmental nuclei
TSE transmissible spongiform encephalopathy
UPR unfolded protein response
v/v volume to volume ratio
vCJD variant Creutzfeldt-Jakob disease
VMAT vesicular monoamine transporter
VN vestibular nuclei
VSV-G vesicular stomatitis virus envelope

PrP^{L} toxic species

PrP^{Sc} disease-associated prion protein

X-gal 5-bromo-4-chloro-3-indolyl- beta-D-galactopyranoside

β-gal β-galactosidase

w/v – weight in volume ratio

wpi weeks post inoculation

1 Introduction

1.1 Prions and prion disease

Prion diseases are transmissible neurodegenerative disorders affecting animals and humans. They are also known as transmissible spongiform encephalopathies (TSE), as they can be transmitted in the same species or between species via different routes of infection. According to the protein only hypothesis, the pathogenic event leading to prion disease is associated with a conformational rearrangement of the normal cellular prion protein, PrP^{C} (C for cellular), to an abnormally folded isoform, PrP^{Sc} (Sc for Scrapie, the TSE affecting sheep) (Prusiner, 1982). At the histopathological level, prion affected brains show typical neuropathological features, like spongiform vacuolation, marked neuronal loss, astrogliosis and microglial proliferation, and accumulation of the disease-associated isoform of the prion protein.

1.1.1 Prion diseases in animals

The first transmissible spongiform encephalopathy (TSE) was seen in Europe in the 18th century. It affected sheep and was denominated "scrapie", due to the predominant symptom of sheep scraping themselves. Since then, a variety of prion diseases have been described in other animals, including chronic wasting disease of deer and elk, transmissible mink encephalopathy, BSE in cattle, and feline transmissible encephalopathies.

1.1.1.1 Scrapie

Scrapie naturally occurs in sheep and goats: affected animals show loss of co-ordination, an uncontrollable urge to itch, excitability and progressive paralysis resulting in death. The neuropathological hallmarks of scrapie include global neuronal loss and cytoplasmic vacuolation, typical spongiform degeneration characterizing the TSEs (Foster et al., 2001). In the 19th century transmissibility studies were unsuccessful, due to failure to recognize the long incubation periods. First successful transmission was achieved in 1939, by inoculating scrapie into goats (Cuillé and Chelle, 1936), and further confirmation of the disease transmissibility were obtained accidentally when lymphoid tissue used to vaccinate sheep against louping ill virus caused scrapie in the

inoculated sheep (Gordon, 1946). Since then, scrapie has been transmitted experimentally into other species including laboratory mice (Chandler, 1961) but has never been proven to be a risk to human health (reviewed in (Brown and Bradley, 1998)).

1.1.1.2 Chronic wasting disease

Chronic wasting disease (CWD) is a prion disease of deer (Williams and Young, 1980), elk (Williams and Young, 1982), and moose (Baeten et al., 2007), occurring predominantly in North America. Clinical signs of CWD are non-specific and subtle in early phase of disease and commonly include weight loss and behavioural changes. Pathogenesis studies have revealed deposition of PrP^{Sc} both in the central nervous system (CNS) and extraneural tissues (lymphoid tissue, pancreas, skeletal muscle). CWD was first recognized in captive animals in Colorado, but epidemiological studies showed widespread occurrence of CWD both in farmed and free-ranging cervids in a number of other US States and in Canada. Horizontal transmission (Miller and Williams, 2003), potentially through excreta contaminating the environment, has led to a surge in CWD research, focused on understanding species susceptibility, transmission and pathogenesis, spatial epidemiology, diagnostic tools, strains, and cervid PrP structure, thanks to the generation of transgenic mice susceptible to CWD (Browning et al., 2004). To date, transmission to human has not been observed.

1.1.1.3 Transmissible mink encephalopathy

Transmissible mink encephalopathy (TME) has been described in captive animals mainly in the USA, and is believed to be transmitted by feeding animal tissues from scrapie-infected sheep or TSE-infected cattle (Marsh, 1992). Successful experimental transmission has been reported in hamsters (Kimberlin and Marsh, 1975) and similarities between TME and BSE in a mouse model have been noted (Baron et al., 2007), but TME is not considered related to BSE in cattle.

1.1.1.4 BSE

Bovine spongiform encephalopathy (BSE) or “mad cow disease” as it is colloquially known, was first observed in the UK in 1986 reviewed in (Smith and

Bradley, 2003). Source of contamination has been identified to be meat and bone meal (MBM), a high protein supplement, originating from tissue waste from various species, fed to young calves. Since the first appearance, approximately 180,000 cattle have developed the disease (Anderson et al., 1996; Ghani et al., 2003; Ghani et al., 2002). Furthermore, several cases appeared in zoo ungulates (Kirkwood et al., 1990), house cats (Wyatt et al., 1991) and zoo felines (Kirkwood and Cunningham, 1994) presumably from feeding of bone meal.

The initial hypothesis for the transmission route was that BSE may have arisen from scrapie infected sheep carcasses rendered into MBM (meat and bone meal) (Wilesmith et al., 1988; Wilesmith et al., 1991; Smith and Bradley, 2003). However, the BSE strain is molecularly and biologically different to the strain causing scrapie, arguing against this hypothesis (Bruce et al., 1994). An alternative hypothesis is that a sporadic case of BSE arose by chance in cows and initiated the epidemic (Weissmann and Aguzzi, 1997).

In 1988 the first control measures were applied and ruminant carcasses were banned in cattle fed in the UK. Some BSE cases were still identified after the ban, and the emergence of variant CJD in 1996 (Will et al., 1996; Collinge and Rossor, 1996) urged re-enforcement of the ban. Other European countries enforced the 1996 UK ban in 2001.

1.1.2 Human prion diseases

Human prion diseases can be classified according to their aetiology as sporadic, inherited or acquired.

Historically, they have been categorized as the clinicopathological syndromes of Creutzfeldt-Jakob disease (CJD), Gerstmann-Sträussler-Scheinker syndrome (GSS), fatal familial insomnia (FFI) and kuru; they are all potentially transmissible. These disorders are rare, affecting one to two people per million world-wide per annum (Collinge, 2005), but are considered of great interest because of their unique biology and for the threat to public health that the BSE epizootic could represent.

Genetic susceptibility for the development of prion disease is conferred by a polymorphism at amino acid residue 129 of the prion protein [which encodes

methionine (M) or valine (V)]. Methionine homozygotes (codon 129MM) are at a slightly higher risk of developing prion disease, maybe due to the increased propensity of PrP to form PrP^{Sc}-like structures, as shown *in vitro* (Tahiri-Alaoui et al., 2004). Heterozygosity (codon 129MV) is believed to confer resistance by inhibiting homologous PrP protein-protein interactions (Palmer et al., 1991).

1.1.2.1 Sporadic CJD

Sporadic CJD (sCJD) represents around 85% of all human prion diseases. It is a rapidly progressive multifocal dementia: the initial symptoms in about a third of the cases are fatigue, sleep disorders and decreased appetite; behavioural and cognitive symptoms in another third of the patients, and a final third have focal signs such as visual loss, cerebellar ataxia, aphasia and motor deficit (Johnson, 2005). Men and woman are affected equally, with age at onset of 60 years (Brown et al., 1994), and a mean duration of 5 months, and 90% of the patients are dead within a year (Johnson and Gibbs, Jr., 1998). Characteristic MRI patterns, with changes in the basal ganglia, electroencephalogram (EEG) readings, showing synchronized biphasic or triphasic sharp-wave complexes, and elevation of 14-3-3 protein in the cerebrospinal fluid (CSF) are diagnostic tools for sCJD (Steinhoff et al., 2004; Tschampa et al., 2005) but none of them are 100% specific or sensitive. Therefore, definitive diagnosis is confirmed *in vivo* by brain biopsies (carried out to exclude other tractable CNS disorders such as vasculitis) or more commonly by post-mortem examination. The salient pathological findings are deposition of abnormal PrP and variable spongiform changes of the CNS grey matter and the spinal cord. The aetiology of sCJD is uncertain: sporadic generation of abnormally folded prion protein can result from spontaneous mutation in the prion gene (*PRNP*) (Brown et al., 1987; Collinge, 1997), or random misfolding of prion protein, as a rare stochastic event resulting in a cascade of prion protein misfolding into the pathogenic isoform (Collinge, 1997). Homozygosity at codon 129 of human prion protein increases susceptibility to sCJD (Mead, 2006).

1.1.2.2 Inherited prion diseases

Inherited prion diseases represent 15% of prion diseases, distributed into three principal phenotypes, familial CJD (fCJD), GSS syndrome and FFI. The diagnosis of these diseases requires a combination of clinical features, a family history consistent with autosomal dominant inheritance and a prion protein gene (*PRNP*) disease-causing mutation. Clinical features include various combinations of adult-onset neurological signs and symptoms like dementia, psychiatric symptoms, myoclonus and brainstem related disturbances (autonomic, visual and movement impairment). Neuropathology varies considerably, depends on the mutation and can even vary between patients with the same mutation (Chapman et al., 1993; Barbanti et al., 1996; Wadsworth et al., 2006). It can consist of spongiform degeneration and astrogliosis in the cortex and deep nuclei in fCJD; multiple amyloid plaques in GSS; neuronal loss and astrogliosis in the thalamus and the inferior olivary nucleus in FFI (DeArmond and Prusiner, 1997).

Over thirty distinct mutations have been documented (Mead, 2006), consisting of three types: point mutations leading to amino acid substitutions, premature stop codons, and insertion of octapeptide repeats within an unstable region rich in proline, glycine, and glutamine (OPRI). It is still unclear how mutations in the *PRNP* gene can lead to the disease. It has been hypothesized that thermodynamic changes may favour the transition to the disease-associated prion isoform or that subtle structural differences in the mutant proteins may affect inter-molecular signalling in various ways (Riek et al., 1998; Swietnicki et al., 1998).

1.1.2.3 Acquired prion diseases

1.1.2.3.1 Kuru

Kuru was the first identified acquired prion disease, emerging in the 1950s in the Eastern Highlands of Papua New Guinea among people of the Fore linguistic group (Mead et al., 2003). In 1959, Hadlow suggested similarity between kuru and scrapie in epidemiology, clinical signs and pathology (Hadlow, 1959). Following his observation, Gajdusek and colleagues succeeded in transmission of “kuru like syndrome” to chimpanzee inoculated with brains tissue of kuru patient, after an incubation period of

18-21 months (Gajdusek et al., 1967). Kuru predominantly affected woman and children practicing ritual cannibalism as a bereavement ceremony. The epidemic is thought to have begun when an individual with sCJD was consumed at one of these rituals. In the late 1950s the Australian government banned endocannibalism, effectively stopping kuru transmission. Clinically, kuru is a progressive cerebellar ataxia (Collinge et al., 2008), with cognitive changes occurring just in advance stages (Zigas and Gajdusek, 1957; Hornabrook, 1968). Disease onset ranges from 5 to 60 years, and its duration can last from 3 months to 3 years (Collinge et al., 2008). Kuru incubation periods vary, from as little as 4.5 years to over 50 years (Collinge et al., 2006). Neuropathology is characterized by spongiform changes and PrP^{Sc} plaques (Alpers, 1987). The genotype of residue 129 has a profound effect on the incubation period and susceptibility to kuru: the MM genotype has the shortest incubation period (Lee et al., 2001), followed by VV homozygotes and MV heterozygotes, whose incubation times has been reported to be >50 years (Collinge et al., 2006). Recently the 127V polymorphism has been shown to be an acquired prion disease resistance factor selected during the kuru epidemic. Variants at codons 127 and 129 of *PRNP* are believed to represent the population genetic response to an epidemic of prion disease (Mead et al., 2009b).

1.1.2.3.2 Iatrogenic CJD

The reported routes of transmission of iatrogenic CJD have been implantation of dura mater grafts, treatment with human growth hormone derived from the pituitary glands of human cadavers, corneal transplants and use of contaminated neurosurgical instruments (Brown et al., 1992; Brown et al., 2000) and EEG electrodes (Bernoulli et al., 1977; Masters et al., 1979; Bernoulli, 1980). Since 1985, over 100 cases of iCJD have occurred after neurosurgical use of human cadaveric dura mater (Brown et al., 2000). In 1985, the occurrence of CJD in human growth hormone recipients (Koch et al., 1985; Gibbs et al., 1985; Powell-Jackson et al., 1985) provided evidence of transmission of CJD via human growth hormone, because of the discrepancy between the young age of the patients and the one usually observed in CJD. After that, the product was withdrawn in most countries, but over 130 young adults have developed iCJD 30 years after discontinuing the injections (Brown et al., 2000), with such a long

incubation period probably due to the peripheral route of inoculation. The initial presentation is characterized by progressive cerebellar syndrome, while other features, like dementia, develop late. The resemblance to kuru clinical progression may be due to the common peripheral route of infection (Will, 2003; Wadsworth and Collinge, 2007). The codon 129 genotype has been proved to be linked to susceptibility and incubation period (Collinge et al., 1991; Huillard d'Aignaux et al., 1999).

1.1.2.3.3 Variant CJD

Concerns about transmission of BSE to humans arose following a report in 1995 of cases of apparent sCJD in unusually young people in the UK (Britton et al., 1995; Bateman et al., 1995; Tabrizi et al., 1996). More cases manifested the following year, leading to the recognition of a new clinicopathological type of human prion disease, denominated 'variant' CJD (vCJD) (Will et al., 1996). The link between BSE and vCJD, suspected on the basis of the epidemiology, was then supported by experimental data on strain typing. sCJD and vCJD prion strains have a different SDS-PAGE migration pattern following limited proteinase K digestion. Analysis of vCJD samples showed a pattern different from the other forms of CJD known hitherto. This new pattern was designated type 4 (or type 2b according to an alternative classification by Gambetti, reviewed in (Kovacs and Budka, 2009)) and proved to be the same as BSE (Collinge et al., 1996). Furthermore, transmission studies in transgenic and wild type mice confirmed that vCJD is caused by the same strain causing BSE in cattle (Hill et al., 1997; Bruce et al., 1997). This raised the possibility of a major epidemic occurring in the UK and other countries as a result of dietary exposure to BSE prions (Collinge, 1999; Ghani et al., 2003). Another serious threat to public health was feared for the iatrogenic exposure of pre-clinical vCJD via medical and surgical procedures (Collinge, 1999; Peden et al., 2005).

By July 2010, 173 cases of vCJD have been reported in the UK (de Marco et al., 2010). Recently, a large-scale immunohistochemical examination for lymphoreticular prion protein in tonsil specimens, collected in Britain, predicted a prevalence of disease-related prion protein in the British population of 109 per million (de Marco et al., 2010)

Clinical manifestation of vCJD is characterised predominantly by psychiatric disturbances (Spencer et al., 2002). Individuals initially present with progressive cerebellar symptoms and then develop dementia. Age of onset ranges between 16-51 years and disease duration varies from 9-35 months (Knight, 2006). Characteristic neuropathological features are widespread spongiosis, gliosis and neuronal loss. PrP^{Sc}-positive 'florid amyloid plaques' are present in high numbers both in the cerebrum and cerebellum (Will et al., 1996), and are different from the ones seen in kuru because they are surrounded by vacuoles (Alpers, 1987). Unlike other human prion diseases, PrP^{Sc} is also present in non-CNS tissues (Wadsworth et al., 2001; Peden et al., 2006; Wadsworth et al., 2007).

Until recently, all vCJD cases documented had been homozygous for methionine at *PRNP* codon 129 (Collinge et al., 1996). However, in 2009 the clinical diagnosis of vCJD was made in an heterozygous subject (Kaski et al., 2009), and it is believed that more cases may be found, probably with prolonged incubation time. In mice prion disease susceptibility and incubation periods are known to be affected by other genetic loci (Stephenson et al., 2000; Lloyd et al., 2001; Lloyd et al., 2002; Lloyd et al., 2009). Recently, two novel candidate loci, *RARB* and *STMN2*, have been identified as potential vCJD risk factors in a genome-wide association study (Mead et al., 2009a).

1.1.3 Nature of the infective agent and protein-only hypothesis

First observations of resistance of sheep scrapie to formaldehyde were obtained in the 1940s (Gordon, 1946). The original assumption of viral origin of the infectious agent was challenged 20 years later, when Alper first hypothesized that the infectious agent was devoid of nucleic acid (Alper et al., 1967), after the demonstration of resistance to inactivation of infectivity by ultraviolet irradiation and high temperature (Alper et al., 1966). These observations led Griffith to propose in 1967 that a protein alone could be an infectious agent (Griffith, 1967), challenging one of the central dogmas of biology. The scepticism of the scientific community was partially overcome years later, when Prusiner and co-workers achieved considerable purification of the scrapie agent, and found that its physicochemical properties were typical of proteins and inconsistent with nucleic acid. Prusiner coined the term 'prion' (proteinaceous infectious

particle),"small proteinaceous infective particles that resist inactivation by procedures which modify nucleic acids" (Prusiner, 1982). Shortly after, a scrapie-associated protein which correlated with infectivity was isolated from infected hamster brain (McKinley et al., 1983). This protein was found to be aggregated, highly insoluble in non-ionic detergents and partially protease resistant and was designated PrP^{27-30} for its molecular mass of 27 – 30kDa.

1.1.3.1 Prion protein gene

Determination of the amino acid sequence of the prion protein co-purifying with scrapie infectivity led to recovery of cDNA clones from scrapie infected Syrian hamster and murine brain libraries. PrP mRNA was found to be the product of a host gene, called *Prnp*, expressed equally in infected and uninfected animals (Oesch et al., 1985; Chesebro et al., 1985). The normal product of the gene was defined as PrP^{C} (from '*C*ellular' isoform of the protein) and it became clear that PrP^{27-30} was derived from a larger molecule of 33-35 KDa, designated as PrP^{Sc} (from the '*Sc*rapie' isoform of the protein). The two isoforms PrP^{C} and PrP^{Sc} have the same primary structure but differ in their secondary and tertiary structure, which affect their physicochemical properties. The identification of these isoforms led Prusiner to update and elaborate the protein-only model of infectivity originally proposed by Griffith, providing a model by which prions could 'replicate' and be infectious (Prusiner, 1989).

The PrP gene is a single copy gene consisting of two (or three, differentially spliced) exons in hamster (Basler et al., 1986) and human (Puckett et al., 1991), and three exons in mice (Westaway et al., 1994). Human *PRNP* has been mapped to the short arm of chromosome 20 and the mouse *Prnp* gene has been mapped to the homologous murine chromosome 21 (Sparkes et al., 1986). In all species examined, the open reading frame is contained entirely in the last exon (Kretzschmar et al., 1986b; Puckett et al., 1991) and encodes 253-257 amino acids (254 in the mouse). The primary sequence of PrP includes a hydrophobic signal sequence consisting of 22-24 C-terminal amino acids (22 in the mouse) which is cleaved off when the GPI anchor is added.

1.1.3.2 Structural characteristics of PrP^C and PrP^{Sc}

It is now widely recognized that PrP^{Sc} is derived from PrP^C (Borchelt et al., 1990) and no covalent differences between PrP^C and PrP^{Sc} have been demonstrated (Caughey and Raymond, 1991). Expression of recombinant PrP in *E.coli* allowed determination of the three dimensional conformation of the cellular form by NMR spectroscopy (Riek et al., 1996). The mature PrP^C consists of an N-terminal region of about 100 amino acids, which is unstructured when the isolated molecule is in solution, and a C-terminal domain of around 100 amino acids, composed of three α-helices and a short anti parallel β-sheet (PrP^C structure will be discussed in further details in paragraph 1.1.4). The N-terminal region contains a series of highly conserved octapeptide repeats which are implicated in copper binding (Brown et al., 1997a) and may play a role in the normal protein functions (Brown, 1999; Pauly and Harris, 1998).

The structure of PrP^{Sc} has not yet been determined, because material extracted from affected brains is highly aggregated, detergent insoluble and not suitable for high resolution structural studies. However, Fourier Transform Infrared Spectroscopy (FTIR) and circular dichroism studies have demonstrated that PrP^{Sc} is rich in β-sheet (Gasset et al., 1993; Pan et al., 1993). PrP^{Sc} contains ~43% beta sheet and 34% alpha helix, while PrP^C contains only 3% beta sheet (Pan et al., 1993). From this observation, it has been suggested that the infective process results from a switch from the predominantly alpha-helical PrP^C to the predominantly beta sheet PrP^{Sc} (Caughey et al., 1991; Gasset et al., 1993; Pan et al., 1993).

The PrP^{Sc} protease-resistant core has been shown to re-arrange into amyloid rods, which stain with Congo red, and show birefringence, typical of amyloids (Prusiner et al., 1983).

1.1.3.3 Models of prion conversion and replication

Two main models have been proposed for the prion conversion process. The first is commonly known as the “heterodimer model”, or the “template directed conversion model” in which PrP^{Sc} binds PrP^C and acts as a template, forcing refolding of PrP^C (Prusiner, 1991).

The second is known as “nucleated or seed polymerization model” (Come et al., 1993). This model postulates that PrP fluctuates between a dominant native state (PrP^{C}) and a series of minor conformations. One or a set of minor conformations can associate in a supra-molecular structure made up of misfolded monomers (PrP^{Sc}). Experiments with β-PrP, a recombinant protein mimicking PrP^{Sc}, showed that β-PrP aggregation occurs slowly until a critical size is reached and the misfolded proteins form a stable ‘seed’ structure. Once a stable seed is formed, further recruitment of misfolded PrP or β-PrP monomers can occur as an irreversible process driven thermodynamically by intermolecular interactions. This second mechanism could explain all three aetiologies of human prion disease: initiation of the pathogenic self-propagating conversion reaction may be induced following exposure to a ‘seed’ of aggregated misfolded monomers following prion inoculation (acquired), as a rare stochastic conformational change (sporadic), or as an inevitable result of expression of a pathogenic mutant PrP^{C} form, prone to form misfolded monomers (inherited) (Collinge, 2005). It still remains to be confirmed if such alternative protein conformational states are enough to adopt PrP^{Sc} conformation and cause prion disease alone, or other cellular cofactors are needed (Figure 1.1).

Conversion of PrP^{C} to PrP^{Sc} has been achieved in cell-free systems *in vitro* but infectivity of the de novo generated PrP^{Sc} could not be established (Kocisko et al., 1995; Kocisko et al., 1994; Hill et al., 1999). The development of a more sophisticated *in vitro* conversion technique called Protein Misfolding Cyclical Amplification (PMCA) (Castilla et al., 2005) has allowed much more efficient replication and detection of PrP^{Sc} and has helped to demonstrate that infectious material can be produced in a cell-free system, which when inoculated into mice leads to scrapie-like disease (Bruce et al., 1994; Supattapone, 2004). Additionally, synthetic prions that polymerise into fibrils *in vitro* have also been shown to be infectious *in vivo* (Legname et al., 2004).

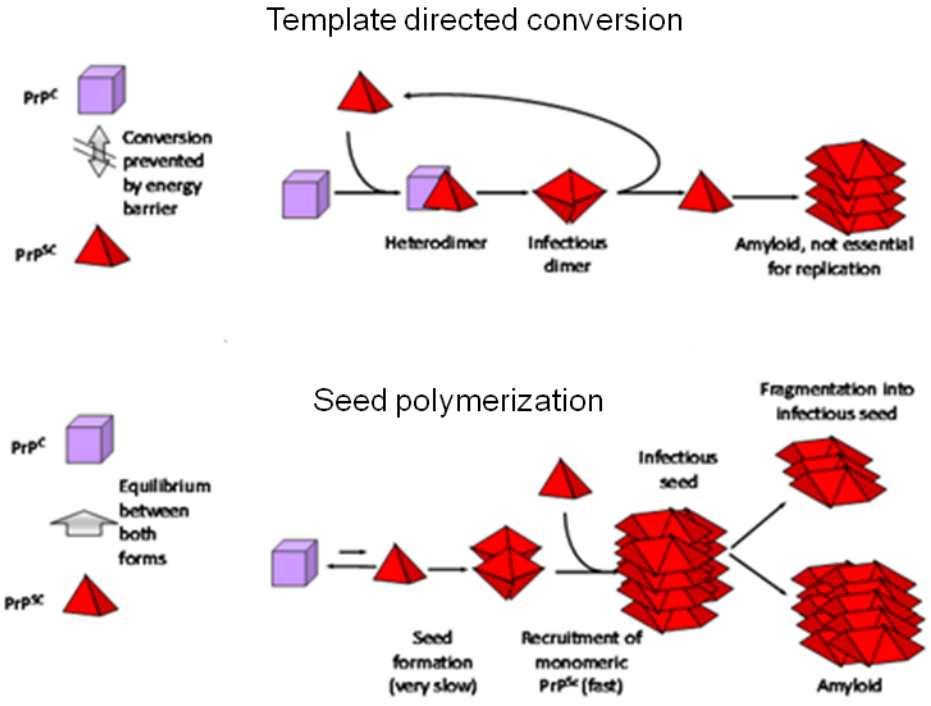

Figure 1.1 Models for prion conversion

According to the 'heterodimer' or 'template directed conversion model' (top panel), PrP^{Sc} binds PrP^{C} and acts as a template, catalysing the refolding of PrP^{C} into PrP^{Sc}. According to the 'seed polymerization model' (bottom panel), PrP fluctuates between a dominant native state (PrP^{C}) and a series of minor conformations. One or a set of minor conformations can associate in a supra-molecular structure made of misfolded monomers (PrP^{Sc}). Monomer association occurs slowly until a critical size is reached and the misfolded proteins form a stable 'seed' structure. From this point, further recruitment of misfolded PrP can occur rapidly, as an irreversible process driven thermodynamically by intermolecular interactions. Adapted from an illustration of Prof. Sebastian Brandner.

1.1.3.4 Prion strains and transmission barriers

Prions exist as distinct isolates or strains. Prion strains can be propagated in lines of inbred mice and maintain their biological properties, with distinct incubation time and neuropathology (Bruce et al., 1992). Strains are not believed to be encoded by differences in primary structure, as they can be serially propagated in inbred mice with the same *Prnp* genotype, and can be re-isolated in mice after passage in intermediate species with different PrP primary structure (Bruce et al., 1994).

Because of the lack of a nucleic acid, the protein-only hypothesis faces the challenge to explain how a single peptide chain can encode multiple disease phenotypes. Some strains show biochemical difference in the propagated PrP^{Sc}. For example, two TME prion strains, hyper (HY) and drowsy (DY), produce different PrP^{Sc} fragment sizes, upon limited proteolysis (Bessen and Marsh, 1994). Distinct human PrP^{Sc} types have been identified by proteolytic fragment size and glycoform ratios, following proteinase K digestion (Peretz et al., 2001). These biochemical properties can imprint their characteristic on the recipient PrP: studies with human isolates in transgenic mice showed that PrP^{Sc} fragment sizes following proteinase K digestion, and ratios of the three principle glycosylated isoforms are maintained. Also, the characteristic molecular signature of the BSE prion strain is maintained in experimental transmissions and across several mammalian species, including humans (Collinge et al., 1996). Differential proteinase K digestion kinetics (Kuczius and Groschup, 1999), thermal or chaotrope denaturation curves, conformation-dependent immunoassay (Safar et al., 1998; Safar et al., 2000), metal binding (Wadsworth et al., 1999), and the propagation of strain

associated biochemical characteristics from in *vitro* produced prions (Kocisko et al., 1994; Bessen et al., 1995; Castilla et al., 2005) provide further evidence that distinct prion strains are associated with different conformational states of PrP. On the opposite side of the coin is the concept of "species barrier" or "transmission barrier": transmission of prion diseases between different mammalian species is generally less efficient than within the same specie. Early studies hypothesized that the 'barrier' resides in the PrP primary structure; for example, transgenic mice expressing hamster PrP, unlike wild-type mice, are highly susceptible to Sc237 hamster prions (Prusiner et al., 1990). However, it is now clear that prion strain type also affects the ease of transmission from one species to another. The most obvious example is the transmission study of human prion disease. It has proven difficult to transmit classical CJD prions to conventional mice, whereas transgenic mice expressing human PrP in the absence of mouse PrP completely lack the species barrier (Hill et al., 1997; Collinge et al., 1995b). However, vCJD prions transmit much more readily to wild-type mice, whereas transmission to humanized mice is inefficient, despite having a PrP primary structure identical to that of the classical CJD (Hill et al., 1997). "Transmission barrier" has been proposed as a more appropriate term than "species barrier", because two strains propagated in the same host may have completely different barriers when propagated in another species.

To unify the concept of strains and transmission barrier, the "conformational selection model" has been postulated (Collinge, 1999). This states that the number of PrP^{Sc} types or strains in mammalian prion disease is limited by thermodynamic stability and the need to replicate at a rate above that of clearance naturally occurring *in vivo*. Ease of transmission from one species to another will thus depend on the overlap between the permissible conformations for PrP^{Sc} derived from the donor species, and those of the host species; two species with no permissible PrP^{Sc} conformations in common would have a larger barrier to transmission. Therefore, in this model, host PrP primary structure influences which of the possible PrP^{Sc} types are thermodynamically favoured with respect to conformation, and kinetically selected during propagation, and the transmission barrier is determined by the degree of overlap between the subset of PrP^{Sc} types allowed in the host and donor species (Figure 1.2).

The conformational selection model can also accommodate the well-known phenomenon of "strain mutation" (Bruce, 1993). Strain mutation occurs when a strain does not "breed true" upon passage in a new host and generates a distinct strain. This phenomenon may occur when the host and donor have different or identical primary structure, suggesting that modifier loci have an effect on strain selection (Asante et al., 2002; Lloyd et al., 2004).

In line with the conformational selection hypothesis, strain mutation can be seen as the selection of a novel PrP^{Sc} conformer as a result of host PrP^{C} not being able to adopt the donor PrP^{Sc} conformation. In this scenario, two possibilities can be hypothesized: a strain can exist as a molecular clone and strain mutation generates a distinct PrP^{Sc} type; or strains consist of an 'ensemble' of molecular species, where one PrP^{Sc} type is preferentially propagated by its usual host (Figure 1.3). However, an alternative host may select a less populous subspecies in the ensemble, because propagation of this subspecies is more favoured in the new environment, giving rise to a strain shift. The second hypothesis has been favoured, given the high degree of molecular diversity observed in prion isolates (Collinge and Clarke, 2007).

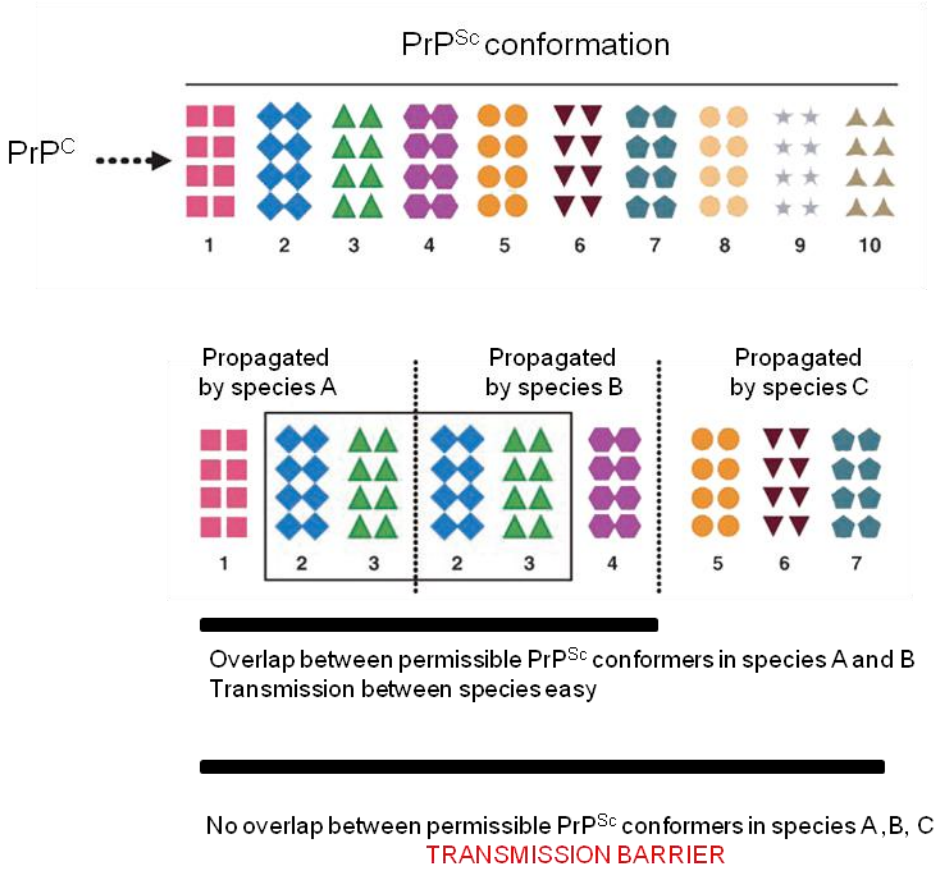

Figure 1.2 The conformational selection model explains the phenomenon of transmission barrier

Each PrP primary structure is compatible with a subset of PrP^{Sc} conformation. Ease of transmission from the donor species to the host species depends on the overlap between the permissible conformations for PrP^{Sc} derived from the donor species, and those of the host species. Two species with no permissible PrP^{Sc} conformations in common have a larger barrier to transmission. Adapted from (Collinge and Clarke, 2007).

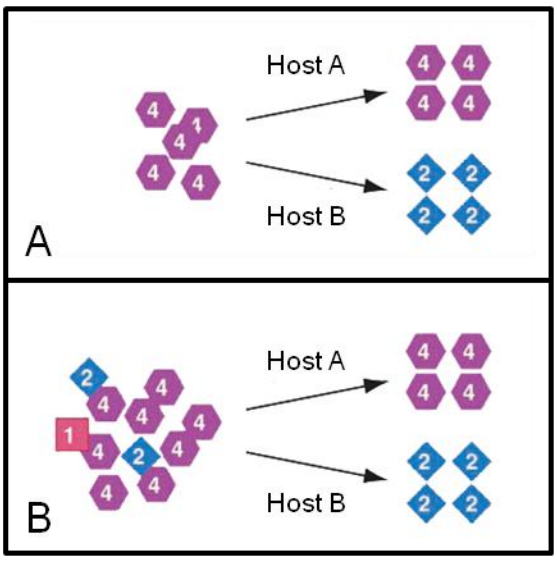

Figure 1.3 Strain shift or mutation

Strain mutation occurs when a novel PrP^{Sc} conformer is selected as the host PrP^{C} cannot adopt the donor PrP^{Sc} conformation. Two models, not mutually exclusive, can explain this phenomenon. A. In a clonal strain, a direct strain mutation causes a different PrP^{Sc} type. B. A strain consisting of an ensemble of molecular species breeds true when it is propagated in a host that preferentially propagates the dominant PrP^{Sc} type (Host A), but may change in a host that selectively propagates a minor component of the ensemble (Host B), generating a mutant strain . Adapted from (Collinge and Clarke, 2007)

1.1.4 Cellular prion protein

1.1.4.1 Prion protein structure

Prion protein is a highly conserved glycoprotein. In human it is encoded on the short arm of chromosome 20, and in mice on chromosome 21 (Sparkes et al., 1986). Human PrP^{C} is translated as a 253 amino acid polypeptide containing at both termini two signal sequences. In the endoplasmic reticulum (ER) the protein undergoes post-translational modification. The N-terminal signal peptide is cleaved off during processing and PrP^{C} can be variably glycosylated at two asparagine residues, resulting in un-, mono-, or diglycosylated species (Haraguchi et al., 1989). The C-terminus is removed upon attachment of the glycosylphosphatidylinositol (GPI) moiety (Basler et al., 1986; Stahl et al., 1987; Turk et al., 1988). In the mature peptide, the N-terminus is basic and unstructured, while the C-terminus forms a domain with three α-helices and a short anti-parallel β-sheet (Knaus et al., 2001; Eghiaian et al., 2004; Haire et al., 2004).

Within this domain, the two cysteins form an internal disulphide bond. Structural information about the N-terminal segment of PrP^{C} is incomplete. This region contains five octapeptide repeats that constitute the major Cu^{2+} binding site (Hornshaw et al., 1995). Additional Cu^{2+} binding sites are localized outside the octapeptide repeat (Jackson et al., 2001). Mutations in the N-terminal segment of PrP have been identified as the cause of some human prion diseases, raising the possibility that it may be an important factor in some PrP^{Sc} conformations and disease manifestation (Hill et al., 2006; Mead, 2006; Mead et al., 2006).

The middle of the protein is a highly conserved hydrophobic region, whose function is still debated: historically, contrasting reports disputed its function as a transmembrane domain (Lopez et al., 1990; Stahl et al., 1990) (Figure 1.4). Further studies have demonstrated that peptides from this region can span membranes and suggested that this could occur during cellular trafficking (Forloni et al., 1993; Glover et al., 2001). Because small peptides from this region can adopt an apoptosis-inducing conformation, it has been suggested that the hydrophobic domain may be an important part of an infectious prion (Forloni et al., 1993; Gasset et al., 1992). Recently, a stress protective function has been proposed for this hydrophobic domain (Rambold et al., 2008), because of the propensity of the domain to promote dimer formation and the relationship between dimerization and stress-protective activity.

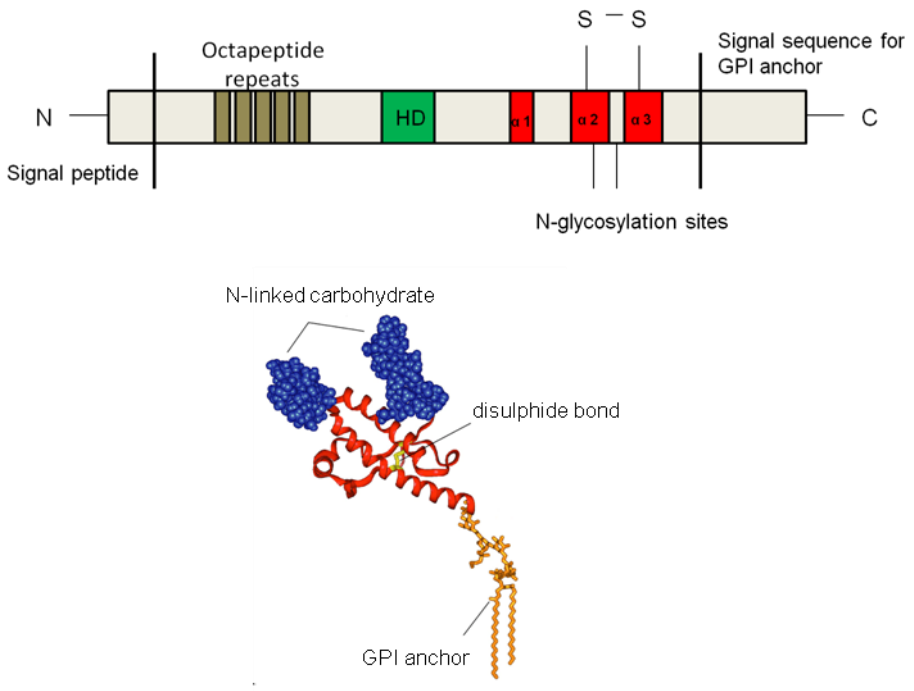

Figure 1.4 Linear and three-dimensional structure of human PrP

Human PrP comprises an N-terminus and C-terminus signal peptide (in white); an octapeptide region (in grey) a hydrophobic domain (in green); the α-helices (red). A disulphide bond is formed between the cystins in α2 and α3. Two potential glycosylation sites are localized in α2 and the linker between α2 and α3. Adapted from (Jackson and Clarke, 2000).

1.1.4.2 PrP^C localization and trafficking

After processing in the ER and Golgi apparatus, mature PrP^C is bound to the cell surface by the GPI anchor (Stahl et al., 1987). At the cell surface PrP^C constitutively cycles between plasma membrane and early endosomes (Shyng et al., 1993). Different hypotheses on the pathways of internalization have been suggested. The main pathway of internalization seems to depend on clathrin-mediated endocytosis: PrP^C may bind, through a basic amino acid motif in the N-terminal region to a transmembrane protein containing a localization signal for coated pits (Shyng et al., 1994; Sunyach et al., 2003). Because of the presence of PrP clusters in caveolae or caveolae domains, a caveolae-mediated endocytic pathway has been proposed (Vey et al., 1996; Peters et al., 2003). However, as caveolae do not occur in mammalian neurons (Morris et al., 2006), these

observations are not relevant to trafficking in neurons. Another proposed mechanism of PrP^C internalisation involves lipid rafts. Rafts are constituted by sphingolipids and cholesterol molecules that form a platform for the attachment of membrane proteins (Simons and Ikonen, 1997). It has been shown that in neurons PrP^C associates with lipid rafts, and leaves the rafts to traverse the detergent-soluble (non-raft) membrane. PrP^C then enters coated pits for endocytosis, and cycles back to the cell surface via the perinuclear sorting compartments (Sunyach et al., 2003).

1.1.4.3 PrP expression during development in the nervous system

PrP expression is tightly regulated throughout development and post-natally in both a temporal and region-specific manner. In the developing embryo, *in situ* hybridisation experiments reported expression of PrP from 13.5 days in the brain, spinal cord, in the peripheral nervous system and in ganglia and nerve trunks of the autonomic nervous system (Manson et al., 1992).

Initial *in situ* hybridization studies indicated that in the adult, PrP expression was restricted to neuronal cells (Kretzschmar et al., 1986a), but subsequently it has also been shown in astrocytes (Moser et al., 1995), in other glial cells, and in ependymal cells in the rat (Verghese-Nikolakaki et al., 1999).

PrP mRNA levels have been shown to increase in the early postnatal days in hamster and mouse (McKinley et al., 1988; Lazarini et al., 1991; Mobley et al., 1988). Regional differences include early post-natal expression in the brainstem and neocortex, intermediate expression in the hippocampus and thalamus, and delayed expression in the basal forebrain (Mobley et al., 1988). High PrP^C expression is also found in the parasympathetic, the enteric nervous system, and the neuroendocrine system (Ford et al., 2002). Outside the central nervous system, PrP^C expression is also detected on lymphocytes (Cashman et al., 1990) and on follicular dendritic cells(McBride et al., 1992).

1.1.4.4 PrP^C physiological function

Despite a conspicuous number of studies on prion cell biology, PrP^C function remains elusive. Hypotheses on PrP^C functions have been based on its localization and

on its interactors (Westergard et al., 2007; Nieznanski, 2010). For example, a role in cell adhesion has been proposed because PrP^C is located at the cell surface and it gets recycled between the plasma membrane and the endocytic compartments. The observed interaction of PrP^C and neuronal adhesion molecules supports this hypothesis (Schmitt-Ulms et al., 2001).

A putative role in cell signalling has been suggested by the demonstration that PrP^C binds to stress-inducible protein 1 (STI1) and mediates neuro-protection through a cAMP/PKA signalling pathway (Zanata et al., 2002). Moreover, antibody-mediated cross-linking of PrP^C triggers signal transduction through the non-receptor tyrosine kinase Fyn (Mouillet-Richard et al., 2000). PrP^C also interacts directly with proteins involved in signalling pathways, like Grb2, Synapsin, and Pint1 (Spielhaupter and Schatzl, 2001).

Additional roles in synaptogenesis (Kanaani et al., 2005), copper homeostasis (Vassallo and Herms, 2003) and neuroprotection (Kuwahara et al., 2000; Roucou et al., 2005; Khosravani et al., 2008) have also been suggested. Recently, PrP^C has been shown to act as a functional receptor for Aβ oligomers in brain slices (Lauren et al., 2009), raising the possibility of crosstalk between prion and Alzheimer's disease.

To shed light on PrP^C function, different knock out mouse models have been generated. In the first knockout line produced, $Prnp^{0/0}$ mice (named 'Zurich I') (Bueler et al., 1992), codons 4 to 187 of the *Prnp* open reading frame (ORF) were replaced by a cassette encoding the Neomycin phosphotransferase selection gene cassette ("Neo-Cassette"). In the second line, designated $Prnp^{-/-}$ (Manson et al., 1994), the ORF was interrupted by the Neo-Cassette. The two lines were derived in different genetic backgrounds, neither expressed detectable PrP^C, and surprisingly both were developmentally and phenotypically grossly normal (Bueler et al., 1992) . It was therefore hypothesized that PrP is either not an essential protein or functional compensation was occurring during development.

The creation of a conditional, adult-onset *Prnp* knockout mouse (Mallucci et al., 2002) circumvented this possibility. Adult-onset *Prnp* knockout mice were created by crossing mice carrying a 'floxed' *Prnp* gene on a $Prnp^{0/0}$ background with $Prnp^{0/0}$ mice expressing Cre recombinase under the control of the neurofilament heavy chain (NFH)

promoter. In these mice, the NFH promoter became active at around 9 - 10 weeks of age, leading to Cre-mediated excision of the *Prnp* transgene in neuronal cells. The mice remained healthy following ablation of neuronal PrP^C, confirming the limited effects of loss of PrP function found in previous models. Mallucci's mouse model will be discussed in further detail in the following chapters of this thesis.

Three lines of PrP knockout mice, created by deletions beyond the ORF, spanning the 5'splice acceptor site, developed a neurodegenerative phenotype (Moore et al., 1999; Sakaguchi et al., 1996; Rossi et al., 2001), but this was shown to result from expression of the downstream *Prnd* gene, encoding the doppel protein (Dpl) (Flechsig et al., 2003; Rossi et al., 2001). Further intensive studies on the first knockout mice have shown some subtle neurophysiological and metabolic abnormalities. Both synaptic function (Collinge et al., 1994; Manson et al., 1995) and intrinsic features of hippocampal cells (Colling et al., 1996; Mallucci et al., 2002) have been shown to be altered upon loss of PrP expression. Furthermore, altered circadian rhythms and sleep disturbance have been reported in PrP null mice (Tobler et al., 1996), an interesting finding in light of the sleep disturbances characteristic of FFI.

Metabolically, reduced $Cu^{2+/}Zn^{2+}$-dependant superoxide dismutase (SOD) activity has been reported in vivo in $Prnp^{0/0}$ mice and neurons derived from these mice exhibit increased vulnerability to oxidative stress *in vitro* (Brown et al., 1997b). These studies suggested a role for PrP in neuroprotection from oxidative stress. The neuro-protective role for PrP^C was further supported by the observation that serum-deprivation induced apoptosis is significantly higher in cultured $Prnp^{0/0}$ cells (Kuwahara et al., 1999), and PrP^C protects human primary neurons (Bounhar et al., 2001) and yeast (Li and Harris, 2005) against Bax-mediated cell death.

Another abnormality that suggested a function for PrP^C is associated to neuronal nitric oxide synthase (nNOS) metabolism: in $Prnp^{0/0}$ mice nNOS is mislocalised and its activity is reduced compared to wild type mice. Since PrP^C and nNOS are both associated with lipid rafts in wild type animals, it has been suggested that PrP^C targets nNOS to the cholesterol-rich microdomains (Keshet et al., 1999).

Recently, ablation of PrP^C in neurons has been shown to trigger chronic demyelinating polyneuropathy. This phenotype could be suppressed by PrP^C neuronal

expression, but not in Schwann cells, therefore suggesting an important role of neuronal PrP^{C} for myelin maintenance (Bremer et al., 2010).

1.1.5 Prion mediated neurotoxicity

Although the role played by PrP^{C}, PrP^{Sc} and the conversion mechanism in neurotoxicity have been extensively studied, the molecular basis of prion-mediated neurotoxicity is still poorly understood. Indeed, the nature of the neurotoxic species is still under debate.

1.1.5.1 The role of PrP^{C} in prion disease

As previously discussed, the physiological role of PrP^{C} has still not been clarified. Nevertheless, the loss of a critical PrP function has been proposed as a possible mechanism by which PrP^{Sc} formation might result in neurodegeneration (Hetz et al., 2003a). However, the lack of a clear cut phenotype in the knockout mice (Bueler et al., 1992; Manson et al., 1994; Mallucci et al., 2002) strongly argues against this hypothesis.

The role of abnormal PrP^{C} processing in prion pathology is also under debate. It has been shown that PrP^{C}-null primary neurones *in vitro* are more sensitive to oxidative stress (Brown et al., 1997b) and the exposure of cells to the synthetic peptide PrP106–126, used as a model for PrP^{Sc} (Forloni et al., 1993), results in microglial activation and the production of reactive oxygen species (ROS) (Combs et al., 1999). Also, in *Prnp*-null mice the expression of N-terminally truncated PrP^{C} has been shown to induce rapid degeneration of cerebellar neurones, which can be rescued by co-expression of wild type PrP^{C} (Shmerling et al., 1998). The N-terminal region has been proposed to have cytoprotective activity, as an N-terminally truncated PrP^{C} mutant has been shown to activate Bax-dependent and independent cell death pathways, (Li et al., 2007).

Abnormal PrP^{C} trafficking has been proposed to have a role in prion mediated neurotoxicity. Most PrP^{C} molecules are anchored to the membrane by the GPI moiety, but a small fraction can be cytosolic. Following inefficient translocation in the ER, PrP can assume two transmembrane topologies, CtmPrP- C transmembrane PrP with an extracellular C-terminus, and NtmPrP- N transmembrane PrP with an extracellular N-terminus (Hegde et al., 1998). In the former, the N terminus is exposed to the cytosol

and the C-terminus is in the ER lumen, whereas in the latter the N-terminus is inside the ER and the C-terminus faces the cytosol. In healthy organisms these forms do not exceed 10% of total PrP, but in TSEs they may constitute up to 30%. Mutations in the hydrophobic domain cause increased generation of CtmPrP, like GSS linked P105L and A117V (Hegde et al., 1998; Kim and Hegde, 2002). Other PrP mutants, associated with FFI and CJD, D177N may be miss-targeted to the cytosol as a result of retrograde transport from the ER (Ma and Lindquist, 2001). Generally, the quality control within the cell would trigger degradation of cytosolic PrP^{C} by the ubiquitin-proteasome system. However, PrP^{Sc} has been shown to inhibit the proteosome (Kristiansen et al., 2007) and inhibition of proteosome activity leads to protein accumulation in the cytosol (Ma and Lindquist, 2001; Ma et al., 2002). Cytoplasmic PrP^{C} aggregates are not toxic themselves, but mutants lacking the signal sequence and the GPI anchor remain in the cytoplasm and can cause neurodegeneration both *in vivo* and *in vitro* (Ma et al., 2002).

1.1.5.2 PrP^{Sc} neurotoxicity

PrP^{Sc} itself has been proposed as the toxic species. This hypothesis comes from the spatial correlation of PrP^{Sc} aggregates and the most damaged areas in prion disease, and from *in vitro* experiments showing that both full-length PrP^{Sc} (Hetz et al., 2003b) and shorter PrP peptides are toxic to primary neuronal cultures (Forloni et al., 1993).

However, the idea that neurodegeneration is caused by formation of PrP^{Sc} is strongly challenged by studies showing that PrP^{C}-null tissue remains healthy and free of pathology when exposed to PrP^{Sc} (Brandner et al., 1996; Mallucci et al., 2003).

Despite the fact that PrP^{Sc} accumulation correlates with neurodegeneration and prion disease manifestation, there are circumstances in which prion disease occurs in the absence of detectable PrP^{Sc} accumulation or abundant PrP^{Sc} deposition is observed in absence of neurodegeneration. For example, PrP^{Sc} levels are barely detectable in brain homogenates from FFI patients and transgenic FFI mice (Collinge et al., 1995a). Also, mice inoculated with BSE prions exhibit neuronal death, without detectable PrP^{Sc} (Lasmézas et al., 1997). In contrast, accumulation of PrP^{Sc} in the absence of any spongiform degeneration has been reported in a single GSS patient (Piccardo et al., 2007). Moreover, inoculation of a patient's brain homogenate to recipient mice resulted

in almost complete absence of disease transmission, although PrP-amyloid deposition was elicited in some of the inoculated mice.

Neurotoxicity due to PrP^{Sc} is also hard to prove in light of subclinical infection, where high levels of PrP^{Sc} accumulate in the absence of clinical symptoms (Hill et al., 2000; Hill and Collinge, 2003b; Hill and Collinge, 2003a).

1.1.5.3 Lessons from adult PrP knockout mice

It has been suggested that the conversion to a toxic species must occur in neurons to be pathogenic (Mallucci et al., 2003).

Mallucci et al. showed the effect of neuronal PrP^{C} depletion on the course of disease and on neuropathological change, in animals with established prion disease. Two lines of transgenic mice were used (tg 46 and tg37). They express PrP^{C} from a MloxP transgene at ~1 and ~3x wild type levels on a *Prnp* null background. After intracerebral inoculation with Rocky Mountain Laboratory (RML) prions these animals succumb to scrapie ~12 and ~18 weeks post inoculation. To test the effect of PrP depletion during prion disease, these transgenic mice were crossed with NFH-Cre mice, expressing the enzyme Cre recombinase under control of Neurofilament Heavy Chain promoter. In the double transgenic NFH-Cre/M*lox*P mice, PrP is normally expressed in neuronal and non-neuronal cells until ~10 -12 week of age. The Neurofilament promoter activated at 10-12 weeks of age, thus activating the Cre recombinase in neurons, which mediates genomic recombination resulting in loss of sequence located within the two loxP sites (Figure 1.5)

NFH-Cre/M*lox*P (tg 37/63) mice were inoculated with RML prions at 3 or 4 weeks of age, and prion replication and CNS infection proceeded normally until Cre-mediated PrP depletion occurred. Control M*lox*P (tg37) mice were inoculated in parallel. In double transgenic animals, neuronal PrP^{C} depletion prevented progression to clinical disease and resulted in long term survival of the infected animals. While control animals succumbed to scrapie ~18 (tg46) and ~12 (tg37) weeks post infection, NFH-Cre/tg37 and NFH-Cre/tg46 remained asymptomatic >57 wpi and >58 wpi respectively (Figure 1.6). Neuropathologically, scrapie-infected control animals (tg37) showed degeneration of hippocampal CA1 and CA3 neurons from 10 wpi, severe neuronal loss

by 12 wpi and shrinkage of the entire hippocampus. Asymptomatic prion-infected animals with PrP^{C} depletion were protected from neuronal loss up to 48 weeks post inoculation. One hallmark of the RML prion strain is spongiosis and early spongiform changes were present both in control tg37 and double transgenic tg37/63 (NFH-Cre/M*lox*P) mice at 8wpi, but not in mice with Cre-mediated neuronal PrP^{C} depletion examined as early as 10 wpi, or up to 48 wpi (Figure 1.7). To allow more time for development of pathology before PrP^{C} depletion, the double transgenic animals were inoculated at one week of age. Under these conditions, neuropathological changes occurring at 8 wpi were reversed after Cre expression at ~ 10 wpi. However, PrP^{Sc} accumulation progressed over a prolonged period of observation, reflecting prion replication in glial cells, where Cre is not expressed. Even though abnormal PrP continued to accumulate, NFH-Cre mice did not develop symptoms of prion disease.

In conclusion, this study demonstrated that arresting neuronal conversion of PrP^{C} to PrP^{Sc}, by depleting the former, prevents the progression from pre-clinical to clinical infection. Also, adult neuronal PrP^{C} depletion reverses early neurodegenerative changes caused by the RML prion strain and protected against neuronal loss, despite continued prion replication and PrP^{Sc} deposition.

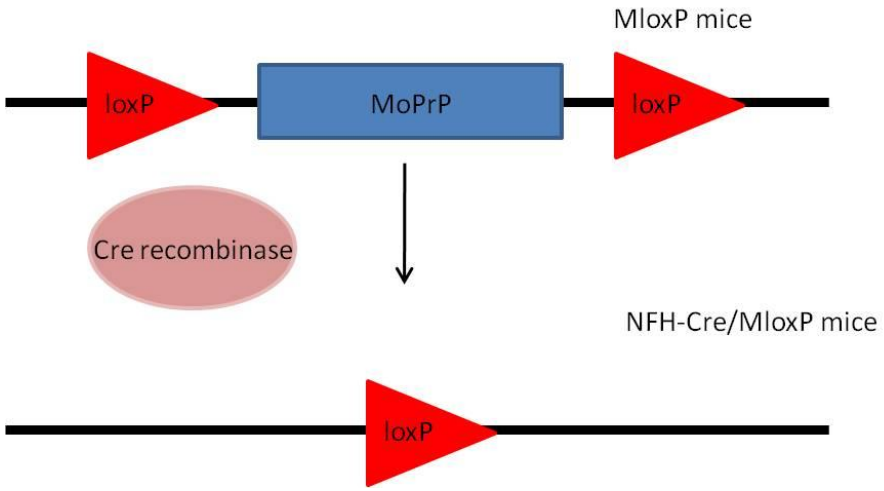

Figure 1.5 Schematic drawing of PrP Cre-mediated recombination in NFH-Cre/M*lox*P mice

M*lox*P mice encode the M*lox*P construct, containing the floxed murine PrP (MoPrP) coding region between two loxP sites. In NFH-Cre/M*lox*P mice, Cre expression mediates the excision of M*lox*P PrP sequences between the two lox P sites.

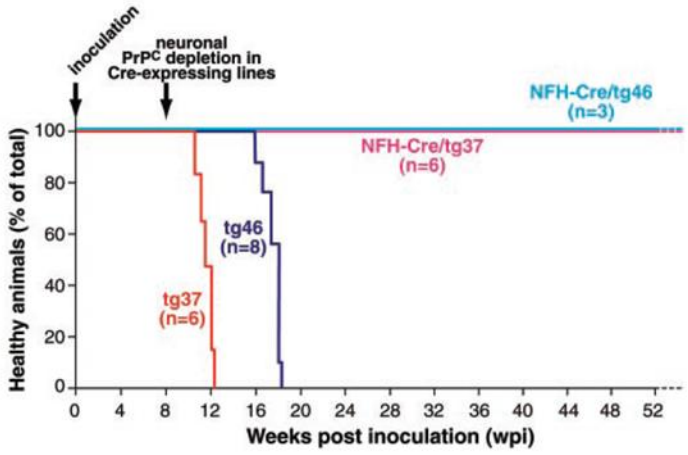

Figure 1.6 Increased survival in RML inoculated NFH-Cre/M*lox*P mice after Cre-mediated neuronal PrP depletion

M*lox*P and NFH-Cre/M*lox*P mice were inoculated at ~3, 4 weeks of age. Around ~8 weeks post inoculation (wpi), Cre-mediated recombination occurred in NFH-Cre/M*lox*P mice. M*lox*P mice succumbed to prion infection at ~12 and ~ 16 wpi (respectively tg37 and tg 46), while NFH-Cre/M*lox*P mice remain asymptomatic by 52 wpi. Figure from (Mallucci et al., 2003).

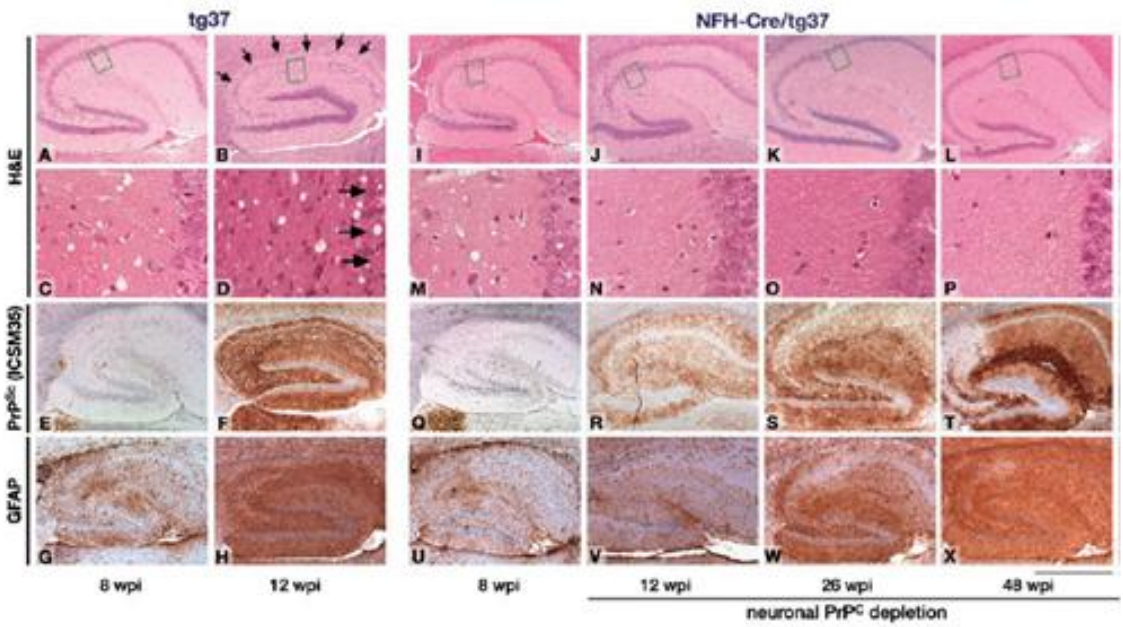

Figure 1.7 Progression of prion pathology in the hippocampus of RML inoculated M*lox*P (tg37) and NFH-Cre/M*lox*P (NFH-Cre/tg37) mice

Sections were stained with haematoxylin and eosin (H&E) and immunostained with an anti-GFAP antibody for detection of astrocytosis and with ICSM35 antibody for PrP^{Sc} deposition. Panel B and D show severe loss of CA1 to CA3 neurons (arrows) and shrinkage of the entire hippocampus (B) in terminally ill tg37 mice. No neuronal loss was seen in asymptomatic prion-infected mice with Cre-mediated PrP^{C} depletion up to 48 wpi (panel J, K, and L). In NFH-Cre/tg37 mice, early spongiosis was seen at 8 wpi (C and M), but was not seen at 12, 26, and 48 wpi (N, O, and P), despite continued PrP^{Sc} accumulation and gliosis (R to T and V to X). Scale bar = 80 µm in C, D, and M to P; =320 µm in all the other panels. Picture taken from (Mallucci et al., 2003).

1.1.5.4 The concept of the "toxic species"

It is clear that the major pathological changes in prion disease do not result from loss of PrP^{C}. Indeed, it is believed that the major pathological changes in prion disease do not result from PrP^{C} loss of function and PrP^{Sc} does not cause neurotoxicity directly but exhibits its toxicity only where PrP^{C} is also expressed (Brandner et al., 1996). It has therefore been suggested that a neurotoxic intermediate is formed during the conversion reaction (Hill et al., 2000; Hill and Collinge, 2003a). This intermediate has been termed PrP^{L}, for 'lethal' and it is believed to acquire a transient structure or conformation in the process of conversion between PrP^{C} and PrP^{Sc}.

This model had been further optimized to accommodate the apparent split between the identity of the propagating infectious agent and toxic species (see for review (Collinge and Clarke, 2007). Four steps are envisaged in the process of PrP^{Sc} formation:

$$PrP^{Sc} + PrP^{C} \xrightarrow{k_1} PrP^{Sc}{:}PrP^{C} \xrightarrow{k_2} PrP^{Sc}{:}PrP^{L} \rightarrow PrP^{Sc}{:}PrP^{Sc} \rightarrow PrP^{Sc} + PrP^{Sc}$$

The formation of classical intermediates is not catalysed by end products: the relative levels of toxicity and infectivity are determined by the ratio of the initial rate of conversion (k1) to the rate of maturation (k2). This model can explain also subclinical infection: a relatively slow rate of initial conversion (k1) would keep the level of PrP^{L} low, because its rate of loss through maturation (k2) would be prevailing. Thus, a large amount of PrP^{Sc} or infectivity would build up, but with little or completly no toxicity (Collinge and Clarke, 2007). Experimental evidence recently provided support for the model suggesting uncoupling of prion infectivity and toxicity (Sandberg et al., 2011). Mice expressing different levels of PrP^{C} were inoculated with the same dose of RML prions, and the prion titre in their brains was compared at different time points. It was found that prion propagation occurs in two distinct phases. In phase 1, prions propagated exponentially until a defined limit titre is reached. After this point, there is a pathway switch and phase 2 is constituted by an infectivity plateau that continues until the onset of clinical disease. The production of toxic species occurs in phase 2 and is linearly dependent on PrP^{C} expression levels; therefore length of this phase is inversely proportional to PrP^{C} expression level. In Sandberg's study, maximal prion titre was reached long before clinical signs in conventional mice with wild type PrP^{C} expression, suggesting that toxic species do not accumulate until infectivity saturates and clinical signs occur once the toxic threshold is crossed. These data can easily be accommodated in the PrP^{L} general model: Production of PrP^{L} is proportional to PrP^{C} concentration and clinical onset occurs when PrP^{L} reaches a toxic threshold (Sandberg et al., 2011) (Figure 1.8). Other alternative models have been hypothesized to explain the split between infectivity and toxicity: for example, fission of infectious particles may stop; leading to

further growth but no increase in number of infectious particles; or a key cellular component may be depleted.

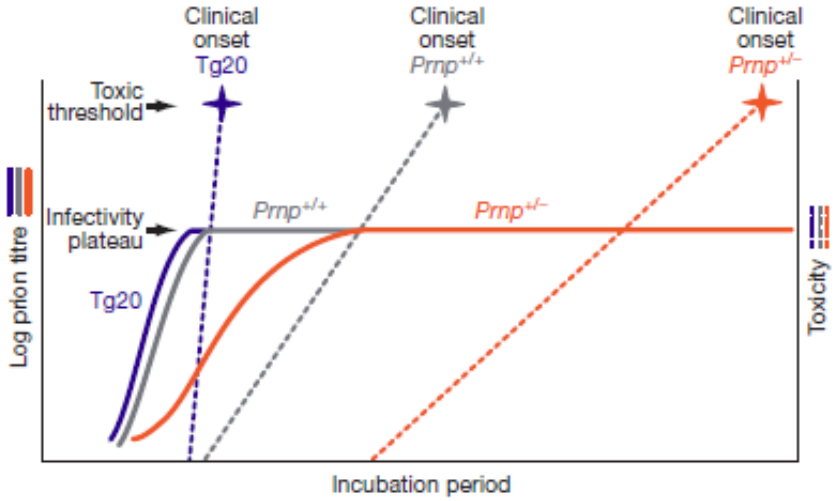

Figure 1.8 Model of prion infectivity and toxicity

Mice expressing different levels of PrP^C (Tg20, eight-fold wild type PrP^C expression level; *Prnp* $^{+/+}$, wild type PrP^C expression level; *Prnp* $^{+/-}$, 50% PrP^C expression level) were inoculated with the same dose of RML prions, and the prion titre in their brains was compared at different time points. It was found that prion propagation occurs in two distinct phases. In phase 1, prions propagated exponentially (solid line) until a limiting titre of prion is attained, independent of PrP^C expression level. After this point, there is a pathway switch and in phase 2 (dotted line) toxic species are produced, linearly dependent on PrP^C expression levels. Toxic species do not accumulate until infectivity saturates and clinical signs occur once the toxic threshold is crossed. Figure from (Sandberg et al., 2011).

1.1.5.5 Mechanism for prion-mediated neurodegeneration

As no specific histopathological marker for PrP^L exists, the identity of the toxic species is still unknown. Therefore, the production of a toxic species is indirectly visualized by variable accumulation of abnormal prion protein aggregates following the PrP^C to PrP^{Sc} conversion event. Different types of abnormal PrP accumulation are detected by immunohistochemical methods. These deposits are highly variable in intensity, pattern, (synaptic deposition or formation of coarse granular deposits) and distribution within the CNS (Reiniger et al., 2011) . These differences are strain-dependent. Therefore, abnormal deposition pattern, in conjunction with spongiform changes and glial activation patterns are used to characterize different prion strains.

Spongiform changes are the most typical alteration induced by prion diseases. The name "spongiform encephalopathies" comes indeed from the vacuolation observed in the affected brains: small, round or oval vacuoles in the brain tissue, give the tissue a typical sponge appearance. The degree of the spongiform changes can vary significantly even within the same brain. Although it is the most typical manifestation of prion disease, its significance is still unclear, and different scenarios have been proposed: It may arise from abnormal membrane permeability and increased water content in the neurons(Kovacs and Budka, 2008); from autophagy (Liberski et al., 2004; Liberski, 2004); or due to production of abnormal PrP within the lysosomal compartment, which would cause disruption of the lysosomal membrane, destruction of the neuronal cytoskeleton and initiation of vacuolation (Laszlo et al., 1992). TSE-infected mink of the Chediak-Higashi genotype, with abnormalities in membrane-bound organelles, manifest no vacuolation (Marsh et al., 1976), therefore supporting last hypothesis on spongiosis generation.

Another typical manifestation used to characterise prion diseases is widespread glial activation within the brain. Histopathologically, this can be confirmed with antibodies against glial fibrillar acidic protein (GFAP) to visualise reactive astrocytes. However, the contribution of inflammation to brain dysfunction is still unclear. Upon accumulation of PrP^{Sc} deposits, microglia get activated and are attracted to the site of injury (Williams et al., 1994). It is still under debate if glial activation is triggered by PrP^{Sc} accumulation directly or by the neurodegenerative changes in neurons upon prion replication, and if inflammation is the cause or the consequence of neuronal degeneration. Expression profiling showed up-regulation of inflammatory genes upon PrP^{Sc} accumulation in the brain before neuronal damage (Hwang et al., 2009). Moreover, neuropathology time course studies showed astrocytes and microglia activation weeks before neuronal loss, coinciding with the first changes in neuronal morphology (Perry et al., 2002; Eikelenboom et al., 2002). *In vitro* experiments proved that neurotoxic activity of the aggregated PrP fragment is enhanced in the presence of microglia (Brown et al., 1996; Bate et al., 2002). Alternatively, activated microglia could play a positive role in removing PrP^{Sc} deposits and slowing down the progression of the disease (McHattie et al., 1999).

Other neuropathological changes typical of prion diseases are synaptic alteration and neuronal loss. However, the molecular mechanisms underlying these neurodegenerative pathways are still not completely understood, as well as their temporal sequence in the affected brain areas. Synaptic dysfunction is considered one of the first events of neurodegeneration. The process of prion conversion is believed to impact on the integrity and functionality of the synaptic structure. Various evidences point to this direction. For example, in a mouse model of prion infection, synaptic alteration appeared concomitantly with PrP^{Sc} deposition and behavioural changes like impairment of burrowing, glucose consumption and increase open field activity months before neuronal loss (Cunningham et al., 2003). Also, in the Cre-mediated adult knock out model mice, synaptic impairment was reported as the first manifestation of the disease (Mallucci et al., 2007). At early stage of the disease, PrP^{Sc} has been shown to accumulate in the lipid rafts, detaching caveolin and synaptophysin at this site. This may lead to impaired synaptic activity (Russelakis-Carneiro et al., 2004). Dendritic loss follows synaptic dysfunctions. This mechanism has been proposed to be due to changes in the expression and cleavage of Notch-1(Ishikura et al., 2005). Although spongiform changes and abnormal PrP accumulation are the typical hallmarks of prion pathology, neuronal loss is believed to be the ultimate cause of chronic brain deterioration and fatal outcome of prion disease. Neuronal death is a prominent feature of prion diseases and there is a good correlation between the type of clinical symptoms observed in each disease and the brain region exhibiting the greatest extent of cell death (Budka, 2003). Two main pathways have been implicated in neuronal loss, autophagy and apoptosis.

Autophagy is an intracellular degradation system: cellular organelles with proteins are sequestered in the “autophagosome”, a double layered vesicle. Once in the cytoplasm the autophagosome fuses with the lysosome and forms the “autophagolysosome”. Lysosomal hydrolysis can degrade the content of the autophagolysosome. It has been proposed that autophagy is a protective mechanism by which the cell fights the diseases through digestion of misfolded aggregates (Moreau et al., 2010).

Apoptosis is programmed cell death, executed by “caspases”, a large family of cysteine proteases. Apoptosis may be triggered by mitochondrial stress or ER stress. In

prion disease both pathways may be activated. Apoptosis induced by aggregated PrP peptide fragments or cytosolic PrP proceeds via the mitochondrial pathway (O'Donovan et al., 2001; Hachiya et al., 2005). However, neither Bax deletion or Bcl-2 overexpression decreases neuronal death in prion infection (Coulpier et al., 2006; Steele et al., 2007)

Alternatively, chronic ER stress results in activation of ER-resident caspases that in turn cleave and activate downstream caspases. Neurons exposed to PrP^{Sc} exhibit extensive ER stress, resulting in release of calcium and activation of the UPR (Hetz and Soto, 2006). Up-regulation of ER-resident caspases has been observed *in vitro*, in brains of prion infected mice and in sCJD and vCJD (Hetz et al., 2003b; Hetz et al., 2003b). Another proposed mechanism by which ER stress leads to neurodegeneration is the disruption of Calcium homeostasis, with release of Calcium from the ER (Hetz et al., 2003b; Florio et al., 1996). Increased Calcium in the cytoplasm deregulates downstream calcium-dependent phosphatases Calcineurin (CaN) activity. It has been shown that CaN activation is implicated in neuronal death induced by PrP^{Sc} and synthetic peptides (Agostinho and Oliveira, 2003). Moreover, CaN activity increases in the brains at the beginning of the symptomatic phase (Mukherjee et al., 2010).

1.1.5.6 The concept of clinical target areas

Early studies in the 70s and the 80s focussed on the effect of different route of infection on clinical phase of prion disease. It was reported that scrapie replication phase in the brain was shorter after peripheral intraperitoneal (i.p.) infection rather than direct intracerebral infection (i.c.) in the anterior brain (Kimberlin and Walker, 1983; Kimberlin and Walker, 1986; Kimberlin and Walker, 1982). This observation led to the proposal that the development of clinical prion disease depends on infection spreading, replicating, and producing cell dysfunction and cell death in specific "clinical target areas". Further investigations proved that intraspinal injection (i.s.) produced shorter incubation time than i.c (Kimberlin et al., 1987). Comparison of the vacuolar lesion profiles produced at clinical stage showed that both i.c. and i.s. route of injection directly initiate a local infection at their respective sites and the location of these sites determines the length of incubation. Moreover, the distribution of vacuoles was similar

for the three routes of infection, but severity of the lesion profiles was different; they were more severe i.c. than i.p. and i.s. This difference was attributed to the duration of the scrapie replication phase in the brain, in agreement with conclusions from other studies which showed that the severity of lesions in a given area is limited by the time available before the host dies (Cole and Kimberlin, 1985; Bruce and Dickinson, 1985).

An important corollary to these observations is the speculation that the duration of the neural phase of scrapie pathogenesis is determined by the complexity of the pathways between the injection site and the postulated clinical target areas in which scrapie should replicate for the disease to develop (Kimberlin et al., 1987).

Different approaches have been used to evaluate the brain regions that could be the clinical target areas of prion disease and many studies have pointed to the brainstem as an important area.

For example, analysis on the route of transport of the TME strain Hyper (HY), following injection in the sciatic nerve in hamsters, showed that it can spread by retrograde transport along specific motor pathways of the spinal cord. As a result, the infection targets brain regions that control vestibular and motor function, like the lateral vestibular nucleus in the brainstem and the cerebellum. In this experimental model, the specific targeting of prion pathology to brain nuclei with a functional role in coordination, balance and motor activity was considered responsible for the early onset of clinical signs (Bartz et al., 2002). More recently, a histopathological comparison between PrP overexpressing T*ga20* mice (also known as Tg20) and wild type C57BL/6 inoculated with three prion strains (RML, Me7 and 22L) showed that abnormal PrP accumulation was lower in the overexpressing mice compared to the wild type in all the brain regions except for brainstem and thalamus. This implied that one or both of these structures may be clinical target areas of prion disease, and that abnormal PrP accumulation in the other brain regions did not progress because the clinical target areas were already impaired and determined the clinical disease (Karapetyan et al., 2009).

1.1.6 Therapeutic strategies in prion disease

The uncertainties about the identity of the prion neurotoxic species and the possible mechanisms of neurodegeneration have been an obstacle to the development of a successful therapeutic strategy against prion disease.

Although the recent development of a prototype blood test for diagnosis of vCJD in symptomatic individuals could pave the way to diagnosis of asymptomatic vCJD prion infections(Edgeworth et al., 2011), diagnosis is not currently possible without clinical manifestation, resulting in a short window of time for therapeutic intervention.

Despite numerous attempts, no therapy is available and to date prion diseases remain fatal. However, a number of proof-of-principles studies have shown that therapy for prion disease is an achievable goal. Possible stages for interruption of prion formation could target PrP^{C}, PrP^{Sc} or the process of conversion between the two isoforms.

Compounds that are able to reduce PrP^{Sc} accumulation in prion infected cells include Congo red, polyanionic compounds, amphotericin B, porphyrins and Quinacrine. *In vivo* use of these molecules has been disappointing, showing only small increases in the incubation period in animal models (reviewed in (Trevitt and Collinge, 2006).

However, a compound that binds PrP^{Sc} is likely to be specific for a particular strain or conformation, and blocking the propagation of a major component of the strain ensemble would just result in a sub-strain becoming dominant. Moreover, the currently available cell lines for screening are susceptible to mouse prions but not human prions, and PrP^{Sc} reduction could be triggered by off-site effects linked to the specific cell lines, rather than a genuine PrP^{Sc} reduction.

The Quinacrine study is an example of the obstacles to turn compounds into actual therapy: while it can cure prion infected cells in the nanomolar range, *in vivo* data showed no increase in survival time in infected mice (Collins et al., 2002; Doh-ura et al., 2004); NMR studies showed no interaction with PrP at a physiologically relevant concentration (Vogtherr et al., 2003) and no efficacy has been shown in human trials (Collinge et al., 2009).

Other compounds, such as branched polyamines (Supattapone et al., 1999) and a tyrosine kinase inhibitor (Ertmer et al., 2004) are able to enhance the endogenous clearance of PrP^{Sc} *in vitro*. However, as they do not prevent de novo formation of PrP^{Sc}, they would only have therapeutic value if the formation of a toxic species occurs downstream of PrP^{Sc} production.

As prions cannot propagate in the absence of PrP^{C} (Bueler et al., 1993; Brandner et al., 1996), and it has been hypothesized that infectivity and neurotoxicity can be uncoupled and mediated by different molecular species (Collinge and Clarke, 2007), stabilizing PrP^{C} in order to prevent the conversion process is another therapeutic strategy.

High throughput screening of a large library of compounds has been set up to identify high quality drug-like molecules for their property of stabilizing PrP^{C} *in vitro* (Nicoll and Collinge, 2009). As these compounds are not licensed drugs, before any clinical trials can be undertaken, eventual hits will need extensive *in vivo* testing for toxicological and pharmacokinetic properties.

Proof of principle for the PrP^{C} stabilizing strategy is provided by another class of therapeutic agents, PrP antibodies. Antibodies against several PrP epitopes have been shown to inhibit PrP^{Sc} replication *in vitro* and transgenic mice expressing anti-PrP μ chains are protected against peripheral prion infection (reviewed in (Trevitt and Collinge, 2006). Passive immunization with anti-PrP monoclonal antibodies has been proven to reduce PrP^{Sc} accumulation and prion infectivity in the spleen of peripherally infected mice, even when antibodies were given at the point of maximal PrP^{Sc} accumulation. In addition, treated animals survived 300 days more than untreated animals. Since antibodies do not cross the blood brain barriers, no effect was seen in intracerebrally infected mice (White et al., 2003). However, in a different study, when administered intracerebrally, anti-PrP antibodies have been shown to cause severe neuronal apoptosis (Solforosi et al., 2004), suggesting further investigations are needed to determine the consequences of PrP binding in the CNS.

Active immunization is limited by immunotolerance to PrP, which is highly expressed in the immune system, and studies aiming to overcome this problem have shown just modest effects (Sigurdsson et al., 2002; Schwarz et al., 2003).

A way to circumvent the handicap represented by the inability of antibodies to cross the blood brain barrier in passive immunization, and the host tolerance in active immunization, is to combine active and passive immunotherapy. Anti-PrP scFv (single-chain variable fragment) has been shown to be able to reduce proteinase K-resistant PrP in infected cells. Brain delivery of anti-PrP scFv through peripheral treatment has been envisaged by use of recombinant adeno-associated virus or lentivirus as a delivery system (Campana et al., 2009). However, to date no *in vivo* experiments have shown the effect of this double approach in an experimental model of prion disease.

The demonstration that removing neuronal PrP^C in adult mice is harmless (Mallucci et al., 2002) and prevents prion disease progression in an established prion infection (Mallucci et al., 2003) has set the basis for a therapeutic approach based on the removal or elimination of PrP^C.

Potential treatments aimed at removing PrP^C for direct therapeutic possibilities in humans must be achieved using extrinsic means. The RNA interference (RNAi) technology offers opportunities to realize therapeutic gene silencing *in vivo*.

1.1.6.1 RNA interference

RNA interference (RNAi) is a sequence-specific mechanism for post-transcriptional gene silencing naturally occurring in eukaryotes, initiated by a double-stranded RNA (dsRNA), either exogenously introduced into the cell, or endogenously encoded as microRNAs (miRNAs).

The process of RNAi can be divided into an initiation step and an effector step. In the initiation step, Dicer, a cytoplasmic ribonuclease, recognizes the exogenously introduced dsRNA and cleaves it into 21–23 nucleotides (nt) sequences, called short interfering RNAs (siRNAs) (Zamore et al., 2000). In the effector step, both siRNAs and miRNAs interact with RISC, a multi-protein RNA-induced silencing complex. The siRNA duplex is unwound and the strand which is least thermodynamically stable within the 5' antisense region is loaded into RISC (Khvorova et al., 2003), becoming the "guide" for locating complementary target mRNAs within the cell (Martinez et al., 2002) (Figure 1.9).

The homology between the guide strand and the mRNA controls whether RISC initiates endonucleolytic activity or translational arrest of the target mRNA. SiRNAs have a higher degree of homology and therefore mediate degradation of target mRNAs, whereas miRNAs silence gene expression through translational repression, as the target mRNA is not perfectly complementary. The other strand, denominated "passenger", is not incorporated into RISC and get cleaved by RISC itself (Matranga et al., 2005; Rand et al., 2005).

Cleavage of both the passenger strand and the target mRNA is due to the endonuclease Slicer. Slicer has been shown to be a highly conserved protein called Argonaute 2 (Ago-2) (Liu et al., 2004; Song et al., 2004).

To use RNAi as a biological tool, siRNA duplexes can be synthesized and introduced for direct loading into RISC. Otherwise, recombinant vectors can be used to obtain stable, long-term expression of interfering RNA sequences. SiRNA duplexes are advantageous because they can bypass the cellular defence mechanisms for recognition of long viral dsRNA. On the other hand, unmodified siRNAs are unstable *in vivo* and cannot cross the blood-brain-barrier (White and Mallucci, 2009)

To be used in conjunction with recombinant vectors, siRNAs are expressed as short hairpin RNAs (shRNAs). ShRNAs are duplexes of 19 – 29 nt, corresponding to the sense and antisense strands of a 'traditional' siRNA, separated by a short loop sequence. Once transcribed within the cell by an endogenous RNA Polymerase, Dicer recognises the shRNAs, and cleaves off the loop region to generate a functional siRNA (Meister and Tuschl, 2004).

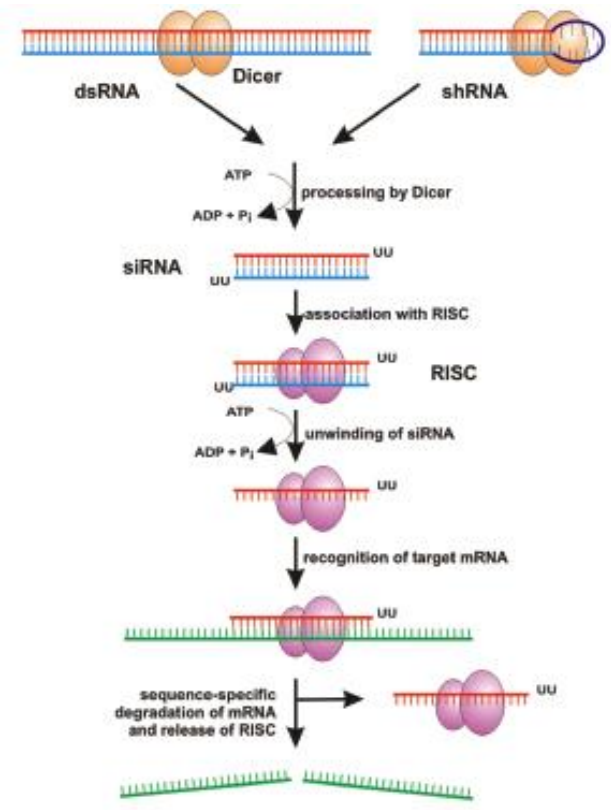

Figure 1.9 The process of RNAi

The process of RNAi can be divided into an initiation step and an effector step. In the initiation step, Dicer, a cytoplasmic ribonuclease, recognizes the exogenously introduced dsRNA and cleaves it into 21–23 nucleotides (nt) sequences, called short interfering RNAs (siRNAs). In the effector step, the siRNAs interact with RISC, a multi-protein RNA-induced silencing complex. RISC unwinds the siRNA and loads the strand which is the least thermodynamically stable within 5' antisense region. This strand becomes the "guide" for locating complementary target mRNAs within the cell. Once the mRNA is degraded, RISC is released. Adapted from (Rutz and Scheffold, 2004)

1.1.6.2 RNAi in the treatment of neurodegenerative diseases

Different recombinant viruses, including retroviruses, adenoviruses, adeno-associated viruses, and herpes-simplex viruses can be used for efficient delivery of shRNA-expressing vectors to neuronal cells *in vivo*. Lentiviruses, a member of the retrovirus family, are a common choice for expression of shRNA in the CNS (Naldini et al., 1996; Blomer et al., 1997), because of their ability to transduce and integrate into the genome of post-mitotic cells such as neurons.

Recently virally mediated RNAi has been used successfully as a therapeutic treatment in models of a number of different neurodegenerative diseases, including mouse models of spinocerebellar ataxia, (Xia et al., 2004), Huntington disease (Harper et al., 2005) (Rodriguez-Lebron et al., 2005), Alzheimer's disease (Singer et al., 2005), and Amyotrophic lateral sclerosis (ALS) (Raoul et al., 2005). These studies suggested that virally mediated RNAi against PrP could be a useful therapeutic approach in prion disease.

1.2 The brainstem and its main functions

The brainstem is located between the higher centres of the central nervous system and the spinal cord. It is anatomically divided into mid brain, pons and medulla, (Figure 1.10) and is critically important for motor and autonomic control.

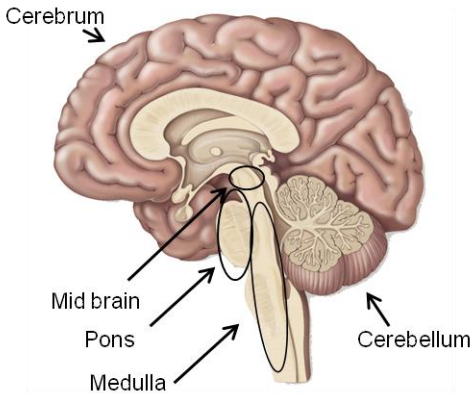

Figure 1.10 The human brainstem

The human brainstem is localized between the cerebrum and the spinal cord and it is anatomically divided into mid brain, pons and medulla.

The midbrain connects the forebrain to the rest of the brainstem. Some major regions in the midbrain are: the cerebral peduncles, which anchor the rest of the brain to the brainstem; the tegmentum, with the red nucleus, origin of the rubrospinal tract; the substantia nigra, a motor centre whose degeneration leads to muscle tremors in Parkinson Disease; the tectum, consisting of the superior colliculus and inferior colliculus, involved in visual and hear attention; the medial lemniscus, that carries

sensory information from the lower nuclei of the brainstem to the thalamus. In the midbrain are also located the nuclei of two cranial nerves that control eye movements: cranial nerve III (oculomotor) and IV (trochlear).

The pons in humans appears as an anterior protuberance rostral to the medulla. In rodents it is contiguous to the midbrain, with the latero-dorsal tegmental nucleus spanning the midbrain and the pons tegmentum. The pons white matter includes tracts conducting signals from the forebrain to the cerebellum and medulla and tracts that carry sensory information to the thalamus. The nucleus of the motor and sensory part of the cranial nerve V (trigeminal) is located in the pons. Pontine nuclei are involved in relaying signals from the forebrain to the cerebellum and in control of autonomic functions like sleep, hearing, equilibrium, taste, eye movement, facial expression and sensation, swallowing, bladder control and posture and respiration.

Although the functional role of the pons in the generation and control of respiratory rhythm and pattern is not fully understood, the pontine regions have been shown to interact with the medullary compartments and these interactions modulate respiratory network activity and control of respiratory phase transition (Cohen, 1979; Okazaki et al., 2002; Cohen and Shaw, 2004; Ezure, 2004; Ezure and Tanaka, 2006; Dutschmann and Herbert, 2006; Alheid and McCrimmon, 2008).

Pontine connections are critical for coordinating the activity of expiratory muscles and upper airway musculature during expiration and expression and regulation of post inspiratory activity (Dutschmann and Herbert, 2006).

Of particular interest for the control of autonomic function are the locus coeruleus (LC), and the pontine respiratory group (PRG), constituted by the Kölliker-Fuse nucleus and the parabrachial complex, composed by the lateral parabrachial nucleus (LPN) and medial parabrachial nucleus (MPN). The LC is implicated in control of homeostatic functions (Svensson and Thoren, 1979; Bhaskaran and Freed, 1988), sleep (Aston-Jones and Bloom, 1981), circadian regulation of arousal and performance (Aston-Jones et al., 2001), control of breathing (Oyamada et al., 1998; Fabris et al., 1999; Biancardi et al., 2008), with central respiratory network activity (Coates et al., 1993; Biancardi et al., 2008) and chemosensitive signalling (Elam et al., 1981; Filosa et al., 2002). The LC is also involved in cardiovascular function (Sved and Felsten, 1987).

The caudal border of the pons can be located at the intersection of the caudal edge of the cerebellar peduncles and the dorsal surface of the brainstem. The nucleus of the VII nerve (facial nerve) marks the beginning of the medulla. Three nerve tracts are located in the medulla. The cortico-spinal tract is constituted by nerve fibres that carry motor signals from the cerebrum to the spinal cord, to stimulate skeletal muscles. Two more nerve groups, the gracile fasciculus and cuneate fasciculus carry sensory signals from the spinal cord to the brain. In addition, many of the medulla's sensory and motor functions are mediated through the last four cranial nerves, which begin or terminate here: cranial nerves IX (glossopharyngeal), X (vagus), XI (accessory), and XII (hypoglossal).

Historically, different parts of the medulla have been regionalized according to their role in regulating main body functions like motor control, cardiovascular and respiratory activity. Control of excitability of limb motor neurons used to be attributed to the vestibular nuclei (Kuypers, 1981); other nuclei that can be considered to be involved in motor control are the nucleus prepositus hypoglossi, known to be a neural integrator of horizontal eye movements and also involved in postural balance control (Seo et al., 2004); and the olive, which sends climbing fibres to the cerebellum, contributing to the cerebellar motor coordination and learning executed by the Purkinje cells (McKay et al., 2007).

The cardiovascular system has been thought to be mainly regulated through neurons located in the nucleus of the solitary tract (NTS) and parts of the medullary reticular formation, known as rostral ventro-lateral medulla (Loewy and Spyer, 1990). The heart has an internal pacemaker and goes on beating even if all nerves to it are detached. However the NTS and the RVLM are involved in the regulation of blood pressure[1] and vasomotor tone[2].The NTS is the site of afferent baro[3]- and

1 The force that the blood exerts against a vessel wall (Saladin, 2004).

2 Constant nervous stimulation of the muscles of the blood vessels needed to maintain a resting level of contraction (Saladin, 2004).

chemoreceptors[4] fibres (Mifflin, 1992; Mifflin, 1993; Paton et al., 2001; Andresen and Peters, 2008) and the RVLM is the so called "vasomotor centre" of the medulla (Lindgren, 1961), which exerts sympathetic control over blood vessels throughout the body, integrating three autonomic reflexes—baroreflexes[5], chemoreflexes[6], and the medullary ischemic reflex[7].

The circuitry responsible for generating and shaping the respiratory pattern, as well as transmitting this pattern to the motor neurons controlling the respiratory muscles was located in the ventro-lateral portion of the NTS and ventro-lateral reticular formation (Feldman, 1986). Specifically, in the ventral reticular formation, nuclei involved in the respiratory rhythm generation pattern (Richter and Spyer, 2001) and modulation are organized in the so called "ventral respiratory column". This continuous region starts in the pons with the PRG and continues in the brainstem with the retrotrapezoid nucleus/parafacial respiratory group, the Bötzinger complex and the Pre-Bötzinger complex (PBC) (Figure 1.11**)** (Bianchi et al., 1995; Richter and Spyer, 2001;

---

3 Stretch receptors detecting changes in blood pressure. When the BP rises, the baroreceptors' signalling rate rises. This input inhibits the sympathetic cardiac and vasomotor neurons, reduces sympathetic tone, and excites the vagal fibres to the heart, causing a reduction in the heart rate and cardiac output and in the blood pressure. Baroreflexes are important chiefly in short-term regulation of BP, for example in adapting to changes in posture (Saladin, 2004).

4 Receptors detecting changes in blood pH and concentrations of O2 and CO2. Located within small organs called aortic bodies and carotid bodies and in particular sites in the brainstem (Saladin, 2004).

5 Autonomic, negative feedback response to changes in blood pressure, detected by baroreceptors (Saladin, 2004)

6 Autonomic response to changes in blood pH and concentrations of O2 and CO2. The primary role of chemoreflexes is to adjust respiration to changes in blood chemistry, but they have a secondary role in stimulating vasomotion. Hypoxemia (O2 deficiency), hypercapnia (CO2 excess), and acidosis (low blood pH) stimulate the chemoreceptors and act through the vasomotor centre to cause widespread vasoconstriction. This increases overall BP, thus increasing the perfusion of the lungs and the rate of gas exchange (Saladin, 2004).

7 Autonomic response to a drop in perfusion of the brain. Within seconds, the cardiac and vasomotor centres of the medulla oblongata send sympathetic signals to the heart and blood vessels to induce an increase in heart rate and contraction force and widespread vasoconstriction. These actions raise the blood pressure and, ideally, restore normal perfusion of the brain (Saladin, 2004).

Feldman et al., 2003; Feldman and Del Negro, 2006; Smith et al., 2007; Spyer and Gourine, 2009). The exact mechanism by which interconnected brainstem respiratory neurons orchestrate the respiratory control is still under debate. Main questions are if the rhythm is generated from a discrete group of pacemaker neurons or results from integrated activity of diffuse networks of inspiratory and expiratory neurons that excite and inhibit each other (Nicholls and Paton, 2009). The PBC has been regarded as the kernel of rhythm generation (Smith et al., 1991).

A growing body of evidence suggests that functions controlled by the medulla are so connected that it is not possible to segregate autonomic and somatic regions. For example, the vestibular nuclei have projections to the nucleus of the solitary tract, the medullar reticular formation and the parabrachial nucleus in the pons (Balaban and Beryozkin, 1994; Yates et al., 1994; Yates et al., 1995; Balaban, 1996; Porter and Balaban, 1997; Stocker et al., 1997); they contribute to cardiovascular and respiratory regulation during movement and changes of posture (Yates et al., 2002; Yates et al., 2003); portion of medial and inferior vestibular nuclei have been shown to mediate autonomic responses and the afferent pathways from brainstem and spinal cord to these regions of the vestibular nuclei have been identified (Jian et al., 2005). Moreover, regions controlling cardiovascular and respiratory activity are juxtaposed and interwoven so that it is still an open question if the same neurons participate in both activities (Nicholls and Paton, 2009), considering also that neuromodulators within a particular region of the brainstem affect the cardiovascular system by acting concomitantly on breathing and vice versa (Coddou et al., 2009; Pilowsky et al., 2009).

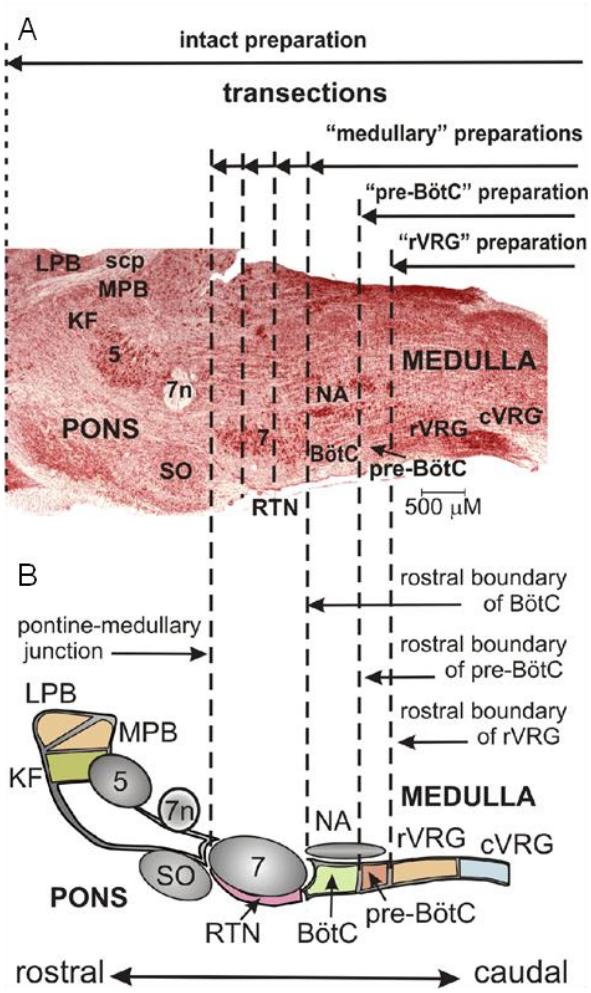

Figure 1.11 Respiratory regions in the brainstem

A. Parasagittal section of rat brainstem stained with in neutral red stain, at the level of NA, VRG, nucleus of the 7th nerve, and lateral pons. B. Schematic diagram of the spatial arrangement of respiratory-related structures in the brainstem. Vertical dashed lines indicate different levels, which delineate rostral extent of reduced preparations (solid horizontal lines with arrows) usually adopted in experimental approaches. "Medullary preparations", obtained after transections through various rostral-caudal levels of the facial nucleus or rostral boundary of Bötzinger; "pre- Bötzinger preparation", after transection at rostral boundary of pre- Bötzinger Complex; "rVRG preparation", after transection at rostral boundary of rVRG. List of abbreviation: 5, V or trigeminal nucleus; 7n, VII or facial nerve; cVRG, caudal VRG; KF, Kolliker-Fuse nucleus; LPB, lateral parabrachial nucleus; MPB, medial parabrachial nucleus; RTN, retrotrapezoid nucleus; scp, superior cerebellar peduncle; SO, superior olive. Figure from (Smith et al., 2007).

1.2.1.1 The brainstem in prion disease

Prion disease-related pathology in the brainstem has been reported for different experimental and naturally occurring prion diseases. In hamsters, orally infected with 263K prions, the first target areas of prion pathology are the dorsal motor nucleus of the vagus nerve and the NTS. In this model system, for the first time the spread of infection was reported to occur via the vagus nerve rather than along the spinal cord (Beekes et al., 1998). In a murine model of BSE, early vulnerability of the central serotonergic system, located in the brainstem, was supported by behavioural and anatomical-pathological observation (Vidal et al., 2009). Recently, in BSE affected cattle, PrP27-30 has been found both in the rostral brainstem, and in the obex, where the fourth ventricle narrows to became the central canal of the spinal cord. Therefore this study suggested that these areas could be useful specimens for a BSE surveillance program (Polak and Zmudzinski, 2011). Moreover, in BSE infected cattle, spongiform lesions and abnormal PrP accumulation was reported in the auditory brainstem nuclei and associated with clinical dysfunction of the auditory system. These findings could be used for ante-mortem BSE diagnosis. For human prion disease, sCJD associated neuropathological abnormalities in the brainstem were considered a late event in the disease progression(Masters and Richardson, 1978). However, more recently a study on 33 sCJD patients with clinical signs suggestive of brainstem involvement challenged this view (Iwasaki et al., 2005). The authors found brainstem atrophy in the pontine base was evident in patients with diseases of prolonged duration. Neuronal loss, prominent in the pons, and pyramidal tract degeneration affected some but not all the patients with prolonged disease. The motor nuclei of pons and medulla, the motor nucleus of the vagal nerve and the locus coeruleus were preserved from neuronal loss, but slight to mild gliosis was identified in some of the patients with prolonged disease. Although PrP deposition showed a granular and diffuse pattern, it was not associated with disease duration or neuronal degeneration until late stage and was mainly localized in the pontine nucleus, the inferior olivary nucleus, substantia nigra and quadrigeminal body, whereas many patients showed mild deposition in the motor nuclei of the brainstem and the locus coeruleus. The authors concluded that PrP deposition occurred as an early

event in sCJD, however, as signs suggestive of brainstem impairment may result from pathologic involvement of basal ganglia and cerebral cortex, this study failed to evaluate the relationship between clinical signs and pathology in the brainstem (Iwasaki et al., 2005).

1.3 Thesis hypotheses

We hypothesised that prion disease onset and progression is due to prion pathology and neurodegeneration in specific nuclei in the brainstem, fundamental for survival. The brainstem is responsible for the control of autonomic functions, and autonomic failure is observed both in humans and in animal models of prion disease. We set out to characterise the identity of these brainstem nuclei, and therefore identify the 'clinical target areas of prion disease'.

Previous studies have shown that PrP conditional knock-out mice survived long term to RML inoculation and were protected against neuronal loss and behavioural changes. We first hypothesized that upon other prion inoculations (Me7 and Mouse-adapted BSE) NFH-Cre/M*lox*P mice would survive long term compared to non-depleted M*lox*P mice (chapter 3), and that this effect would be due to Cre-mediated depletion of PrP in specific vital brainstem nuclei.

However, Cre-mediated depletion in Me7 and Mouse-adapted BSE inoculated NFH-Cre/M*lox*P mice did not produce a long term survival comparable to previous published data in RML inoculated NFH-Cre/M*lox*P mice, and we revised our hypothesis. Specifically, we considered that the different outcome may be due to different tropism of different prion strains, and that neuronal PrP depletion does not protect one or more areas responsible for disease onset and progression in Me7 and Mouse-adapted BSE inoculation to the same extent as in RML inoculation.

We envisaged two different scenario: we hypothesised that clinical target areas may be the last regions accumulating abnormal prion protein and neurodegenerative changes (chapter 4), or the first regions affected by prion accumulation, effectively being rate-limiting in the disease progression (chapter 5). In chapter 4 we challenged the 'last target areas hypothesis', by comparing the pathology in the late stage RML and Me7 inoculated M*lox*P and NFH-Cre/M*lox*P mice; in chapter 5 we investigated the 'first

target areas hypothesis' by comparing prion pathology in RML and Me7 inoculated M*lox*P and NFH-Cre/M*lox*P mice at early asymptomatic stage of prion infection.

In our experiments NFH-Cre/M*lox*P mice did not survive RML inoculation as previously published (cf. chapter 5 and Mallucci et al. 2002). This discrepancy led us to hypothesise that the pattern of Cre expression in the NFH-Cre expressing line had changed over time and that recombination in the double transgenic line did not occur in the proposed clinical target areas with sufficient efficacy to stop the disease progression. These hypotheses are investigated in chapter 6.

Finally, chapter 7 describes the production of lentivirus encoding shRNA against PrP, exploring the hypothesis that an extrinsic tool for focal knock-down of PrP in select brain areas could protect against prion-mediated neurodegeneration.

1.4 Aims of the thesis

Identification of clinical target areas of prion disease in mouse models:

- To characterize the pathology progression in brains of M*lox*P and NFH-Cre/M*lox*P mice infected with Me7 and Mouse-adapted BSE prion strains.
- To characterize and compare the end-stage lesion profile in the brainstem of RML and Me7 infected M*lox*P and NFH-Cre/M*lox*P mice.
- To characterize and compare the first areas of prion pathology in the brainstem of RML and Me7 infected M*lox*P and NFH-Cre/M*lox*P mice.

Characterisation of the NFH-Cre/M*lox*P mouse model:

- To characterize Cre-mediated recombination in NFH-Cre/Ml*ox*P mouse model and its effect on the incubation time upon prion infection.

Therapeutic approach to prion disease:

- To reproduce lentivirus encoding shRNA against PrP to be used as an extrinsic tool for focal knock-down of PrP in selected brain areas

1.5 Outline of the thesis

- In **chapter 3** we describe experiments that were designed to characterise prion pathology in brains of M*lox*P and NFH-Cre/M*lox*P mice infected with Me7 and Mouse-adapted BSE prion strains. We compare these newly acquired data with existing data, published by Mallucci et al (Mallucci et al., 2003). At this stage only Me7 and mouse-adapted BSE inoculations were carried out. An unexpected outcome prompted us to review, and ultimately repeat the RML inoculations of M*lox*P and NFH-Cre/M*lox*P mice (chapter 4). We formulate two hypotheses on clinical target areas of prion disease, the "first target areas" hypothesis and the "last target areas" hypothesis.

- In **chapter 4**, we analyse the survival of RML, Me7 and MRC2 (slightly modified mouse-adapted BSE strain) inoculated M*lox*P and NFH-Cre/M*lox*P mice and describe a detailed histopathological characterisation of the end stage prion pathology in the brainstem of RML and Me7 inoculated M*lox*P and NFH-Cre/M*lox*P mice. These experiments highlighted a discrepancy to the original data of Mallucci, in that RML inoculated NFH-Cre/M*lox*P mice no longer survived >52 weeks but succumbed to disease after 35 weeks. This discrepancy prevented us from testing a specific aspect of the anatomical target areas hypothesis (late target areas scenario) as RML, Me7, and MRC2 inoculation all succumbed to prion disease and RML and Me7 inoculated mice had extensive prion deposition in the brain stem.

- In **chapter 5**, we then addressed a second scenario of the target area hypothesis by examining early stage pathology in the brainstem. Here we describe that RML and Me7 show identical target areas at early stage. In addition, a detailed account of the pathology of the disease progression in these target areas is provided. We find that the target areas show severe pathology at end stage and therefore support the scenario of "clinical target area" being the first target of prion pathology.

- In **chapter 6** we set out to understand the discrepancy between the original data (i.e. long survival of RML inoculated NFH-Cre/M*lox*P mice, as

described in the introduction and chapter 3) and the current results, (i.e. short survival of these mice). We analysed the time course of Cre-mediated recombination in the brain both NFH-Cre/M*lox*P mice using both NFH-Cre/M*lox*P mice and a reporter strain and discovered that the recombination pattern has changed over time and this explains the different results.

- **Chapter 7** describes a different, complementary approach to PrP depletion, using a lentivirus to express shRNA.

2 Materials and methods

2.1 Mice

All animal work, including prion inoculation and mice culling, conformed to the United Kingdom regulations and institutional guidelines and was performed under Home Office project license (70/6454).

M*lox*P and NFH-Cre/M*lox*P transgenic mice were generated as described in (Mallucci et al., 2002) on a *Prnp*$^{0/0}$ background so that all PrP expression is from the PrP (M*lox*P) transgene. The genetic background is predominantly FVB after ten generations of backcrossing. All animals were hemizygous for one or both transgenes (M*lox*P alone or also with NFH-Cre).

ROSA26 mice supplied as homozygous were crossed to homozygous NFH-Cre mice, so to obtain mice hemizygous for both transgenes (LacZ and NFH-Cre).

Mice were housed in a temperature- and light-controlled room with 12 hrs. light/dark cycles in groups of four to six mice. All mice had unlimited access to food and water.

2.1.1 Genotyping

Mice were assessed for the presence of transgenes by ear biopsies which were used for DNA extraction and subsequent analysis by polymerase chain reaction (PCR).

2.1.2 Prion inoculation

Prion inoculation of mice was performed by designated staff, according to established local protocols. One week old mice were anaesthetised with isofluorane in an inhalation chamber until pinch reflexes were absent. They were then inoculated with 20µl of 1% brain homogenate of either Me7 (I6302), Mouse-adapted BSE (I873), RML (I8700), Me7 (I9458), MRC2 (I9467) (in PBS) using a 1ml insulin syringe and a 26-gauge hypodermic needle inserted 3-4 mm into the right parietal lobe. Mice were allowed to recover in a cage placed on a heated pad prior to being replaced in their home cage.

2.1.2.1 Prion inoculum preparation and titration

Prion inocula were prepared by Dr Jonathan Wadsworth.

Me7 (I6302), Mouse-adapted BSE (I873), RML (I8700), Me7 (I9458), MRC2 (I9467) prion inocula were prepared as a 10% (w/v) brain homogenate in Dulbecco's phosphate buffered saline lacking Ca2+ or Mg2+ ions (D-PBS). RML (I8700), Me7 (I9458) and MRC2 (I9467) were titred by bioassay in Tg20 mice; RML titration was performed by Dr Malin Sandberg. To obtain the titre of stock 10% Me7 (I9458) and stock 10% MRC2 (I9467), new 2ml aliquot of I9458 or I9467 10% PBS stock brain homogenate were thawed and passed through an orange (25G) syringe and needle. For each titration, the 10% homogenate was serially diluted 10-1, 10-2, 10-3, 10-4, 10-5, 10-6, 10-7, and 10-8. The first 10 fold dilution used sterile Dulbecco's PBS lacking Ca2+ and Mg2+ ions (D-PBS) as diluent (0.5ml of 10% homogenate I9458 or I9467 plus 4.5ml D-PBS). Subsequent dilutions were made using 1% normal CD1 brain in D-PBS as diluent. The dilution series was generated by serial transfer of 100µl into 900µl 1% CD1 brain homogenate. 1% normal CD1 brain homogenate was prepared from a stock of 10% normal CD1 brain homogenate diluted in D-PBS and passaged through an orange (25G) syringe and needle (2 ml 10% normal CD1 brain homogenate plus 18ml D-PBS). Each dilution was passed through an orange (25G) syringe needle at each step and frozen as a single aliquot at -80 ºC.

For each dilution, 6 Tg20 mice (~ 6 weeks old) were intracerebrally inoculated with 30µl of inoculum.

Prion titres were calculated using the Reed–Meunch formula:

LD50 = log10 dilution above 50% - (I x log h)

where

LD50 = median lethal dose, to kill half of the experimental population

I = (% scrapie-sick in the group above 50% - 50%) / (% scrapie-sick in the group above 50%) - (% scrapie-sick in the group below 50%)

h = the dilution factor (in this case 10)

I8700 titre= 8.2 Log LD50 /g brain;

I9458 titre= 9 Log LD50 / g brain;

I9467=8 Log LD50/ g brain.

2.1.3 Diagnosis of scrapie symptoms

Mice were examined daily for appearance of scrapie symptoms or other illness.

Early indicators of prion disease include erect ears, rigid tail, piloerection, and ungroomed appearance, slight hunched posture, and clasping of hind limbs when lifted; confirmatory signs include ataxia, generalized tremor, impaired breathing activity, loss of righting reflex, or limb paralysis. Animals were culled as soon as clinical prion disease was confirmed or if they showed signs of distress or loss of up to 20% of body weight. All symptoms were recorded on videotape prior to culling of the animal.

2.1.4 Removal of brains and embryos

Terminally scrapie-sick animals or animals sick for other reasons were culled and the brains removed according to local safety regulations in a class I cabinet within the secure pathogen-free mouse facility. Brains to be analysed histologically were fixed either in formalin buffer or 4% PFA; brains to be used for PCR and qPCR were snap frozen and different brain areas dissected for DNA extraction. Embryos were dissected by designated staff, and processed for histology or molecular analysis (PCR, qPCR).

2.2 Immunohistochemistry

2.2.1 β-galactosidase staining assay

Brains were fixed in formalin (Pioneer Research) for 30min at room temperature (RT), cut sagittally and then incubated for a further 30min in formalin. The brains were then permeabilised, by shaking for 2hrs in permeabilisation buffer, consisting of β-gal staining solution (10mM Phosphate buffer, pH= 7-7.2, [Fisher Chemicals], 150mM NaCl [Fisher Chemicals], 1mM MgCl2 [Sigma], 3.3mM K4Fe(CN)63H2O [Sigma], 3.3mM K3Fe(CN)6 [Sigma]), 1% MgCl2 [Sigma], 0.02% Igepal (Fluka BioChemika) and 0.0 1% Sodium Deoxycholate (Sigma). The brains were then incubated overnight at 37°C with shaking in ‘permeabilisation’ buffer and 1% X-Gal (Merck) (dissolved in N,N-dimethylformamide [Sigma]). X-Gal is cleaved by β-galactosidase expressed by the LacZ gene yielding galactose and 5-bromo-4-chloro-3-hydroxyindole. This compound is then oxidized into 5,5'-dibromo-4,4'-dichloro-indigo, an insoluble blue

product. The brains were photographed using a Nikon Coolpix 995 camera mounted on a Zeiss Stemi SV11 microscope to record the pattern of β-galactosidase staining.

2.2.2 Preparation of paraffin blocks

Brains from time-culled and terminally ill mice were fixed in 10% buffered formal saline (BFS). Brains were cut in three pieces, corresponding to frontal, medial, and caudal brain and every piece was separately processed and embedded in paraffin wax by the MRC Prion Unit histology support team. Serial coronal sections from the most caudal block, corresponding to the brainstem, were cut at a nominal thickness of 3µm, placed on to Super-frost slides and allowed to dry at 37°C for a minimum of 2 hours, before they were transferred to a 60°C oven for another 2 hours.

2.2.3 Pre-treatment prior to immunostaining: Re-hydration and de-hydration of wax embedded sections

Wax embedded sections were re-hydrated prior to staining and then de-hydrated after staining. For the re-hydration process, wax was removed by sequential transfer of the sections into 3 separate xylene solutions. They were placed in the first xylene solution for 5 minutes and then the other two for 2 minutes each. The sections were then transferred to 100% ethanol for 2 minutes followed by 2 minutes in 100%, 90% and 70% ethanol respectively. The samples were then rinsed with tap water. For de-hydration of stained sections before mounting onto slides, the opposite procedure was carried out: the sections were incubated for 2 minutes in each of a series of increasing ethanol concentrations (70%, 90%, 100%, 100%) and then placed into xylene solution for a further 2 minutes.

2.2.4 Immunostaining of paraffin-embedded sections

Sections from prion infected mice were stained with haematoxylin and eosin and immunostained with ICSM35 and anti-GFAP antibody to assess spongiosis, abnormal PrP accumulation, and gliosis respectively.

Selected sections were also stained with anti-NK1 receptor and anti-tyrosine hydroxylase antibody to identify the pre-Bötzinger complex and the locus coeruleus.

To confirm Cre-mediated recombination in NFH-Cre/ROSA 26 mice, selected sections were stained with anti-β galactosidase antibody.

Immunostaining was carried out on a on a Ventana automated immunohistochemical staining machine using a basic diaminobenzidine detection system according to the manufacturer's instructions (Ventana Medical Systems, Tucson, AZ). Stained sections were dehydrated and mounted with Pertex, a xylene-based mounting medium.

2.2.4.1 Haematoxylin and Eosin staining

To assess spongiosis, sections were stained with haematoxylin and eosin. Re-hydrated sections were immersed in haematoxylin for 5 minutes and then rinsed with tap water. They were then placed into a solution of 1% acid alcohol (1% concentrated HCl in 100% ethanol) for 20 seconds to differentiate nuclear size and rinsed again with cold running water. They were then immersed in eosin (0.5% aqueous solution) for 20 seconds and washed with cold running water. The sections were de-hydrated and mounted with Pertex.

2.2.4.2 Immunostaining with the PrP-specific antibody ICSM35

To assess abnormal PrP accumulation, re-hydrated brain sections were pre-treated in 1xTris-EDTA buffer at high pressure for 5 minutes followed by 5 minutes at low pressure. To facilitate detection of PrPSc, the sections were immersed in 98% formic acid for 5 minutes. On the Ventana automated immunohistochemical staining machine, sections were incubated for 16 minutes with a low concentration of protease (iView/Ventana Medical Systems), incubated in Superblock for 10 min, then exposed to ICSM35 (1μg/mL; D-Gen) for 32 minutes at a concentration of 1:3000, followed by biotinylated anti-mouse IgG secondary antibody (SA-HRP; iView); colour was developed with 3,3'- diaminobenzidine tetrahydrochloride (iView). The sections were dehydrated and mounted with Pertex.

2.2.4.3 Immunostaining for the astroglial marker GFAP

To assess gliosis, re-hydrated brain sections were pre-treated by heating in the microwave for 25 minutes in 1xTris-EDTA solution and then rinsed with tap water before automated immunostaining. Sections were incubated in the primary rabbit anti-GFAP antibody (Dako/Z0334) for 32 minutes at a concentration of 1:1,000, followed by biotinylated anti mouse IgG secondary antibody (SA-HRP; iView); colour was developed with 3,3- diaminobenzidine tetrahydrochloride (iView). The sections were dehydrated and mounted with Pertex.

2.2.4.4 Immunostaining for NK1 -receptor

To confirm the identity of the pre-Bötzinger complex, re-hydrated sections were heat pre-treated in cell conditioning buffer (SCC, 95°C for 24 minutes) on the Ventana machine and immunostained with Rabbit polyclonal anti -NK1 receptor, (Pierce PA1-32229) for 2 hours at a concentration of 1:200. Specific swine anti-rabbit secondary antibody (Dako/E0353) was used at a concentration of 1:200, and colour developed with 3, 3'- diaminobenzidine tetrahydrochloride (iView). The sections were dehydrated and mounted with Pertex.

2.2.4.5 Immunostaining for β- galactosidase

To investigate the efficacy of Cre-mediated recombination, sections from NFH/Cre-ROSA26 mice were assessed for β-galactosidase expression. Re-hydrated sections were pre-treated as for GFAP staining but immunostained with anti-β galactosidase antibody (Millipore AB1211-5MG) for 2 hours at concentration of 1:100. Specific swine anti- rabbit secondary antibody (Dako/E0353) was used at concentration of 1:200, and colour developed with 3, 3'- diaminobenzidine tetrahydrochloride (iView). The sections were dehydrated and mounted with Pertex.

2.2.4.6 Immunostaining for tyrosine hydroxylase

To assess the level of expression of tyrosine hydroxylase in the locus coeruleus of MloxP and NFH/Cre-MloxP mice, re-hydrated sections were pre-treated as for GFAP staining and immunostained with anti- tyrosine hydroxylase antibody (Abcam, ab111)

for 32 minutes at 42°C, at concentration 1:2000, followed by biotinylated anti-mouse IgG secondary antibody (SA-HRP; iView), and colour developed with 3,3-diaminobenzidine tetrahydrochloride (iView). The sections were dehydrated and mounted with Pertex.

2.2.5 Neuropathological analysis

Sections of brains from time-culled and end stage clinically sick mice were examined blind. Identification of brainstem nuclei was carried out by using comparable tables of the Paxinos and Franklyn mouse atlas (Paxinos and Franklin, 2004), based on stereotaxic coordinates.

Spongiosis, abnormal PrP deposition and gliosis were evaluated semi-quantitatively, on a scale from 0 to 3. Pictures were taken with a ColorView II digital camera (www.soft-imaging.de) mounted on a ZEISS Axioplan microscope and composed with Adobe Photoshop.

2.3 Techniques involving nucleic acids

2.3.1 Extraction of DNA from tails, ear biopsies, brain samples, and embryos.

Tails and ears biopsies were provided by the Animal Facility. Brain samples and embryos were dissected as in paragraph 2.1.4. Samples were transfer to new Eppendorf tubes and submerged in 0.5ml of lysis buffer (50 mM Tris-HCl pH=8 [Sigma]; 100 mM EDTA pH=8 (Fluka BioChemika); 100mM NaCl (Fisher Chemicals), 1% SDS (BioChemika) containing 20µl of Proteinase K (Roche) at 20mg/ml of Proteinase K (Roche) and digested for at least 2 hours or overnight at 55°C, shaking at 500 rpm. After digestion, 160µl of Protein Precipitate Solution (Promega) was added to each sample. Samples were vortexed to ensure complete mixing, incubated on ice for 5 minutes, to allow separation of phases, and spun at 13000 rpm for 5 minutes. The supernatant was then transferred to fresh Eppendorf tubes and 490 µl of Isopropanol (Fisher Chemicals) was added to precipitate DNA. The samples were centrifuged for 5 min at ≥13000 rpm and the supernatant discarded. The pellet was washed in 200µl of 70% Ethanol (Fisher Chemicals) and the samples spun down at 13000 rpm for 5 minutes. The supernatant

was discarded and the DNA pellets air-dried for 10 minutes. The DNA was resuspended in 50-200 µl of TE buffer, (10mM TrisHCl: 1mM EDTA), pH=7.5.

2.3.2 Polymerase chain reaction

PCR reactions were performed in a 25µl reaction volume in autoclaved microfuge tubes. All PCR primers were obtained from MWG Biotech and dissolved in sterile water to a concentration of 100pmol/µl. 2x MangoMix (Bioline, BIO-25044) ready to use pre-optimized reaction mix, containing MangoTaq™ DNA Polymerase, dNTPs, red and orange, reference dyes and Mg2+ (final concentration 2.5mM) was used, according to the manufacturer specifications. 1µl of DNA sample was dissolved in 24µl of mastermix. All PCRs had a common initial heating phase of 94°C for 5 minutes and a final elongation step of 72°C for 10 minutes. The PCR products were stored at 4°C or at -20°C for longer periods of time.

LoxP PCR (M*lox*P and NFH/Cre-M*lox*P mice genotyping)

Primers:	Lox forward (B):	5'-TTG GTT AGG GTA GCG GTA CAT-3'	
	Lox reverse (D):	5'-ATC AGT CAT CAT GGC GAA CCT-3'	
	band size =	490bp	
	RBforward:	5'-AAT AGA GGC ACT CCC TTC AC-3'	
	RBreverse:	5'-GGT AAG CCC TTG ACC TAA AA-3'	
	Expected band size=	340bp	
Master Mix:	Mango Mix x2 =	12.5µl	
	Primers* =	1µl	* (B+D: Rbf+Rbr= 5:7)
	H_2O =	10.5µl	
	DNA=	1µl	
Cycle conditions			
	Denaturing	94°C 45''	
	Annealing	57°C 60''	
	Extension	72°C 1'30''	
	33 cycles		

Cre PCR (genotyping of NFH-Cre mice)

Primers:	454:	5'-TCG ACC ATG CCC AAG AAG AAG-3'

455: 5'-ACG TTT TCT TTT TCG GAT CCG CCG CAT-3'

Expected band size = 450 bp

98: 5'-GAT CTA TGT GAG TGC GAG GCT AGC-3'

99: 5'-TCA AAC CAG ATG GCA CTG AAG ACT-3'

Expected band size = 100bp

Mix: Mango Mix x2 = 12.5µl

Primers* (5:3) = 1µl * (454+455:98+99=5:3)

H_2O = 10.5µl

DNA = 1µl

Cycle conditions

Denaturing 94°C 45''

Annealing 57.8°C 50''

Extension 72°C 1'30''

29 cycles

CosTet PCR (recombination within the MoPrP transgene in NFH-Cre/M*lox*P mice)

Primers: CosSHa F: 5'- GCT GTC AAG GAA TAG GCC TG-3'

CosSHa R: 5'- AGA GCT ACG GTG GAT AAC C-3'

Expected band sizes= 1150 or 300bp, depending on occurrence of recombination

Mix: Mango Mix x2 = 12.5µl

Primers = 1 µl

H_2O = 10.5 µl

DNA= 1 µl (100ng)

Cycle conditions

Denaturing 94°C 45''

Annealing 62°C 1'

Extension 72°C 1'

2.3.3 Real time polymerase chain reaction (qPCR)

Real-time PCR was carried out on a 7500 Fast Real-time PCR System (Applied Biosystems) in a total volume of 25µl, using 100ng of genomic DNA template and 2x TaqMan gene expression master mix (ABI, 4369016). Primers and probe were designed using the Primer Express 3.0 Sequence software. Primers were supplied by MWG Biotech, dissolved in sterile water at a concentration of 100pmol/µl; the 6-FAM TaqMan MGB probe supplied by Applied Biosystems dissolved in sterile water was aliquoted to avoid repeated freeze and thawing. Taqman Rodent GAPDH control reagent (Tamra-Vic probe, 4008313, ABI) was used within the reaction as an endogenous control according to the manufacturer's instructions. Standard curves were derived for both probes and used to calculate the quantity of gene-specific DNA in the reaction. Reactions were carried out in 96 well-plates in quintuplicate. Controls without DNA were included in every plate.

Primers:	qMloxP 5':	5'-TCA TTT TGC AGA TGA GTC GA GAT-3'
	qMloxP 3':	5'-CAC AAG AAC GAG GAA GTA CAA GCA-3'
Probe:	qMloxP:	5'-TAC ATT ATA CGA AGT TAT CTC GAC-3'

Mix:	Gene Expression Mix x2 =	12.5µl
	Primers mix (10µM each) =	1µl
	Probe (10µM) =	1µl
	GADPH =	0.75µl
	H_2O =	0.25µl
	DNA (10ng) =	10µl

Cycle conditions

	Segment 1	50°C 2'
	Segment 2	95°C 10'
	Segment 3 (40 replicates)	95°C 15''
		60°C 1'

2.3.4 Plasmid DNA minipreps

Qiagen miniprep kits were used to perform preparation of up to 20µg of high purity plasmid DNA, according to the manufacturer's protocol (Qiagen QIAprep

Miniprep Handbook, 2004). Briefly, 1 - 5ml of overnight LB culture containing selective antibiotic was centrifuged for 15 minutes at 4°C at 6000g. The supernatant was discarded and the bacterial pellet resuspended completely in 250µl buffer P1. The cells were lysed by addition of 250µl buffer P2 at room temperature for 5 minutes. 350µl chilled buffer P3 was added to precipitate DNA. The tubes were mixed immediately for 10 times to avoid localised precipitation. The lysate was centrifuged at 13,000rpm for 10 minutes, and the supernatant applied to a QIAprep spin column. To bind the plasmid DNA, the column was centrifuged at 13,000rpm for 1 minute and the flow-through discarded. Trace nuclease activity was removed by washing the column with 500µl Buffer PB and centrifugation as before for 1 minute. 750µl Buffer PE containing ethanol was added and the column centrifuged for 1 minute to remove remaining impurities. The flow-through was discarded and the column re-centrifuged at 13,000rpm for 1 minute to remove residual ethanol. The column was placed into a clean 1.5ml tube and 30 - 50µl of Buffer EB was added to the centre of the membrane. The column was incubated at room temperature for 1 minute before centrifuging at 13,000rpm for a final minute to elute the purified plasmid DNA.

2.3.5 Maxipreps of plasmid DNA

Qiagen maxiprep kits were used to prepare up to 1 mg of high purity plasmid DNA, under the manufacturer's instruction (Qiagen HiSpeed Plasmid Purification Handbook, 2001). The purification protocol is based on a modified alkaline lysis method followed by binding of plasmid DNA to an anion-exchange resin under suitable low salt and pH conditions. 250ml of saturated LB culture was centrifuged for 15 minutes at 4°C at 6000g to obtain the bacterial pellet. Following removal of the supernatant, the pellet was resuspended in 10ml buffer P1 containing 100µg/ml of RNAse A. 10ml buffer P2, containing NaOH-SDS, was added to lyse the cells. The tubes were thoroughly mixed and incubated at room temperature for 5 minutes. The SDS disrupts cell membranes releasing DNA and proteins which are then denatured by the NaOH. 10ml chilled neutralisation buffer P3 containing potassium acetate was added. The lysates were inverted 10 times and immediately poured into the barrel of a QIAfilter cartridge. Incubation at room temperature for 10 minutes allowed the precipitated material to form

a layer on top of the solution, preventing clogging of the filter. During this time, 10ml equilibration buffer QBT was added to a HiSpeed Maxi Tip and allowed to drain through the column by gravity flow. The cap was removed from the QIAfilter outlet and the plunger inserted to filter the lysate into the equilibrated Maxi Tip. The cleared lysate entered the anion-exchange resin by gravity and plasmid DNA was bound to the resin. 60 ml of buffer QC was used to remove contaminants. 15 ml of high salt elution buffer EB was then added to elute the DNA off the resin. To precipitate the DNA, 0.7 volumes of isopropanol was added to the eluted DNA and incubated for 5 minutes at room temperature. The eluate/isopropanol mixture was transferred into a 30ml syringe attached to a QIAprecipitator Maxi Module. Insertion of the plunger into the syringe forced the mixture through the QIAprecipitator which traps the precipitated DNA. 2ml of 70% ethanol was added to the syringe and forced through the QIAprecipitator to wash the DNA. Finally, a new 5ml syringe was attached to the QIAprecipitator and the purified plasmid DNA was eluted by the addition of 1ml TE.

2.3.6 Spectroscopic measurement of DNA

Nucleic acid concentrations were determined by spectroscopic analysis on a NanoDrop ND-1000 Spectrophotometer (NanoDrop Technologies). The pedestal was cleaned with dH2O before measurement of a 1µl blank. 1.5µl samples of unknown DNA concentration were then measured and the 260/280 absorbance determined for assessment of nucleic acid purity. Samples with a ratio of ~1.8 were considered sufficiently pure.

2.3.7 Restriction enzyme digestion

DNA digestion by specific restriction enzymes (endonucleases) was performed using 1-5 units of enzyme per µg of plasmid DNA at 37°C for a minimum of 1 hour. Restriction enzymes (New England Biolabs) were used with appropriate 10x NEB buffers giving optimal salt and pH conditions for the reaction. The volume of enzyme used was less than 1/10th of the total reaction volume to prevent inhibition of the enzyme by high glycerol concentration.

2.3.8 Ligation of DNA

USB T4 DNA ligase was used for all ligation reactions of DNA fragments. Ligation reactions were set up using a wide range of molar ratios of insert DNA: vector DNA from 0.5:1 to 100:1.

Routine controls were performed to check the efficiency of ligation by re-ligating the cut vector alone, and to check complete digestion of the vector by omitting T4 DNA ligase.

Vector DNA, insert DNA and ddH2O to a total volume of 15 μl were added to a microfuge tube. The mixture was placed on ice and 1 μl (1-3U/μl) T4 DNA ligase and 1.5 μl 10x ligase buffer (10mM MgCl2, 1mM ATP, 50mM Tris-HCl pH 7.5, 10mM DTT, and 25μg /ml BSA) were added. Ligation was performed at room temperature for 30 minutes or overnight at 16°C.

2.3.9 Transformation of DNA into E.coli

100μl competent cells were thawed on wet ice and mixed with 1 - 10μl ligation mix in a chilled 1.5ml microfuge tube. The mixture was incubated on ice for 30 minutes. The cells were heat-shocked by incubation in a 42°C waterbath for 90 seconds, then transferred back to ice for a further 2minutes. 900μl LB medium was added and the suspension was incubated at 37°C, with shaking at 225rpm for 1 hour to allow the cells to recover. The cells were pelleted by centrifugation at 4,000rpm for 5 minutes and resuspended in 100μl LB medium before spreading onto LB Agar plates with the appropriate antibiotic selection.

To select transformants, the cells plated on LB Agar medium were incubated overnight at 37°C. Colonies evident the following day were picked with a pipette tip and incubated overnight in 5ml of LB containing the appropriate selective antibiotic at 37°C, 225rpm. Cultures were used fresh or stored at 4°C for several days before use in small or large-scale DNA preparation.

2.3.10 Agarose gel electrophoresis

DNA fragments were separated according to size by electrophoresis through agarose gels.

A 1% agarose mini-gel was made by heating 1.5g of electrophoresis-grade agarose (Invitrogen) in 150ml of 1x TAE buffer in a microwave oven until it dissolved. The gel was cooled to approximately 50°C and ethidium bromide solution (10mg/ml) was added to a final concentration 0.02% v/v. The molten gel was then poured into a gel tray fitted with the appropriate comb(s) (Hybaid). Gel sizes varied (mini, midi and maxi) according to number of samples to be loaded and the fragment separation required. DNA samples were mixed with 1/10th volume of 10x loading buffer (containing Bromophenol Blue as a tracking dye). The samples were loaded into individual wells of the gel. A molecular weight marker was also loaded on each gel to allow determination of DNA fragment sizes by comparison. Electrophoresis was performed in appropriate tanks (Hybaid) containing 1x TAE buffer at 2.5-5V/cm until the fragments were adequately separated.

DNA was visualised by examining the gel on a BioRad Gel Doc 1000 imaging system under UV light. Gels were photographed and analysed using Quantity One software (version 4.5.1, BioRad).

2.3.11 Extraction of DNA from agarose gel

DNA was electrophoresed on an agarose gel as described above. The gel was placed on a 302nm UV transilluminator (UV products Ltd) and the desired band of DNA excised using a clean scalpel blade. All DNA extractions from agarose were performed using the QIAquick Gel Extraction Kit (QIAGEN) according to manufacturer's instructions. This kit solubilises the agarose and passes it through a mini column containing a silica membrane. The DNA binds to the membrane in a salt and pH-dependent manner and any contaminants pass through. The DNA can then be washed with ethanol-containing buffer to remove the salt and eluted using a higher pH buffer. The gel slice was weighed in a 1.5ml tube and 3 volumes of Solubilisation and Binding Buffer QG was added. If the slice weighed over 400mg, it was split into 2 equal parts and extracted separately to avoid overloading a single column. The agarose was

solubilised by heating it in Buffer QG at 50°C for 10 minutes and vortexing every 2 - 3 minutes. 1 gel volume of isopropanol was added to the sample and mixed by vortexing briefly. The sample was then loaded onto a QIAquick column in a 2ml collection tube and centrifuged for 1 minute at 13,000 rpm to bind the DNA to the membrane. To remove any traces of agarose, 0.5 ml of Buffer QG was applied to the column; it was re-centrifuged for 1 minute at 13,000rpm. The DNA was washed and any salts removed by adding 0.75ml of the ethanol-containing Buffer PE before centrifuging at 13,000rpm for 1 minute. The flow-through was discarded and the column centrifuged again at 13,000 rpm for 1 minute to remove residual ethanol which may interfere with downstream applications. To elute the DNA, the column was placed in a fresh 1.5ml tube and 50µl of Buffer EB was added. The column was incubated at room temperature for 1 minute to allow the increased pH to elute the DNA off the silica membrane. The purified DNA was collected by centrifugation at 13,000 rpm for 1 minute.

2.3.12 DNA Sequencing

Purified DNA was resuspended in TE buffer pH 7.5 at 50ng/µl and sequenced using an ABI 377 automated sequencer with sequencing primers at 2pmol/µl. All DNA sequencing was performed by G. Adamson.

2.4 Cell culture

All media and solutions were bought pre-sterilised, and sterile plastic ware was used. All procedures, including preparation of media, were performed in a laminar flow tissue culture hood. Water-baths and incubators were cleaned and sterilised regularly. All solutions and media were pre-warmed to 37°C prior to use.

2.4.1 Propagation of N2A cells

N2A cells were maintained in OptiMEM (Invitrogen) containing HEPES buffer, 2400mg/l sodium bicarbonate, hypoxanthine, thymidine, sodium pyruvate, L-glutamine, trace elements, growth factors, and phenol red reduced to 1.1 mg/l, supplemented with 10% v/v foetal calf serum (FCS) (Invitrogen), and 50U/ml each of penicillin and streptomycin (Sigma), in vented plastic flasks (NUNC, Fisher Scientific) in a humidified

incubator, in an atmosphere of 5-7% CO2 at 37°C. The medium was changed every 3 days, and cells were seeded 1:3-1:8 every 5-7 days or when they had reached 85% confluence. To seed the N2A cells, all medium was aspirated from the flask or dish, fresh growth medium was added and the cells were gently pipetted up and down until a homogenous suspension was attained and then diluted as necessary in fresh medium and transferred to a new flask.

When an accurate number of cells had to be seeded they were lifted as usual, a 500µl aliquot was stained with trypan blue and cells counted using a haemocytometer (Hausser Scientific Company) on a phase microscope, prior to seeding into fresh flasks with an appropriate volume of medium.

2.4.2 Propagation of HEK293 cells

Cells were propagated in growth medium consisting of Dulbecco's Modified Eagle Medium (DMEM) High Glucose containing 4500 mg/l D-glucose and 4mM L-glutamine (Gibco BRL), supplemented with 10% v/v foetal calf serum (FCS)(Invitrogen), 50U/ml each of penicillin and streptomycin (Sigma) and 50 mg/ml Geneticin® (Gibco BRL) to maintain expression of the large T antigen. They were maintained in vented tissue culture flasks (NUNC, Fisher Scientific) in a humidified incubator, in an atmosphere of 5-7% CO_2 at 37°C. The medium was changed every 3 days, and cells were seeded 1:10 2 times a week or when they had reached 85% confluence. To seed the cells, old medium was aspirated off, the cells were rinsed with sterile PBS and trypsin-EDTA 1x solution (0.05% trypsin, 0.5mM EDTA) (Gibco BRL) was added sufficient to cover the cell monolayer. The flask was placed at 37°C for 2-5 minutes until the cells detached, and an excess volume of growth medium was added, inhibiting further activity of the trypsin. The cell suspension was aspirated, and placed in a polypropylene tube (Falcon) and centrifuged at 1500g for 5 minutes. The supernatant was discarded and the cell pellet was resuspended in fresh growth medium, taking care to avoid clumping of the cells and transferred to a fresh flask.

When an accurate number of cells had to be seeded they were lifted as usual, 500µl aliquot was stained with trypan blue and counted using a haemocytometer

(Hausser Scientific Company) on a phase microscope, prior to seeding into fresh flasks with an appropriate volume of medium.

2.4.3 Cryopreservation of cells

Low passage cells which were 85% confluent were harvested as above. After centrifugation, the cell pellet was placed on ice and resuspended in DMEM with 20% FCS and 10% DMSO, at a final concentration of 1 x 10^6 cells /ml. 1.5ml aliquots were frozen at -20°C and then stored overnight at -70°C before transfer to liquid nitrogen for long term storage. When reanimating frozen cells for experimental use, they were rapidly thawed at 37°C and diluted in nine volumes of fresh media. The suspension was then centrifuged at 1000*g* for 5 minutes, the supernatant discarded and the cells resuspended in fresh media and seeded in flasks or dishes.

2.5 Lentiviral procedure

2.5.1 Design and preparation of shRNA insert oligonucleotides

To convert siRNA sequences into the required format for expression as shRNA molecules from the pLL3.7 lentivector, a stem and loop sequence was designed and appropriate restriction enzyme sequence added at the 5' and 3' ends.

The design of oligonucleotide shRNA-Cl8 is shown below. All shRNA oligonucleotides were designed likewise.

siRNA sequence = TAGGAGATCTTGACTCTGA

- addition of the loop sequence to end- TTCAAGAGA

  TAGGAGATCTTGACTCTGATTCAAGAGA

- addition of the reverse complement to end

  TAGGAGATCTTGACTCTGATTCAAGAGATCAGAGTCAAGATCTCCTA

- addition of the terminator sequence

  TAGGAGATCTTGACTCTGATTCAAGAGATCAGAGTCAAGATCTCCTATTTTTTC

- creation of the antisense strand

TAGGAGATCTTGACTCTGATTCAAGAGATCAGAGTCAAGATCTCCTATTTTTT

ATCCTCTAGAACTGAGACTAAGTTCTCTAGTCTCAGTTCTAGAGGATAAAAAA

- addition of restriction HpaI (5') and Xho I (3') restriction enzyme sequence

5′- AACTAGGAGATCTTGACTCTGATTCAAGAGATCAGAGTCAAGATCTCCTATTTTTTC-3′

3′-TTGATCCTCTAGAACTGAGACTAAGTTCTCTAGTCTCAGTTCTAGAGGATAAAAAAGAGCT-5′

All oligonucleotides were obtained from MWG Biotech and resuspended in ddH_2O.

2.5.2 Annealing of oligonucleotides

60pmol of sense and antisense oligonucleotides were added to 48µl Annealing Buffer (Xeragon) and denatured by heating to 95°C for 10 minutes. The temperature was reduced to 70°C and then every 10 minutes it was reduced by 10°C (70°- 60°-50°-40°) and then allowed to cool gradually to room temperature overnight to promote annealing of complementary oligonucleotides.

2.5.3 Recombinant lentivirus production

The lentiviral production protocol used was provided by Prof Greg Towers and required 6 days per preparation.

Day 1-seed HEK293 cells: cells were seeded by splitting a confluent plate 1:4, approximately 24 hours before transfection into a 100mm plate with 8 ml complete media and incubated at 37°C in 5% CO2.

Day 2-transfection: DNA was diluted in a 1.5ml Eppendorf tube to a total volume of 15µl with TE pH 8.0

1 µg p8.91 (gag-pol expression vector)

1 µg pMDG2 (VSV-G expression vector)

1.5 µg pLL3.7 DNA (lentiviral vector)

For each transfection mix, 200µl of OptiMEM (Invitrogen 51985-026) were added to a second Eppendorf tube and 10µl of Fugene (1988387/1815075 Roche Diagnostic) were added to the centre of the tube without touching the sides. The mixture was mixed, by flicking. DNA was then added to the OptiMEM Fugene mix and flicked once again. The Eppendorf was then left at room temperature for 15 minutes and in this time the plated cells were fed fresh complete pre-warmed medium. After 15 minutes, the

OptiMEM/Fugene mix was added to the cells drop wise and the plates swirled to ensure complete mixing. The cultures were incubated at 37°C.

Day 3-media change: approximately 24 hours following the transfection, the medium containing the transfection mix was replaced with 10 ml of fresh complete medium.

Day 5, 6-virus collection: the lentivirus containing supernatant was harvested at 48 and 72 hours after media change. The medium was collected in a 10 ml syringe (SZR-150-052C Fisher) and filtered through a 0.45μM filter (Nalgene Syringe filters 513-1902 VWR). The supernatant was stored at -80°C.

2.5.4 Transduction of HEK293 cells

A serial dilution method was used to determine the titre of each lentivirus. 2 x 10^5 HEK293 cells were plated in each well of a 6 well plate and incubated overnight. The following day, the lentiviral stock was thawed and serial dilutions prepared in 1 ml of complete culture medium. Polybrene was added at a final concentration of 8μg/μl to neutralise the charge of the plasma membrane and promote interaction with the virus. The culture media was removed from the cells and the viral dilutions added. One well received polybrene only to control for its effects on the cells. The plates were incubated at 37°C overnight and the culture medium replaced the following day. Four days post-transduction, the cells were examined for GFP expression by fluorescence microscopy and harvested for FACS analysis.

2.5.5 Determination of lentiviral titre

Cells were harvested as usual and washed in 5ml PBS, spun at 1500rpm for 5min at 4°C twice. The total number of cells was then determined. Cells were resuspended at a density of $1x10^6$cells/100μl and transferred to FACS tubes (Becton-Dickinson). The cells that received polybrene only were used as a negative control to gate for living GFP-negative cells. GFP-positive cells in the transduced samples were detected in FL1 and their proportion determined by gating. At least 20,000 cells were analysed. FACS analysis was carried out using an LSRII flow cytometer (BD Biosciences) with FloJo

software (Tree Star Inc., Ashland, Oregon, USA), or a Beckman Coulter Cytomics FC500 Flow Cytometer (MCP System) using CXP Software.

2.5.6 Measurement of PrP knockdown

N2A cells were harvested, washed, and resuspended in a correct volume for a final density of $1x10^6$cells/100µl as previously described. 100µl of cells were transferred to an Eppendorf and spun at 1500rpm for 5min at 4°C. The supernatant was removed, and cells resuspended in 100µl of primary antibody ICSM18 at final concentration of 5µg/ml.

Cells were incubated on ice for 20-30 minutes, and then spun at 1500 rpm for 5 minutes at 4°C. The supernatant was removed carefully, without disturbing the cell pellet, and cells were washed twice in PBS, by sedimenting at 1500 rpm for 5 min at 4°C. Cells were resuspended in 100µl of secondary antibody PE-Goat anti-mouse (BD Pharmnigen, 550589), diluted 1:50 in PBS and incubated on ice for 30 min. 100µl PBS was added and cells were spun at 1500rpm for 5min at 4°C. Cell pellet was resuspended in 500 µl of PBS. Data were collected using Beckman Coulter Cytomics FC500 Flow Cytometer (MCP System) and analysed using CXP software. Background fluorescence was measured using cells stained with secondary antibody only.

3 Effect of Cre-mediated recombination in Me7 and Mouse-adapted BSE prion infected mice

3.1 Background

The protective effect of neuronal PrP^{C} depletion on the course of disease in mice with established prion disease has been investigated in a milestone work from Mallucci et al. (Mallucci et al., 2003).

This study has been described in detail in paragraph 1.1.5.3. Briefly, it demonstrated that arresting neuronal conversion of PrP^{C} to PrP^{Sc} by depleting the former prevents the progression from pre-clinical to clinical infection and it suggested that the generation of a toxic species must take place in neurons to be pathogenic. Also, adult neuronal PrP^{C} depletion reversed early neurodegenerative changes caused by the RML prion strain and protected against neuronal loss, despite continued prion replication and PrP^{Sc} deposition.

3.2 Aims

- To assess the effect of Cre-mediated PrP recombination on survival in mice infected with prion strains other than RML
- To follow the progression of prion pathology in the brains of prion infected M*lox*P and NFH-Cre/M*lox*P mice

3.3 Experimental setup

In order to minimise incubation times, M*lox*P tg37 rather than tg 46, and NFH-Cre/tg37 rather than NFH-Cre/tg46 were used in all of the following experiments, as tg37 mice express PrP^{C} at higher levels. Therefore, from now on I will refer to tg37 as M*lox*P and NFH-Cre/tg37 as NFH-Cre/M*lox*P.

To take advantage of the window for reversing prion pathology, M*lox*P and NFH-Cre/M*lox*P mice were inoculated with Mouse adapted-BSE and Me7 prions at one week of age. The Mouse-adapted BSE inoculum (I874) was derived from a pool of five natural BSE affected brainstems sub-passaged twice in C57 BL/6 mice (Lloyd et al.,

2004). The mouse adapted scrapie strain Me7 has been extensively studied for prion related hippocampal damage.

For each group a statistically significant number of animals were culled at different time points for histopathological analysis. Sagittal sections were stained with haematoxylin and eosin (H&E) to follow progression of spongiosis, and ICSM 35 antibody for abnormal PrP deposition. Furthermore, for each group, a significant number of animals were used to study survival.

I joined this project when it was already started: the experimental set up was planned by Prof. Giovanna Mallucci and her team. Prion inoculation and mice culling were carried out at the animal house facility by specialized personnel. The MRC Prion Unit histopathology support group performed the histology. I took over from Prof Mallucci's team for the histopathological analysis that I carried out with the help of Jackie Linehan and Prof. Sebastian Brandner.

3.4 Results

3.4.1 Extended survival of prion infected NFH-Cre/MloxP mice

PrP^C depletion increased survival in double transgenic NFH-Cre/MloxP mice for both prion inoculations.

M*lox*P control mice succumb to the Me7 prion strain at ~17 wpi (n=6) whereas mice that have undergone neuronal PrP^C depletion developed signs of scrapie at ~29 wpi (n=9), p value <0.0005 (Figure 3.1 A).

Upon Mouse-adapted BSE infection, M*lox*P mice succumbed in ~20 wpi (n=7) but mice with neuronal PrP^C depletion survived up to ~33 wpi (n=10), p value <0.0005 (Figure 3.1 B).

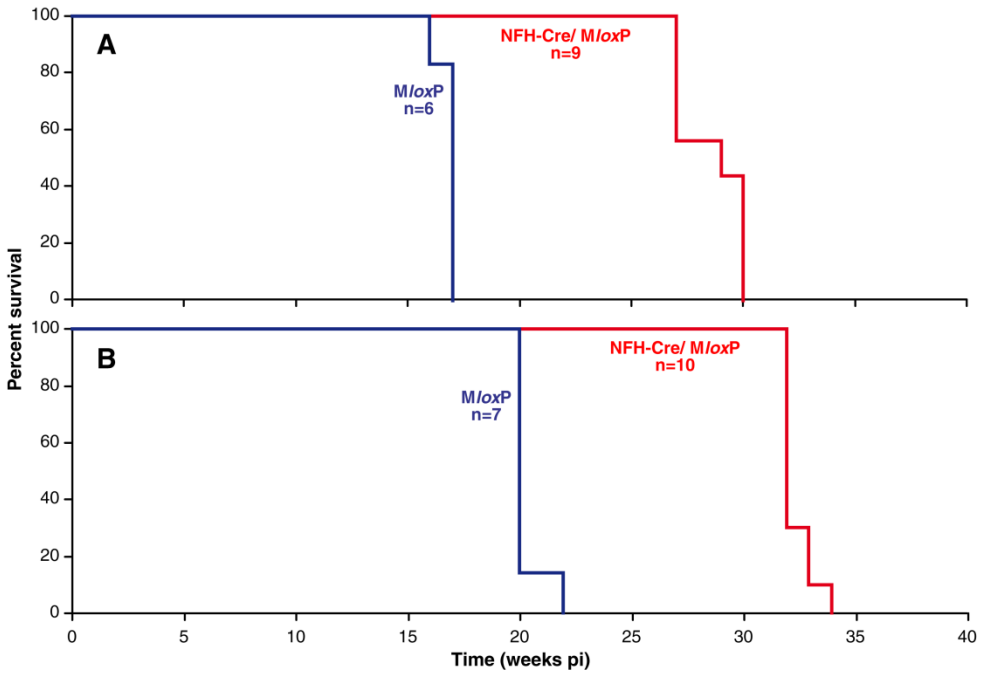

Figure 3.1 Increased survival in prion infected NFH-Cre/M*lox*P mice after Cre-mediated neuronal PrP depletion

A. Mice were inoculated with Me7 prions at one week of age. M*lox*P mice (blue line) succumbed to the infection at ~17 wpi (n=6); NFH-Cre/M*lox*P mice (red line), undergoing PrP^{C} depletion developed signs of scrapie at ~29 wpi (n=9), p value <0.0005. B. Mice were inoculated with mouse-adapted BSE prions at one week of age. M*lox*P mice (blue line) succumbed in ~20 wpi (n=7) but mice with PrP^{C} depletion (red line) survived up to ~33 wpi (n=10), p value <0.0005.

3.4.2 Time course of prion pathology in mice infected with Me7 prion strains

Abnormal PrP deposition in Me7 inoculated M*lox*P mice was first found at 8 wpi, localized in the thalamus and the brainstem; by 10 wpi deposition was observed in the cortex and hippocampus and became more intense in the thalamus and brainstem. Prion accumulation continued for the following four weeks, eventually spreading to cerebellum by 16 wpi. At end stage of the disease, (~17 wpi) abnormal PrP accumulation was widespread in all brain areas.

In NFH-Cre/M*lox*P mice, the pattern of PrP deposition at 8 wpi was similar to that observed in M*lox*P mice, but at 10 wpi the abnormal PrP deposition was milder. By 12 wpi, prion deposition mimicked that observed in M*lox*P mice, with intense staining in the thalamus and brainstem. From this time point, the pattern differed from the

M*lox*P: at ~16 wpi deposition had spread to cerebellum, striatum and cortex, but the thalamic nuclei, which were the first area of accumulation, and the hippocampus were spared. The areas of maximal deposition were already established by 20 wpi: cortex, caudo-putamen, frontal thalamus, posterior hippocampus, brainstem and cerebellum. At the end stage of disease (~29 wpi) frontal hippocampus and ventral thalamic nuclei showed milder abnormal accumulation compared to end stage M*lox*P mice (Figure 3.2 A).

Spongiosis in Me7 inoculated M*lox*P mice was not as severe as in RML infected animals. It was first localized at 10 wpi in the thalamus and caudate nucleus. By 12 wpi it targeted the hippocampus and by end stage it affected all the brain areas. The Me7 prion pathology in M*lox*P mice did not involve hippocampal neuronal loss, unlike RML infection in the same mouse model (Mallucci et al., 2003). Neuronal loss was found just in one of the analysed mice.

Spongiosis in Me7 infected NFH-Cre/M*lox*P mice differed slightly from that observed in control animals. It was first found at ~12 weeks post inoculation in the thalamus and cortex. By 20 wpi, the whole brain was mildly spongiotic; with no particular area being specially targeted (Figure 3.2 B). As spongiosis is not a strong hallmark of the Me7 prion strain, in the M*lox*P model it was not possible to use this paradigm to compare with the rescuing effect on spongiosis previously seen in RML infected NFH-Cre/M*lox*P mice (Mallucci et al., 2003).

At ~28 wpi, in NFH-Cre/M*lox*P mice, cerebellar pathology emerged. Neuronal loss, localized to the granular layer of cerebellum, was observed. Layers F11.9-12 were affected the most. No cerebellar pathology was observed in M*lox*P mice at the end stage of the disease (Figure 3.3).

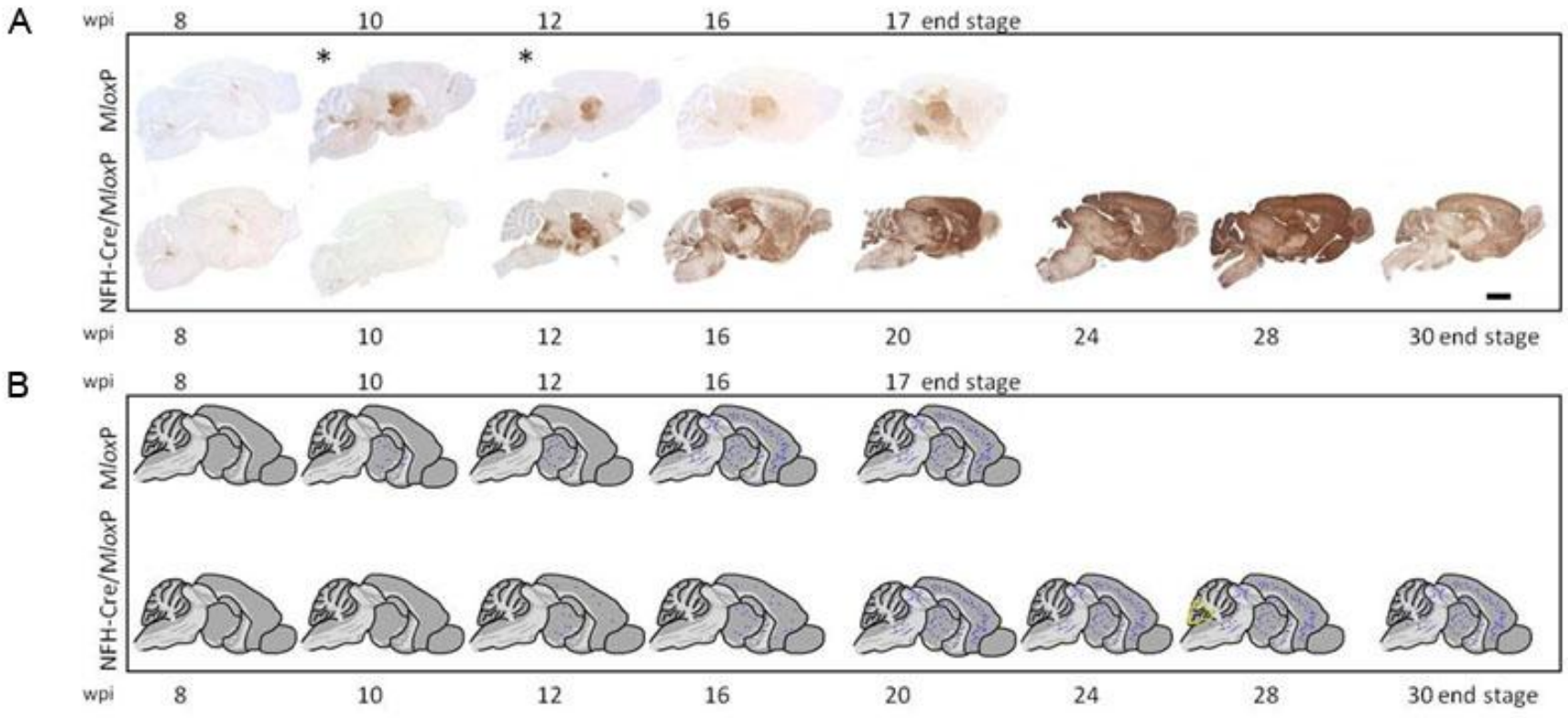

Figure 3.2 Progression of prion pathology in Me7 inoculated M*lox*P and NFH-Cre/M*lox*P mice

Me7 inoculated M*lox*P and NFH-Cre/M*lox*P mice were time culled at different times post infection (wpi). 3 brains per group were analysed.

A. Representative progression of abnormal PrP deposition: in Me7 inoculated M*lox*P mice it was first found at 8 wpi, in the thalamus and the brainstem; by 10 wpi it spread to the cortex and hippocampus and became more intense in the thalamus and brainstem; by 16 wpi it interested the cerebellum. At end stage of the disease, (~17 wpi) abnormal PrP accumulation was widespread in all brain areas, with maximal intensity in the thalamus and brainstem. In NFH-Cre/M*lox*P mice, the pattern of PrP deposition at 8 wpi was similar to that observed in M*lox*P mice, but at 10 wpi the abnormal PrP deposition was milder. At 12 wpi,

intense staining was localized in the thalamus and brainstem; at ~16 wpi deposition spread to cerebellum, striatum and cortex, but the thalamic nuclei, which were the first area of accumulation, and the hippocampus were spared. At 20 wpi the areas of maximal accumulation were: cortex, caudo-putamen, frontal thalamus, posterior hippocampus, brainstem and cerebellum. At the end stage of disease frontal hippocampus and ventral thalamic nuclei showed milder abnormal accumulation compare to end stage MloxP mice.

Brains have been stained with ICSM 35 antibody, scale bar= 1.7 mm for brains labelled with *; 2.2 mm for all the other brains.

B. Representative progression of spongiosis: Brains have been stained with H&E and a schematic of the results has been drawn.

In Me7 inoculated M*lox*P mice spongiosis was first localized at 10 wpi in the thalamus and caudate nucleus. By 12 wpi it targeted the hippocampus and by end stage it involved all the brain areas. Neuronal loss was found in just one of the analysed samples. Spongiosis in Me7 infected NFH-Cre/M*lox*P mice was first found at ~12 weeks post inoculation in the thalamus and cortex, it spread to the hippocampus and by 20 wpi, the whole brain was mildly spongiotic, with no particular area being specially targeted. At 28 wpi, the cerebellum was severely affected. The yellow line delimits the cerebellar foliae most affected.

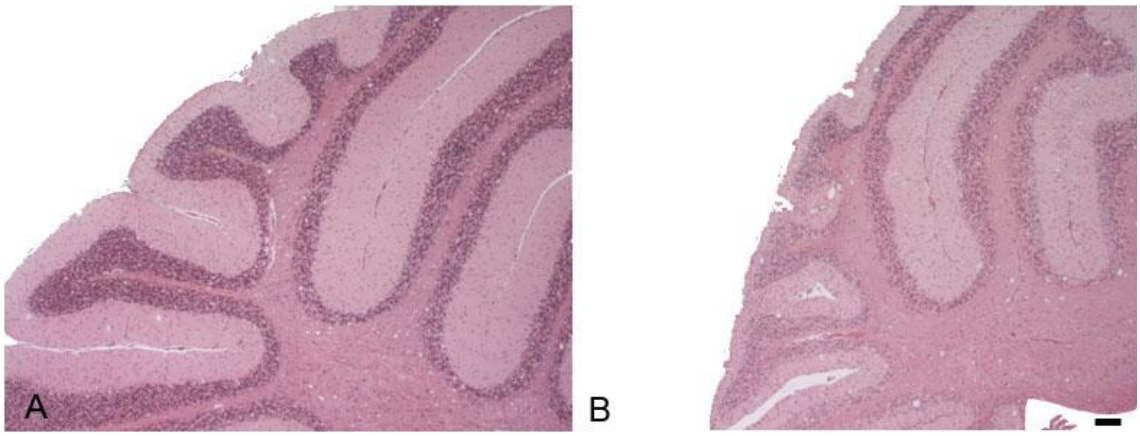

Figure 3.3 Cerebellar pathology in end-stage Me7 inoculated NFH-Cre/M*lox*P mice

A. Cerebellar foliae are not spongiotic in M*lox*P mice at the end-stage of Me7 infection

B. layers F11.9-12 in the cerebellum of NFH-Cre/M*lox*P mice are highly spongiotic, and also show neuronal loss and shrinkage of the tissue. Brains have been stained with H&E, scale bar = 435 μm

3.4.3 Time course of prion pathology in mice infected with Mouse-adapted BSE prion strain

In M*lox*P mice infected with Mouse-adapted BSE, deposition of abnormal PrP started at 8 wpi in the thalamus, hippocampus and brainstem and its intensity was constant for the following 4 weeks. At 16 wpi, abnormal deposition of PrP reached the cortex and the striatum and at the end stage of the disease (~20wpi) the areas of maximal accumulation were the brainstem and striatum.

NFH-Cre/M*lox*P mice accumulated abnormal PrP at 10 wpi in dorsal thalamic nuclei and brainstem. By 12 wpi, fronto-dorsal thalamus staining was more intense; prion accumulation had also spread to dorsal hippocampus, leaving the frontal hippocampus spared, as already observed in Me7 mice. Abnormal PrP accumulation reached the striatum at 16 wpi, as in control animals. From this time, the pattern of accumulation was established, with focal areas in brainstem and striatum until ~28 wpi. In the last 4 weeks, (28-33 wpi) prion accumulation spread to the cortex and cerebellum. The degree of accumulation in the first targeted areas was constant during this period. The only areas that were spared were frontal hippocampus and ventral thalamus. Indeed, in the thalamus abnormal PrP accumulation occurred as a peculiar ring shape (Figure 3.4 A)

Hippocampal neuronal loss and spongiosis was not a neuropathological feature of this prion strain in our experimental model. Mild spongiosis was localized in the areas of prion accumulation (brainstem, ventral thalamus and ventral striatum) at the end stage of the disease.

In NFH-Cre/M*lox*P mice, the progression of spongiosis was similar to that in M*lox*P mice, being localized to the brainstem, ventral thalamus and ventral striatum at 16 wpi. In one sample it appeared earlier in the disease (12 wpi) and was widespread in the cortex, hippocampus, thalamus, and striatum. At 24 wpi spongiosis was also localized in the dorsal thalamus and cortex. From this time point until end stage of the disease, spongiosis was localized in the same areas affected by prion accumulation, keeping the cerebellum intact (Figure 3.4 B).

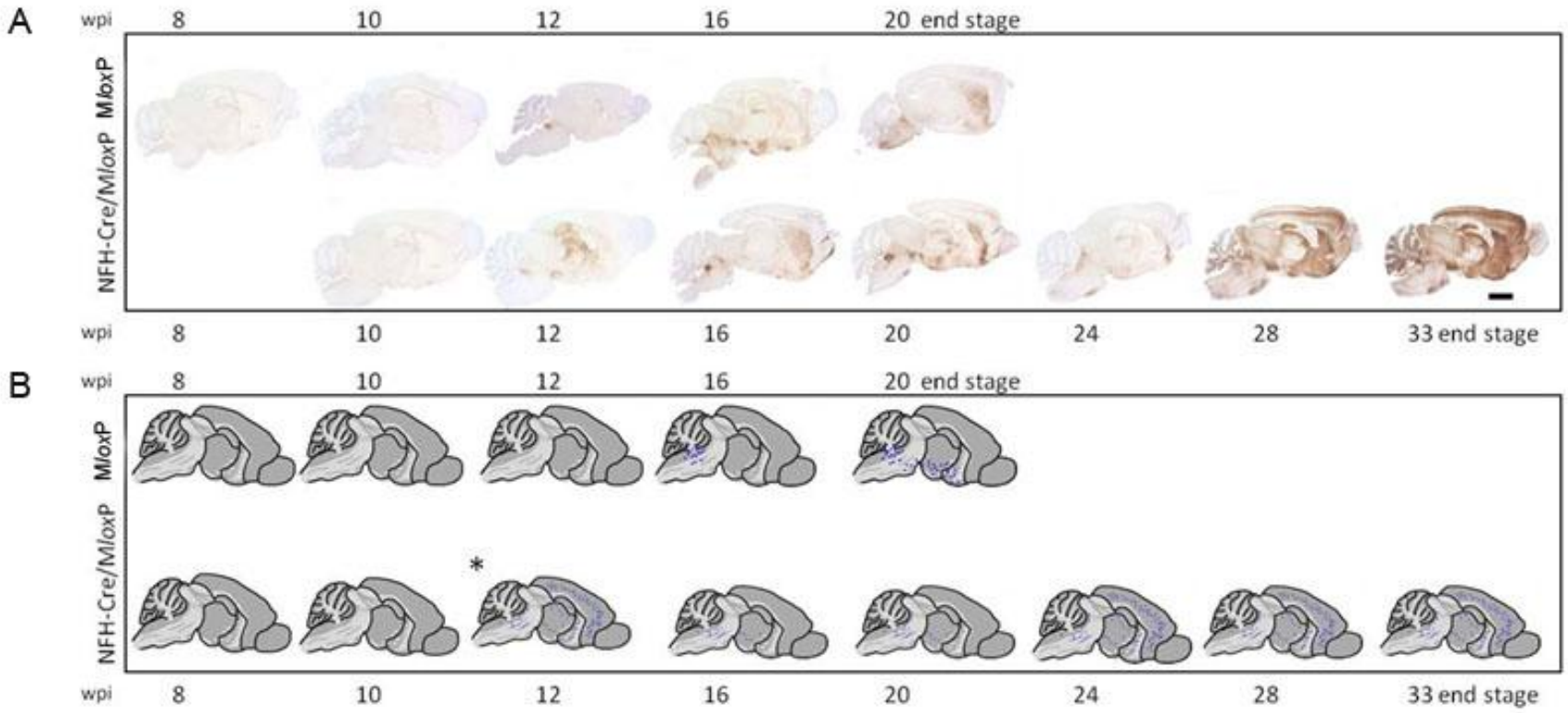

Figure 3.4 Progression of prion pathology in mouse-adapted BSE inoculated M*lox*P and NFH-Cre/M*lox*P mice

Mouse-adapted BSE inoculated M*lox*P and NFH-Cre/M*lox*P mice were time culled at different times post infection (wpi). 3 brains per group were analysed. No brain was available for NFH-Cre/M*lox*P mice at 8wpi.The star * indicates that just one brain out of 3 had the represented phenotype; the other two resembled the previous time point.

A. Representative progression of abnormal PrP deposition: in Mouse-adapted BSE M*lox*P inoculated mice started at 8 wpi in thalamus, hippocampus and brainstem. At 16 wpi, abnormal deposition of PrP reached the cortex and the striatum and at the end stage of the disease (~20wpi) the areas of maximal

accumulation were the brainstem and striatum. In NFH-Cre/M*lox*P mice abnormal PrP accumulation was found at 10 wpi in dorsal thalamic nuclei and brainstem. By 12 wpi, deposition was intense in the thalamus and dorsal hippocampus, whereas the frontal hippocampus was spared. Abnormal PrP accumulation reached the striatum at 16 wpi, as in M*lox*P mice. From this time, the pattern of accumulation was established, with focal areas in the brainstem and striatum until ~28 wpi. In the last 4 weeks, (28-33 wpi) prion accumulation spread to the cortex and cerebellum. The degree of accumulation in the first targeted areas was constant during this period. The only areas spared from abnormal PrP accumulation were frontal hippocampus and ventral thalamus, where abnormal PrP accumulation occurred as a peculiar ring shape. Brains have been stained with ICSM 35 antibody, scale bar= 2.2mm.

B. Representative progression of spongiosis: Brains have been stained with H&E and a schematic of the results drawn. In M*lox*P mice mild spongiosis was localized to the areas of prion accumulation (brainstem, ventral thalamus and ventral striatum) from 16 wpi. In NFH-Cre/M*lox*P mice, spongiosis appeared at 12 wpi in one sample, indicated with a star, and was widespread in the cortex, hippocampus, thalamus, and striatum. At 16 wpi it localized to the brainstem, ventral thalamus and ventral striatum. At 24 wpi spongiosis was localized also in the dorsal thalamus and cortex. From this time point until end stage of the disease, spongiosis was localized in the same areas affected by prion accumulation, keeping the cerebellum intact.

3.5 Discussion

The survival data in this pilot experiment showed a clear difference in the effect of neuronal PrP^C depletion in the course of different prion infections. Indeed, loss of neuronal PrP was effective in delaying progression of the disease after both Me7 and Mouse-adapted BSE prion inoculation, but it did not completely protect as previously observed for RML infection (Mallucci et al., 2003). In addition, some important observations were made both for neuropathology and the survival of infected animals.

First, it is important to consider that different prion strains have different lesion profiles. Indeed, the hippocampus, which was the main area analysed in Mallucci's experiment, is a prominent site for prion accumulation in Me7 but not in Mouse-adapted BSE inoculated mice. Second, the rescue effect of prion pathology observed in the hippocampus of RML infected animals is not seen in the Me7 infection. In this case, spongiosis in the hippocampus of double transgenic animals appears later in the disease (16 wpi vs. 12 wpi in control animals) but then remained constant as the disease progressed. This could be due to a miss-coupling of the kinetics of Cre recombination and prion pathology targeting the hippocampus.

Other areas appear to be a common target for Me7 and Mouse-adapted BSE prions, like thalamus and brainstem. Even in these areas, a slowing of the disease progression, with later appearance of spongiosis is the only effect of PrP^C depletion and no rescue of pathology was observed. It is also noticeable how recombination affects abnormal PrP deposition: recombination is known to occur with higher efficiency in areas enriched in neurons (Mallucci et al., 2002), like hippocampus and thalamus, and indeed the thalamus in both Me7 and Mouse-adapted BSE infection and the hippocampus in Me7 infection were cleared of abnormal PrP accumulation.

The slowing of the disease progression is in accordance with the increased survival of NFH-Cre/M*lox*P mice. In contrast with RML infection, Me7 and Mouse-adapted BSE infected mice did not survive long term asymptomatically. We reasoned that the different lesion profile could be responsible for this outcome and that neuronal PrP^C recombination do not protect one or more areas responsible for the onset of disease in Me7 and Mouse-adapted BSE to the same extent as in RML infection.

Specific anatomical target areas, “clinical target areas”, have been hypothesized to be responsible for disease onset, progression and the clinical phenotype (Kimberlin and Walker, 1983; Kimberlin and Walker, 1986; Kimberlin et al., 1987).

We suggest that a comparison of end stage infected M*lox*P and NFH-Cre/M*lox*P mice and asymptomatic RML infected NFH-Cre/M*lox*P mice, could facilitate identifying these anatomical and functional target areas. Two scenarios could be hypothesized: “clinical target areas" responsible for the fatal outcome of the disease could be either the very first regions to be affected and become rate-liming in the disease progression or, alternatively, the target areas are the last regions to start accumulating abnormal prion protein.

In the first scenario, the clinical target areas are the first sites of prion accumulation and pathology, both in M*lox*P and NFH-Cre/M*lox*P mice. Comparison of the published data (i.e. RML inoculated NFH-Cre/M*lox*P mice survive for > 52 weeks) with the data obtained here (i.e. Me7 inoculated NFH-Cre/M*lox*P mice survive ~ 28 weeks), would allow the conclusion that the difference of incubation time is due to the different involvement of the anatomic target areas. It must be assumed, that such a difference is caused by the different kinetics of the prion accumulation, for example that Me7 accumulates faster than RML in a specific areas. In the context of our model of neuronal depletion, the colonisation of an area with prions may precede the recombination event, causing a clinical phenotype.

In the second scenario (last target area), the clinical target areas can be identified by comparing late stage RML inoculated NFH-Cre/M*lox*P mice with end stage NFH-Cre/M*lox*P mice inoculated with Me7 or Mouse-adapted BSE. In this scenario, mice would be able to survive the infection in a pre-clinical stage- i.e. accumulating prions without developing clinical showing signs of prion disease, until the colonisation of the critical target areas that cause a fatal outcome. Therefore, clinical target areas of prion pathology should be distinguishable at the end stage of the disease in the M*lox*P mice infected with any prion strains, and in the late stage NFH-Cre/M*lox*P mice infected with prions strains that still develop clinical prion disease, but these areas should be partially or totally spared from prion pathology in RML infected NFH-Cre/M*lox*P mice surviving long term.

In order to further investigate and validate these hypotheses, a new experiment was set up. The results are described in the following chapters.

3.6 Summary

It was previously shown that Cre-mediated neuronal PrP^{C} depletion in RML infection reversed early spongiform changes, prevented progression to clinical disease, despite the accumulation of extra-neuronal PrP^{Sc} (Mallucci et al., 2003).

Here we showed that the effect of neuronal PrP^{C} depletion is different with different prion strains. Upon Me7 and Mouse-adapted BSE inoculation, depleted mice survive longer than non-depleted mice but still develop clinical symptoms; however the prion pathology progressed more slowly but it was not rescued upon depletion of neuronal PrP by recombination. We speculate that the difference may be due to the cross-talk between Cre-mediated recombination and areas preferentially targeted by prion pathology, the so called "clinical target areas" (Kimberlin and Walker, 1983; Kimberlin and Walker, 1986; Kimberlin et al., 1987). Basically, Cre-mediated recombination could occur in one or more clinical target areas before they are targeted by the RML induced prion pathology, but not Me7 or Mouse-adapted BSE related prion pathology. Therefore, Cre-mediated recombination prevents progression to clinical disease in RML but not in Me7 or Mouse-adapted BSE infection. To evaluate which are the clinical target areas and if they are first or last areas affected in the course of a given infection, a new experiment was set up which is described in the following chapter.

4 Prion pathology in the brainstem of RML and Me7 M*lox*P and NFH-Cre/M*lox*P infected mice

4.1 Introduction

The idea of specific anatomical target areas preferentially affected in prion disease is not new (Kimberlin and Walker, 1983). According to the "clinical target areas" hypothesis, specific vital brain regions are targets of prion pathology and determine clinical onset in prion-infected animals. More recent studies have supported the hypothesis that specific vital brain regions may be preferentially affected, and have rejected the hypothesis that generalised high level of PrP^{Sc} in the central nervous system is the reason for accelerated pathogenesis and disease (Karapetyan et al., 2009).

M*lox*P and NFH-Cre/M*lox*P infected mice are useful tools to further investigate the hypothesis of clinical target areas in prion disease. In the previous chapter we described that NFH-Cre/M*lox*P mice, which in previous studies showed resistance to clinical disease following RML prion inoculation, were not resistant to inoculation with other prion strains. Me7 and Mouse-adapted BSE inoculated NFH-Cre/M*lox*P mice survived significantly longer than their respective PrP overexpressing M*lox*P mice, but still succumbed to prion disease. We therefore reasoned that, comparing the brain areas affected by prion pathology in terminally ill M*lox*P mice, terminally ill NFH-Cre/M*lox*P mice and resistant RML inoculated NFH-Cre/M*lox*P mice, may enable us to pin-point the vital areas in which Cre-mediated recombination prevents prion pathology.

Terminally ill prion infected mice usually show signs of tremor, balance control and gait impairment in conjunction with impaired respiratory rate. The brainstem is the centre of control of vital activities, such as cardiovascular and respiratory functions. Moreover, some anatomical regions in the brainstem (so-called nuclei) in this heterogeneous area also supervise motor control. Therefore, we reasoned that a detailed analysis of the brainstem nuclei would reveal important information on "clinical target areas" of prion disease.

Work from Iwasaki et al. examined the brainstem of 33 sCJD patients (Iwasaki et al., 2005), looking for a connection between clinical symptoms suggestive of brainstem involvement and brainstem pathology. Brainstem atrophy,

neuronal loss, pyramidal tract degeneration and PrP deposition were reported particularly in patients with prolonged disease, but the authors hypothesized that abnormal PrP deposition in the brainstem occurs in the early stage of the sCJD disease process. However, this study showed high variability and failed to determine a correlation between clinical signs and brainstem lesions. The authors suggested that a conclusive evaluation of the connection between clinical signs and brainstem impairment is difficult because the same symptoms could derive from overlapping involvement of basal ganglia or cortex (Iwasaki et al., 2005).

Therefore, a controlled and reproducible system, such as an animal model could circumvent the problem of variability of clinical signs in patients and the variable distribution of pathological features in human samples.

The organization of the brainstem has been described as a segregation between nuclei involved in motor control and neuronal populations implicated in the control of homeostatic activity (Brodal, 1981). This model of brainstem circuitry, based on segregation between activities, generally attributes the control of skeletal muscle contraction to the medial pontine and reticular formation and the vestibular nuclei, and the regulation of respiration and blood pressure to areas such as the nucleus of the solitary tract and the lateral medullary reticular formation (Yates and Stocker, 1998). Although this segregation has proven to be inaccurate (Yates et al., 2002; Yates et al., 2003), we used it as an approximate approach to investigate the involvement of the brainstem in prion pathology, and analysed different brainstem nuclei as involved in motor or autonomic control.

In this chapter I will discuss our study, which aims at the identification of the brainstem nuclei in transgenic mice that show the most significant prion-related pathology and the characterisation of disease progression.

4.2 Aims

- To assess the effect of Cre-mediated recombination of the *Prnp* gene on the survival of mice infected with RML, Me7 and MRC2 prions
- To identify the brainstem nuclei affected by prion pathology in M*lox*P mice inoculated with each of the three prion strains

- To follow the disease progression in PrP-depleted mice, by evaluating the brainstem nuclei affected by prion pathology in NFH-Cre/M*lox*P mice at a time when non-recombined M*lox*P mice were terminally ill.
- To evaluate the prion pathology in the brainstem nuclei at the end-stage of prion disease in NFH-Cre/M*lox*P mice inoculated with each of the three prion strains.

4.3 Experimental set up

M*lox*P and NFH-Cre/M*lox*P mice were inoculated when one week-old with the RML, Me7 or MRC2 prion strains. The inoculum was 1% brain homogenate, designated as I9900 (1% RML I8700), I 9459 (1% Me7 I9458), I 9468 (1% MRC2 9467).

The MRC2 strain was derived from Mouse–adapted BSE inoculum, subpassaged in SJL mice. It is a selected strain rather than an intermediate passage and has been characterised previously (Lloyd et al., 2004). For each group, a statistically significant number of animals were used to analyse survival and to analyse their brains histopathologically. Furthermore, RML, Me7 or MRC2 inoculated NFH-Cre/M*lox*P mice were culled at the time when the respective (non-recombined) M*lox*P mice were terminally ill, and their brains analysed histologically. An additional group of NFH-Cre/M*lox*P mice was inoculated and it was planned to cull at 50 wpi for direct comparison with the experiment performed by Mallucci (Figure 4.1).

For each group, three animals were used for pathological analysis. Brains were fixed, cut coronally into three pieces and processed for paraffin embedding. The block corresponding to the brainstem was sectioned with the microtome by the support team of the histology core facility at the MRC Prion Unit in serial sections and levels. Eight sections were collected for histology at each level. Sections were stained with haematoxylin and eosin (H&E) to assess spongiform changes, ICSM 35 antibody for abnormal prion protein deposition and anti-GFAP antibody to visualise reactive astrocytes and to assess astrogliosis. Sections were analysed microscopically and areas of interest were compared with landmarks in the Paxinos Mouse Brain Atlas and Allen Mouse Atlas (Paxinos and Franklin, 2004; Lein et al., 2007). Degree

of spongiosis, abnormal PrP deposition and gliosis were evaluated semi-quantitatively.

A detailed histological analysis was carried out on RML and Me7 inoculated brains.

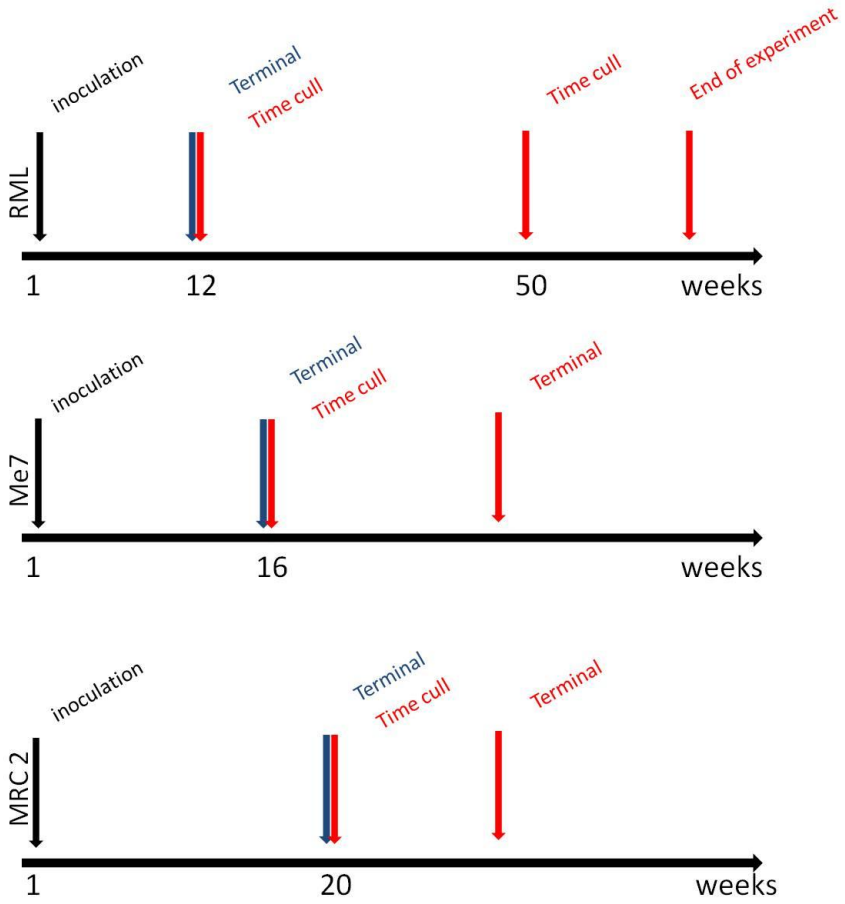

Figure 4.1 Description of the experimental plan

M*lox*P and NFH-Cre/M*lox*P mice were inoculated when one week old with RML, Me7 or MRC2 brain homogenate. Differential survival upon Cre-mediated recombination was to be estimated comparing terminal M*lox*P mice (blue arrow) and terminal NFH-Cre/M*lox*P mice (red arrow) incubation time. Because previous studies showed RML inoculated NFH-Cre/M*lox*P mice to be resistant to prion infection, RML inoculated NFH-Cre/M*lox*P mice were to be culled at the end of the experiment. For histopathological analysis, brains were to be collected form terminally ill M*lox*P and NFH-Cre/M*lox*P mice, and NFH-Cre/M*lox*P mice culled at the time when the M*lox*P mice were terminal, respectively, 12 wpi for RML inoculation, 16 wpi for Me7 inoculation and 20 wpi for MRC2 inoculation. An extra group of RML inoculated NFH-Cre/M*lox*P mice to be culled at 50 wpi was set up for a direct comparison with results reported by Mallucci *et al*.

4.4 Results

4.4.1 Effect on survival

In keeping with previous studies (Mallucci et al., 2003), RML inoculated M*lox*P control mice succumbed to prion disease after approximately 12 weeks (n=10). Surprisingly, the recombined NFH-Cre/M*lox*P mice did not survive for more than 57 weeks but became terminally ill ~35 wpi, (n=18) with the first animal dying at 30 wpi and the last at 38 wpi (Figure 4.2 A).

Me7 prion infected M*lox*P mice succumbed to disease at ~17 weeks (n=9) whereas the PrP^{C} depleted mice developed signs of scrapie at ~29 weeks (n=9) p value <0.0005, consistently with previous observations (cf. chapter 3) (Figure 4.2 B).

MRC2 infected M*lox*P mice succumbed after ~22 weeks (n=12) but PrP^{C} depleted mice survived ~31 weeks (n=14; p <0.0005) (Figure 4.2 C), with an incubation time longer than for Mouse-adapted BSE (cf. chapter 3).

4.4.2 Histopathology in the brainstem of prion infected animals

The pathological phenotype in the brainstem was examined for RML and Me7 prion strains. The semiquantitative evaluation included degree of spongiosis, abnormal PrP deposition and gliosis, using a scoring system ranging from non-existent (0) to severe (3). Spongiosis was scored as mild (= 1), intermediate (= 2) or severe (= 3), taking into account the ratio between vacuoles and healthy tissue in a given nucleus; gliosis was scored as mild (= 1), intermediate (= 2) or severe (= 3), taking into account the proportion of GFAP positive cells and the intensity of GFAP staining. PrP deposition was identified as synaptic or coarse, granular. The first appears as fine abnormal PrP deposition at the synapses and was scored as mild (= 1), intermediate (= 2) or strong (= 3) according to the intensity of deposition; the second is characterized by coarser granular deposition of abnormal PrP, and was scored according to the granular appearance as mild (= 1), intermediate (= 2) or dense (= 3) (Figure 4.3).

The analysis particularly focused on pontine and medullary nuclei involved in gait and balance (vestibular nuclei, prepositus nucleus, olive) and autonomic activity (locus coeruleus, tegmental nuclei, parabrachial nucleus, gigantocellular reticular nucleus, nucleus of the solitary tract, ventro-lateral reticular medulla, pre-

Bötzinger complex). A schematic representation of their position is shown in Figure 4.4.

In addition to the brainstem, the cerebellum was included in the analysis, as it is connected to the brainstem through the olivo-cerebellar pathways.

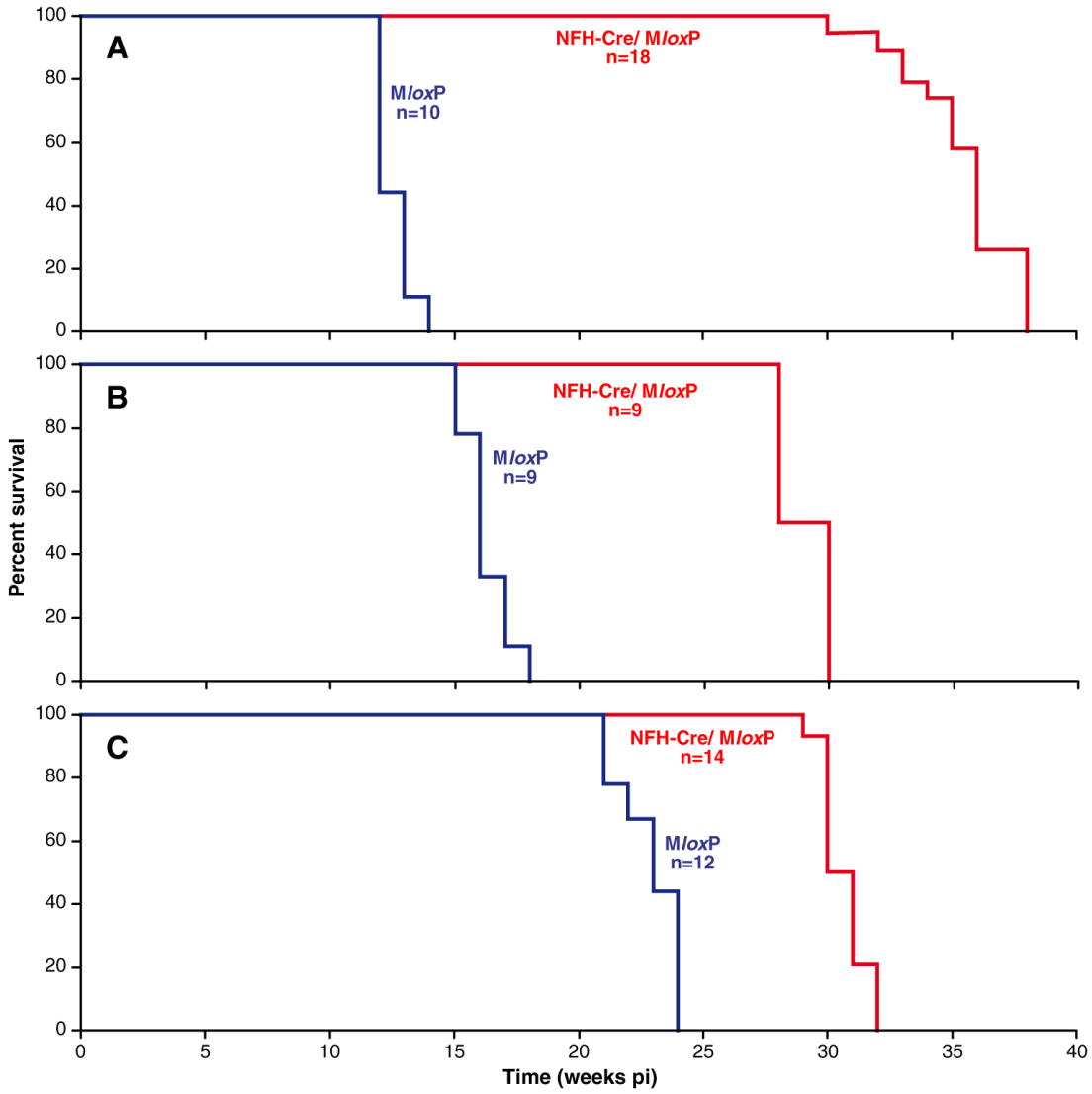

Figure 4.2 Survival curves of RML, Me7 and MRC2 inoculated M*lox*P and NFH-Cre/M*lox*P mice

A. Mice were inoculated with RML prions when one week of age. M*lox*P mice (blue line) became terminally ill at ~12wpi (n=10). In contrast to previous experiments, the recombined NFH-Cre/M*lox*P mice (red line) were not resistant to prion inoculation, and were terminally ill in ~ 35 weeks (n=18), showing a significant increase in the incubation time, p value <0.0005.

B. Mice were inoculated with Me7 prions when one week of age. M*lox*P mice (blue line) succumbed to Me7 prions at ~17 weeks (n=9); NFH-Cre/M*lox*P mice, were terminal at ~29 weeks (n=9) (red line) p value <0.0005, in accordance with previous results reported in chapter 3.

C. Mice were inoculated with MRC2 prions when one week of age. M*lox*P mice (blue line) succumbed in ~22 weeks (n=12), but NFH-Cre/M*lox*P mice, with PrP^{C} depletion survived ~31weeks (n=14), p value <0.0005.

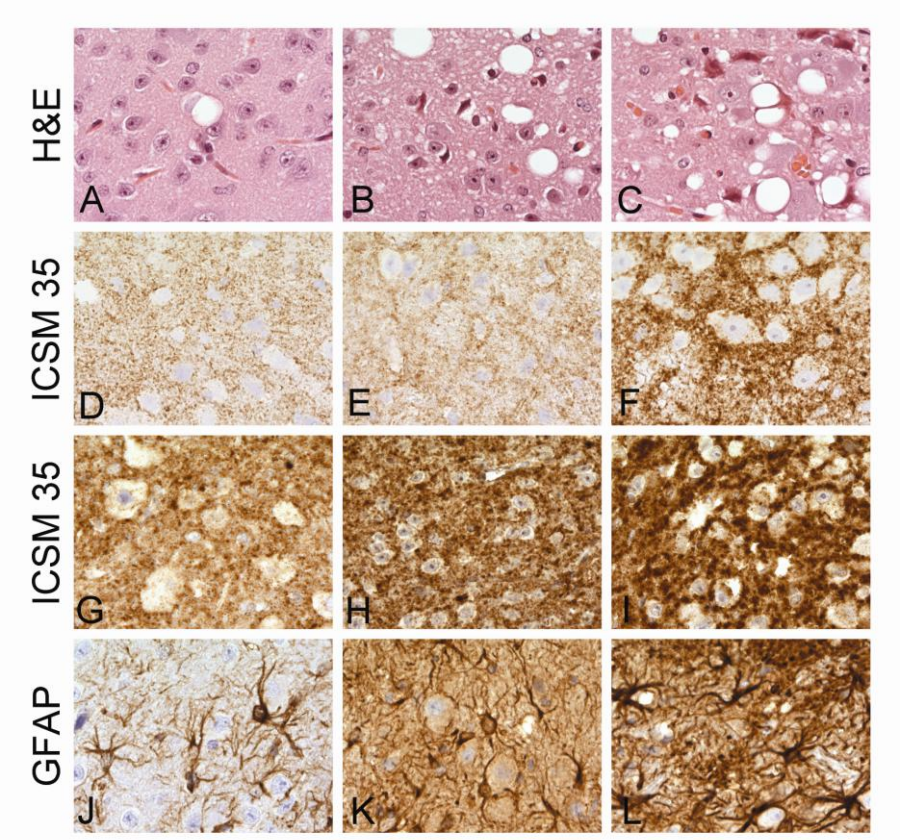

Figure 4.3 Scoring system used to evaluate prion pathology in the brainstem of prion inoculated animals

Spongiosis was scored considering the ratio between healthy tissue and vacuoles in a given nucleus, observed by H&E staining, as mild = 1 (A), intermediate = 2 (B) or severe = 3(C).

Abnormal PrP accumulation was scored according to synaptic density of abnormal PrP deposits (D, E, F) or granularity (G, H, I), as observed by ICSM 35 antibody staining. Synaptic density was scored as mild (D), intermediate = 2 (E) or strong = 3 (F); granularity was scored as mild = 1 (G), intermediate = 2 (H) or dense = 3 (I). Gliosis was scored taking into account proportion of reactive cells and the intensity of GFAP staining, as mild = 1 (J), intermediate = 2 (K) or severe = 3 (L).

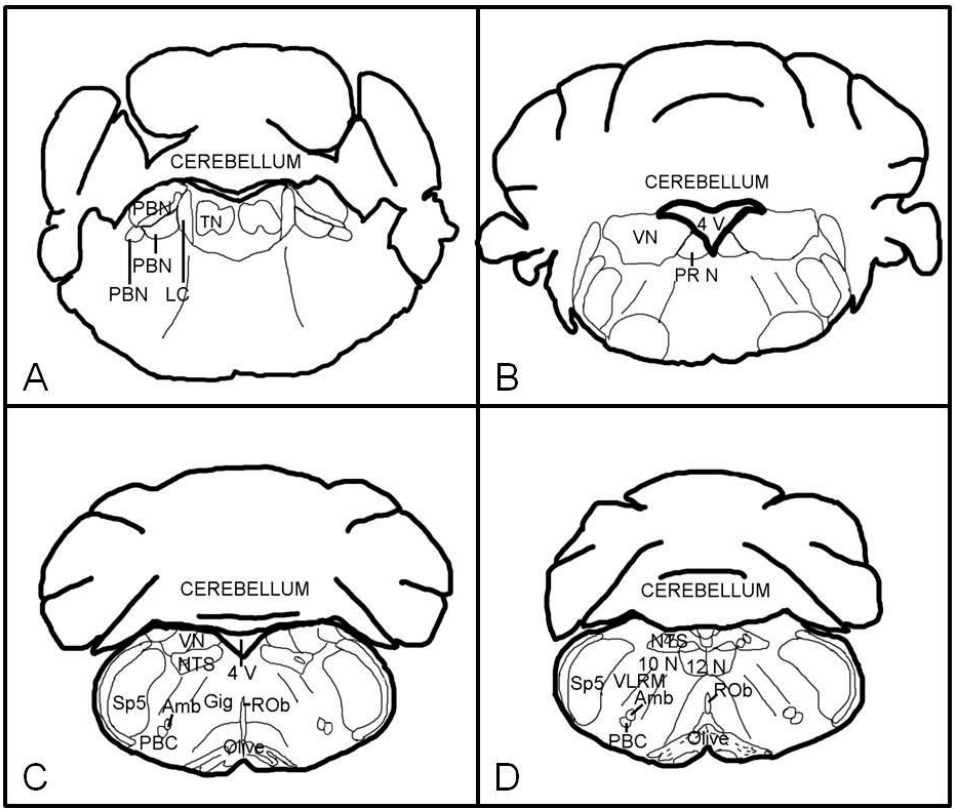

Figure 4.4 Location of the brainstem nuclei

The scheme has been adapted from the Paxinos Mouse Brain Atlas.

A = -5.34 mm from Bregma; B = - 6.00 mm from Bregma; C= - 6.84 mm from Bregma; D = -7.32 mm from Bregma.

List of abbreviations:

PBN = parabrachial nuclei; TN = tegmental nuclei; LC= locus coeruleus; VN= vestibular nuclei;

PR N= prepositus nucleus; 4 V = forth ventricle; NTS= nucleus of the solitary tract; Sp5= spinal nucleus of the V nerve; VLRM= ventro-lateral reticular medulla; Amb= nucleus ambiguous; PBC= pre-Bötzinger complex; ROb = raphe obscurus; 10 N= nucleus of the X nerve; 12N= nucleus of the XII nerve.

4.4.2.1 Brainstem pathology in RML inoculated M*lox*P mice at the end stage of prion disease

The pathological findings in the brainstem of RML infected M*lox*P mice were consistent. Spongiosis ranged between mild in the tegmental nuclei, locus

coeruleus and parabrachial nucleus, to intermediate in the vestibular and prepositus nuclei.

The pattern of abnormal PrP deposition was synaptic, with widespread staining ranging from mild in the autonomic centres, gigantocellular reticular nucleus, nucleus of the solitary tract, ventro-lateral medulla, and pre-Bötzinger complex, intermediate in the motor control areas (vestibular, prepositus nuclei) and autonomic areas (tegmental and parabrachial nuclei), to severe in the locus coeruleus and the olive.

Gliosis did not always correspond to the abnormal PrP deposition, as the areas with severe abnormal PrP deposition (such as tegmental nucleus, parabrachial nucleus and the locus coeruleus) showed relatively mild reactive gliosis, whereas other motor control areas, such as vestibular nucleus, prepositus nucleus and olive showed more severe gliosis.

The cerebellum in these animals was less spongiotic than all the brainstem nuclei analysed, and it showed mild abnormal PrP accumulation and very mild reactive gliosis (Figure 4.5; Table 4.1).

4.4.2.2 Brainstem pathology in RML inoculated NFH-M*lox*P culled at 12 wpi

Prion-related pathology at 12 wpi was markedly different in clinically healthy PrP depleted animals compared to non-recombined M*lox*P mice which were terminal at that time.

In PrP depleted mice, spongiosis was almost completely absent, with only the locus coeruleus being mildly affected. This nucleus showed the most severe accumulation of abnormal PrP. Abnormal PrP deposition in RML-infected NFH-*MloxP* was patchy, and coarse granular, rather than synaptic. Other nuclei with marked PrP deposition were the parabrachial and tegmental nuclei, followed by gigantocellular nucleus, the nucleus of the solitary tract and the olive. Gliosis correlated best with abnormal deposition in the locus coeruleus and the nucleus of the solitary tract, where it was intermediate, but was variable in the other nuclei.

The cerebellum showed a very mild pathology (spongiosis, gliosis and PrP deposition) (Figure 4.6; Table 4.1).

4.4.2.3 Brainstem pathology in RML inoculated NFH-M*lox*P mice at end stage of prion disease

Terminally ill NFH-*MloxP* mice showed an overall pathology that was significantly different from that of RML infected M*lox*P mice. The gigantocellular reticular nucleus, ventro-lateral reticular medulla and the pre-Bötzinger complex were mildly spongiotic, while the other nuclei varied from intermediate to severe spongiosis, with the locus coeruleus being the most affected area. Also the cerebellum showed severe spongiosis, which is interpreted as a consequence of the prolonged incubation time, as it is not seen in terminally ill RML infected M*lox*P mice at 12wpi. The abnormal prion protein deposition in NFH-*MloxP* mice appeared different from that observed in M*lox*P mice, in that the majority of the brainstem was spared from PrP deposition with only a few patchy granules appearing, probably as a result of the removal of neuronal PrP through Cre-mediated recombination. Interestingly, areas with the highest scores were the locus coeruleus, the nucleus of the solitary tract and, outside the brainstem, the cerebellum (Figure 4.7, Table 4.1). For the first time, we also observed accumulation in the tracts of the cranial nerves (Figure 4.8 A), within the perivascular Virchow-Robin spaces and in the brain parenchyma directly surrounding them (Figure 4.8 B). As this was absent in shorter surviving RML infected M*lox*P mice, it can be ascribed to a secondary effect of the prolonged incubation time. The distribution of gliosis in the different nuclei matched the abnormal PrP accumulation (Figure 4.7, Table 4.1).

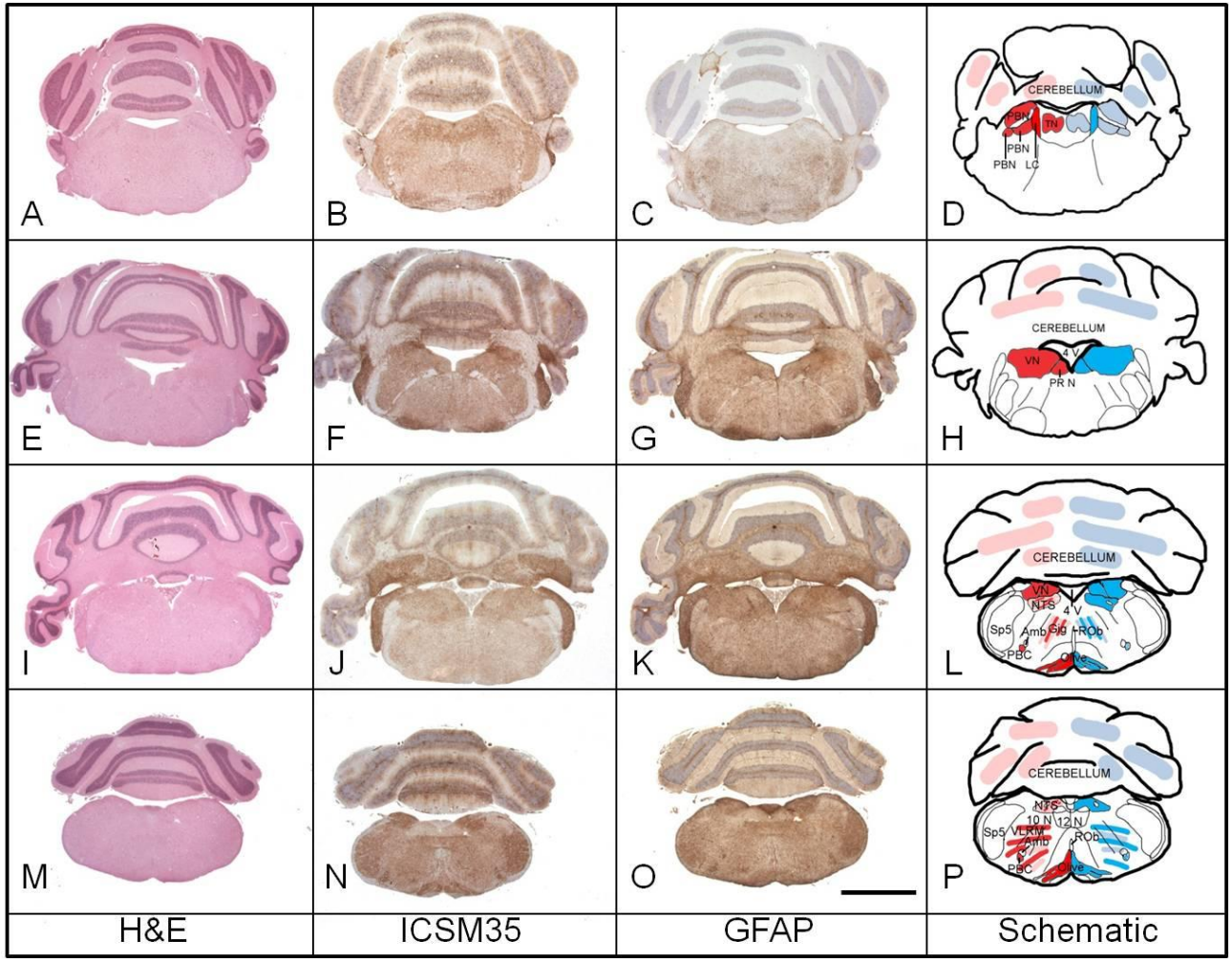

Figure 4.5 Brainstem pathology in RML inoculated M*lox*P mice at end stage of prion disease

Brain sections of RML inoculated M*lox*P mice were stained with haematoxylin and eosin (H&E) (A, E, I, M) and immunostained with ICSM35 antibody for PrP^{Sc} deposition (B, F, J, N) and an anti-GFAP antibody for detection of astrocytosis (C, G, K, O). In D, H, L, P a schematic representation of abnormal PrP deposition (red) and spongiosis (blue) of the brainstem nuclei analysed is shown. Gliosis mimicked the abnormal PrP schematic unless otherwise stated. Spongiosis was intermediate in the vestibular (E,I,H,L) and prepositus (E,H) nuclei and mild in tegmental nuclei (E, H), locus coeruleus and parabrachial nucleus(A,D) and cerebellum (A,E,I,M,D,H,L,P). PrP deposition was severe in the locus coeruleus (B,D) and the olive (N,P); intermediate in the vestibular (F,J, H,L) prepositus (F, H); tegmental and parabrachial nuclei (B,D) , and mild in the gigantocellular reticular nucleus , nucleus of the solitary tract, ventro-lateral medulla, and pre-Bötzinger complex (J, L, N, P) and cerebellum (B,F,J,N,D,H,L,P). Gliosis was intermediate in vestibular nucleus (G), prepositus nucleus(G) and olive (O) and mild//intermediate in the tegmental nuclei (C), parabrachial nucleus (C) and the locus coeruleus(C), the nucleus of the solitary tract, ventro-lateral medulla and pre-Bötzinger complex (K,O).

Scale bar= 4mm; Abbreviations: PBN = parabrachial nuclei; TN = tegmental nuclei; LC= locus coeruleus; VN= vestibular nuclei;

PR N= prepositus nucleus; 4 V = forth ventricle; VN= vestibular nuclei; NTS= nucleus of the solitary tract; Sp5= Spinal nucleus of the V nerve; VLRM= ventro-lateral reticular medulla; Amb= nucleus ambiguous; PBC= pre-Bötzinger complex; ROb = raphe obscurus; 10 N= nucleus of the X nerve; 12 N= nucleus of the XII nerve.

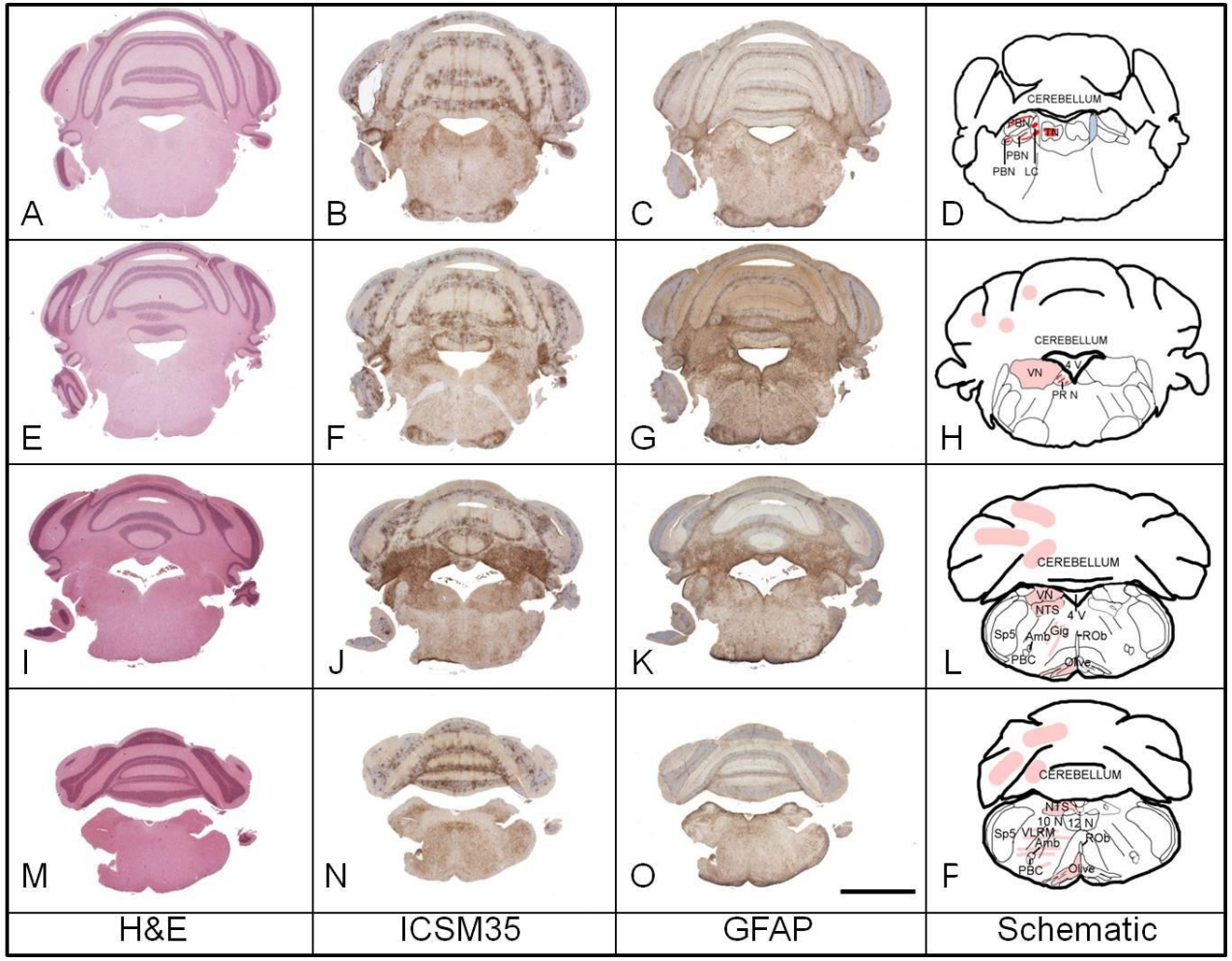

Figure 4.6 Brainstem pathology of RML inoculated NFH-*MloxP* mice at 12 wpi

Brain sections of RML inoculated NFH-Cre/M*lox*P mice culled at 12 wpi were stained with haematoxylin and eosin (H&E) (A, E, I, M) and immunostained with ICSM35 antibody for PrP^{Sc} deposition (B, F, J, N) and an anti-GFAP antibody for detection of astrocytosis (C, G, K, O). In D, H, L, P a schematic representation of abnormal PrP deposition (red) and spongiosis (blue) of the brainstem nuclei analysed is shown. Gliosis mimicked the abnormal PrP schematic unless otherwise stated.

Spongiosis was almost completely absent everywhere, but it was mild in the locus coeruleus (A, D). This nucleus was also the one with the most severe abnormal PrP accumulation (B, D). Other nuclei affected by abnormal deposition were the tegmental and the parabrachial nuclei (B, D) and mildly the gigantocellular nucleus, the nucleus of the solitary tract and the olive (J, N L, F). Gliosis correlated with abnormal deposition in some nuclei like the locus coeruleus (C) and the nucleus of the solitary tract (K) while in the other nuclei it was less evident.

The cerebellum showed a very mild pathology in respect of all the three parameters, as evident in all the pictures of the panel.

Scale bar= 4mm; Abbreviations: PBN = parabrachial nuclei; TN = tegmental nuclei; LC= locus coeruleus; VN= vestibular nuclei;

PR N= prepositus nucleus; 4 V = forth ventricle; VN= vestibular nuclei; NTS= nucleus of the solitary tract; Sp5= Spinal nucleus of the V nerve; VLRM= ventro-lateral reticular medulla; Amb= nucleus ambiguous; PBC= pre-Bötzinger complex; ROb = raphe obscurus; 10 N= nucleus of the X nerve; 12 N= nucleus of the XII nerve.

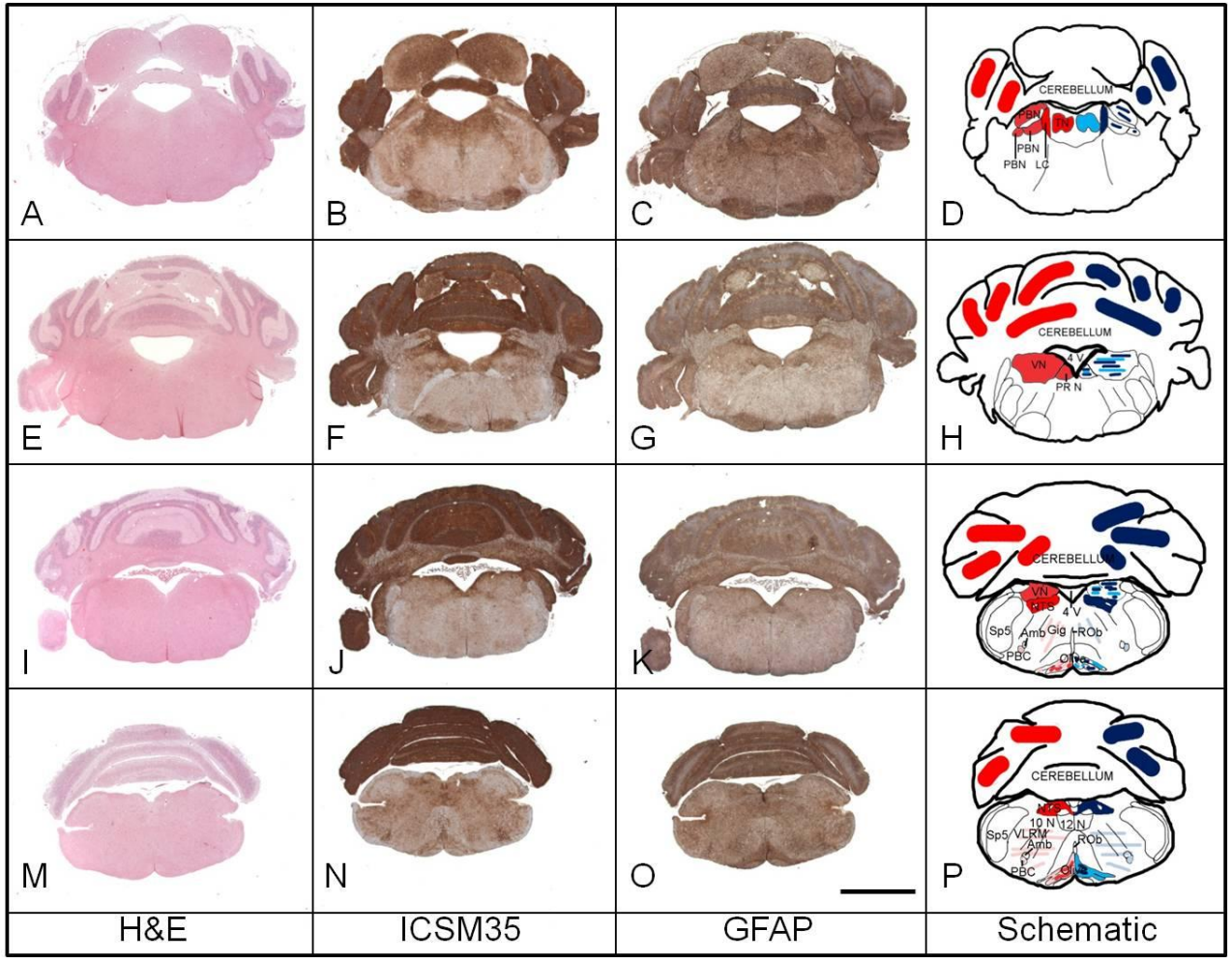

Figure 4.7 Brainstem pathology of RML inoculated NFH-*MloxP* mice at end stage of prion disease

Brain sections of RML inoculated NFH-Cre/M*lox*P mice culled at 12 wpi mice were stained with haematoxylin and eosin (H&E) (A, E, I, M) and immunostained with ICSM35 antibody for PrP^{Sc} deposition (B, F, J, N) and an anti-GFAP antibody for detection of astrocytosis (C, G, K, O). In D, H, L, P a schematic representation of abnormal PrP deposition (red) and spongiosis (blue) of the brainstem nuclei analysed is shown. Gliosis mimicked the abnormal PrP schematic unless otherwise stated.

Spongiosis was spread in all the brainstem nuclei analysed, most severe in the locus coeruleus (A,D) the nucleus of the solitary tract (I,M,L,P) and the cerebellum (A,E,I,M,D,H,L,P),severe/ intermediate in the parabrachial (A,D), vestibular and prepositus nuclei (E,H), tegmental nuclei (A,D) and olive (I,M,L,P) and mild in gigantocellular reticular nucleus, ventro-lateral reticular medulla and the pre-Bötzinger complex (I,M,L, P). The majority of the brainstem was spared from deposition, with just few patchy granules and areas with the maximal scores were the locus coeruleus (B, D), the nucleus of the solitary tract (J, N, L, P) and, outside the brainstem, the cerebellum (B,F, J,N,D,H,L,P).The distribution of gliosis in the different nuclei mimicked the abnormal PrP accumulation (C ,G, K, O, D, H, L ,P).

Scale bar= 4mm; Abbreviations: PBN = parabrachial nuclei; TN = tegmental nuclei; LC= locus coeruleus; VN= vestibular nuclei;

PR N= prepositus nucleus; 4 V = forth ventricle; VN= vestibular nuclei; NTS= nucleus of the solitary tract; Sp5= Spinal nucleus of the V nerve; VLRM= ventro-lateral reticular medulla; Amb= nucleus ambiguous; PBC= pre-Bötzinger complex; ROb = raphe obscurus; 10 N= nucleus of the X nerve; 12 N= nucleus of the XII nerve.

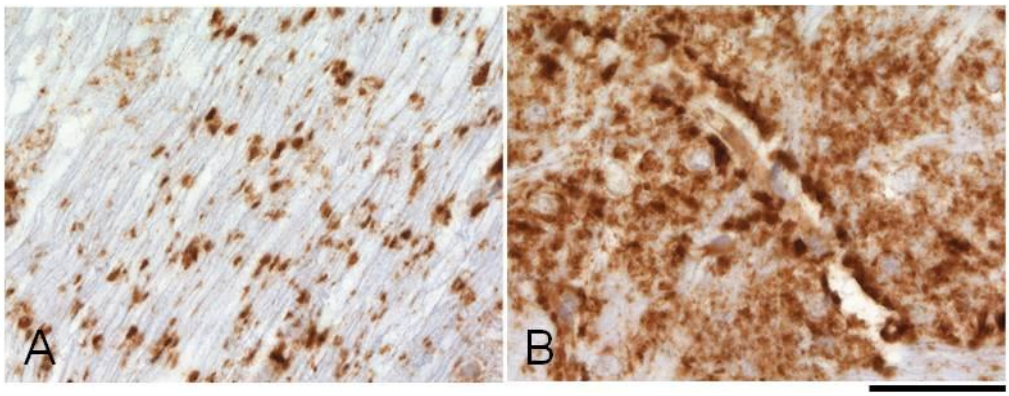

Figure 4.8 Granular PrP deposition in RML inoculated NFH-Cre/M*lox*P mice

In RML inoculated NFH-Cre/M*lox*P mice PrP deposition was also found in areas spared in RML inoculated M*lox*P mice, like the tracts of the cranial nerves (A) and the Virchow-Robin spaces (B), suggesting that the prolonged survival allows the spread of prions in areas not primarily targeted by the infection.

Scale bar = 60 µm.

4.4.2.4 Brainstem pathology in Me7 inoculated M*lox*P mice at end stage of prion disease

Because many prion strains elicit a strain-specific pathological phenotype, the histopathological features of terminally ill Me7 inoculated M*lox*P mice were different from those of end stage RML inoculated M*lox*P. All scored nuclei showed high degree of spongiosis, ranging from intermediate in the pre-Bötzinger complex to severe in the locus coeruleus, the tegmental and parabrachial nuclei, and slightly less in the nucleus of the solitary tract and vestibular and prepositus nuclei. Abnormal PrP deposition was both synaptic and granular and it correlated well with spongiosis, with strong deposition in the vestibular and prepositus nucleus, locus coeruleus, tegmental and parabrachial nuclei, nucleus of the solitary tract. Among the motor control areas, the olive showed severe accumulation. As an exception, the pre-Bötzinger complex, which was just mildly spongiotic, showed severe abnormal PrP accumulation. The reactive astrogliosis was uniformly distributed, ranging from intermediate to severe.

As observed in the pilot experiment of Me7 inoculation in M*lox*P mice (chapter 3) and in RML infected M*lox*P mice, the cerebellum was not among the most severely affected areas. Abnormal PrP deposition was scored lowest among all the examined areas, and spongiosis and gliosis were intermediate (Figure 4.9, table 4.1).

4.4.2.5 Brainstem pathology in Me7 inoculated NFH-Cre/M*lox*P mice culled at 16 wpi

PrP depletion significantly reduced pathological changes in brainstem nuclei of Me7 infected NFH-Cre/*MloxP* mice at 16 wpi. Spongiosis was reduced and scored as mild throughout, with the exception of the locus coeruleus with intermediate score. This was also the only nucleus with intermediate levels of PrP accumulation, followed by the olive, the gigantocellular nucleus and the nucleus of the solitary tract. The pre-Bötzinger complex was the nucleus in which the effect of PrP depletion was more evident: PrP accumulation was scored as severe in M*lox*P mice and NFH-Cre/M*lox*P mice showed just mild accumulation. The locus coeruleus exhibited the (relatively) strongest gliosis (intermediate), followed by the nucleus of the solitary tract. In the cerebellum, pathology was very mild, confirming the

previous observation that this area of the brain is not one of the first targets of prion deposition and pathology. (Figure 4.10; Table 4.1)

4.4.2.6 Brainstem pathology in Me7 inoculated NFH-Cre/M*lox*P mice at the end-stage of prion disease

Marked spongiosis in the brainstem of these mice was a consistent feature, albeit slightly less that in terminally ill, undepleted mice. The most affected nucleus was the locus coeruleus with strong spongiosis, prion protein deposition and reactive astrogliosis. As observed in RML inoculated NFH-Cre/M*lox*P mice at end stage, the nucleus of the solitary tract and the cerebellum showed severe deposition, while the other nuclei ranged from mild (pre-Bötzinger complex) to intermediate, confirming an overall protection of prion deposition (probably due to Cre-mediated recombination) (Figure 4.11; Table 4.1). PrP accumulation in the tracts of the cranial nerves and in the Virchow-Robin spaces was also observed, similar to that in RML infected NFH-Cre/M*lox*P mice (Figure 4.12). Gliosis was congruent to abnormal PrP accumulation. It was generally intermediate, milder in the pre-Bötzinger complex and gigantocellular nucleus and most severe in the cerebellum and locus coeruleus (Figure 4.11; Table 4.1).

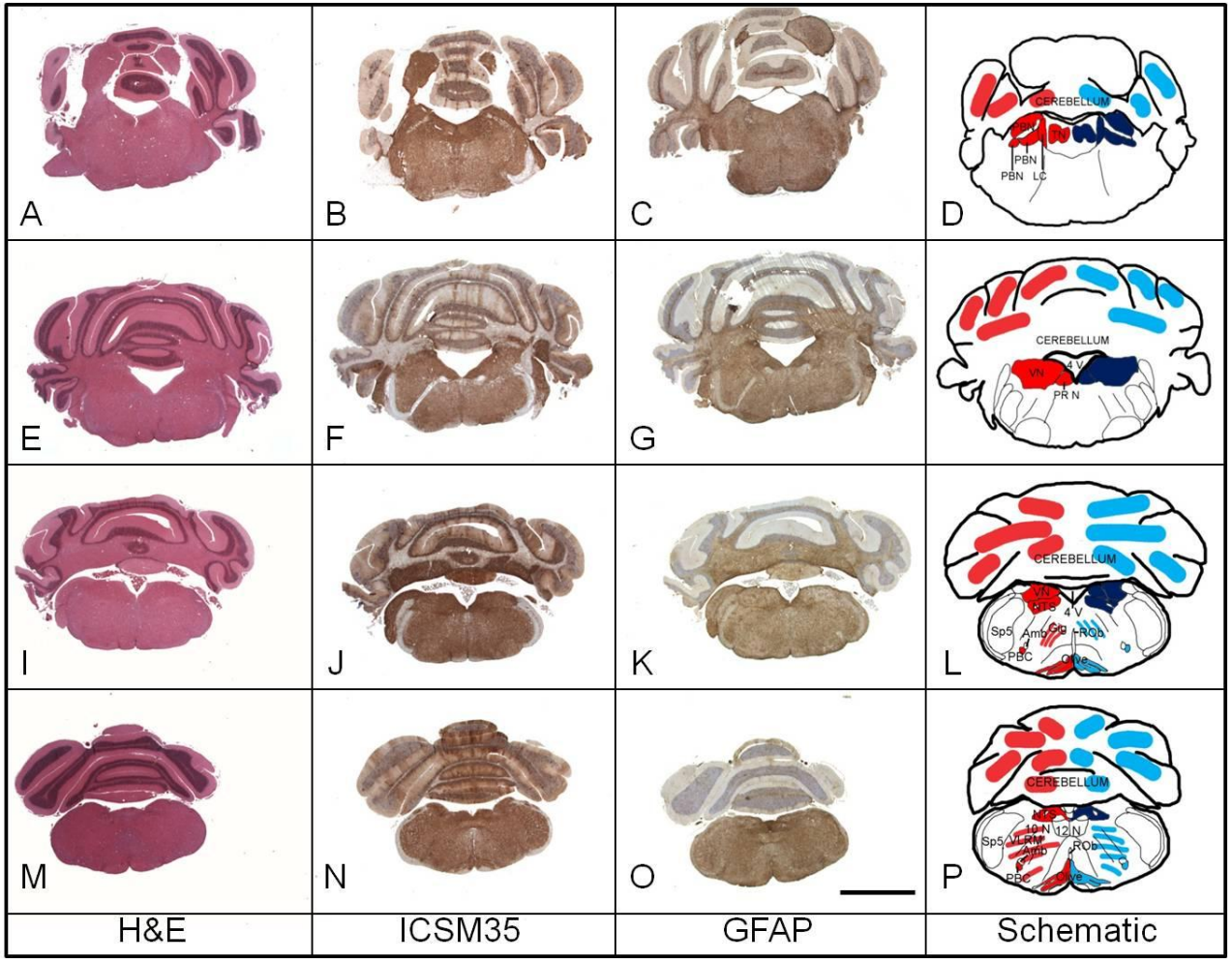

Figure 4.9 Brainstem pathology in Me7 inoculated M*lox*P mice at end stage of prion disease

Brain sections of Me7 inoculated M*lox*P mice were stained with haematoxylin and eosin (H&E) (A, E, I, M) and immunostained with ICSM35 antibody for PrP^{Sc} deposition (B, F, J, N) and an anti-GFAP antibody for detection of astrocytosis (C, G, K, O). In D, H, L, P a schematic representation of abnormal PrP deposition (red) and spongiosis (blue) of the brainstem nuclei analysed is shown. All the scored nuclei showed high degree of spongiosis: severe in the locus coeruleus (A, D), the tegmental and parabrachial nuclei (A, D), the vestibular and prepositus nuclei (E, I, H, L) and the nucleus of the solitary tract (I, M, L, P), and intermediate in the pre-Bötzinger complex, ventro-lateral reticular medulla and olive (I, M, L, P). Abnormal PrP deposition correlated with spongiosis, being more severe in nuclei where spongiosis was also severe, like locus coeruleus (B, D), tegmental and parabrachial nuclei (B, D), vestibular (F, H), nucleus of the solitary tract (J, N, L, P). The pre-Bötzinger complex, which was just mildly spongiotic, showed severe abnormal PrP accumulation (J, N, L, P). The reactive astrogliosis was uniformly distributed (C, G, K, O, D, H, L, P).

Scale bar= 4mm; Abbreviations: PBN = parabrachial nuclei; TN = tegmental nuclei; LC= locus coeruleus; VN= vestibular nuclei;

PR N= prepositus nucleus; 4 V = forth ventricle; VN= vestibular nuclei; NTS= nucleus of the solitary tract; Sp5= Spinal nucleus of the V nerve; VLRM= ventro-lateral reticular medulla; Amb= nucleus ambiguous; PBC= pre-Bötzinger complex; ROb = raphe obscurus; 10 N= nucleus of the X nerve; 12N= nucleus of the XII nerve.

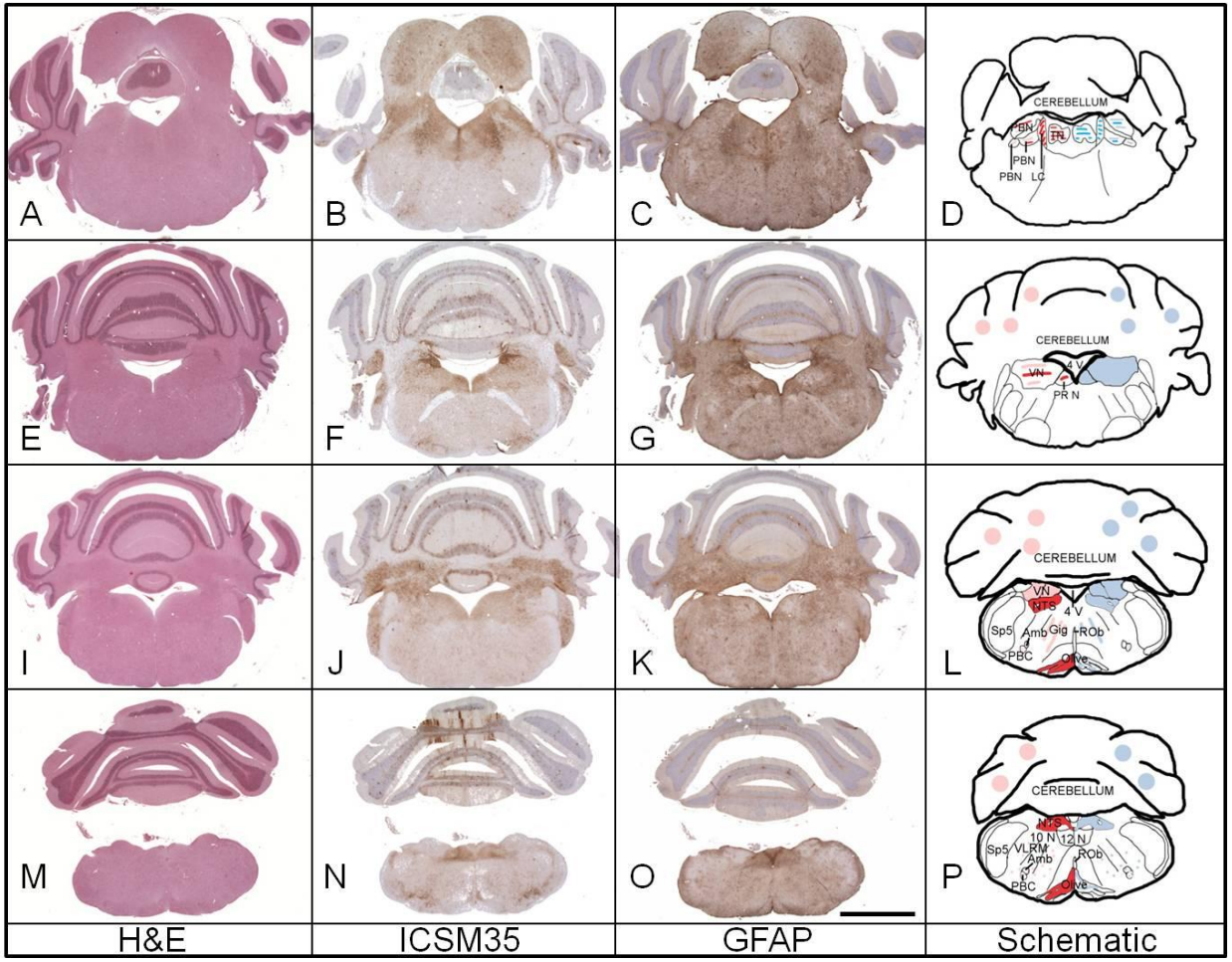

Figure 4.10 Brainstem pathology of Me7 inoculated NFH-*MloxP* mice at 16 wpi

Brain sections of Me7 inoculated M*lox*P mice were stained with haematoxylin and eosin (H&E) (A, E, I, M) and immunostained with ICSM35 antibody for PrP^{Sc}

deposition (B, F, J, N) and an anti-GFAP antibody for detection of astrocytosis (C, G, K, O). In D, H, L, P a schematic representation of abnormal PrP deposition (red) and spongiosis (blue) of the brainstem nuclei analysed is shown. Spongiosis was reduced everywhere compared to Me7 inoculated M*lox*P mice at end stage of prion disease: all the other nuclei analysed were mildly spongiotic (A, E, I, M, D, H, L, P) the only nucleus showing intermediate level of spongiosis was the locus coeruleus (A, D). Abnormal PrP accumulation was more intense in the locus coeruleus (B,D), nucleus of the solitary tract (J, N, L, P) and olive (N, O) followed by the parabrachial and tegmental nuclei (B, D), vestibular and prepositus nuclei (F, H) and gigantocelluar reticular nucleus (J, L). Deposition was mild in the pre-Bötzinger complex and ventro-later reticular medulla (J, N, L, P). The distribution of gliosis in the different nuclei mimicked the abnormal PrP accumulation (C, G, K, O, D, H, L, P)

In the cerebellum, spongiosis, abnormal accumulation and gliosis were very mild.

Scale bar= 4mm; Abbreviations: PBN = parabrachial nuclei; TN = tegmental nuclei; LC= locus coeruleus; VN= vestibular nuclei;

PR N= prepositus nucleus; 4 V = forth ventricle; VN= vestibular nuclei; NTS= nucleus of the solitary tract; Sp5= Spinal nucleus of the V nerve; VLRM= ventro-lateral reticular medulla; Amb= nucleus ambiguous; PBC= pre-Bötzinger complex; ROb = raphe obscurus; 10 N= nucleus of the X nerve; 12N= nucleus of the XII nerve.

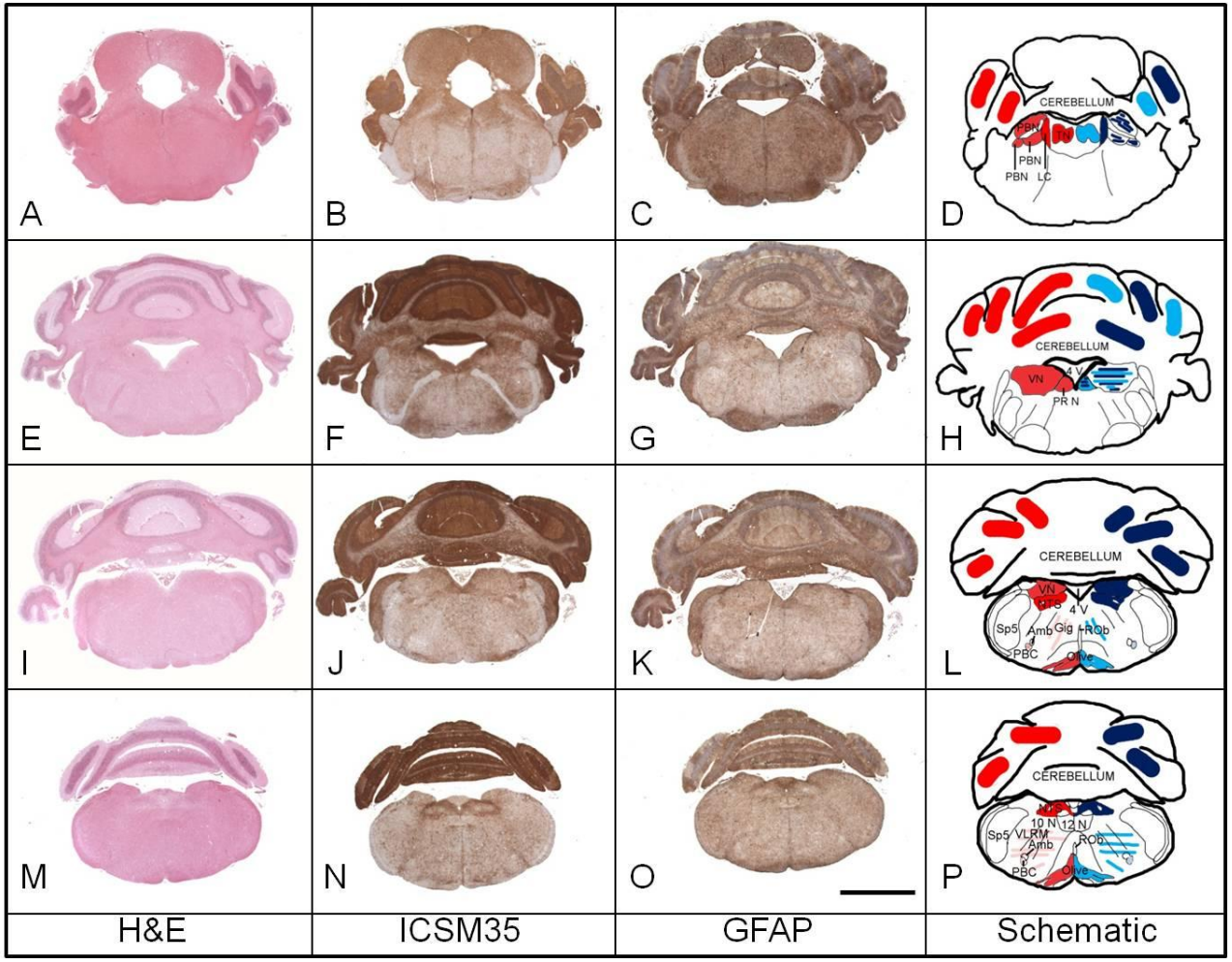

Figure 4.11 Brainstem pathology of Me7 inoculated NFH-*MloxP* mice at end stage of prion disease

Brain sections of Me7 inoculated NFH-Cre/M*lox*P mice were stained with haematoxylin and eosin (H&E) (A, E, I, M) and immunostained with ICSM35 antibody for abnormal PrP deposition (B, F, J, N) and an anti-GFAP antibody for detection of astrocytosis (C, G, K, O). In D, H, L, P a schematic representation of abnormal PrP deposition (red) and spongiosis (blue) of the brainstem nuclei analysed is shown.

Spongiosis was severe in the locus coeruleus (A, D), parabrachial nuclei (A, D) and nucleus of the solitary tract; (I, M, L, P); severe/intermediate in the tegmental nuclei (A, D), vestibular nuclei (E, H), prepositus nucleus (E, H), and cerebellum (A, E, I, M, D, H, L, D, P) and intermediate in the gigantocellular nucleus (I, L), ventro-lateral medulla and olive (M, P). It was mild in the pre-Bötzinger complex (I, M, L, P). The locus coeruleus had also the high degree of abnormal PrP accumulation (B, D), with the cerebellum (B, F, J, N, D, H, L, P) and the nucleus of the solitary tract (J, N, L, P). PrP deposition was intermediate in the tegmental (B, D), parabrachial (B, D), vestibular (F, H) and prepositus nuclei (F, H), and in the olive (N, P); and mild in the gigantocellular nucleus (J, L), ventro-lateral reticular medulla and pre-Bötzinger complex (N, P).

Gliosis was occurred in the same areas of abnormal PrP accumulation and ranged from mild in the pre-Bötzinger complex (K, O) and gigantocellular nucleus (K) to severe in the cerebellum (C, G, K, O) and locus coeruleus (C).

Scale bar= 4mm; Abbreviations: PBN = parabrachial nuclei; TN = tegmental nuclei; LC= locus coeruleus; VN= vestibular nuclei;

PR N= prepositus nucleus; 4 V = forth ventricle; VN= vestibular nuclei; NTS= nucleus of the solitary tract; Sp5= Spinal nucleus of the V nerve; VLRM= ventro-lateral reticular medulla; Amb= nucleus ambiguous; PBC= pre-Bötzinger complex; ROb = raphe obscurus; 10 N= nucleus of the X nerve; 12N= nucleus of the XII nerve.

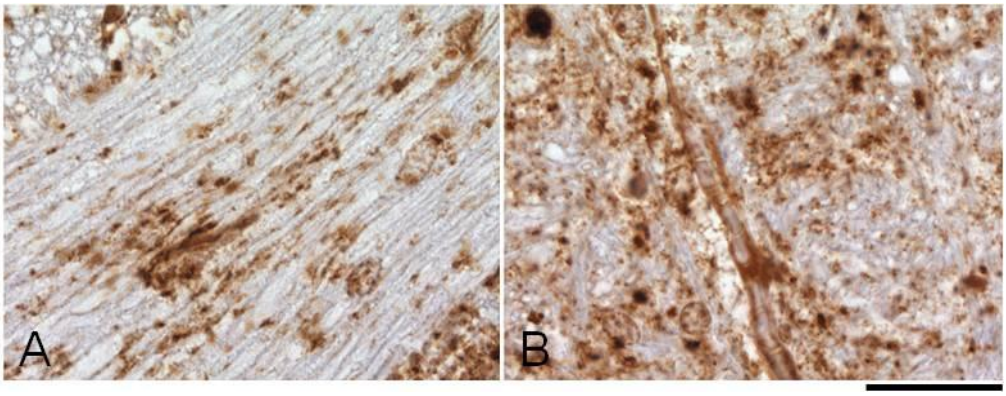

Figure 4.12 Diffuse PrP deposition in Me7 inoculated NFH-Cre/M*lox*P mice

In Me7 inoculated NFH-Cre/M*lox*P mice PrP deposition was found also in the tracts of the cranial nerves (A) and the Virchow-Robin spaces (B). This characteristic deposition was previously found in RML inoculated NFH-Cre/M*lox*P mice, and highlighted the similarity in the lesion profiles of RML and Me7 inoculated NFH-Cre/M*lox*P mice. Scale bar = 60 µm.

	End-stage RML infected M*lox* P mice										
	motor control				autonomic activity						
	V N	PR N	Olive	CRBM	T N	L C	PBN	Gig	NTS	VLRM	PBC
spongiosis	2.0	2.0	1.5	1.1	1.3	1.4	1.3	1.5	1.7	1.5	1.3
abnormal PrP	2.0	2.3	3.0	1.0	2.0	3.0	1.7	1.5	1.3	1.3	1.5
gliosis	2.0	2.3	2.0	0.7	0.8	1.0	0.6	1.5	0.5	1.5	1.3

	RML infected NFH-Cre/M*lox* P mice time culled at 12 wpi										
	motor control				autonomic activity						
	V N	PR N	Olive	CRBM	T N	L C	PBN	Gig	NTS	VLRM	PBC
spongiosis	0.0	0.0	0.2	0.0	0.0	0.7	0.3	0.2	0.0	0.0	0.0
abnormal PrP	1.0	1.5	1.2	1.0	1.7	2.5	1.7	1.0	0.8	1.0	0.5
gliosis	0.5	1.0	1.0	1.0	0.8	0.8	0.8	1.0	1.0	0.8	1.0

	End-stage RML infected NFH-Cre/M*lox* P mice										
	motor control				autonomic activity						
	V N	PR N	Olive	CRBM	T N	L C	PBN	Gig	NTS	VLRM	PBC
spongiosis	2.6	2.5	2.5	2.8	2.1	3.0	2.6	1.0	2.8	1.0	1.1
abnormal PrP	1.9	2.3	1.5	3.0	2.3	3.0	2.3	1.0	3.0	0.8	1.4
gliosis	2.0	2.4	2.0	3.0	1.9	3.0	2.0	1.3	2.6	1.5	1.2

	End-stage Me7 infected M*lox* P mice										
	motor control				autonomic activity						
	V N	PR N	Olive	CRBM	T N	L C	PBN	Gig	NTS	VLRM	PBC
spongiosis	2.8	2.8	2.2	2.0	3.0	3.0	3.0	2.3	2.8	2.2	1.8
abnormal PrP	2.8	2.8	3.0	1.8	2.8	3.0	2.8	2.2	3.0	2.2	3.0
gliosis	2.3	2.7	2.5	2.0	2.3	2.7	2.0	2.0	2.3	2.0	2.3

	Me7 infected NFH-Cre/M*lox* P mice time culled at 16 wpi										
	motor control				autonomic activity						
	V N	PR N	Olive	CRBM	T N	L C	PBN	Gig	NTS	VLRM	PBC
spongiosis	0.8	1.0	0.7	0.7	1.3	2.0	1.5	0.7	1.0	0.7	0.5
abnormal PrP	1.3	1.3	2.3	0.5	1.8	2.5	1.7	1.3	2.3	0.7	1.0
gliosis	0.5	1.3	0.7	0.5	1.5	2.0	1.0	1.2	1.8	1.3	1.2

	End-stage Me7 infected NFH-Cre/M*lox* P mice										
	motor control				autonomic activity						
	V N	PR N	Olive	CRBM	T N	L C	PBN	Gig	NTS	VLRM	PBC
spongiosis	2.5	2.8	2.0	2.5	2.5	3.0	2.8	1.8	2.7	2.0	1.2
abnormal PrP	1.8	1.8	2.0	3.0	2.3	3.0	2.3	1.2	3.0	1.2	1.3
gliosis	1.8	2.0	2.5	2.2	2.0	2.8	2.3	1.5	2.8	1.8	1.2

Table 4.1 Scoring of brainstem nuclei pathology

Sections spanning the area of interest were stained with haematoxylin and eosin to follow progression of spongiosis, ICSM 35 antibody for abnormal PrP deposition and anti-GFAP antibody to follow gliosis progression. Sections were analysed microscopically and degree of spongiosis, abnormal PrP deposition and gliosis in different brainstem nuclei were evaluated, using a scoring system ranging

from non-existent (0) to maximum (3). For every group, a minimum of 3 brains were analysed and their scores averaged.

4.4.3 Comparison of end stage pathology after Me7 and RML infection of NFH-Cre/M*lox*P mice: selection of a new strain?

Individual prion strains have different incubation times and show distinct pathology upon inoculation. As shown so far, RML and Me7 inoculated M*lox*P mice showed distinct pathology. Yet, in RML or Me7 infected NFH-Cre/M*lox*P mice, abnormal PrP deposition in the analysed coronal levels showed similarities both for phenotype of deposition and affected nuclei. (i) In both cases the phenotype of PrP accumulation was granular rather than synaptic; (ii) the most affected nuclei were the locus coeruleus, the nucleus of the solitary tract, and the cerebellum; (iii) in both infections, abnormal deposition was also observed in the cranial nerves and Virchow-Robin spaces. The observation that inoculations with the two different prion strains generate perfectly super imposable phenotypes suggested that depletion of neuronal PrP in the NFH-Cre/M*lox*P line may have selected a specific strain that might not have been the dominant species in the prion inoculum ensemble, in line with the strain selection model described in paragraph 1.1.3.4. The phenotype of these two infections is indeed different from the respective undepleted controls (RML in M*lox*P mice and Me7 in M*lox*P).

Strain selection is a phenomenon that can occur upon passaging of an inefficiently propagating strain in a new host, resulting in a new, distinct strain (Bruce, 1993). It can occur upon inter-species transmission, because the PrP sequence of the host is different from that of the inoculum, or in intra-species transmission, suggesting an effect of modifier loci on strain selection (Lloyd et al., 2004). Recently, Li e al. showed how environmental modifications can affect strain selection pressure and favour an otherwise rare strain. The changes determining the strain shift were shown to be the host or chemical selection. The prion conformer dominating a brain-adapted prion ensemble replicated less rapidly than a cell-adapted form, once passaged from brain to susceptible cells. However, when the cell-adapted ensemble was returned to brain, the brain-adapted form became dominant again. Similarly the use of an inhibitor achieved selection for a resistant sub-strain, whereas, in its absence, the susceptible sub-strain outgrew its resistant counterpart (Li et al., 2010).

To test the hypothesis that passaging prion strains in neuronal PrP-depleted NFH-Cre/M*lox*P mice resulted in the selection of a new strain from the ensemble, a small scale experiment was set up. We planned to test this hypothesis both in mice and cells. Firstly, we planned to compare the survival and the lesion profile of mice injected with the original RML inoculum and mice injected with inoculum derived from RML passaged in NFH-Cre/M*lox*P mice; we also planned to use the two inocula in the scrapie cell assay (SCA) in PK1 cells (Klohn et al., 2003), as these cells allow propagation of RML prions but not of other prion strains.

4.4.3.1 Experimental setup

One brain from a terminally ill RML inoculated NFH-Cre/M*lox*P mouse was used to generate a 10% brain homogenate (I10716) to be used for infection. 1% of I10716, designated I10717, and the same RML brain homogenate used in the infection of M*lox*P and NFH-Cre/M*lox*P (I9900) were injected into 6 Tg20 overexpressing mice (Fischer et al., 1996) and 6 FVB wild type mice. A graphical representation of the experiment is shown in Figure 4.13. The PrP overexpressing Tg20 line was chosen because of its reduced incubation time. The wild-type mice have the same genetic background as the two transgenic lines used in the previous analysis (M*lox*P and NFH-Cre/M*lox*P). Mice were kept under observation from the first appearance of scrapie signs and culled when terminally ill. Their brains were taken for histopathology, fixed in BFS, and embedded in three pieces, to obtain coronal sections as described in 4.3.

At the time of writing this thesis, the only results available so far are mouse survival data. Future work will be needed to analyse the pathology profiles and to perform the SCA.

4.4.3.2 Different survival in I 9900 and I 10717 inoculated Tg20 overexpressing mice but not in FVB wild type

Tg20 overexpressing mice inoculated with subpassaged RML prions survived shorter than Tg20 mice inoculated with the original RML prion inoculum (56 +/- 3 days vs. 61 +/- 2 days; n=6, $p<0.004$). Wild type mice inoculated with subpassaged RML or original RML prion inoculum showed no difference in the incubation time (175+/- 8 days vs. 171 +/- 8 days; n=5) (Figure 4.14).

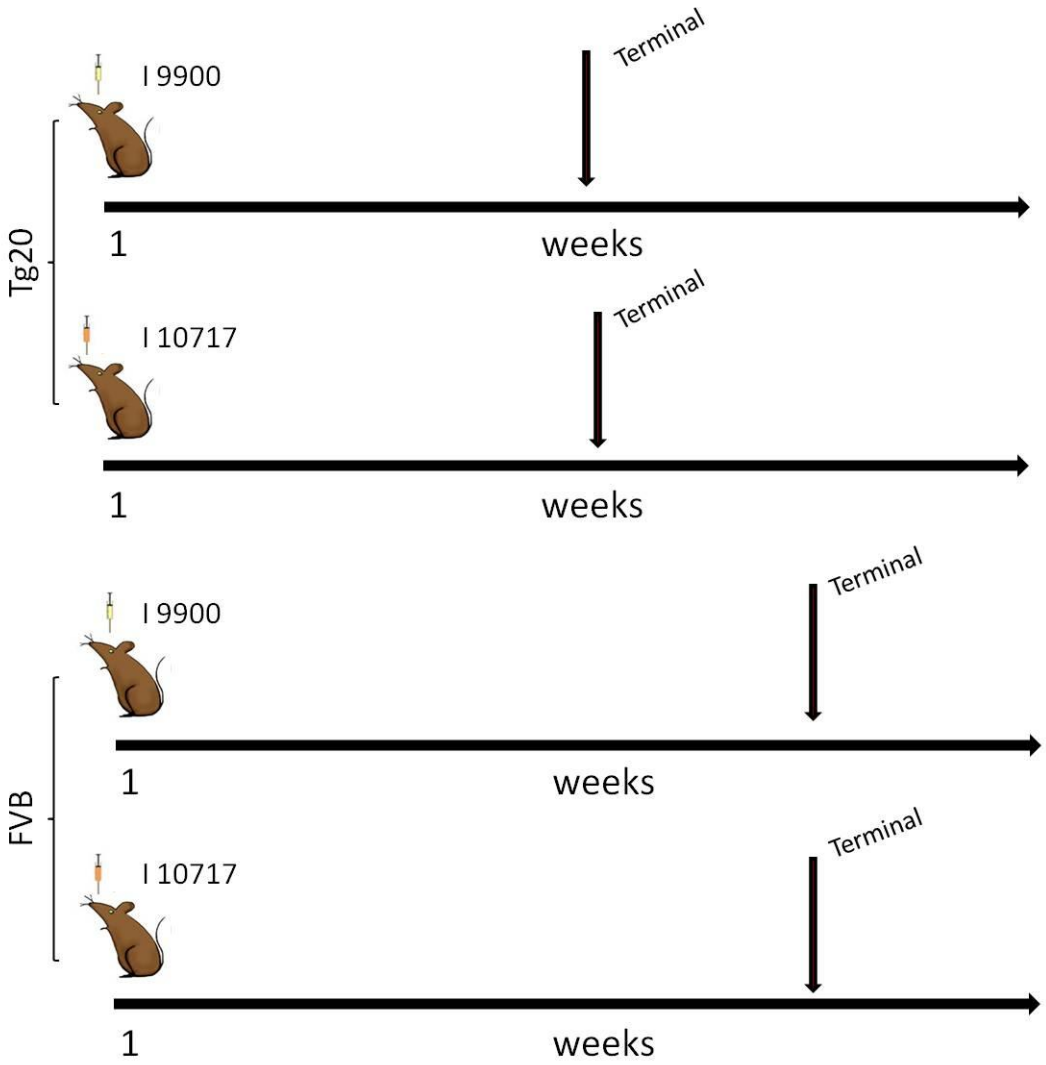

Figure 4.13 Is NFH-Cre/M*lox*P mouse line selecting a new strain? Description of the experimental plan

Abnormal PrP deposition in different coronal levels showed striking similarities in RML or Me7 inoculated NFH-Cre/M*lox*P mice both for phenotype of deposition and nuclei affected. This observation suggested that depletion of neuronal PrP in the NFH-Cre/M*lox*P line may have selected a new specific strain, not the previous dominant species in the prion inocula ensemble. To test the hypothesis that passaging of prion strains in neuronal depleted mice results in the selection of a new strain, we planned to compare the survival and the lesion profile of mice injected with the original RML inoculum (I9900) and mice injected with inoculum derived from RML passaged in NFH-Cre/M*lox*P mice (I 10717).

PrP overexpressing Tg20 and wild type FVB mice were inoculated with I9900 and I 10717. Mice were kept under observation from the first appearance of scrapie signs and culled when terminally ill and their brains were prepared for histopathological analysis.

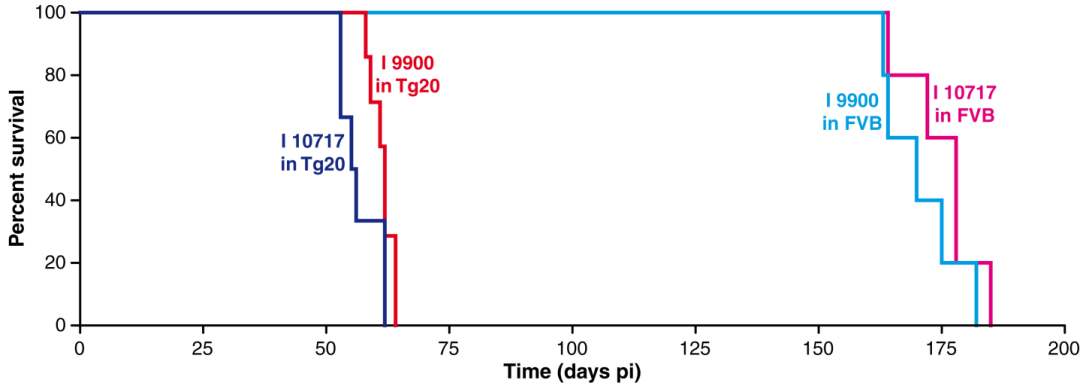

Figure 4.14 Different survival in I 9900 and I 10717 inoculated Tg20 overexpressing mice but not in FVB wild type

6 Tg20 PrP over expressing mice were inoculated with the original RML inoculum (I9900) and 6 Tg20 PrP over expressing mice were inoculated with RML subpassaged in NFH-Cre/M*lox*P mice (I17017). I 17017 inoculated Tg20 mice survived less than I9900 Tg 20 inoculated mice (56 +/- 3 days vs. 61 +/- 2 days; n=6, $p < 0.004$).

5 wild type FVB mice, inoculated with I9900 and 5 wild type FVB mice, inoculated with 17017 showed no difference in the incubation time (175+/- 8 days vs. 171 +/- 8 days;).

The discrepancy between the two results suggests that the RML inoculum is under a different strain selection in PrP overexpressing and wild type mice, however, histopathological analysis and further studies are required for conclusive results.

4.5 Discussion

Clinical target areas are defined as specific anatomical and functional areas of the CNS that are targets of prion infection and pathology, and therefore are thought to cause the clinical phenotype (Kimberlin and Walker, 1983). We hypothesised that these areas are either the first or the last targets of prion pathology.

In the "first target area" scenario, an area that first accumulates toxic species would be rate limiting in the disease process. This area would have to be relatively tolerant to a continuous accumulation of prion toxicity and would cause neurological dysfunction when high levels of toxicity exceed a critical threshold, manifesting as clinical phenotype. Conceptually different would be the "last target area hypothesis". In this case, a generalised widespread accumulation of "toxic species" in the context of prion disease would occur in the CNS. This widespread accumulation would not cause clinical impairment, until it localizes in vital areas. Therefore, the last areas that become functionally impaired would be the target areas, the impairment of which would cause the clinical symptoms. These areas would be relatively sensitive to prion accumulation compared to surrounding structures.

A previous study had shown that RML inoculated NFH-Cre/M*lox*P mice, undergoing adult neuronal PrP depletion through Cre-mediated recombination, are resistant to prion infection. Even though infected mice accumulated abnormal PrP in non-recombined cells, they did not succumb to the disease (Mallucci et al., 2003). Here we have shown that neuronal depletion of PrP in adult NFH-Cre/M*lox*P mice inoculated with Me7 and Mouse–adapted BSE slowed down the disease progression but these mice eventually succumbed to prion infection.

We approached the hypothesis that clinical target areas are the last targets, by comparing the difference in pathology between RML and other prion strains (Me7 and MRC2, the strain derived by passaging Mouse-adapted BSE in SJL mice), at the end stage of prion disease. We hypothesized that the clinical target areas could be one or more nuclei localized in the brainstem for the following reasons: First, its nuclei are in control of essential body functions, such as motor control, generation of the respiratory rhythm and regulation of the blood pressure. Second, the clinical signs that define an experimental mouse as terminally ill are suggestive of brainstem malfunction affecting both motor control (unsteady gate, tremor and ataxia), and respiratory control (abnormal breathing rate). Notably, in human prion disease, a

detailed analysis relating clinical signs suggestive of brainstem function impairment to histopathology is compromised because such clinical signs may mask the involvement of basal ganglia and cortex.

We inoculated RML, Me7 or MRC2 prion strains into M*lox*P mice, overexpressing PrP and NFH-Cre/M*lox*P mice that undergo neuronal Cre-mediated recombination and loss of PrP expression.

Our intention was to compare the pathology of terminally ill RML, Me7 or MRC2 infected M*lox*P mice, terminally ill Me7 or MRC2 infected NFH-Cre/M*lox*P mice and long term surviving RML infected NFH-Cre/M*lox*P mice and look at brainstem nuclei in RML infected NFH-Cre/M*lox*P mice that were protected from prion-mediated toxicity. These areas would have represented the clinical target areas in prion disease, because their absence or reduced pathology would have been sufficient to protect RML inoculated NFH-Cre/M*lox*P mice from progression to a clinical stage.

In contrast to previous studies, NFH-Cre/M*lox*P mice showed clinical signs of prion disease after ~35 weeks and ultimately succumbed to prion disease. These mice behaved like Me7 or MRC2 infected NFH-Cre/M*lox*P mice in that they survived significantly longer than their M*lox*P counterparts, but still developed clinical signs and succumbed to the disease (Figure 4.2). There are a number of possibilities to explain the discrepancy between the data reported here and that published previously by Mallucci et al. (Mallucci et al., 2003). Most important are the inocula and the inoculated mouse line. According to the most recent theory on prion strains, every strain exists as an ensemble and the cross-talk with the host environment defines which prion species will be successfully propagated (Collinge and Clarke, 2007). Although in both cases an RML inoculum was used, the two inocula came from different brain homogenates. This difference did not affect the incubation time in M*lox*P mice, which was ~12 weeks for both inocula, but may have had an effect in neuronal PrP depleted NFH-Cre/M*lox*P mice.

The second possibility is a change occurring in the transgenic mouse lines. NFH-Cre/M*lox*P mice are the result of a cross between PrP overexpressing M*lox*P mice and recombinase-Cre expressing NFH-Cre mice. It has previously been reported that Cre-mediated recombination in NFH-Cre/M*lox*P mice occurs at 9 weeks of age and it affects the entire neuronal population (Mallucci et al., 2002). The

Mallucci study was carried out almost ten years ago, and since then the Cre-expressing mice (NFH-Cre) have been continuously bred under a strict genotyping regime. The possibility of a change in the efficacy or pattern of Cre expression has been reported in other studies (Turlo et al., 2010). In light of the discrepancy between these results and those obtained previously for survival of RML infected NFH-Cre/M*lox*P mice, a change in the Cre expression pattern, selected by accident through continuous breeding cannot be excluded.

Since the original premise of the experiment had changed, we were unable to approach our original question as planned. Nevertheless, our pathological analysis showed some characteristics of the end stage prion pathology in M*lox*P and NFH-Cre/M*lox*P mice.

Our first observation was the different pathology of RML or Me7 infected M*lox*P mice.

Every strain has a define lesion profile and the first obvious difference between RML and Me7 infected M*lox*P brain was the phenotype of abnormal PrP accumulation, synaptic in RML and granular in Me7 inoculated mice. The overall degree of spongiosis, abnormal accumulation and gliosis was stronger in Me7 infected M*lox*P mice, but the incubation time was greater for these mice than for RML infected M*lox*P mice. Moreover, in RML infected M*lox*P mice the pathology was more heterogeneous, ranging from mild to severe, whereas in Me7 infected M*lox*P mice prion pathology was severe in the majority of the scored nuclei (Figure 4.5 and 4.9).

Data obtained from RML or Me7 infected NFH-Cre/M*lox*P mice showed the significant effect of PrP depletion on disease progression. RML and Me7 infected NFH-Cre/M*lox*P mice, time culled when the M*lox*P "counterparts" manifested terminal disease (i.e. at 12 wpi for RML and at 16 wpi for Me7), showed mild pathology (Figure 4.6 and 4.10). The locus coeruleus was the only nucleus to show intermediate abnormal PrP accumulation at 12 wpi in RML infected NFH-Cre/M*lox*P mice and at 16 wpi in Me7 infected NFH-Cre/M*lox*P mice. As an effect of Cre-mediated recombination, we would have expected absence or significantly reduced prion deposition in areas whose cells underwent PrP depletion. The neuronal deposition of PrP in the locus coeruleus suggests that recombination was not as efficient as in the other brainstem areas. The prion deposition pattern in RML

infected NFH-Cre/M*lox*P mice was granular, similar to that in Me7 infected NFH-Cre/M*lox*P mice. In addition to the locus coeruleus, in Me7 infected NFH-Cre/M*lox*P mice culled at 16 wpi, the nucleus of the solitary tract showed abnormal PrP accumulation. Spongiosis and gliosis in these two nuclei were less prominent than abnormal PrP deposition in the Me7 infected mice, and almost non-existent in RML infected NFH-Cre/M*lox*P mice (Figure 4.6 and 4.10).

Despite the general differences of pathological features between terminally ill Me7 and RML, infected NFH-Cre/M*lox*P showed a surprisingly similar pattern of prion protein deposition (Figure 4.7 and 4.11). Both inocula caused strong spongiosis, gliosis and prion protein deposition in the locus coeruleus and the nucleus of the solitary tract (involved in autonomic activity) whereas the nuclei involved in the motor control (vestibular nucleus, prepositus nucleus and olive) showed reduced abnormal accumulation compared to the M*lox*P mice and similar spongiosis and gliosis. Clearly, in these last nuclei (vestibular, prepositus and olive), recombination is efficient in reducing availability of the PrP substrate for conversion in disease-associated PrP accumulation. However, a contribution due to clearance of abnormal PrP cannot be excluded at this stage but it could not be further investigated in this project. No recovery of spongiosis in the brainstem of NFH-Cre/M*lox*P mice was observed, highlighting the difference with the Mallucci's study on recovery of spongiform degeneration in the hippocampus of NFH-Cre/M*lox*P RML inoculated mice.

It is interesting to note how prolonged incubation time allowed spreading of the pathology to areas that are not normally affected in M*lox*P mice. In both RML and Me7 infected NFH-Cre/M*lox*P mice, abnormal PrP deposition, spongiosis and gliosis were found in the cerebellum, and for the first time abnormal PrP accumulation in the tracts of the cranial nerves, in the Virchow-Robin spaces and in the brain parenchyma surrounding them was observed (Figure 4.8 and 4.12).

Analysis of RML infection in M*lox*P and NFH-Cre/M*lox*P mice showed that the phenotype of the prion pathology was different in these two mouse lines, with prion accumulation shifting from synaptic to granular. Because the overall characteristic of prion pathology in RML infected NFH-Cre/M*lox*P mice was very similar to that of Me7 infected NFH-Cre/M*lox*P mice, we reasoned that the change of prion deposition phenotype could be explained by a strain shift or strain selection.

To test the strain selection hypothesis, we inoculated RML and RML passaged in NFH-Cre/M*lox*P mice into mice overexpressing PrP (Tg20) and wild-type mice (FVB).

The preliminary data showed here are not conclusive. In PrP overexpressing Tg20 mice, the two inocula gave rise to different incubation times (Figure 4.14). However, detailed neuropathology is needed to evaluate the phenotype of PrP deposition and determine if overall prion pathology is the same. Intriguingly, there was no difference in incubation time in wild type mice (Figure 4.14). The discrepancy between PrP overexpressing and wild type mice suggests a number of possibilities, considering that a strain is defined by the cross-talk between the prion inoculum and the host. The kinetics of prion propagation and clearance need to be considered, as well as the targeted areas in which propagation occurs. The hypothetical new strain enriched in the NFH-Cre/M*lox*P mice may be favoured in Tg20 overexpressing mice but not in wild type mice because the kinetics of propagation in the target areas are different. Another hypothesis is that the original RML ensemble undergoes different selective pressure in NFH-Cre/M*lox*P, Tg20 or FVB mice. In both cases, the pathological analysis and comparison between RML and RML subpassaged in NFH-Cre/M*lox*P infected M*lox*P, NFH/Cre-M*lox*P, Tg20 and FVB mice would shed the light on these two hypotheses. On the other hand, the *in vitro* approach, using the scrapie cell assay could be a relatively easy tool to test if there is a difference between the two inocula. If a strain shift has occurred, a consequence of this phenomenon is that, although RML and Me7 cannot be considered the same strain in NFH-Cre/M*lox*P mice because of the difference in the incubation time, the 12 wpi time culled RML infected NFH-Cre/M*lox*P mice can be considered informative as an earlier time point in the progression of the Me7 infection, in light of the high degree of similarity among the end stage pathologies for these prion strains.

In conclusion, the analysis of the lesion profiles of RML and Me7 infected M*lox*P and NFH-Cre/M*lox*P mice did not highlight any nuclei that could be defined as clinical target areas.

In NFH-Cre/M*lox*P mice, Cre-mediated recombination reduced the level of abnormal PrP deposition almost everywhere, except in the locus coeruleus, the nucleus of the solitary tract and the cerebellum. The locus coeruleus and the nucleus

of the solitary tract were also severely affected by prion pathology in M*lox*P mice; therefore they seem to be interesting candidates as critical target areas. In the vestibular nuclei, the depletion reduced the amount of abnormal PrP accumulation, but not the spongiform changes. The locus coeruleus and the nucleus of the solitary tract are involved in the control of autonomic function, while the vestibular nuclei are historically classified as the centre for the motor control. However, more recent studies have suggested an involvement in autonomic regulation. These nuclei, therefore, also seem to be potential candidates for critical functional areas for the clinical phenotype.

However, because RML infected NFH-Cre/M*lox*P mice reached a clinical stage, by comparison with terminally ill mice, we could not evaluate the spared areas that could represent clinical target areas of prion disease.

Because a clinical target area could be an area targeted early by the pathology and could represent the centre from which the pathology spreads to other regions, we decided to investigate which are the early targets of prion infection in the brainstem. A detailed investigation of lesion profiles at early stage of the disease both in RML and Me7 infected M*lox*P and NFH-Cre/M*lox*P mice was set up and is the topic of chapter 5.

Moreover, a more detailed analysis of recombination in every brainstem nuclei was required to further evaluate which nuclei undergoes efficient recombination, and how recombination affects prion pathology. The investigation of spatial and temporal characteristics of Cre-mediated recombination is the topic of chapter 6.

4.6 Summary

In this chapter we investigated if clinical target areas are the last targeted areas in course of prion infection by comparing M*lox*P and NFH-Cre/M*lox*P mice infected with RML, Me7 or MRC2 prion strains. In contrast with a previous study, we found that in all three inoculations, NFH-Cre/M*lox*P PrP depleted mice have a prolonged survival compared to their M*lox*P counterpart (35 wpi vs. 12 wpi for RML, 28 wpi vs. 16 for Me7 and 32 vs. 20 wpi for MRC2); however RML infected NFH-Cre/M*lox*P mice were not resistant to prion infection, as previously observed. This difference could be due to a change in the expression pattern of Cre

recombinase in NFH-Cre/M*lox*P mice. Further investigations on the temporal and spatial characteristic of Cre mediated recombination are reported in chapter 6.

Because RML infected NFH-Cre/M*lox*P developed signs of clinical disease, we could not use the comparison between terminally ill M*lox*P and surviving recombined NFH-Cre/M*lox*P mice to identify clinical target areas for prion disease. Nevertheless, we collected data on pathology in Me7 and RML infected end-stage M*lox*P and recombined NFH-Cre/M*lox*P mice and NFH-Cre/M*lox*P mice time-culled at time when the M*lox*P mice were terminal. We scored nuclei involved in motor and autonomic control and looked for areas that are severely affected both in RML and Me7 infected M*lox*P and NFH-Cre/M*lox*P mice.

We found that:

- The locus coeruleus is the nucleus whose pathology is consistently severe across the various infections analysed;
- Prolonged incubation time allows a re-distribution of prion pathology in infected NFH-Cre/M*lox*P mice, with areas not otherwise targeted in the control mice.
- NFH-Cre/M*lox*P mice have a similar pathology phenotype in RML or Me7 infection and we hypothesized a shift of strains. We tested this hypothesis by passaging the original RML inoculum used and the inoculum derived from the brain of a NFH-Cre/M*lox*P mouse infected with RML in overexpressing Tg20 and wild type FVB mice, but the results shown here are not fully conclusive and further work is required.

To investigate if clinical areas could be the first target areas in prion infection, we describe the pathology profile at early time points RML or Me7 infected mice in the following chapter.

5 First target areas of prion pathology

5.1 Introduction

"Clinical target areas" for prion disease are defined as areas of the brain where prion infection spreads and produces cell dysfunction leading to clinical manifestation of the disease (Kimberlin and Walker, 1983; Kimberlin and Walker, 1986; Kimberlin et al., 1987). The actual identity of these target areas remains speculative, but it has been suggested that clinical target areas may be located in the brainstem. Firstly, the brainstem controls vital functions. Clinical signs indicative of brainstem involvement (such as impaired respiration and unsteady balance and gait) are typical in experimental models of prion disease. Widespread deposition of PrP^{Sc} in the brainstem has been reported as an early pathologic event in human sCJD (Iwasaki et al., 2005), and in our pilot study described in chapter 3 we found accumulation of abnormal PrP in the brainstem of Me7 and Mouse-adapted BSE inoculated M*lox*P and NFH-Cre/M*lox*P mice very early on in the disease progression.

In chapter 4, we had planned to use the RML or Me7 inoculated M*lox*P and NFH-Cre/M*lox*P mice to investigate the clinical target areas for prion disease. RML inoculated NFH-Cre/M*lox*P mice have been shown to be resistant to RML infection (Mallucci et al., 2003). We had hypothesized that, in NFH-Cre/M*lox*P mice, Cre-mediated recombination protected one or more brainstem nuclei from prion pathology, and stopped the progression to clinical phenotype, even in presence of continuous abnormal PrP accumulation in the remainder of non-recombined cells. We had found in our preliminary study, described in chapter 3, that this effect was not common to other prion strains, as Me7 or Mouse-adapted BSE inoculated NFH-Cre/M*lox*P mice survived longer than their M*lox*P counterparts but eventually developed prion disease. Therefore, our aim was to compare the longer surviving RML infected NFH-Cre/M*lox*P mice with end-stage RML and Me7 infected M*lox*P and Me7 inoculated NFH-Cre/M*lox*P mice to pinpoint the critical areas that led to the clinical phenotype.

We hypothesised two different scenarios: clinical target areas could be the last or the first sites of prion replication.

We set up the experiment described in chapter 4 to explore the first hypothesis. For this hypothesis to be verified, mice should be able to sustain the infection in a pre-clinical stage- i.e. accumulating abnormal PrP without showing clinical signs - until the infection reached one or more "critical areas", determining their degeneration and causing clinical prion disease. Therefore, clinical areas of prion pathology should have been unaffected or less severely affected in asymptomatic RML infected NFH-Cre/M*lox*P mice at the late stage of disease, and affected in terminally ill RML infected M*lox*P mice, Me7 infected M*lox*P mice and Me7 infected NFH-Cre/M*lox*P mice.

Surprisingly, we found that RML inoculated NFH-Cre/M*lox*P mice showed a prolonged incubation time but were not resistant to prion disease. Moreover, the prion pathology in the brainstem of RML infected NFH-Cre/M*lox*P mice was very similar to the pathology of Me7 infected NFH-Cre/M*lox*P mice. In contrast, RML or Me7 inoculated M*lox*P mice had different lesion profiles, but the locus coeruleus (LC) and the nucleus of the solitary tract (NTS) were found to be the structures of abnormal PrP accumulation common to all the end stage phenotypes analysed.

The unexpected development of clinical signs in ~35 wpi in RML inoculated NFH-Cre/M*lox*P mice led us to change our experimental approach. Therefore, we decided to investigate the early stage of prion infection in M*lox*P and PrP depleted NFH-Cre/M*lox*P mice, looking for the first targets of prion pathology in RML and Me7 inoculated mice.

5.2 Aims

- To identify the first target areas of prion pathology in experimental models of prion disease
- To follow the disease progression in these areas.

5.3 Experimental set up

6 M*lox*P and 6 NFH-Cre/M*lox*P mice were inoculated when one week old with RML, Me7 or MRC2 prion strains, in the form of 1% inoculum, respectively I9900 (1% RML I 8700), I 9459 (1% Me7 I 9458), I 9468 (1% MRC2 I 9467).

Inoculated mice were culled at an early time point of the disease: RML infected mice were culled at 6 wpi, based on previous published data (White et al.,

2008); Me7 and MRC2 inoculated mice at 8 wpi, based on our observation in chapter 3. Because MRC2 is derived from Mouse-adapted BSE prions, we assumed early pathology could be present at 8 wpi as observed in the parental strain in chapter 3. A schematic representation of the experimental setup is illustrated in Figure 5.1.

Brains were fixed, cut coronally into three pieces and processed for paraffin embedding. The block corresponding to the brainstem area of RML and Me7 infected mice was sliced with the microtome by the support team of histology core facility at the MRC Prion Unit. Eight consecutive sections for each level were collected and used for histology. Sections were stained with haematoxylin and eosin (H&E) to examine the progression of spongiform changes, ICSM 35 antibody for abnormal prion protein deposition, and anti-GFAP antibody to visualise reactive astrocytes and to assess astrogliosis. Sections were analysed microscopically and areas of interest were evaluated by comparison with the Paxinos Mouse Brain Atlas and Allen Mouse Atlas (Paxinos and Franklin, 2004; Lein et al., 2007; Lein et al., 2007). Degree of spongiosis, abnormal PrP deposition and gliosis were evaluated, using a semi-quantitative scoring scale. Selected sections were stained with anti-tyrosine hydroxylase (TH) and anti-Neurokinin 1 (anti-NK1) receptor antibodies, as indicated in the results sections. Once the first targeted areas had been evaluated, samples from end-stage mice were re-analysed to follow the progression of prion associated pathology.

Due to time constraints it was only possible to carry out the histological analysis on the RML and Me7 inoculated brains.

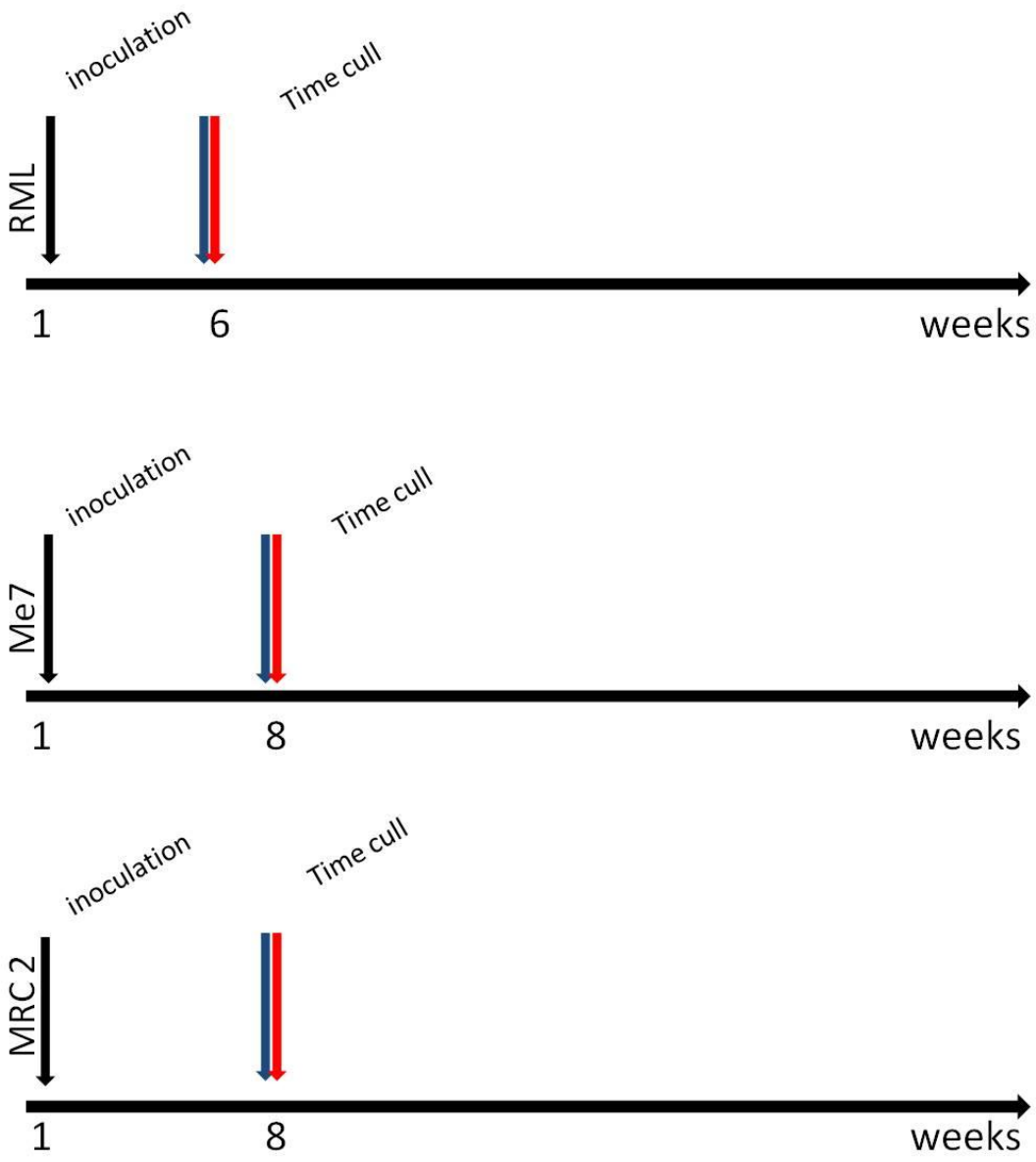

Figure 5.1 Description of the experimental plan

To assess the areas of early pathology in prion inoculated mice, 6 M*lox*P and 6 NFH-Cre/M*lox*P mice were inoculated at one week of age with RML, Me7 or MRC2 prion strains, and culled at an early asymptomatic stage, and their brainstem analysed histopathologically. RML inoculated mice were culled at 6 wpi, based on previously published data (White et al., 2008); Me7 inoculated mice were culled at 8 wpi, based on our observation described in chapter 3; MRC2 inoculated mice were culled at 8 wpi because this strain is derived from Mouse-adapted BSE prions, whose early pathology is present at 8 wpi, as described in chapter 3.

5.4 Results

5.4.1 First targeted areas in RML and Me7 inoculated M*lox*P and NFH-Cre/M*lox*P mice

Analysis of the brainstems of prion infected M*lox*P and NFH-Cre/M*lox*P mice at an early asymptomatic stage (RML, 6 wpi; Me7, 8 wpi) showed early prion pathology in the locus coeruleus (LC), the nucleus of the solitary tract (NTS) and the pre-Bötzinger complex (PBC). Early prion pathology in these nuclei manifested as deposition of disease-associated prion protein and reactive gliosis. However no spongiform changes were observed at this time (Figure 5.2).

Locus coeruleus

In M*lox*P mice at an early, asymptomatic stage of the disease (RML, 6 wpi; Me7, 8 wpi), abnormal PrP accumulation in the locus coeruleus (LC) was scored as intermediate. As already observed for later stages, in RML inoculated mice the abnormal PrP accumulation was of the synaptic type, while in Me7 inoculated mice it was granular. Some reactive gliosis was also recognisable in both infections, in the absence of spongiosis (Figure 5.3).

In NFH-Cre/M*lox*P mice abnormal PrP accumulation was reduced in comparison to M*lox*P mice. In both cases (RML and Me7) abnormal accumulation of PrP was granular. RML inoculated mice were culled at 6 wpi, i.e. 7 weeks of age and Me7 inoculated mice at 8 wpi, i.e. 9 week of age. At 8 wpi, abnormal PrP deposition in NFH-Cre/M*lox*P mice was reduced compared to the accumulation in M*lox*P mice, suggesting that PrP depletion had occurred, even if was not complete. Abnormal PrP deposition was comparable between RML inoculated mice at 6 wpi and Me7 inoculated mice at 8 wpi. This suggested that the depletion occurred before 6 wpi (7 weeks of age), and that from 6 wpi to 8 wpi there was no further increase of abnormal PrP deposition. Gliosis was present in both RML and Me7 inoculated NFH-Cre/M*lox*P mice, although less diffuse than in M*lox*P mice. No spongiosis was present (Figure 5.4).

Nucleus of the solitary tract

In the nucleus of the solitary tract (NTS), prion pathology at the early stage was very subtle. In M*lox*P mice the abnormal accumulation was mild in RML inoculated mice and very mild in Me7 inoculated mice, whereas the gliosis was more

evident. As for the LC, the tissue did not show any spongiosis. In recombined NFH-Cre/M*lox*P mice, while gliosis was comparable to gliosis in M*lox*P mice, abnormal deposition was reduced and no spongiform changes were present (Figure 5.5).

Pre-Bötzinger complex

In the ventral medulla, an area characterized by small and medium-sized strictly interconnected neurons, showed mild abnormal PrP accumulation both in RML and Me7 infected M*lox*P mice. The anatomical mapping corresponds to the pre-Bötzinger complex (PBC). The identity of this nucleus was confirmed by staining with anti-NK1 receptor antibody, which specifically labels pre-Bötzinger neurones within the brain stem (Gray et al., 1999). The PBC, both in RML and Me7 infected M*lox*P mice, showed the same pattern of pathology as the nucleus of the solitary tract, with mild prion protein accumulation and gliosis, and absence of spongiosis. In the recombined RML inoculated or Me7 inoculated NFH-Cre/M*lox*P mice, abnormal accumulation was less than in the non-recombined M*lox*P mice. This suggested that at an early stage of prion pathology, recombination had occurred in this nucleus but it was not completely protective. Gliosis was comparable between M*lox*P and NFH-Cre/M*lox*P in both RML and Me7 inoculated mice, and spongiosis was absent (Figure 5.6).

The first areas showing prion pathology in RML or Me7 inoculated M*lox*P and NFH-Cre/M*lox*P mice were the same. We decided to study in further detail the progression of pathology in RML and Me7 inoculated mice, by comparing the appearance of prion deposition, spongiosis and gliosis in each area of interest in the course of the disease.

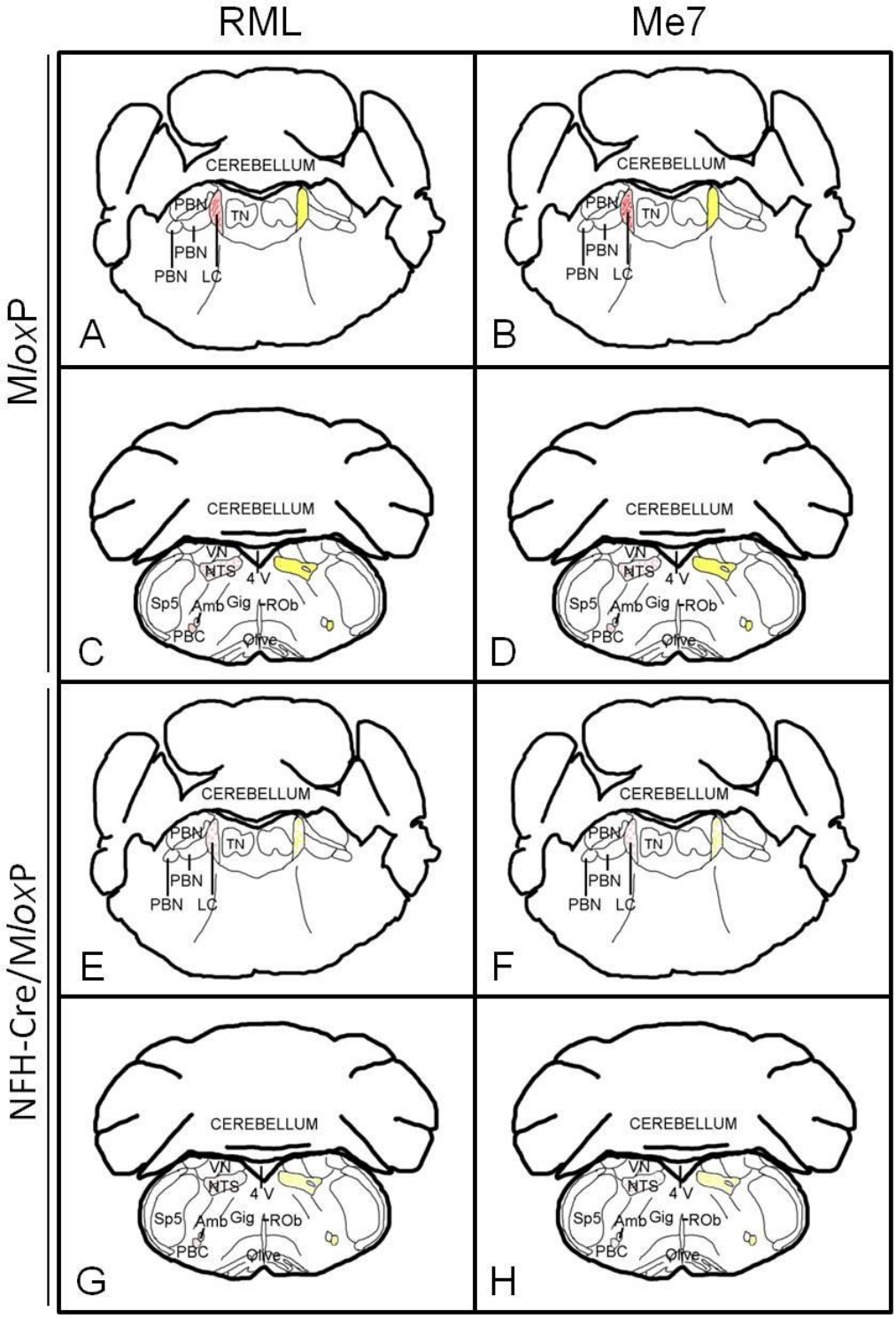

Figure 5.2. Schematic representation of first targeted areas in the brainstem of RML and Me7 M*lox*P and NFH/Cre-M*lox*P inoculated mice

Early prion pathology in the brainstems of RML and Me7 inoculated of M*lox*P and NFH-Cre/M*lox*P mice, time culled at an early asymptomatic stage (RML, 6 wpi; Me7, 8 wpi), manifested with deposition of disease-associated prion protein (red/pink) and reactive gliosis (yellow) in the locus coeruleus (LC), the nucleus of the solitary tract (NTS) and the pre-Bötzinger complex (PBC). No

spongiform changes were observed at this time point.

The scheme has been adapted from the Paxinos Mouse Brain Atlas. A, B, E, F = -5.34 mm from Bregma; C, D, G, H = - 6.84 mm from Bregma. List of abbreviations: PBN = parabrachial nuclei; TN = tegmental nuclei; LC= locus coeruleus; VN= vestibular nuclei; 4 V = fourth ventricle; NTS= nucleus of the solitary tract; Sp5= spinal nucleus of the V nerve; Amb= nucleus ambiguous; PBC= pre-Bötzinger complex; ROb = raphe obscurus.

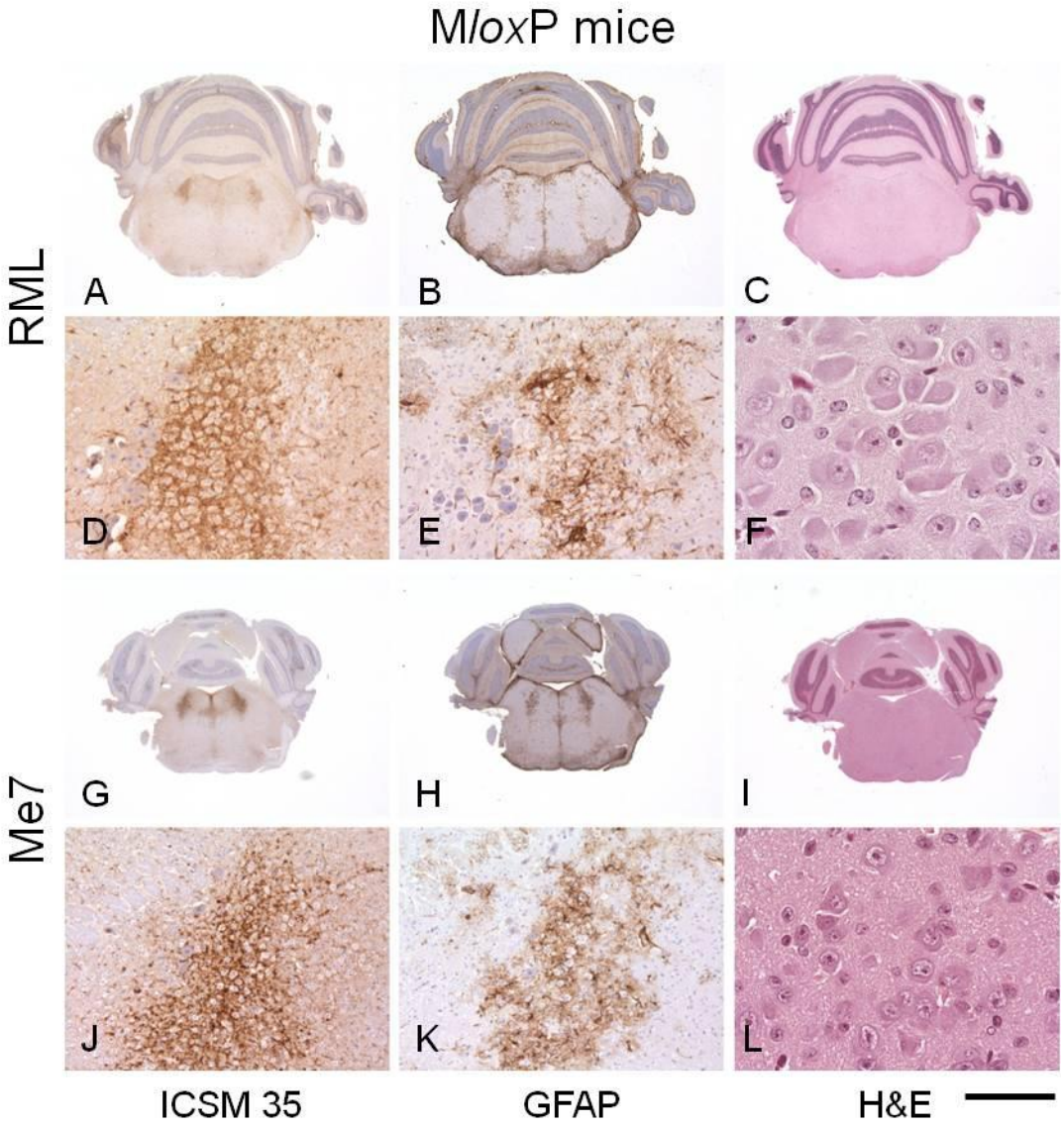

Figure 5. 3 Early prion pathology in the locus coeruleus of RML and Me7 inoculated M*lox*P mice

RML and Me 7 inoculated M*lox*P mice were culled at 6 and 8 wpi. Brain sections were immunostained with ICSM35 antibody for abnormal PrP deposition (A, D, G, J), anti-GFAP antibody for detection of astrocytosis (B, E, H, K), and stained with haematoxylin and eosin (H&E) (C, F, I, L) to assess spongiform changes. In the locus coeruleus (LC) of RML and Me7 inoculated M*lox*P mice, abnormal PrP accumulation was intermediate. In RML inoculated mice the phenotype of abnormal PrP accumulation was synaptic (A, D), while in Me7 inoculated mice it was granular (G, J). Mild reactive gliosis was also recognisable in both RML (B, E) and Me7 (H, K) inoculated M*lox*P mice, but no spongiosis (C, F, I, L). Scale bar= 4 mm in A, B, C, G, H, I; 164 µm in D, E, J, K,; 84 µm in F, L.

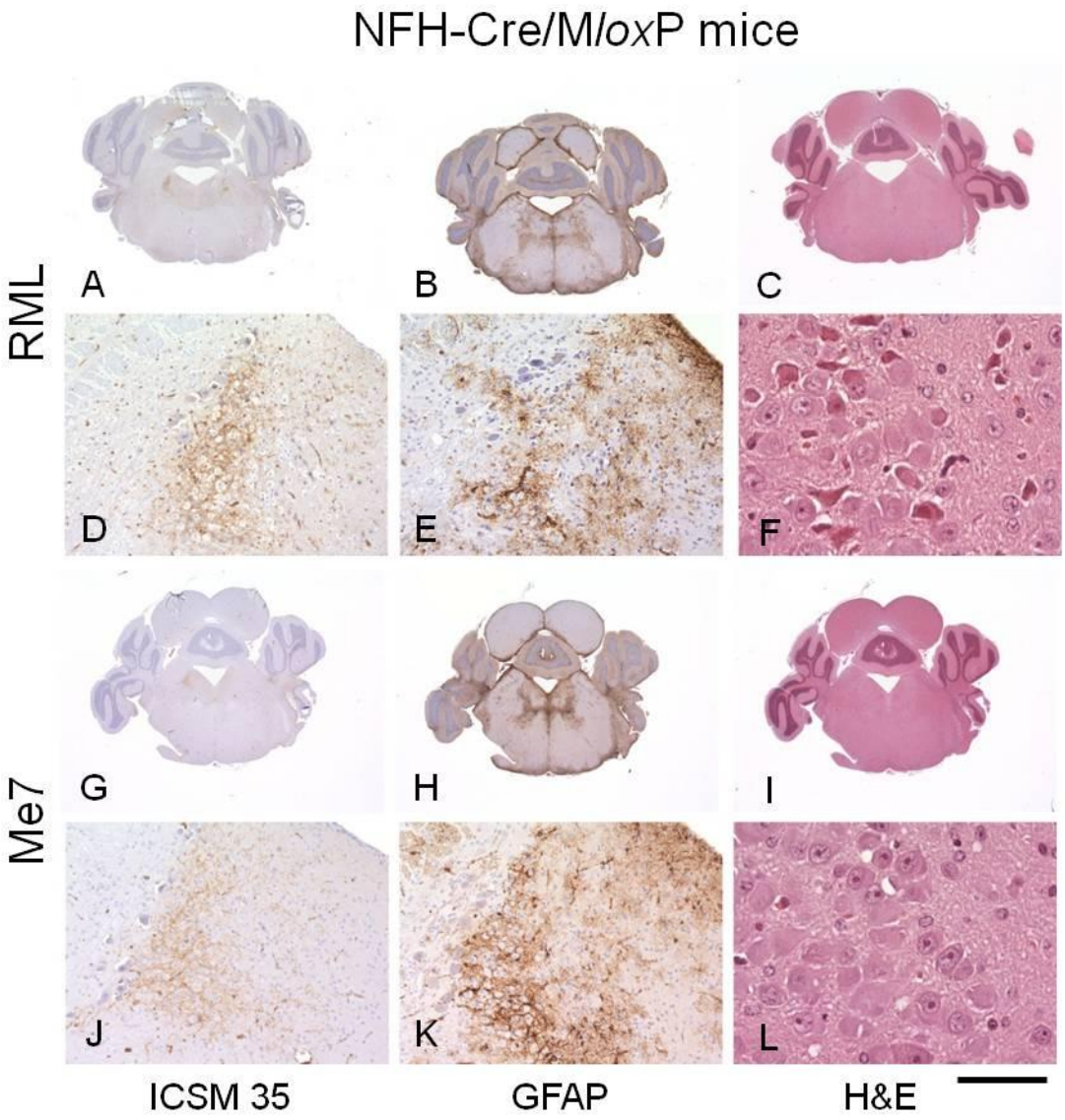

Figure 5.4 Early prion pathology in the locus coeruleus of RML and Me7 inoculated NFH-Cre/M*lox*P mice

RML and Me 7 inoculated NFH-Cre/M*lox*P mice were culled at 6 and 8 wpi. Brain sections were immunostained with ICSM35 antibody for abnormal PrP deposition (A, D, G, J), anti-GFAP antibody for detection of astrocytosis (B, E, H, K), and stained with haematoxylin and eosin (H&E) (C, F, I, L) to assess spongiform changes. In the locus coeruleus (LC) of RML and Me7 inoculated NFH-Cre/M*lox*P mice, abnormal PrP accumulation was mild. In both RML (A, D), and Me7 (G, J) inoculated mice the phenotype of abnormal PrP accumulation was granular. Mild reactive gliosis was also recognizable in both RML (B, E) and Me7 (H, K) inoculated M*lox*P mice, but no spongiosis (C, F, I, L). Scale bar= 4 mm in A, B, C, G, H, I; 164 µm in D, E, J, K; 84 µm in F, L.

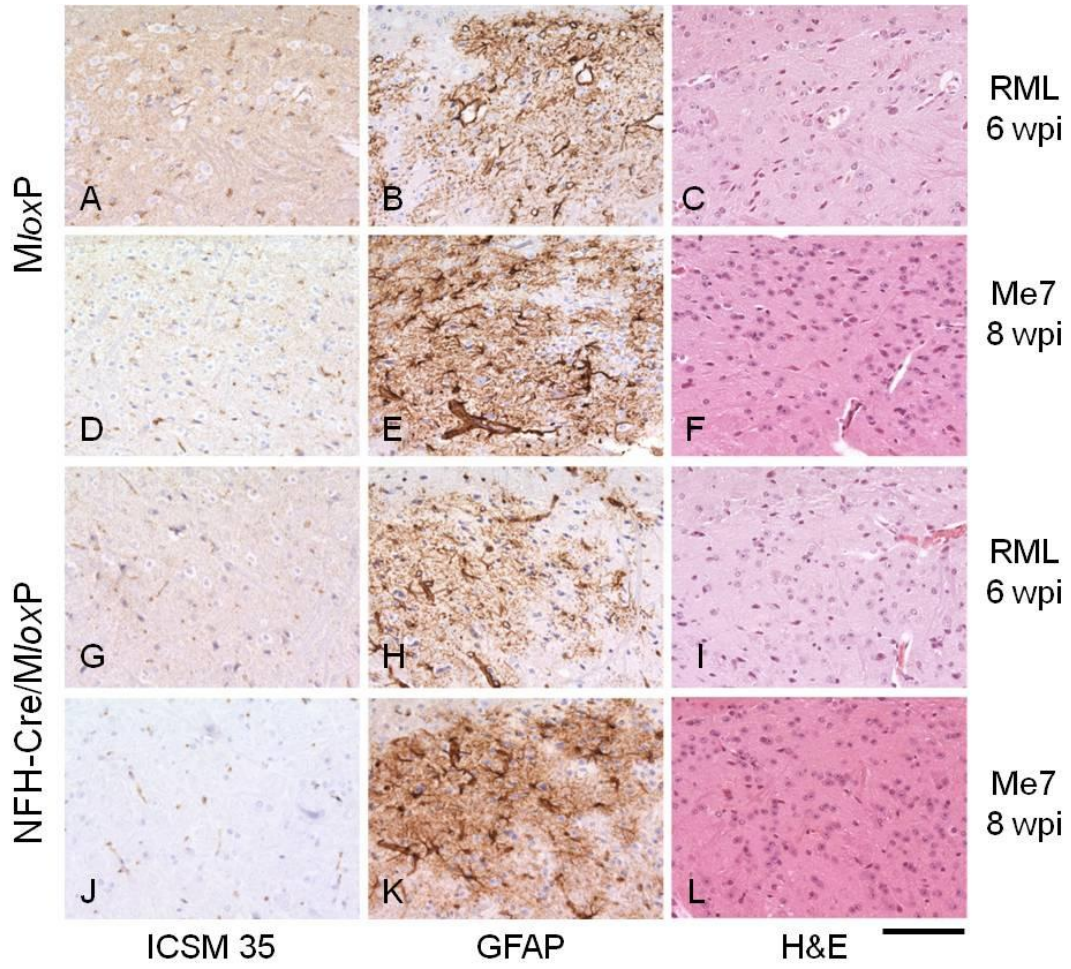

Figure 5.5 Early prion pathology in the nucleus of the solitary tract (NTS) of RML and Me7 inoculated M*lox*P and NFH-Cre/M*lox*P mice

RML and Me7 inoculated M*lox*P and NFH-Cre/M*lox*P mice were culled at 6 and 8 wpi. Brain sections were immunostained with ICSM35 antibody for abnormal PrP deposition (A, D, G, J), anti-GFAP antibody for detection of astrocytosis (B, E, H, K), and stained with haematoxylin and eosin (H&E) (C, F, I, L) to assess spongiform changes. In RML and Me7 inoculated M*lox*P mice abnormal deposition was mild, with synaptic phenotype in RML infection (A) and granular phenotype in Me7 infection (D). In RML (G) and Me7 (J) inoculated NFH-Cre/M*lox*P mice abnormal accumulation was milder than in M*lox*P mice. Gliosis was comparable between RML and Me7 inoculated M*lox*P and NFH-Cre/M*lox*P mice (B, E, H, K), and no spongiosis was evident (C, F, I, L). Scale bar= 84 µm.

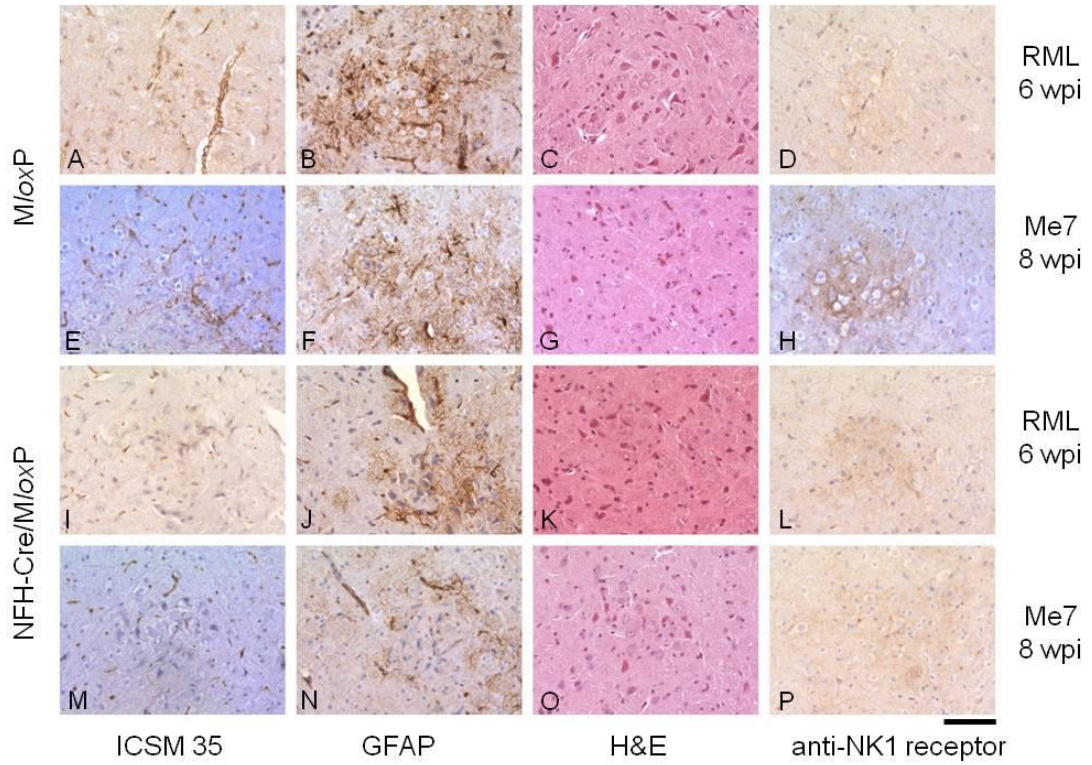

Figure 5.6 Early prion pathology in the pre-Bötzinger complex of RML and Me7 inoculated M*lox*P and NFH-Cre/M*lox*P mice

RML and Me7 inoculated M*lox*P and NFH-Cre/M*lox*P mice were culled at 6 and 8 wpi. Brain sections were immunostained with ICSM35 antibody for abnormal PrP deposition (A, E, I, M), anti-GFAP antibody for detection of astrocytosis (B, F, J, N), stained with haematoxylin and eosin (H&E) (C, G, K, O) to assess spongiform changes and immunostained with anti-NK1 receptor antibody (D, H, L, P), a marker for pre-Bötzinger complex neurons. In the ventral medulla, an area characterized by neurons strictly connected to each other, showed mild abnormal PrP accumulation both in RML and Me7 infected M*lox*P and NFH-Cre/M*lox*P mice (A, E, I, M). This area was identified as the PBC and the identity was confirmed by immunostaining with anti-NK1 receptor antibody (D, H, L, P). Abnormal PrP deposition was mild in M*lox*P mice (A, E) and very mild in recombined NFH-Cre/M*lox*P mice (I, M); gliosis was mild in both M*lox*P (B, F) and NFH-Cre/M*lox*P mice (J, N) and no spongiform changes were observed (C, G, K, O). Scale bar= 84 µm.

5.4.2 Progression of prion pathology in the locus coeruleus of RML inoculated M*lox*P and NFH-Cre/M*lox*P mice

As previously mentioned, at 6 wpi the deposition in RML inoculated M*lox*P mice was scored as intermediate, while in the PrP depleted NFH-Cre/M*lox*P mice it was less pronounced. Moreover, already from this early stage the different phenotype of abnormal PrP deposition (synaptic in M*lox*P and granular in NFH-Cre/M*lox*P) was evident. At this early time point, gliosis was similar in M*lox*P and NFH-Cre/M*lox*P mice and spongiosis was absent. At 12 wpi, M*lox*P mice were terminally ill, whereas the NFH-Cre/M*lox*P mice were asymptomatic and healthy. Strong abnormal accumulation was observed in the LC of M*lox*P mice, while at the same time (12 wpi) the recombined NFH-Cre/M*lox*P mice showed levels of accumulation just slightly higher than at 6 wpi. This was probably due to the Cre-mediated recombination and the depletion of host PrP^{C}. Gliosis was stronger in NFH-Cre/M*lox*P mice than in control M*lox*P mice. Healthy NFH-Cre/M*lox*P mice did not show any spongiform changes, but in M*lox*P mice small, densely packed vacuoles were visible. In terminally ill NFH-Cre/M*lox*P mice spongiosis and prion accumulation were intermediate and severe, comparable to M*lox*P mice, but gliosis was more severe than in M*lox*P mice (Figure 5.7).

5.4.3 Progression of prion pathology in the locus coeruleus of Me7 inoculated M*lox*P and NFH-Cre/M*lox*P mice

In Me7 infected M*lox*P mice at 8 wpi the abnormal accumulation in the LC was intermediate, while in the NFH-Cre/M*lox*P mice, it was milder. Gliosis in both mouse lines was comparable and no spongiosis was evident at this early time. Me7 infected M*lox*P mice were terminally ill at 16 wpi. As discussed in the previous chapter, abnormal PrP accumulation was globally strong. At 16 wpi asymptomatic NFH-Cre-M*lox*P mice showed intermediate accumulation. As already documented in chapter 4, at 16 wpi the LC showed higher accumulation than the surrounding areas. This could be an effect of lower efficacy of PrP depletion, although a less effective clearance in this area cannot be excluded. The difference between LC pathology in M*lox*P and NFH-Cre-M*lox*P mice at 16 wpi was also evident from comparing gliosis and spongiosis. The first was stronger in M*lox*P than NFH-Cre-M*lox*P mice. Spongiosis in M*lox*P mice was characterized by the presence of large and small

confluent vacuoles, whereas in NFH-Cre-M*lox*P mice only a few large vacuoles were recognized. Abnormal PrP accumulation in terminally ill NFH-Cre-M*lox*P mice was severe (see results in Chapter 4), while the surrounding areas were almost spared from abnormal PrP accumulation. In contrast, gliosis was strong both in the LC and surrounding nuclei. Spongiosis at 28 wpi in terminally ill NFH-Cre-M*lox*P mice was comparable with spongiosis observed in terminally ill M*lox*P mice at 16 wpi (Figure 5.8).

5.4.4 TH staining did not show functional impairment in the locus coeruleus of terminally ill mice

The LC is the major noradrenergic nucleus of the brain. We therefore asked if noradrenergic production changed in the course of the disease. To address this question, immunohistochemistry for tyrosine hydroxylase (TH) was performed on brain slices from time culled and terminally ill RML and Me7 inoculated M*lox*P and NFH-Cre/M*lox*P mice. The slices were directly adjacent to those used for H&E, abnormal PrP and GFAP staining.

We expected a reduced number of TH-positive cells but could not detect a change (Figure 5.9). However, the specimens were not appropriate for this analysis, because the levels of the sections were not directly anatomically comparable. To appreciate a change, a more thorough stereotaxic cell count is required, but it could not be performed on the collected slices, because they did not cover the entire volume of the nucleus. This needs to be investigated further in the future.

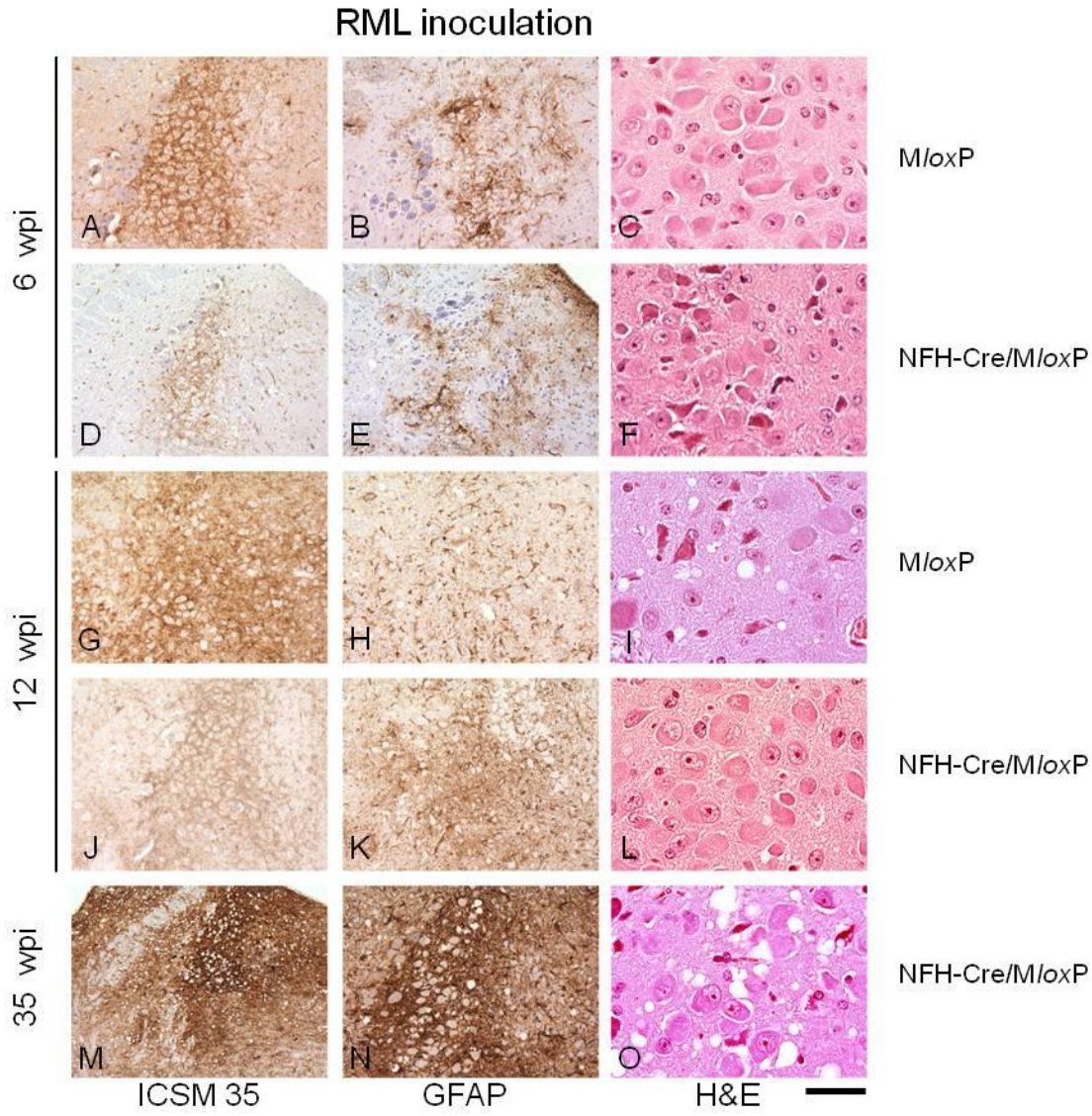

Figure 5.7 Progression of prion pathology in the locus coeruleus of RML inoculated M*lox*P and NFH-Cre/M*lox*P mice

Brain slices of the locus coeruleus of RML inoculated M*lox*P and NFH-Cre/M*lox*P mice at different stages of disease progression were compared. Slices had been immunostained with ICSM35 antibody for Abnormal PrP deposition (A, D, G, J, M), anti-GFAP antibody for detection of astrocytosis (B, E, H, K, N), and stained with haematoxylin and eosin (H&E) to assess spongiform changes (C, F, I, L, O).

At 6 wpi the deposition in RML inoculated M*lox*P mice was synaptic and intermediate (A), while in depleted NFH-Cre/M*lox*P mice it was granular and mild (D). At this early time point, gliosis was comparable in M*lox*P and NFH-Cre/M*lox*P mice (B, E) and spongiosis was absent (C, F). At 12 wpi, strong abnormal accumulation was observed in the LC of terminally ill M*lox*P mice, (G), while at the same time (12 wpi) the recombined NFH-Cre/M*lox*P mice showed levels of accumulation just slightly stronger than at 6 wpi (J). This was probably due to the Cre-mediated recombination and the depletion

of host PrP^C. Gliosis was stronger in NFH-Cre/M*lox*P (K) mice than in control M*lox*P mice(H). In M*lox*P mice spongiform changes were characterized by small, dense vacuoles (I), whereas healthy NFH-Cre/M*lox*P mice did not show any spongiform changes (L). In terminally ill NFH-Cre/M*lox*P mice prion accumulation (M) and spongiosis (O) were intermediate and severe, comparably to terminally ill M*lox*P mice (G and E), but gliosis (N) was more severe than in M*lox*P mice (H). Scale bar= 164 µm in A, B, D, E, G ,H M, N; 84 µm in C, F, I, L, O.

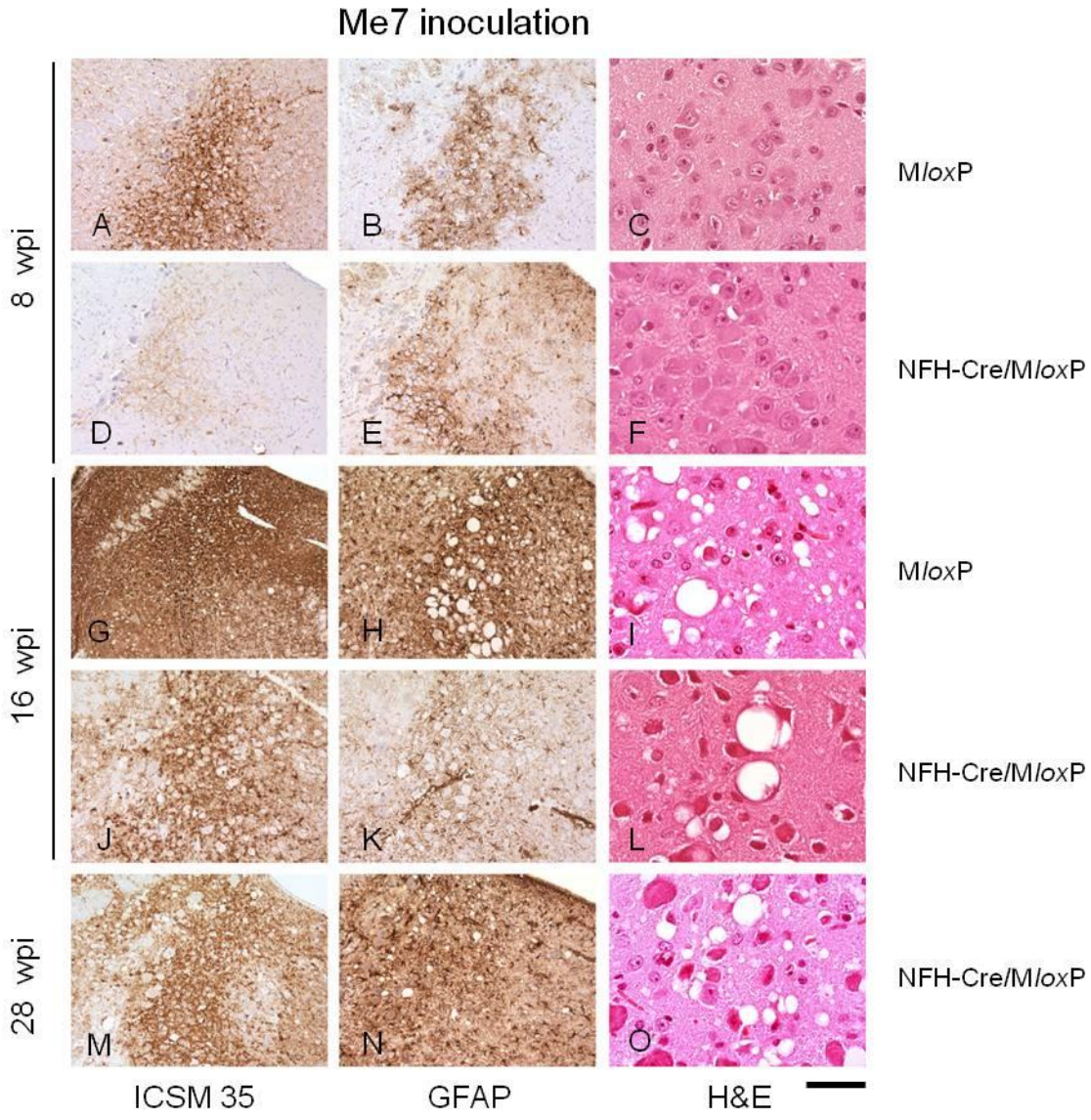

Figure 5.8 Progression of prion pathology in the locus coeruleus of Me7 inoculated M*lox*P and NFH-Cre/M*lox*P mice

Brain slices of the locus coeruleus of Me7 inoculated M*lox*P and NFH-Cre/M*lox*P mice at different stages of disease progression were compared. Slices had been immunostained with ICSM35 antibody for abnormal PrP deposition (A, D, G, J, M), anti-GFAP antibody for detection of astrocytosis (B, E, H, K, N), and stained with haematoxylin and eosin (H&E) to assess spongiform changes (C, F, I, L, O).

At 8 wpi the abnormal accumulation in the LC of M*lox*P was intermediate (A), while in the NFH-Cre-M*lox*P mice it was milder (D). Gliosis in both mouse lines was comparable (B, E) and spongiosis was absent (C, F). In terminally ill Me7 infected M*lox*P mice (16 wpi) abnormal PrP accumulation was strong in the LC (G) and globally. At 16 wpi asymptomatic NFH-Cre-M*lox*P mice showed intermediate accumulation in the LC (J), higher than in the surrounding areas. Gliosis was stronger in M*lox*P (H) than NFH-Cre-M*lox*P mice (K). Spongiform changes in M*lox*P mice were characterized

by both large and small confluent vacuoles (I), whereas in NFH-Cre-M*lox*P mice only a few large vacuoles were seldom present (L). Abnormal PrP accumulation in terminally ill NFH-Cre-M*lox*P mice was severe (M), whereas the surrounding areas were almost spared from abnormal PrP accumulation. Gliosis was strong both in the LC and surrounding nuclei (N). Spongiosis at 28 wpi in terminally ill NFH-Cre-M*lox*P mice (O) was comparable with spongiosis observed in terminally ill M*lox*P mice at 16 wpi (I). Scale bar= 164 µm in A, B, D, E, G, H M, N; 84 µm in C, F, I, L, O..

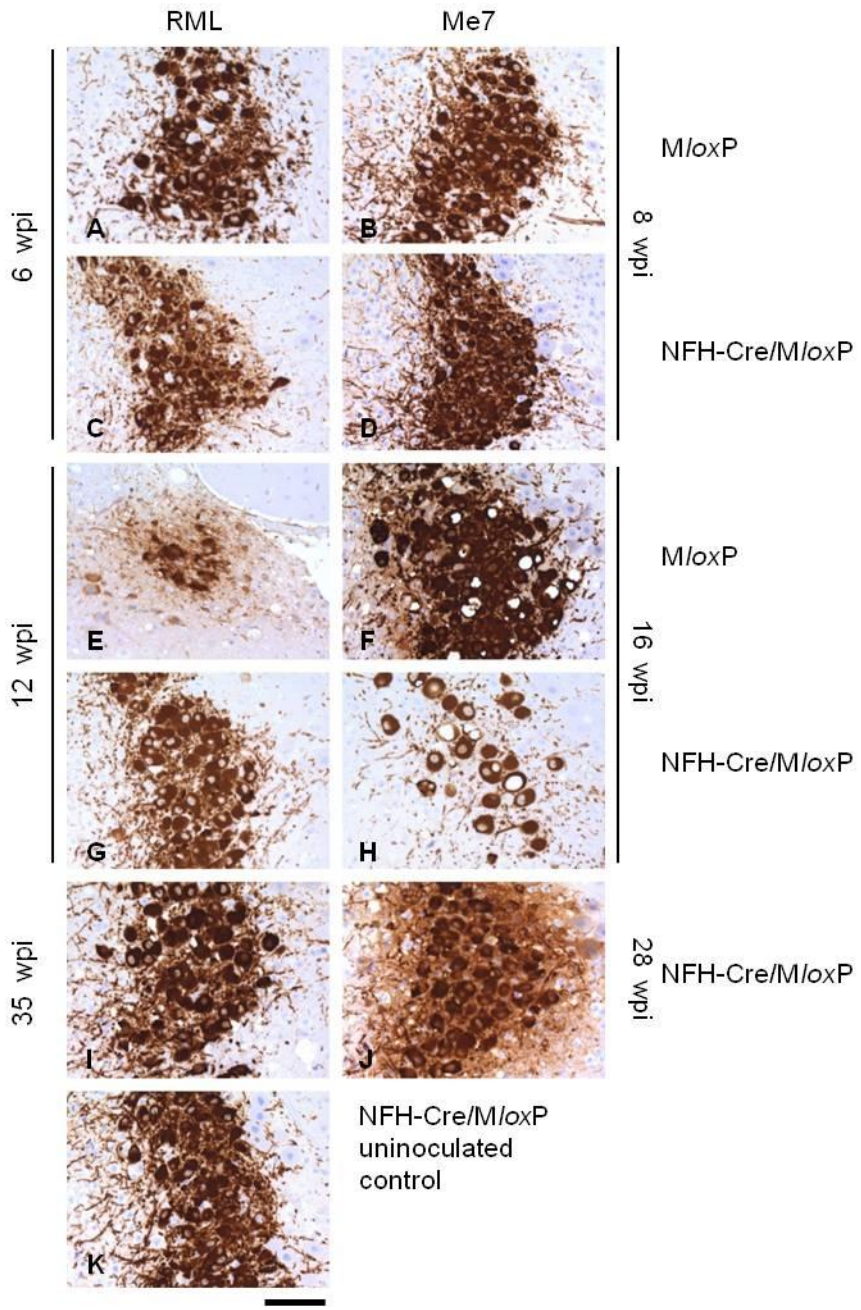

Figure 5.9 Anti Tyrosine hydroxylase staining did not show reduced number of positive cells with the disease progression

Noradrenalin is synthesized from tyrosine by Tyrosine Hydroxylase (TH). To assess if noradrenergic production changed in the course of the disease TH immunohistochemistry was performed on collected brain slices from time culled and terminally ill RML (left) and Me7 (right) inoculated M*lox*P and NFH-Cre/M*lox*P mice. The slices, directly adjacent to those used for H&E, PrP and GFAP staining, were stained with anti-TH antibody. As a control, the LC of uninoculated NFH-Cre/M*lox*P mice was used. We expected a reduced number of TH-positive cells in terminally ill RML and Me7 inoculated M*lox*P (E, F) and NFH-Cre/M*lox*P mice (I, J) compared to early time culled RML and Me7 inoculated M*lox*P (A, B) and NFH-Cre/M*lox*P (C,D) mice and asymptomatic time culled RML and Me7 inoculated NFH-Cre/M*lox*P mice (G,H). However, no change was appreciable because the

levels were not perfectly comparable (for example cfr A, E, H) and they did not encompass the entire volume of the nucleus. A more thorough stereotaxic cell count is required, but it could not be performed on the available slices. Scale bar= 84 μm.

5.4.5 Progression of prion pathology in the nucleus of the solitary tract in RML infected M*lox*P and NFH-Cre/M*lox*P mice

In the NTS at 6 wpi, RML inoculated M*lox*P mice showed mild abnormal accumulation and gliosis, whereas NFH-Cre-M*lox*P mice showed less abnormal PrP accumulation but a similar degree of gliosis. By 12 wpi, when M*lox*P mice were terminally ill, the degree of accumulation was intermediate and gliosis was strong. Spongiosis in the neuropil was recognizable in small confluent vacuoles. The degree of PrP accumulation in healthy NFH-Cre/M*lox*P mice was comparable, but spongiosis had not yet developed, and reactive gliosis was reduced compared both to the terminally ill (12 wpi) M*lox*P mice and 6 wpi culled NFH-Cre/M*lox*P, as if the inflammatory reaction slowed down upon disease progression. In terminally ill NFH-Cre-M*lox*P mice, reactive gliosis was similar to that in terminally ill M*lox*P mice, but abnormal PrP accumulation was stronger than in control mice, and was localized in specific sub-nuclei. A more detailed study, with stereotaxic cell counting is required to unequivocally evaluate which are these areas. Spongiosis in terminally ill NFH-Cre-M*lox*P mice was comparable to that in terminally ill M*lox*P mice, with small vacuoles localized in the entire surface of the nucleus (Figure 5.10).

5.4.6 Progression of prion pathology in the nucleus of the solitary tract in Me7 inoculated M*lox*P and NFH-Cre/M*lox*P mice

At 8 wpi, in Me7 inoculated mice, granular deposition of abnormal PrP was more evident in M*lox*P than in NFH-Cre/M*lox*P mice. Nevertheless, gliosis levels were comparable in both mouse lines. By 16 wpi, M*lox*P mice showed a substantial worsening of pathology, with severe accumulation, gliosis and spongiosis, with small uniformly distributed vacuoles. The corresponding NFH-Cre/M*lox*P mice showed reduced levels of PrP accumulation and gliosis compared to the M*lox*P mice. Spongiosis was mild, with only a few vacuoles seen. At the end stage (28 wpi), NFH-Cre/M*lox*P mice showed strong abnormal PrP deposition and spongiosis. Here, the vacuoles were bigger than observed in M*lox*P mice, and uniformly distributed. Gliosis was intense, but reduced compared to terminally ill M*lox*P mice Figure 5.11.

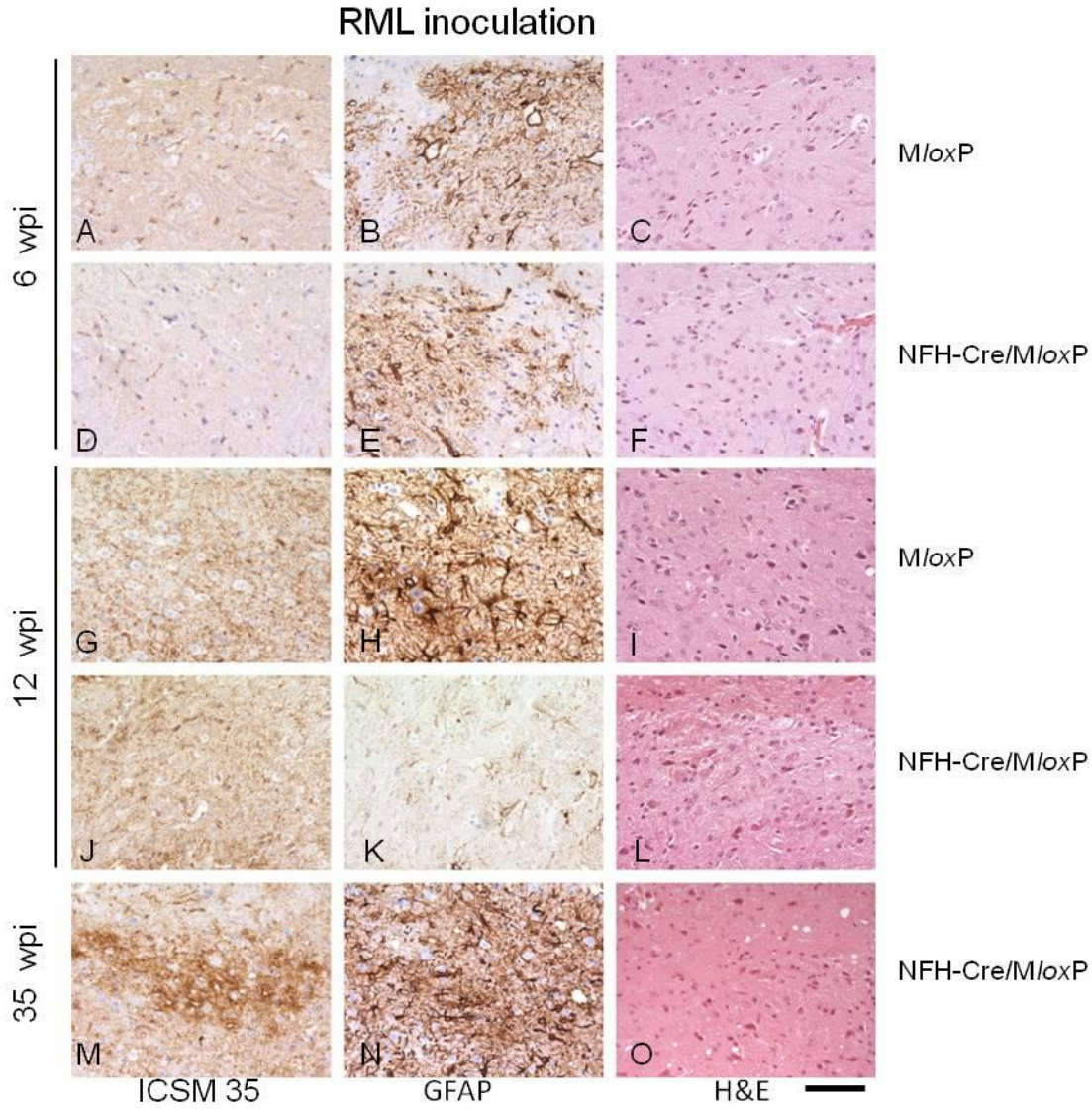

Figure 5.10 Progression of prion pathology in the nucleus of the solitary tract of RML inoculated M*lox*P and NFH-Cre/M*lox*P mice

Brain slices from the nucleus of the solitary tract (NTS) of RML inoculated M*lox*P and NFH-Cre/M*lox*P mice at different stages of the disease progression were compared. Slices had been immunostained with ICSM35 antibody for abnormal PrP deposition (A, D, G, J, M), anti-GFAP antibody for detection of astrocytosis (B, E, H, K, N), and stained with haematoxylin and eosin (H&E) to assess spongiform changes (C, F, I, L, O). At 6 wpi, RML inoculated M*lox*P mice showed mild abnormal PrP accumulation (A) and gliosis (B) and no spongiform changes (C). At the same early stage, NFH-Cre-M*lox*P mice showed mild abnormal accumulation (D), comparable gliosis (E) and no spongiosis (F). In terminally ill M*lox*P mice (12 wpi), the degree of accumulation was intermediate (G), gliosis was strong (H) and spongiosis was characterized by small confluent vacuoles (I). At the same time (12 wpi) the degree of PrP accumulation in healthy NFH-Cre/M*lox*P mice was

comparable (J), reactive gliosis was reduced (K) compared both to terminally ill (12 wpi) M*lox*P mice (H) and 6 wpi culled NFH-Cre/M*lox*P (E), as if the inflammatory reaction slowed down upon disease progression. In 12 wpi time culled NFH-Cre/M*lox*P spongiosis was absent (L). In terminally ill NFH-Cre-M*lox*P mice, abnormal PrP accumulation (M) was stronger than observed in terminally ill M*lox*P mice (G) and seemed to be localized in specific sub-nuclei. Reactive gliosis (N) was similar to the terminally ill M*lox*P mice (H). Spongiosis was characterized by small vacuoles localized in the entire surface of the nucleus (O) and comparable to spongiosis in terminally ill M*lox*P mice (I). Scale bar= 84 μm.

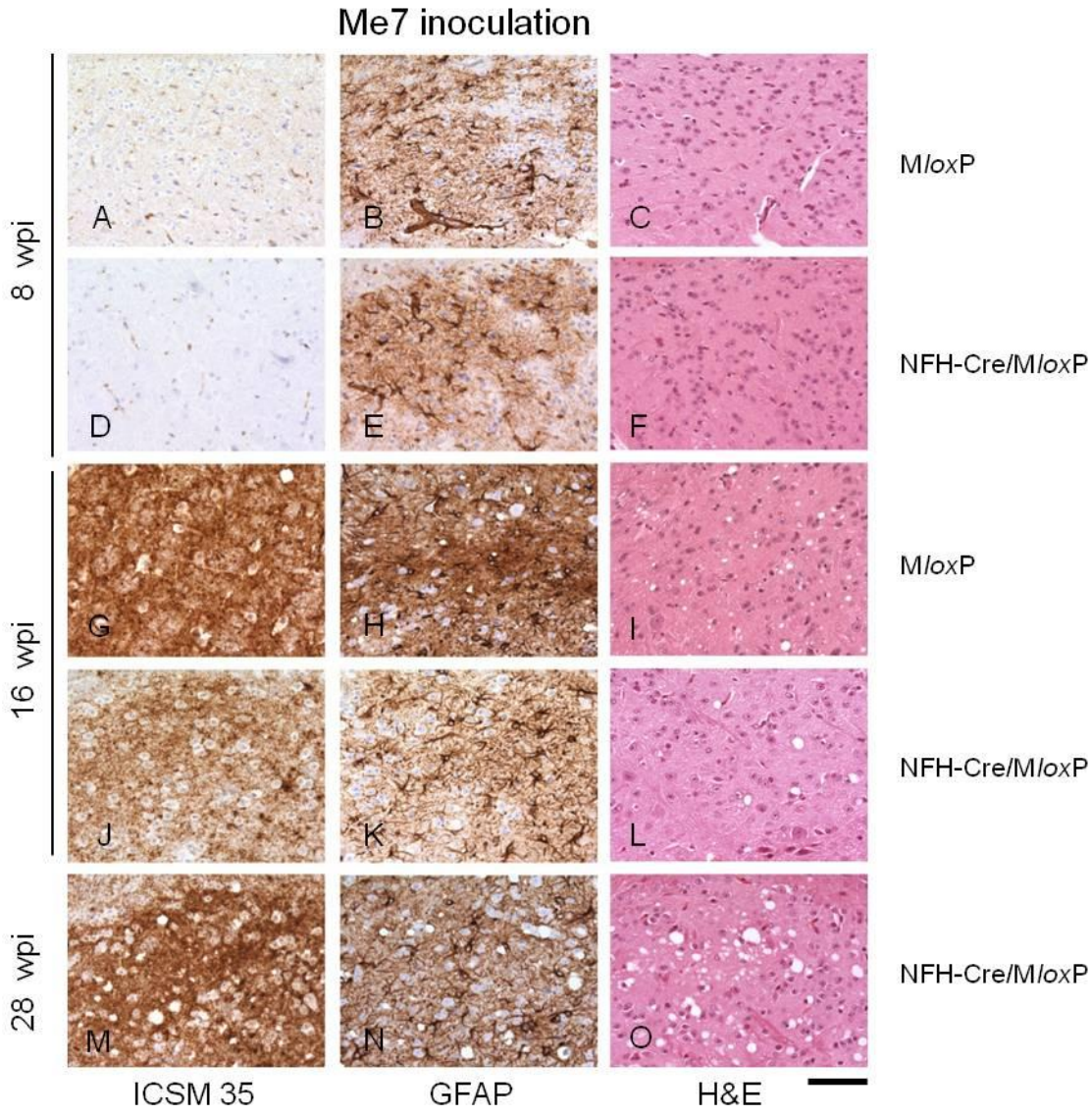

Figure 5.11 Progression of prion pathology in the nucleus of the solitary tract of Me7 inoculated M*lox*P and NFH-Cre/M*lox*P mice

Brain slices of the nucleus of the solitary tract (NTS) of Me7 inoculated M*lox*P and NFH-Cre/M*lox*P mice at different stages of the disease progression were compared. Slices had been immunostained with ICSM35 antibody for abnormal PrP deposition (A, D, G, J, M), anti-GFAP antibody for detection of astrocytosis (B, E, H, K, N), and stained with haematoxylin and eosin (H&E) to assess spongiform changes (C, F, I, L, O). At 8 wpi, in M*lox*P mice, granular deposition of abnormal PrP was mild (A) and even milder in NFH-Cre/M*lox*P mice (D). Gliosis levels were comparable in both mouse lines (B, E) and no spongiform changes were found (C, F). At 16 wpi, terminally ill M*lox*P mice showed diffuse severe abnormal PrP accumulation (G), gliosis (H) and spongiosis characterized by small and uniformly distributed vacuoles (I). At 16 wpi healthy NFH-Cre/M*lox*P mice showed reduced levels of PrP accumulation (J) and gliosis (K) compared to the M*lox*P mice (G, H). Spongiosis was mild, but vacuoles were seldom found. At the end stage (28 wpi), NFH-Cre/M*lox*P

mice pathology was characterized by strong abnormal deposition (M) and spongiosis (O), with bigger vacuoles than observed in M*lox*P mice (I), and uniformly distributed. Gliosis was intense (N), but less than in terminally ill M*lox*P mice (H). Scale bar= 84 µm.

5.4.7 Progression of prion pathology in the pre-Bötzinger complex (PBC) of RML infected M*lox*P and NFH-Cre/M*lox*P mice

In RML infected M*lox*P mice, the PBC showed mild accumulation and gliosis, and absence of spongiosis. In the PBC of RML infected NFH-Cre/M*lox*P mice recombination was not completely protective at 6 wpi. "Recombined" mice accumulated PrP, even if very mildly. Upon disease progression, the effect of recombination became more significant: at 12 wpi, when RML infected M*lox*P mice were terminally ill and RML infected NFH-Cre/M*lox*P mice were healthy, abnormal PrP accumulation was prominent in the PBC of M*lox*P mice, at a level comparable to the rest of the ventral medulla, whereas in recombined NFH-Cre/M*lox*P mice, the PBC showed reduced accumulation compared to the surrounding areas. Although gliosis was comparable between M*lox*P mice and NFH-Cre/M*lox*P mice, spongiosis was evident in terminally ill M*lox*P mice but not in healthy NFH-Cre/M*lox*P mice. Terminally ill NFH-Cre/M*lox*P mice at 35 wpi, showed abnormal PrP accumulation in this nucleus, which was reduced in comparison to the surrounding areas, and not substantially different from that observed in these mice at 12 wpi. Gliosis was also comparable to gliosis in 12 wpi time culled NFH-Cre/M*lox*P mice; the main difference with the earlier time point was in the appearance of spongiosis, with small vacuoles affecting the neuronal perykaria (Figure 5.12).

5.4.8 Progression of prion pathology in the pre-Bötzinger complex of Me7 infected M*lox*P and NFH-Cre/M*lox*P mice

At 8 wpi, PrP deposition and gliosis in Me7 infected M*lox*P mice were very mild. In "recombined" NFH-Cre/M*lox*P mice, PrP deposition was reduced compared to M*lox*P mice, but gliosis was comparable. The PBC of terminally ill M*lox*P mice was severely affected by prion deposition, gliosis and spongiosis, in the form of small and medium size vacuoles. In contrast, in NFH-Cre/M*lox*P mice time-culled at 16 wpi, PrP deposition was mild, and the tissue was not spongiotic, but exhibited reactive gliosis. When NFH-Cre/M*lox*P mice were terminally ill, the effect of PrP depletion was still evident, as in this nucleus there was less deposition then in the surrounding areas, but it was not complete. The PBC of terminally ill NFH-Cre/M*lox*P mice was affected by reactive gliosis and by spongiosis, at a level comparable to terminally ill M*lox*P mice (Figure 5.13).

5.4.9 Early pathology in the forebrain of RML infected mice

To control for prion pathology in the forebrain at an early time point, brain slices encompassing the hippocampus and thalamus of five RML inoculated M*lox*P and five NFH-Cre/M*lox*P mice were stained with anti-PrP antibody. In three out of five M*lox*P mice, abnormal PrP accumulation was localized in the thalamus, as previously reported for M*lox*P mice (White et al., 2008). In two out of five NFH-Cre/M*lox*P mice, abnormal PrP accumulation was detected in the thalamus, but not elsewhere (Figure 14). The thalamus and the brainstem have been indicated to be potential clinical target areas in a study by the group of Weissmann (Li et al., 2010), but a more detailed study of the lesion profile at early time points and an accurate description of disease progression in the forebrain is required.

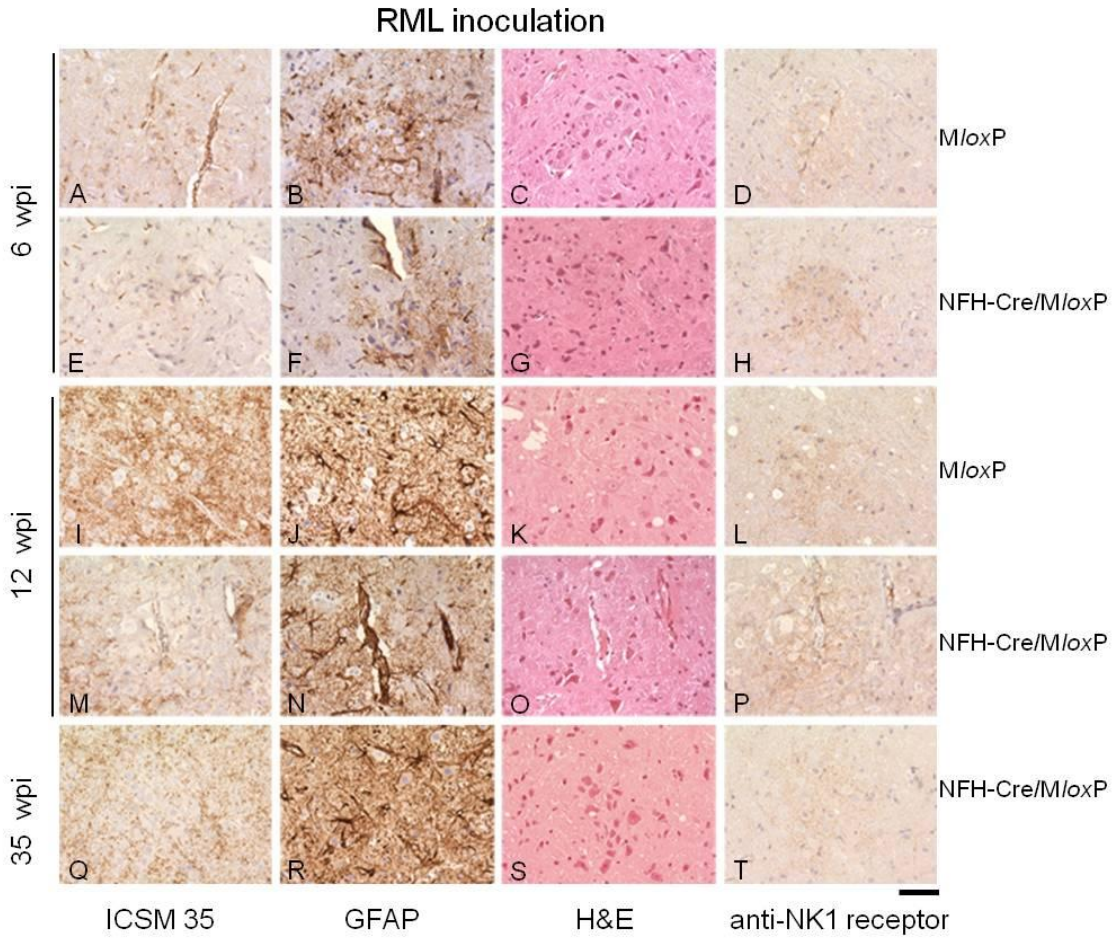

Figure 5.12 Progression of prion pathology in the pre-Bötzinger complex of RML inoculated M*lox*P and NFH-Cre/M*lox*P mice

Brain slices of the pre-Bötzinger complex (PBC) of RML inoculated M*lox*P and NFH-Cre/M*lox*P mice at different stages of disease progression were compared. To confirm the identity of this group of cells, slices were immunostained with ICSM35 antibody for abnormal PrP deposition (A, E, I, M, O), anti-GFAP antibody for detection of astrocytosis (B, F, J, N, R), haematoxylin and eosin (H&E) to assess spongiform changes (C, G, K, O, S) and anti-NK1 receptor antibody (D, H, L, P, T), a marker for PBC neurons. In M*lox*P mice, the PBC showed mild abnormal PrP accumulation (A) and gliosis (B), and absence of spongiosis (C). In NFH-Cre/M*lox*P mice, abnormal PrP accumulation was even milder (E), and gliosis (F) was comparable to M*lox*P mice (B). At 12 wpi, abnormal PrP accumulation was prominent in the PBC of terminally ill M*lox*P mice, at levels comparable to the rest of the ventral medulla (I), whereas in recombined NFH-Cre/M*lox*P mice, the PBC showed reduced accumulation compared to the surrounding areas (M). Although gliosis was comparable between M*lox*P mice (J) and NFH-Cre/M*lox*P mice (N), spongiosis was evident in terminal M*lox*P mice (K) but not in healthy NFH-Cre/M*lox*P mice (O). In terminally ill NFH-Cre/M*lox*P mice (35 wpi), abnormal PrP accumulation was reduced in the PBC in comparison to the surrounding areas (Q), and not substantially different from that observed in these mice at 12 wpi (M). Gliosis (R) was also

comparable to gliosis in 12 wpi time culled NFH-Cre/M*lox*P mice (N).The main difference with the earlier time point was the occurrence of spongiform changes, with small vacuoles (S). Scale bar= 84 µm.

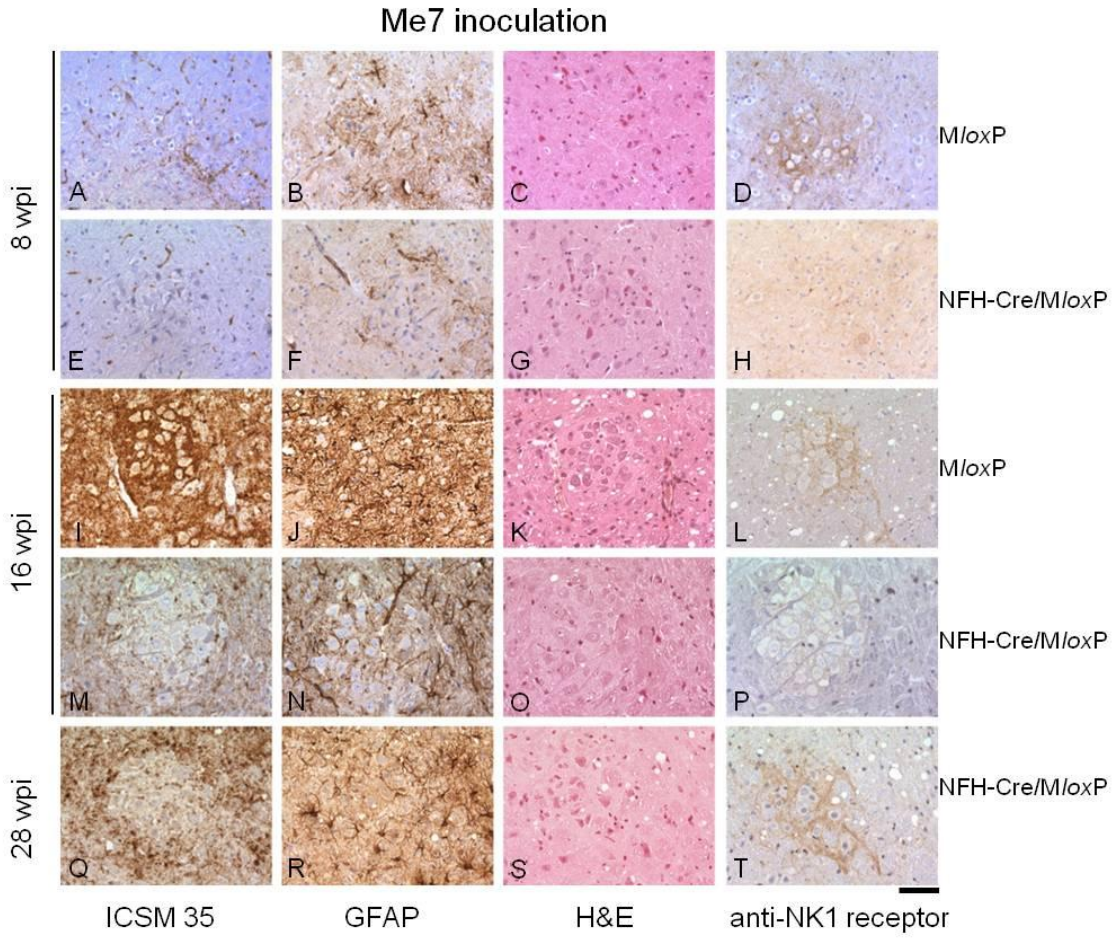

Figure 5.13 Progression of prion pathology in the pre-Bötzinger complex of Me7 inoculated M*lox*P and NFH-Cre/M*lox*P mice

Brain slices of the pre-Bötzinger complex (PBC) of Me7 inoculated M*lox*P and NFH-Cre/M*lox*P mice at different stages of disease progression were compared. To confirm the identity of this group of cells slices were immunostained with ICSM35 antibody for abnormal PrP deposition (A, E, I, M, O), anti-GFAP antibody for detection of astrocytosis (B, F, J, N, R), haematoxylin and eosin (H&E) to assess spongiform changes (C, G, K, O, S) and anti-NK1 receptor antibody (D, H, L, P, T), a marker for PBC neurons. At 8 wpi, PrP deposition (A) and gliosis (B) in the PBC of Me7 infected M*lox*P mice were very mild. In the recombined NFH-Cre/M*lox*P mice, PrP deposition was reduced (E) compared to M*lox*P mice (A), but gliosis was comparable (F) No spongiform changes were recognizable both in M*lox*P (C) and NFH-Cre/M*lox*P mice (G). The PBC of terminally ill M*lox*P mice was severely affected by prion deposition (I), and gliosis (J); small and medium size vacuoles were recognizable (K). In NFH-Cre/M*lox*P mice time-culled at 16 wpi PrP deposition was mild (M), reactive gliosis was mild (N) and the tissue was not spongiotic (O). In terminally ill NFH-Cre/M*lox*P mice (28 wpi), the effect of PrP depletion was evident, as in the PBC there was less deposition then in the surrounding areas (Q) and reactive gliosis (R) and spongiosis (S) were comparable to that in terminally ill M*lox*P mice (J, K). Scale bar= 84 µm.

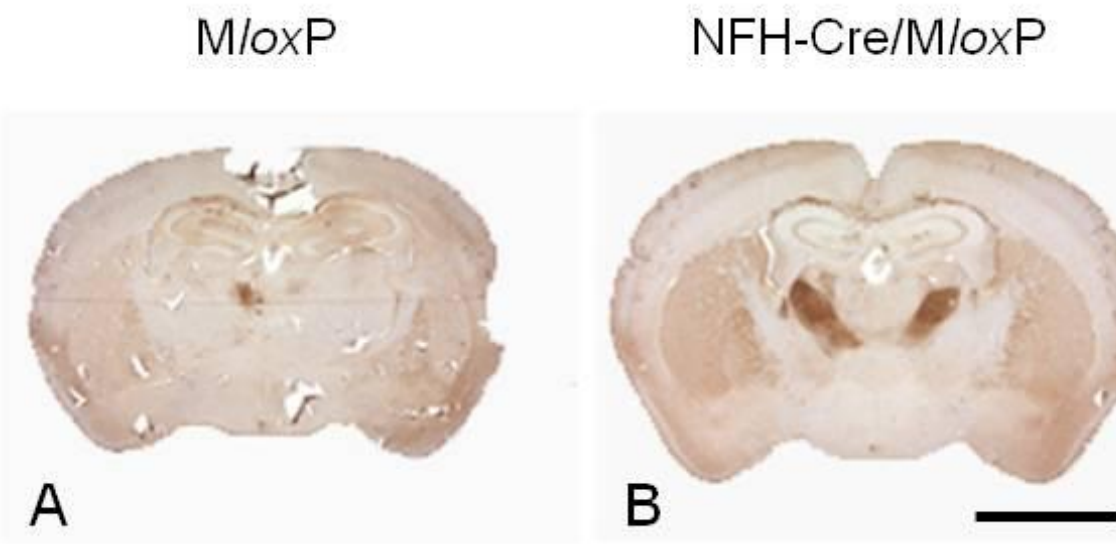

Figure 5.14 Early prion pathology in the forebrain of RML inoculated M*lox*P and NFH-Cre/M*lox*P inoculated mice

Brain slices encompassing the hippocampus and thalamus of five RML inoculated M*lox*P (A) and five NFH-Cre/M*lox*P mice (B), time culled at 6 wpi, were stained with ICSM 35 to assess abnormal PrP deposition in the forebrain. Abnormal PrP accumulation was localized in the thalamus of two out of five M*lox*P (A) and two out of five NFH-Cre/M*lox*P (B) mice. The thalamus and the brainstem, have previously been suggested to be the potential clinical target areas (Li et al., 2010). Scale bar= 4 mm

5.5 Discussion

The aim of this thesis was to investigate the clinical target areas in prion disease. Clinical target areas are regions responsible for the clinical phenotype and ultimately for the (fatal) outcome of prion disease. Previously, sub-clinical infection has been described in genetically modified mice, undergoing adult neuronal Cre-mediated PrP deletion (Mallucci et al., 2003). RML infected NFH-Cre/M*lox*P mice were shown not succumb to prion disease, but survived long-term in a sub-clinical state, while accumulating extra-neuronal PrP. As described in chapter 3, a repeat experiment with different prion strains, did not yield the same results, as Me7 or Mouse-adapted BSE inoculated NFH-Cre/M*lox*P mice survived longer than their respective M*lox*P controls, but developed clinical disease. In light of this difference, we used the adult PrP depleted NFH-Cre/M*lox*P model as tool to investigate the clinical target areas of prion disease.

We hypothesized that the different outcome between RML and other prion infections in neuronal PrP depleted mice was that in RML infected NFH-Cre/M*lox*P mice, PrP depletion stopped the disease progression in one or more specific anatomical regions (clinical target areas), preventing the progression towards clinical phenotype and death. Therefore, by comparing the pathology of subclinical RML inoculated NFH-Cre/M*lox*P mice, terminally ill RML or Me7 inoculated M*lox*P mice and terminally ill Me7 inoculated NFH-Cre/M*lox*P mice, we could pinpoint the clinical target areas for prion disease.

We decided to focus on the pathological analysis of the brainstem for several reasons: (i) the brainstem is critically important for the vital functions of the animal. It controls the respiratory and cardiovascular system, ensuring continuous modulation of respiration, heart rate and blood pressure and balances external inputs such as gravity and movement; (ii) clinical signs suggestive of brainstem involvement are typical in experimental models of prion disease and correlation of clinical signs deriving from brainstem impairment and brainstem pathology in the brainstem of sCJD patient has been reported (Iwasaki et al., 2005); and (iii), our study described in chapter 3, showed accumulation of abnormal PrP in the brainstem of Me7 and Mouse-adapted BSE inoculated M*lox*P and NFH-Cre/M*lox*P mice very early on in disease progression.

We speculated that clinical target areas could be either the first or the last areas affected by prion pathology in the disease progression. In the "last target areas scenario", prion disease would start as a generalised widespread accumulation of "toxic species" in the CNS. This widespread accumulation would not cause clinical impairment, until it localizes in the vital areas. Therefore, the clinical symptoms would be caused by functional impairment of the last targeted areas.

In the "first target areas scenario", prion accumulation would start in a region critical for specific functions or connections. During disease progression, the pathology would eventually spread to secondary target regions. The clinical phenotype would be determined when the molecular events, following prion inoculation, lead to partial or total impairment of the functions of the first targeted area(s). In this scenario, degeneration over time of the first target region(s) determines fatal outcome; therefore clinical phenotype could be avoided by reducing prion accumulation in the clinical target areas or by blocking or slowing down the disease progression in these areas.

In chapter 4 we explored the "last target area hypothesis", by comparing pre-clinical longer surviving RML inoculated NFH-Cre/M*lox*P mice, and end stage M*lox*P mice inoculated with RML or Me7 and NFH-Cre/M*lox*P mice inoculated with Me7. Unexpectedly, the RML infected NFH-Cre/M*lox*P mice also progressed to a clinical phenotype. Although we cannot discard the hypothesis of clinical target areas being last areas targeted by prion infection, we cannot use our original approach to undertake this investigation since the RML inoculated NFH-Cre/M*lox*P mice also progressed to clinical disease. However, we noticed that both RML and Me7 inoculated M*lox*P and NFH-Cre/M*lox*P terminally ill mice had severe prion pathology in the same brainstem areas, namely the locus coeruleus (LC) and the nucleus of the solitary tract (NTS).

Keeping in mind these results, we investigated the first areas of prion pathology in M*lox*P and NFH-Cre/M*lox*P mice, at an early stage of prion infection, i.e. 6 wpi for RML and 8 wpi for Me7 prions. We first analysed prion pathology in Me7 and RML inoculated M*lox*P mice and found that the same three areas in the brainstem were the focus of primary abnormal PrP deposition: the locus coeruleus (LC), the nucleus of the solitary tract (NTS) and the pre-Bötzinger complex (PBC) (Figure 5.2). A higher level of abnormal PrP deposition was found in the LC, in

association with intense gliosis (Figures 5.3). In the NTS and the PBC, both abnormal deposition and gliosis were milder (Figures 5.5. and 5.6). In all three areas, spongiosis was absent (Figures 5.3, 5.5, 5.6).

When we compared the pathology profiles of RML or Me7 infected M*lox*P mice with those of RML or Me7 infected NFH-Cre/M*lox*P mice, we noticed that prion pathology was localized in the same areas (i.e. LC, NTS, PBC), although with reduced intensity in the recombined mice. At 6 wpi RML infected NFH-Cre/M*lox*P mice and at 8 wpi Me7 infected NFH-Cre/M*lox*P mice showed reduced, but intense abnormal accumulation in the LC and reduced gliosis (Figure 5.4). Although abnormal PrP accumulation was reduced in the NTS and the PBC of depleted NFH-Cre/M*lox*P mice, no reduction of gliosis was observed (Figures 5.5 and 5.6).

These data lead to two observations, the first regarding the mouse model used, and the second on the pathological steps in the disease progression. (i) M*lox*P mice overexpress PrP from the M*lox*P transgene ~ 3-4 times wild type level, whilst retaining the regional expression pattern (Mallucci et al., 2002). Therefore, the first sites of abnormal accumulation in M*lox*P mice are representative of the wild type situation. NFH-Cre/M*lox*P mice have been shown to undergo Cre-mediated recombination in all post mitotic neurons throughout the nervous system at ~10 weeks of age (Mallucci et al., 2002). We already noticed a discrepancy between our results and published data on the sub-clinical state of RML infected NFH-Cre/M*lox*P mice. The reduced abnormal accumulation observed in the LC, NTS and PBC suggested that some recombination has already occurred in NFH-Cre/M*lox*P mice in these nuclei at 7 weeks of age (= 6 wpi, the early time point for RML inoculated mice). This difference highlighted the need for a more detailed analysis of recombination in the animal model, which will be discussed in the next chapter. (ii) The pathological steps in the disease progression are characterised by the presence of intermediate gliosis in the NTS and PBC, and suggest that reactive gliosis is an early event in these two brainstem areas, even if the abnormal accumulation has been reduced by recombination.

We also monitored abnormal accumulation in the forebrain of RML infected mice (Figure 5.14) and confirmed that thalamus is another region of early accumulation, as reported previously (White et al., 2008).

To evaluate how neurodegeneration in brain regions correlates with the clinical phase of prion disease, we followed the disease progression in the areas targeted by early pathology. As the degrees of abnormal PrP deposition in the evaluated areas in terminal M*lox*P mice and asymptomatic NFH-Cre/M*lox*P mice (12 wpi for RML infection and 16 wpi for Me7 infection) were comparable, we confirmed once again that PrP^{Sc} is not the toxic species. At 12 wpi and 16 wpi NFH-Cre/M*lox*P mice can be considered to be sub-clinical infections (Hill et al., 2000; Hill and Collinge, 2003b; Hill and Collinge, 2003a), where accumulation of PrP disease associated form does not cause development of clinical symptoms. The functional changes that prion toxicity generates in cells and tissue are not clear, nor are their temporal sequence. In this chapter we showed that progression of pathology in the LC, NTS and PBC of RML and Me7 infected PrP depleted NFH-Cre/M*lox*P mice was slower than in their PrP overexpressing M*lox*P counterparts, probably due to recombination, but in both M*lox*P and NFH-Cre/M*lox*P mice and both infections spongiosis was first observed when in the clinical phase of the disease (12 and 16 wpi for M*lox*P and 35 and 28 wpi for NFH-Cre/M*lox*P mice), (Figures 5.7, 5.8, 5.10, 5.11, 5.12, 5.13). The mechanism behind spongiform changes is still under debate: spongiosis has been linked to abnormal membrane permeability and increased water content in the neurons (Kovacs and Budka, 2008) or to autophagy (Liberski et al., 2004; Liberski, 2004). However, spongiosis represents the ultimate stage of disease progression.

Neurotoxicity in prion disease is believed to be mediated by a lethal PrP species, PrP^{L} (Hill et al., 2000; Hill and Collinge, 2003a), distinct from abnormally folded PrP, PrP^{Sc}. PrP^{L} formation is catalysed by PrP^{Sc}, and PrP^{L} toxic effects occur when the PrP^{L} concentration increases above a local threshold (Collinge and Clarke, 2007).

It has been shown experimentally that prion infectivity and toxicity occur in two separate phases. Phase 1 is a clinically silent exponential phase not rate-limited by prion protein concentration, in which the maximal prion titre is reached; and phase 2 is constituted by a plateau of infectivity that continues until the onset of clinical disease. Phase 2 length is inversely proportional to PrP^{C} expression level. PrP^{L} is believed to be produced in the phase 2, proportionally to PrP^{C} concentration. Therefore, clinical onset occurs when PrP^{L} reaches a toxic threshold (Sandberg et al.,

2011). Other alternative scenarios have been hypothesized to explain the split between infectivity and toxicity: for example, fission of infectious particles may stop, leading to further growth of abnormally folded PrP aggregates but no increase in number of infectious particles; or a key cellular component may be depleted during phase 2, determining clinical onset.

Our data can be accommodated in this general model: although in both M*lox*P and NFH-Cre/M*lox*P mouse lines the LCS, NTS and PBC were the first sites of prion replication, we could assume that in overexpressing M*lox*P mice phase 2 is shorter than in depleted mice, where PrP expression level is lower. However when PrP^{L} reaches the local threshold in these areas, mice become terminally ill. In an alternative scenario, the toxicity event may be impairment at the cellular level in the LC, NTS, and PBC. Indeed, LC, NTS and PBC are particularly important for the survival of an animal, because of their role in autonomic control.

Although due to time constraints it was not possible to set up a functional study to test functional impairment in these areas correlating with clinical stage of prion disease, a literature search supported our view on the vital role of these areas.

The LC is the largest group of noradrenergic neurons in the central nervous system. Noradrenalin or Norepinephrine (NA or NA) is synthesized from tyrosine by TH, with formation of L-dihydroxyphenylalanine (L-DOPA). L-DOPA is converted to dopamine by L-amino acid decarboxylase and dopamine is transported by the vesicular monoamine transporter (VMAT) into synaptic vesicles, where it is converted to NA by the dopamine β-hydroxylase (DBH). NA is inactivated through pre-synaptic reuptake via a selective transporter (NET) and subsequent metabolism. NA acts via three G-protein receptor families, α1, α2, and β. α1 and β are primarily localized post-synaptically, with excitatory functions; α2 receptors are both pre- and post-synaptic and have inhibitory effects. Synaptic availability of NA is regulated by active reuptake via the NET and inhibition of release via presynaptic α2 receptors (Benarroch, 2009). It is estimated that ~50% of all the noradrenergic projections in the central nervous system originate in the LC and are directed towards the forebrain, cerebellum, brainstem and spinal cord.

Through its wide net of connections, the LC has a fundamental role in control of various homeostatic functions (Svensson and Thoren, 1979; Bhaskaran and Freed,

1988; Aston-Jones and Bloom, 1981; Aston-Jones et al., 2001), and cognitive behaviour.

In the context of prion disease pathology, the intriguing characteristics are its involvement in other neurodegenerative syndromes and its role in the control of autonomic functions. In human post mortem studies of Alzheimer Disease, degeneration of the LC correlated with the progression and severity of dementia and increase of Aβ plaque deposition and neurofibrillary tangle formation (Iversen et al., 1983; Bondareff et al., 1987; German et al., 1992; Marien et al., 2004).

Loss of LC neurons has been associated with plasticity changes, in an attempt to compensate for the loss of NA content, including increase in TH expression, sprouting of dendrites in LC neurons, axonal sprouting and down-regulation of α1D and α2C adrenergic receptors in the hippocampus (Szot et al., 2006). In Alzheimer's Disease mouse models, noradrenalin depletion has been shown to contribute to astroglial and microglial activation (Heneka et al., 2006), upregulation of inflammatory markers (Pugh et al., 2007) and elevated inducible nitric oxide synthase (iNOS) and nitric oxide levels in LC projection areas (Heneka et al., 2002). Recently, LC degeneration has been shown to dysregulate adrenergic receptors and to exacerbate Aβ-induced neuroinflammation (Jardanhazi-Kurutz et al., 2011).

In Parkinson's disease, (PD) LC neuronal loss (German et al., 1992; Zarow et al., 2003; Remy et al., 2005) and morphological alterations of synapses and mitochondria have been reported (Baloyannis et al., 2006). Although the significance of LC involvement in PD pathology is not clear, some studies suggested that the LC-NA system may have a role in compensatory mechanisms in early stages of PD. In animal models, neurotoxic LC lesions or knockout of the DBH gene results in more severe dopaminergic cell loss and motor manifestation, and pharmacologic or genetic blockade of NET or administration of the α2 receptor agonist protects dopaminergic neurons (reviewed in (Rommelfanger and Weinshenker, 2007).

Down syndrome (DS) individuals show deficits in contextual learning and memory (Pennington et al., 2003). These tasks are hippocampal-based and mediated by noradrenergic LC inputs. In a mouse model of DS, dysfunction and degeneration of the LC has been shown to be associated with a deficit in contextual learning. However, the postsynaptic hippocampal targets were responsive to noradrenergic

receptor activation, suggesting that restoring NA transmission could reverse cognitive dysfunction (Salehi et al., 2009).

In order to assess the implication of prion pathology in the LC, we compared TH immunoreactivity in the LC of infected mice at end stage and in the course of disease progression (Figure 5.9). No change in TH staining was detected; however this is most likely due to the way the samples were collected: we used some of the sequential sections spanning the LC, collected for the prion pathology analysis. To determine the number of TH positive cells throughout the rostral-caudal extent of the LC, an un-biased stereological method would have been a better approach. However, this would have required a new experiment to collect the appropriate brain slices and therefore it was not pursued. Intrigued by the findings on hippocampal impairment followed by LC degeneration in the mouse model of DS, we attempted VMAT2 and β-adrenergic receptor staining on hippocampal slices, but were unable to optimize a working protocol with the antibodies tested.

The hippocampus is a known target of prion pathology, and rescue of early pathology and behavioural changes has been shown through genomic PrP depletion (Mallucci et al., 2003; Mallucci et al., 2007), and local knock-down through lentiviral-mediated RNAi (White et al., 2008). To discriminate between LC and hippocampus driven behavioural impairment would be difficult in the course of prion disease. However we have now shown that LC pathology temporally precedes hippocampal impairment; therefore it is possible that LC impairment may have a role in some of the hippocampal deficits observed in experimental prion disease. Future experiments involving focal delivery of anti PrP RNAi in the LC could determine if behavioural defects can be rescued.

The LC is implicated in control of respiration (Oyamada et al., 1998; Fabris et al., 1999; Biancardi et al., 2008) and cardiovascular function (Sved and Felsten, 1987). Specifically, LC neurons participate to the central respiratory network, (Coates et al., 1993) and manifest chemosensitive signalling behaviour (Elam et al., 1981; Filosa et al., 2002). The LC has also been shown to be pathologically involved in Rett syndrome (Taneja et al., 2009), and Multiple system atrophy (MSA) (Benarroch et al., 2008). These properties are of particular interest, considering the other nuclei that we also identified as clinical target areas of prion disease.

The NTS is an extraordinary relay nucleus for integration and modulation of autonomic activity. In rats, it has been estimated to contain ~42000 cells, organized in different sub-nuclei (Andresen and Kunze, 1994) that contribute both to respiratory control and cardiovascular activity. Many NTS neurons have respiratory-related activity and central respiratory modulation (Weston et al., 2003; Bailey et al., 2006; Kubin et al., 2006) and respond directly to acid in vitro and detect changes in pCO_2 *in vivo* (Dean et al., 1990; Nattie and Li, 2009). NTS also contains neurons responding to arterial baroreceptors (Rogers et al., 1993; Paton, 1998; Paton, 1999; Zhang and Mifflin, 2000). NTS neurons activated by hypoxia may have a role in impaired ventilator response observed in Multiple System Atrophy (MSA) (Neubauer and Sunderram, 2004).

In prion disease, the NTS has also been shown to be one of the first areas of prion accumulation in a model of oral infection, via the dorsal motor nucleus of the vagal nerve (Beekes et al., 1998; Beekes et al., 1998). Our findings imply that the NTS is a particularly vulnerable area for prion pathology not only for the anatomical connection to the vagus nerve, but even upon intracranial inoculation.

PBC neurons are characterized by Neurokinin 1 receptor immunoreactivity (Gray et al., 1999). We took advantage of this property to confirm the identity of the group of cells showing early abnormal PrP accumulation in the ventral medulla. Different studies indicate that the PBC is the centre of respiratory rhythm generation (Funk et al., 1993; Smith et al., 1991; Ramirez and Richter, 1996; Rekling and Feldman, 1998; Koshiya and Smith, 1999; Smith et al., 1991). In neonatal rat isolated brainstem-spinal cord preparations, removal of the PBC abolishes rhythm generation, with rhythmicity maintained only if the PBC is present (Smith et al., 1991).

The PBC may also contribute to generation of respiratory rhythm in adult mammals. After the early reports in adult cats (Connelly et al., 1992; Schwarzacher et al., 1995) and rats (Sun et al., 1998), the exact location of the PBC has recently been found in human brains (Schwarzacher et al., 2011). In rats, PBC neurons have been described as oval, fusiform or multipolar in shape, small to medium size, also projecting to the NTS (Onimaru et al., 1995). Impairment of the PBC has been shown to occur in Rett Syndrome (Mironov et al., 2009), Sudden Infant Death

Syndrome (SIDS) (Pena, 2010) and Multiple System Atrophy (MSA) (Benarroch, 2007).

Given the role of these nuclei in control of respiratory and cardiac activity, their cellular impairment and neurodegeneration may determine clinical onset; therefore the LC, NTS and PBC could be the clinical target areas of prion disease. Identification of these nuclei as clinical target areas of prion disease will now enable a detailed investigation into the molecular, cellular and neuronal network events that could trigger clinical onset of prion disease.

5.6 Summary

We have found three areas in the brainstem where prion deposition occurs at early time points both in RML and Me7 inoculated M*lox*P and M*lox*P/NFH-Cre mice: the locus coeruleus, the nucleus of the solitary tract and the pre-Bötzinger complex.

We also followed disease progression in these areas and observed that the common trait in terminally ill M*lox*P and M*lox*P/NFH-Cre mice was spongiform changes in these nuclei.

Because of their fundamental role in control of respiratory and cardiac activity, their cellular impairment and neurodegeneration may determine clinical onset. Therefore the LC, NTS and PBC could be the clinical target areas of prion disease. Our analysis suggests that the first target areas of prion deposition are critical, as their degeneration is responsible for the fatal outcome of prion disease.

6 Spatial and temporal characteristic of Cre-mediated recombination

6.1 Introduction

In the previous chapter, the locus coeruleus, the nucleus of the solitary tract and the pre-Bötzinger complex were identified as the first brainstem target areas of prion pathology in an experimental model of prion disease, and we speculated they may represent clinical target areas in prion disease. The experimental model was the neuronal PrP depleted NFH-Cre/M*lox*P mouse line, a thoroughly characterized model (Mallucci et al., 2002). These mice are the result of a cross between NFH-Cre and M*lox*P transgenic mice. NFH-Cre mice express the P1 Cre recombinase under the control elements of the Neurofilament gene (NFH) (Julien et al., 1988) on a PrP null background (FVB *PrnP* $^{0/0}$) (Bueler et al., 1992).

M*lox*P mice encode the M*lox*P construct, containing the floxed murine PrP (MoPrP) coding region between two *lox*P sites, on the FVB *PrnP* $^{0/0}$ background. Mallucci et al. generated lines of M*lox*P mice designated tg46 and tg37 (Mallucci et al., 2002). Tg46 mice express PrP at a level comparable to wild-type, whereas tg37 mice overexpress PrP ~ 3-4 fold the wild type level. Both lines have the same regional pattern of PrP expression as wild-type animals (Sales et al., 1998). Tg46 and tg37 were crossed to NFH-Cre mice: in the double transgenic line, when Cre is expressed, it mediates the excision of MloxP PrP sequence between the two lox P sites. It was shown, using quantitative southern blot analysis on whole brain DNA from double transgenic mice (both NFH-Cre/tg46 and NFH-Cre/tg37), that Cre-mediated deletion of M*lox*P transgene occurred in the majority, probably all the neurons ~10 weeks after birth. Moreover, by crossing Cre-expressing mice with the ROSA26 reporter mice (Soriano, 1999), encoding a LacZ transgene that requires Cre recombinase for activation, it was shown that LacZ is expressed throughout the central and peripheral nervous system, especially in neuron-rich areas, such as hippocampus and brainstem. In NFH-Cre/M*lox*P (NFH-Cre/tg46) mice deletion of the M*lox*P transgene upon Cre activation was confirmed with immunohistochemistry on frozen sections of 12-week old mice, throughout cortex, hippocampus, striatum and cerebellum. Pre-deletion mice, analysed when <10 weeks of age, exhibited a pattern of PrP expression identical to M*lox*P mice (Mallucci et al., 2002). As

discussed in the previous chapters, NFH-Cre/M*lox*P mice were resistant to RML prion infection, even though they accumulated PrP in non-recombined cells. Both NFH-Cre/tg 46 and NFH-Cre/tg37 survived RML prion infection for up to 56 weeks, whereas tg46 and tg37 M*lox*P non-recombined controls succumbed to RML prion infection within 18 and 12 wpi. In addition, depletion of neuronal PrP reversed early spongiform changes and prevented neuronal loss in the hippocampus of NFH-Cre/tg37 mice (Mallucci et al., 2003). Furthermore, RML infected NFH-Cre/tg37 mice recovered early behaviour and synaptic impairment in parallel with spongiosis reversal (Mallucci et al., 2007).

When we set out to investigate clinical target areas for prion pathology in the brainstem, we decided to use the overexpressing M*lox*P tg37 and the NFH-Cre/tg37 mice for comparison with previous studies. However since we had planned to look for clinical target areas in the brainstem, a more detailed investigation of recombination in every brainstem nucleus was clearly required. Moreover, my results presented in chapter 4 showed that the RML infected NFH-Cre/M*lox*P mice were no longer fully protected from clinical disease, but showed a prolonged incubation time compared to RML infected M*lox*P controls. The differences in the results between these two studies suggested that a careful examination of timing and region specification of Cre-mediated PrP knock-out in NFH-Cre/M*lox*P mice was required.

6.2 Aims

- To characterize the timing and regional specificity of Cre-mediated recombination in NFH-Cre/M*lox*P mice.

6.3 Experimental set up

To achieve a detailed characterization of the mouse model, two different approaches were employed:

- A histological approach taking advantage of the ROSA26 reporter line to localize Cre-mediated recombination in different brain areas as indicated by LacZ activation
- A molecular approach to monitor timing and efficacy of Cre-mediated recombination in NFH-Cre/M*lox*P mice in different brain areas

6.4 Results

6.4.1 Characterization of Cre activation in NFH-Cre/ROSA26 mice

Homozygous NFH-Cre mice were crossed with homozygous ROSA26 reporter mice (Soriano, 1999). Thus, every mouse in the litter was hemizygous for both the Cre and the LacZ transgenes.

Expression of the LacZ gene in ROSA reporter mice is repressed by the presence of a stop codon, positioned between 2 loxP sites. When Cre recombinase is expressed in NFH-Cre/ROSA mice, it interacts with the two loxP sites, mediating excision of the stop codon resulting in expression of the product of the LacZ gene, the β-galactosidase enzyme (Figure 6. 1).

Litters of the cross were organized into groups of 5 or more mice to enable time culling at embryonic day 15, post-natal day 2, post-natal weeks 1, 2, 5, 9, 13, 15, 17, 21 and 25. Whole embryos, heads of 2 days old mice and brains of the weekly-based time culling mice were fixed. Occurrence of recombination was monitored through β-galactosidase staining and immunohistochemistry with anti β-galactosidase antibody on fixed samples (Figure 6.2).

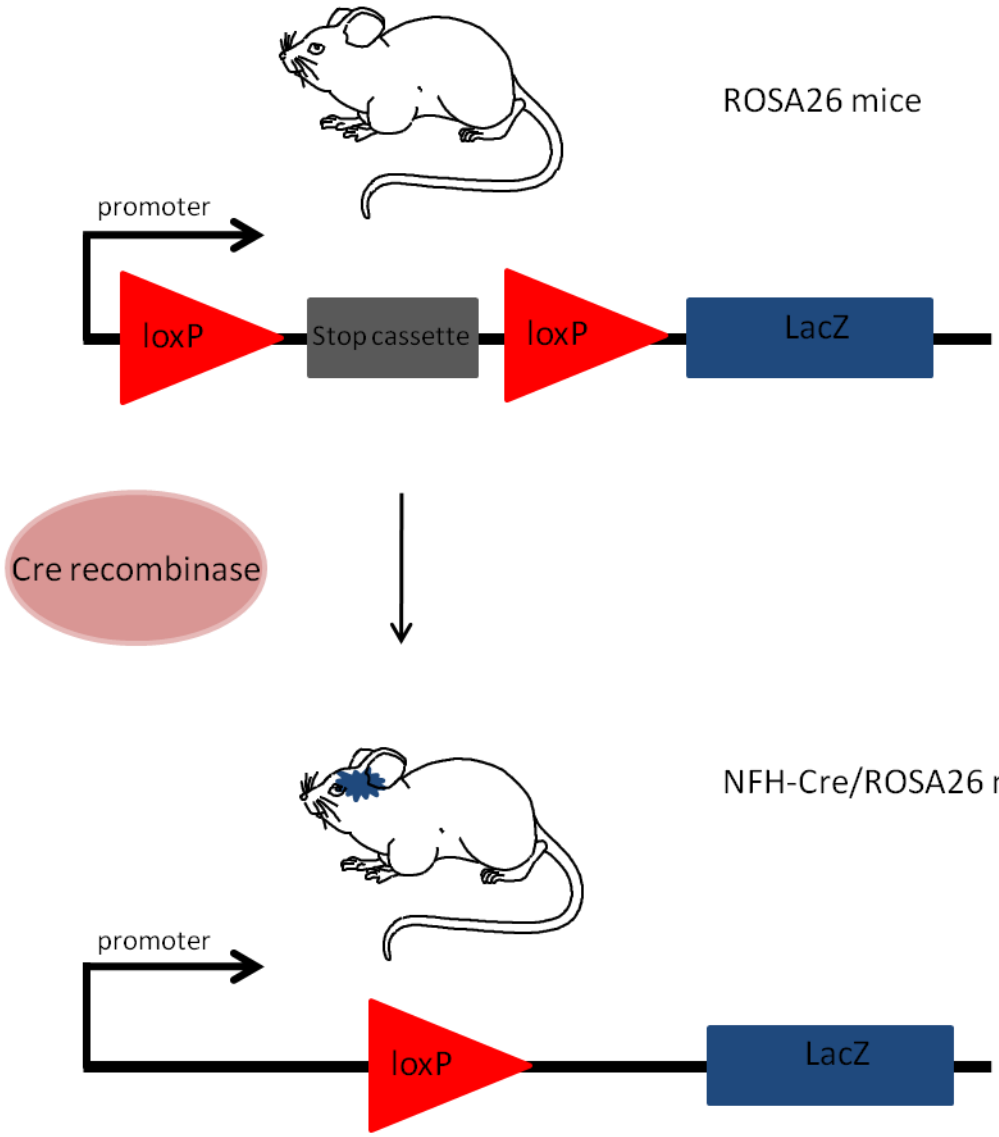

Figure 6.1 Schematic of Cre-mediated recombination in NFH-Cre/ROSA 26 mice

Expression of the LacZ gene in ROSA26 reporter mice is repressed by the presence of a stop codon, positioned between the two loxP sites. Cre recombinase expression mediates excision of the stop codon and expression of the product of the LacZ gene, the β-galactosidase enzyme.

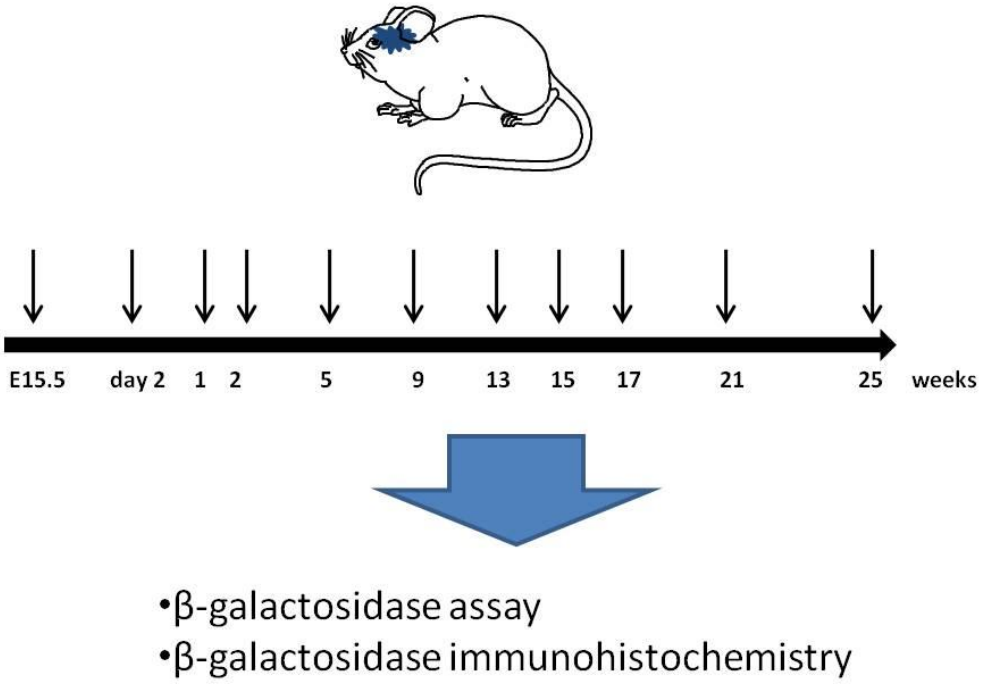

Figure 6.2 Experimental approach

Homozygous NFH-Cre and homozygous ROSA26R mice were crossed. Litters were grouped to 5 or more mice and analysed at embryonic day 15.5, post-natal day 2, and post-natal weeks 1, 2, 5, 9, 13, 15, 17, 21 and 25. After fixation, whole embryos, heads of 2 days old mice or brains of the weekly time culls were analysed by the β-galactosidase assay and/or by immunohistochemical detection of β-galactosidase (Time axis not to scale).

6.4.1.1 β- galactosidase staining assay in NFH-Cre/ROSA26 mice

LacZ encodes the bacterial enzyme β-galactosidase, which hydrolyses β-galactosides into monosaccharides.

β-galactosidase expressing cells can be detected by the β-galactosidase staining assay through exposure to the synthetic compound X-gal (5-bromo-4-chloro-3-indolyl- beta-D-galactopyranoside). β-galactosidase hydrolyses X-gal into galactose and 5-bromo-4-chloro-3-hydroxyindole, a blue insoluble compound. Therefore, β-galactosidase expressing cells assume a characteristic blue colour.

Since this was a straightforward and inexpensive procedure, it was used on brains from early time points, when no recombination should have taken place (Mallucci et al., 2002). Half heads from mice culled at postnatal day 2 (n=9) and half brains from mice culled at postnatal week 2 (n=3) were fixed in 4% PFA and exposed to X-gal containing solution. However, formation of the blue compound was unexpectedly observed in all the stained brains, albeit at different intensities. At post-natal day 2, a mouse brain is still developing, and cells are migrating to their adult location. For this reason, it was not possible to precisely define in which brain areas recombination had occurred (Figure 6.3 A). However, at post-natal week 2, a mouse brain is fully formed. A representative sample of the different patterns observed is shown in Figure 6.3 B. Recombined areas in the brainstem, the hippocampus, the ventral tegmental area, the thalamus were clearly detected. A more detailed analysis on areas of recombination could have been attempted, performing the β-galactosidase assay on 40 µm slices cut on the microtome. However, trials on non-experimental brains, constitutively expressing β-galactosidase, showed a high level of variability, probably dependent on the variable time the slices were in fixative before the application of X-gal solution. Although many efforts were made to optimize the β-galactosidase assay protocol on vibratome sections, a high level of reproducibility could not be achieved. Therefore, a more thorough histological study based on immunohistochemistry for β-galactosidase was undertaken.

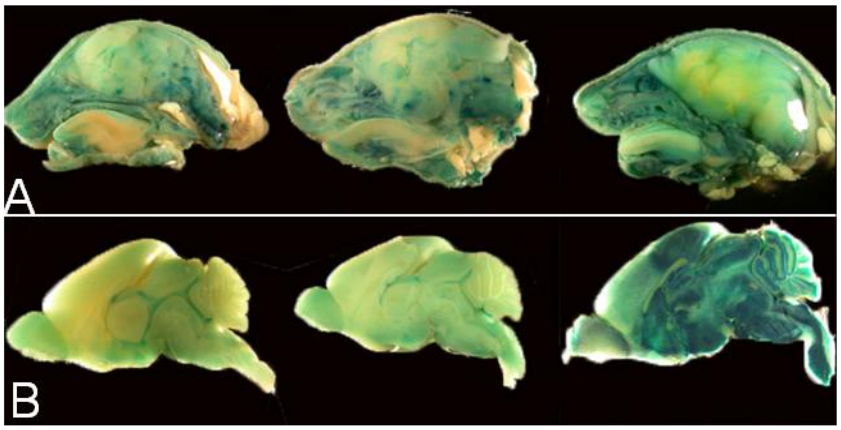

Figure 6.3 β-galactosidase assay in NFH-Cre/ROSA26 mice

β-galactosidase expressing cells can be detected through exposure to the synthetic compound X-gal. β-galactosidase hydrolyses X-gal into galactose and 5-bromo-4-chloro-3-hydroxyindole, a blue insoluble compound. β-galactosidase expressing cells assume a characteristic blue colour.

A. Three heads of NFH-Cre/ROSA26 mice (P2) show a widespread expression of β-galactosidase, indicating that widespread recombination had occurred. At P2 many structures of the mouse brain are still developing and it is not possible to determine precisely in which structures recombination has occurred.

B. Three sagittally dissected brains of NFH-Cre/ROSA26, culled at post natal week 2. The variability of the staining indicates a variable efficacy of recombination.

6.4.1.2 Immunohistochemistry for β-galactosidase expression

The other halves of the brains collected at postnatal day 2 were used for immunohistochemistry with anti- β-galactosidase antibody. β–galactosidase diffusely accumulates in the cytoplasm and typically forms a few intralysosomal dense aggregates. In brains from NFH-Cre/ROSA26 mice at postnatal day 2, β-galactosidase staining was localized in the cerebellum and in the brainstem (Figure 6.4 panel D and E). In mice the cerebellum is only completely formed at postnatal week 1, therefore identity of the cerebellar cells involved in recombination could not be defined. Also, the absence of clear anatomical hallmarks in the brainstem sagittal section did not allow localization of specific brainstem nuclei. For subsequent time points, coronal sections were prepared and analysed. Collected brains were cut into three pieces with the same procedure used in chapter 4, and coronal slices were cut using the microtome by the support team of the histology core facility at the MRC Prion Unit.

At postnatal week 2, β-galactosidase staining was localized in the thalamus, the hippocampus and the brainstem, at the level of the motor nucleus of the 5^{th} nerve, showing both punctuate and diffuse staining (Figure 6.4 panels F, G, I). At post-natal week 5, β-galactosidase positive cells were localized as previously observed in the thalamus, hippocampus and brainstem, and for the first time in the cortex (Figure 6.4 panels K to N). At post-natal week 9, the areas of recombination were the same as at postnatal week 5, but more cells appeared to be involved (Figure 6.4 panels P to S).

This time course study showed that in NFH-Cre/ROSA26 mice, Cre-mediated recombination did not occur simultaneously in all brain areas; but the efficacy of recombination was low in some areas before 9 weeks of age.

Results in chapter 5 indicate that first areas of prion pathology at 6 wpi for RML (post-natal week 7) and 8 wpi for Me7 (post-natal week 9) were the locus coeruleus, the nucleus of the solitary tract and the pre-Bötzinger complex. Thus a more detailed analysis of recombination in these areas was performed.

Through serial coronal sections the exact localization of the mentioned areas in NFH-Cre/ROSA26 mice brains at postnatal week 9 was identified. As in Figure 6.5, β-galactosidase positive cells were present in all the mentioned areas, suggesting that Cre was active and recombination was occurring. However, not all the cells showed positive staining, indicating that recombination was not 100%.

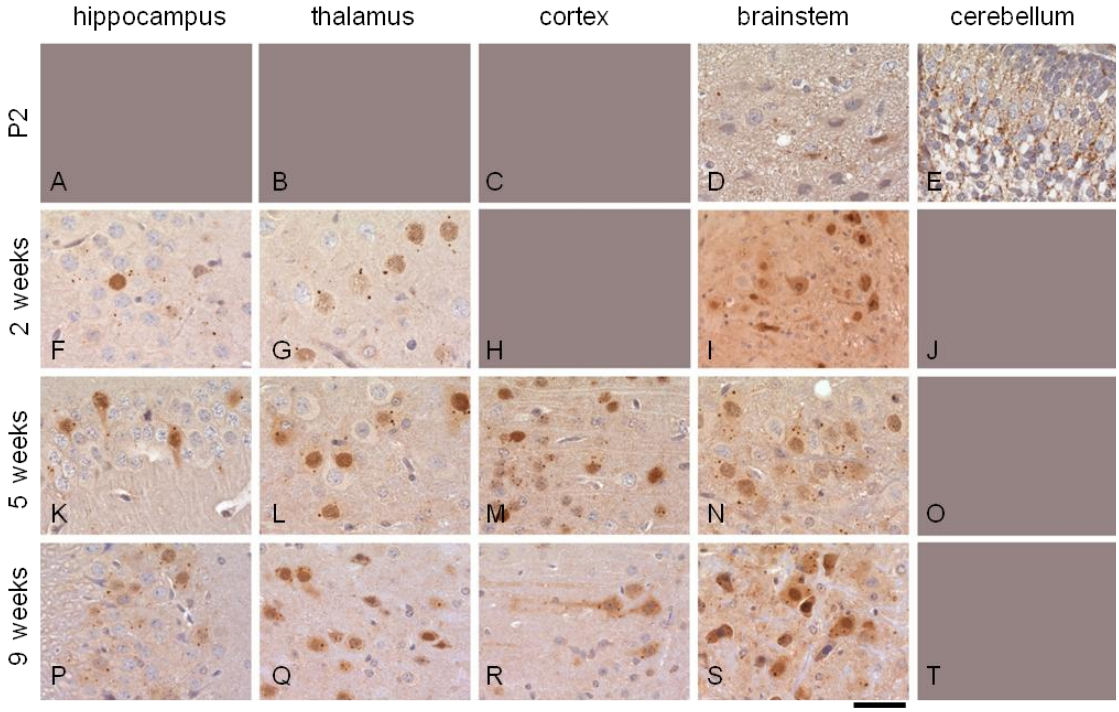

Figure 6.4 Immunohistochemistry for β-galactosidase

Immunostaining for β-galactosidase shows a diffuse accumulation in the cytoplasm as well as few intralysosomal dense aggregates with punctuate staining. In brains from NFH-Cre/ROSA26 mice at postnatal day 2, β-galactosidase staining was localized in the brainstem (D) and in the cerebellum (E). At postnatal week 2, β-galactosidase staining was localized in hippocampus (F), thalamus (G), and in the brainstem (I). At post-natal week 5, β-galactosidase positive cells were detected as previously observed in the hippocampus (K), thalamus (L), and in the brainstem (N) and for the first time in the cortex (M). At post-natal week 9, the areas of recombination were the same as at postnatal week 5 (P to S). Cerebellum from postnatal week 2 (J), 5 (O) and 9 (T) were not available. Scale bar= 84 µm.

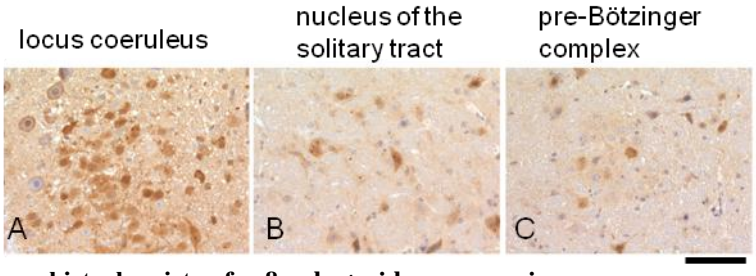

Figure 6.5 Immunohistochemistry for β-galactosidase expression

A. In the locus coeruleus, ca. half of the cells express β-galactosidase, indicating partial recombination. In the Nucleus of the solitary tract (B) and in the pre-Bötzinger complex (C), recombination was less frequent, but still clearly recognisable. Scale bar= 84 µm.

6.4.2 Characterization of Cre activation in NFH-Cre/M*lox*P mice

Homozygous NFH-Cre and homozygous M*lox*P mice were crossed and the litters organized into groups of at least 5 mice to be time culled at embryonic day 15, post-natal day2, post-natal weeks 1, 2, 5, 9, 13, 15, 17, 21, 25 and 32 (Figure 6.6). Embryos, and whole brains were snap–frozen for subsequently analysis. Whole brains were dissected into different brain areas (olfactory bulb, hippocampus, thalamus, caudate nucleus, mid brain, pons, medulla, cerebellum, cortex). From the embryos and the different brain areas, DNA was extracted and analysed.

6.4.2.1 qPCR on dissected brain areas of NFH-Cre/M*lox*P mice

DNA extracted from dissected brain areas from 5 week old NFH-Cre/M*lox*P mice (n=5) were analysed first. 100 ng of DNA from each of the different brain regions was amplified by PCR using a set of primers that anneal outside the M*lox*P sites, CosTet5' and CosTet3'. As shown schematically in Figure 6.7, in absence of recombination this results in a ~1150 bp band, corresponding to the entire M*lox*P transgene. Upon recombination and deletion of MoPrP, a shorter ~250 bp band is produced. However if recombination is not complete, due to the presence of non-neuronal cells or neurons in which recombination is not 100% complete, both bands will be detected.

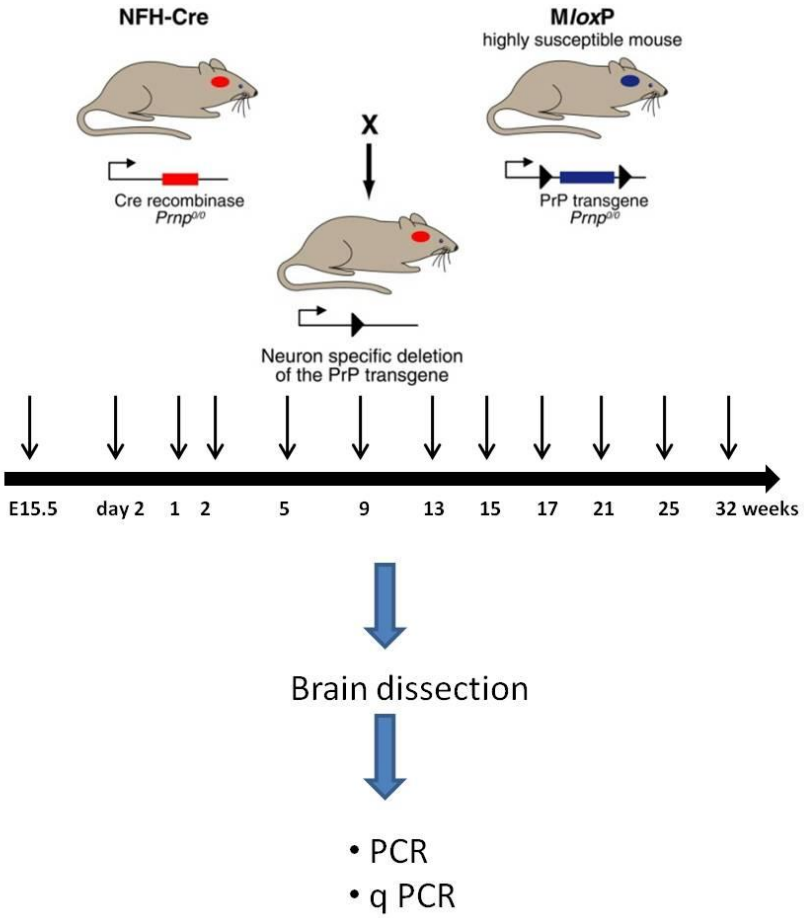

Figure 6.6 Experimental approach

Homozygous NFH-Cre and homozygous M*lox*P mice were crossed and the litters organized into groups of at least 5 mice to be time culled at embryonic day 15, post-natal day2, post-natal weeks 1, 2, 5, 9, 13, 15, 17, 21, 25 and 32. Embryos and whole brains were snap–frozen and analysed. Whole brains were dissected into different brain areas (olfactory bulb, hippocampus, thalamus, caudate nucleus, mid brain, pons, medulla, cerebellum, and cortex). From the embryos and the different brain areas, DNA was extracted and analysed.

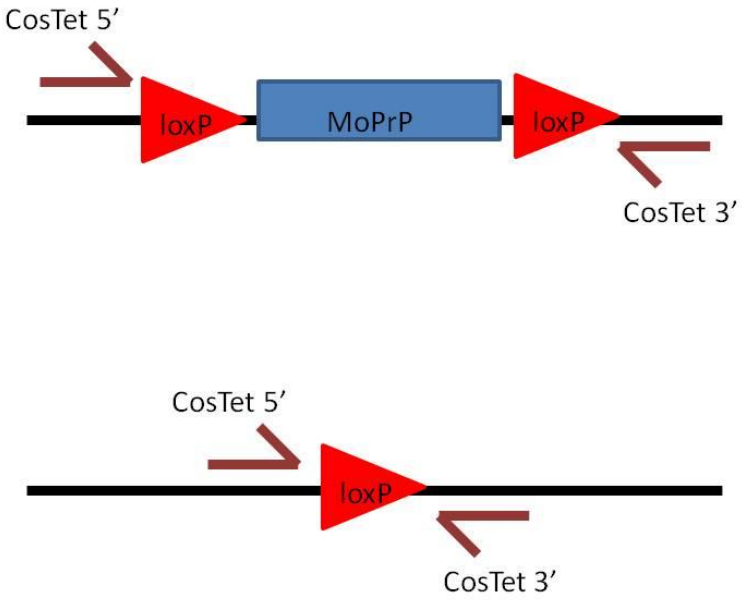

Figure 6.7 Scheme of amplification with Cos tet primers

The primers CosTet5' and CosTet3' in absence of recombination amplify a band of ~1150 bp, corresponding to the entire M*lox*P transgene. In presence of Cre recombinase, the primers amplify two DNA bands, the first (~1150 bp), corresponding to amplification of DNA from un-recombined neurons and non-neuronal cells, and the other of ~250 bp corresponding to amplification of DNA from recombined cells.

In 5 week old NFH-Cre/M*lox*P mice, the 250 bp band was detected in DNA from all the dissected areas, indicating that recombination had occurred. Control hippocampal DNA extracted from M*lox*P mice only yielded the 1150 bp band, indicating the absence of recombination (Figure 6.8).

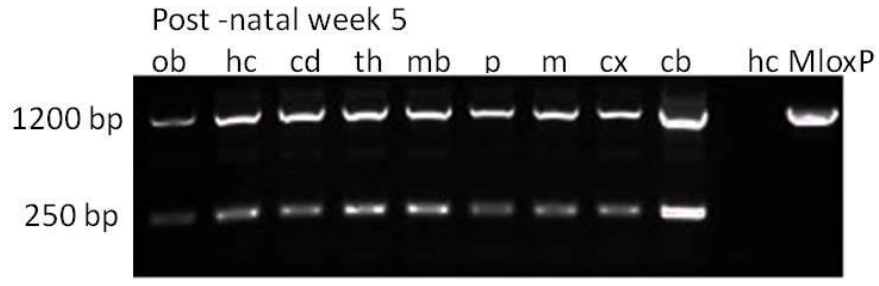

Figure 6.8 Amplification with CosTet primers of DNA from different brain dissected areas of NFH-Cre/loxP mice culled at post-natal week 5

ob=olfactory bulb; hc= hippocampus; cd=caudate nucleus; th=thalamus; p=pons; m=medulla; cx=cortex; cb=cerebellum. In all areas, the CosTet primers amplify both the high and low molecular weight band, indicating the occurrence of recombination. Control hippocampal DNA extracted from MloxP mice showed only the higher molecular weight band.

To confirm the identity of the low molecular weight band and the specificity of the PCR reaction, the 250bp band was sequenced using the CosTet5' and CosTet3' primers. The resulting sequence is shown in Figure 6.9. Recombination was found to occur in all brain areas as early as postnatal week 1 and up to post-natal week 15 (Table 1**)**. Analysis of whole brain embryos indicated the occurrence of recombination at embryonic day 15.5 (Figure 6.10).

The PCR data confirmed the observations from the NFH-Cre/M*lox*P mice that recombination was occurring earlier, but the greater sensitivity of the PCR analysis allowed recombination to be detected in areas not previously detected with histology.

Previous analysis based on Southern blot and histology did not detect Cre-mediated PrP recombination before ~9~10 weeks in any brain area (Mallucci et al., 2002) and real time RT-PCR analysis showed 30-40% reduction of the PrP mRNA in hippocampus of NFH-Cre/M*lox*P mice at 9 week of age compared to 6 and 8 week of age. To further investigate the efficacy of recombination in various brain regions at different time points, a quantitative real time PCR (qPCR) was utilized.

GCTGTCAAGGAATAGGCCTGGGAGGGAGGGGTGGCTGATGCCATGACCGTCACACATTTGTT
CTGCAACAGATGTCAAGTAGCTTCAGCCTGCGTGCTGGACAATGACGTGTTGCTGGAGTACAA
TGATGCCTTGTTCTTCATTTTGCAGATCAGTCGAC**ATAACTTCGTATAGCATACATTATACGAA**
GTTATCTCGACCTCCCTGCTTGTACTTCCTCGTTCTTGTGGTCTAGGCTGGGGGAGGGGTTATC
CACCGTAGCTCTA

Figure 6.9 Sequence of the low molecular weight band

The loxP sequence is highlighted in green.

	ob	hc	cd	th	mb	p	m	cx	cb
1	+	+	+	+	+	+	+	+	+
2	+	+	+	+	+	+	+	+	+
5	+	+	+	+	+	+	+	+	+
9	+	+	+	+	+	+	+	+	+
13	+	+	+	+	+	+	+	+	+
15	+	+	+	+	+	+	+	+	+
17	+	+	+	+	+	+	+	+	+

Table 6.1 Recombination in different brain areas at different times of culling

ob= olfactory bulb; hc= hippocampus; cd=caudate nucleus; th=thalamus; p=pons; m=medulla; cx=cortex; cb=cerebellum.

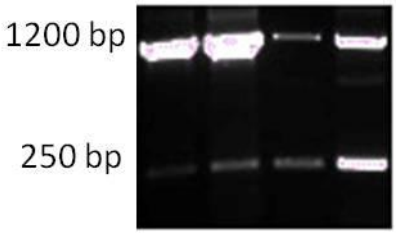

Figure 6.10 Amplification with CosTet primers of DNA from NFH-Cre/M*lox*P embryos

DNA from four embryos was amplified with CosTet primers. In all the samples, both high and low molecular weight bands were observed, indicating the occurrence of recombination.

6.4.2.1.1 Validation of primers and probes for qPCR

Since previous studies had focussed on the hippocampus, this analysis was started in the hippocampus by using a relative quantification method, which analyses changes in gene expression in a given sample relative to a reference sample.

DNA extracted from 9 weeks old mice was selected as the reference sample as by 9 week recombination has been suggested to be complete.

Since measurement of PrP knock-down, i.e. disappearance of amplified signal originating from M*lox*P PrP DNA, could be biased due to signal derived from DNA of non-neuronal cells, where recombination is not thought to occur, a probe spanning the recombined sequence at the break point, specific for recombined DNA

was used. The “gene of interest” was denominated “Recombined lox PrP” (Rec lox PrP). The sequence for primers and probe is shown in Figure 6.11.

GCTGTCAAGGAATAGGCCTGGGAGGGAGGGGTGGCTGATGCCATGACCGTCACACATTTGTT
CTGCAACAGATGTCAAGTAGCTTCAGCCTGCGTGCTGGACAATGACGTGTTGCTGGAGTACAA
TGATGCCTTGTTCTTCATTTTGCAGATCAGTCGACATAACTTCGTATAGCATACATTATACGAA
GTTATCTCGACCTCCCTGCTTGTACTTCCTCGTTCTTGTGGTCTAGGCTGGGGGAGGGGTTATC
CACCGTAGCTCTA

Figure 6.11 Primers and probe for Rec lox PrP qPCR

The primers are in blue and the probe is underlined in pink

For analysis of change in gene expression, the $\Delta\Delta C_t$ method was used (Livak and Schmittgen, 2001). To be able to use the comparative C_t method, a standard curve of the gene of interest and the internal control (housekeeping gene) need to have comparable efficacy, i.e. the efficacy of amplification should not be dependent on the starting DNA concentration of the sample.

One hippocampal DNA sample from a 9 week old mouse was used to prepare serial dilutions of DNA from 100 ng to 6.125 ng, and perform qPCR in quintuplicate for every dilution, using GAPDH as housekeeping gene.

The Rec lox PrP standard curve efficacy obtained with the selected primers and probe was not optimal (R= 0.9643). The standard curve efficacy could have been improved by changing the primers and probe, but the constraint of the small sequence made it impossible. However, the validation experiment showed that the efficiency of the standard curves for the gene of interest and for the reference sample GAPDH were comparable, as the slope of the curve interpolating the delta Ct in function of the logarithm of the DNA concentration was <0.1.

Therefore the actual experiment was performed with the primers and probe that had been designed (Figure 6.12).

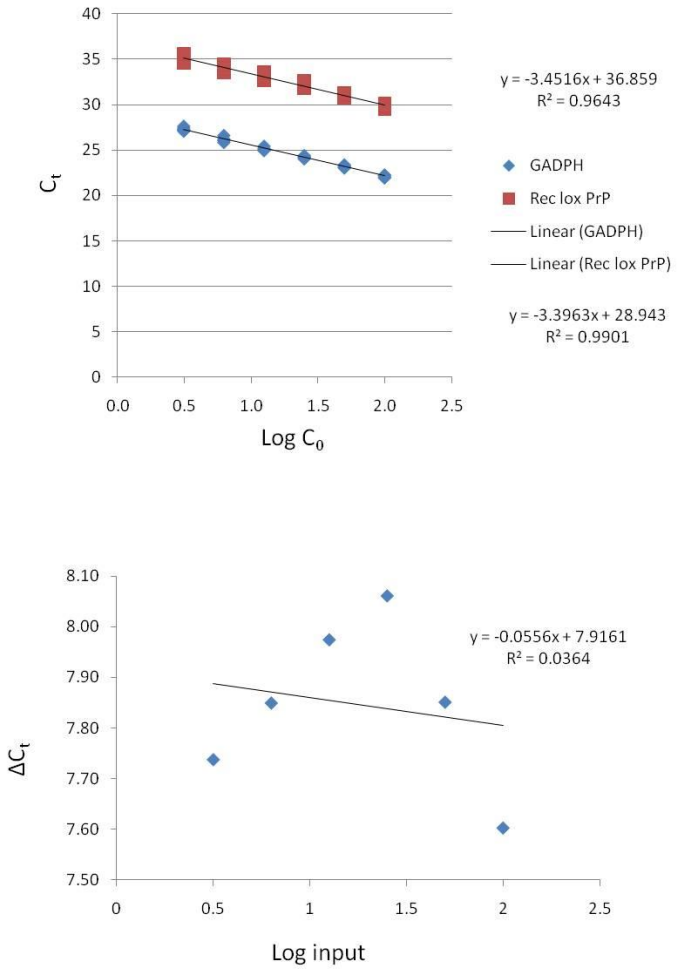

Figure 6.12 Validation experiment for the use of the comparative C_t method

Serial dilutions of the DNA sample from the initial concentration of 100ng down to 6.12 ng were prepared, and used to perform qPCR in quintuplicate for every dilution, with GAPDH as a housekeeping gene. The Rec lox PrP standard curve efficacy obtained with the selected primers and probe was not optimal (R= 0.9643), but the standard curves' efficacy for the gene of interest and for the reference sample GAPDH are comparable, as the slope of the curve interpolating the delta C_t in function of the logarithm of the DNA concentration is <0.1

6.4.2.1.2 qPCR on hippocampus of NFH-Cre/M*lox*P mice at various time points

DNA extracted from hippocampal samples from 9 week old mice were amplified by qPCR (real time PCR). Since at 9 weeks recombination was considered to be the maximal, we assigned the occurrence of recombination at this point an arbitrary value of 100%. Next, samples from the hippocampus of 1-, 2-, 5- , 13-, 32-weeks old mice were amplified: for every time point, 5 samples were used and tested in quadruplicate. In every experiment, 3 M*lox*P hippocampal samples were used as a negative control, and run in triplicate. Recombination was detected as early as

postnatal week 1, but it was not complete: at postnatal week 1 recombination was occurring with an efficacy equal to 10% of the recombination at 9 weeks of age ($p < 0.001$). At postnatal week 2, there was an increase in recombination (40% of the 9 weeks, $p < 0.001$), but still not complete. There was no significant difference in recombination efficacy between postnatal week 9 and 5, 13 or 32 indicating that in the hippocampus, recombination was complete by postnatal week 5 (Figure 6.13). A limit of detection of the qPCR cannot be excluded, but time constraints and limitation in samples did not permit other strategies with different sets of primers and probes to be tested.

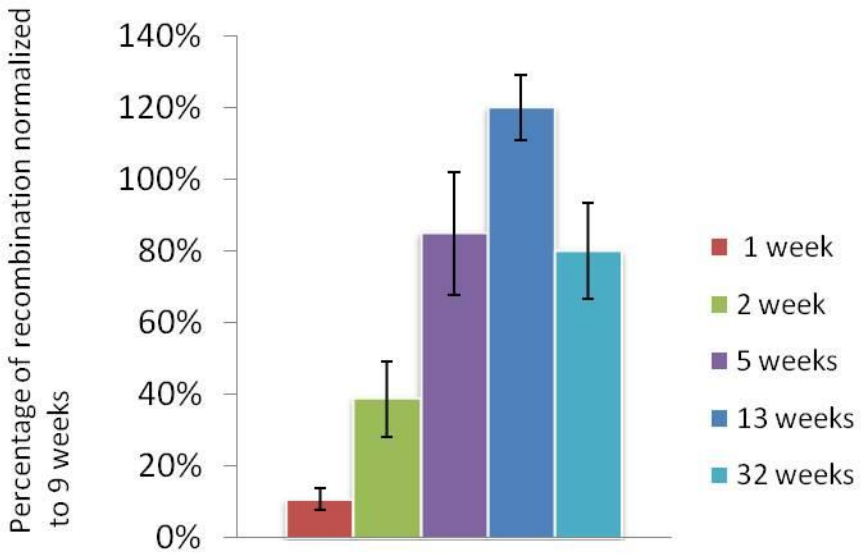

Figure 6.13 Cre-mediated recombination in the hippocampus of M*lox*P mice

DNA hippocampal samples from 9 week old mice was analysed by real time PCR. At 9 weeks the recombination was considered the maximal possible, therefore an arbitrary value=100% was assigned to the occurrence of recombination at this point. Samples from the hippocampus of 1-, 2-, 5- , 13-, 32- weeks old mice were amplified: for every time point, 5 samples were used and tested in quadruplicate. In every experiment, 3 M*lox*P hippocampal samples were used as negative controls, run in triplicate. At postnatal week 1 recombination occurred with an efficacy equal to 10% of the recombination at 9 weeks of age, $p< 0.001$. At postnatal week 2, recombination was 40% of the recombination at 9 weeks of age, ($p< 0.001$). There is no significant difference in recombination efficacy between postnatal week 9 and 5, 13 or 32. This suggests that in the hippocampus, recombination is complete by postnatal week 5.

6.5 Discussion

The Cre/loxP system is widely used to generate conditional knock-out mice, for tissue and/or time specific disruption of expression of a target gene. Chosen DNA sequences can be flanked by loxP elements, and the enzyme Cre can mediate recombination at the loxP sites, leading to excision of the sequence between the two

elements. In double transgenic mice, the pattern of Cre expression determines when and where the floxed transgene is deleted. The specificity of Cre expression is obtained by designing the Cre construct under the control of a defined promoter so that the expression occurs exclusively in a cell type where/when the promoter is active (Nagy, 2000).

This system has been used in the Prion Unit to generate conditional PrP knock-out mice. Cre/loxP double transgenic mice were obtained by crossing the M*lox*P transgenic mice with the Cre transgenic mice. In the Cre expressing mice, Cre expression was under the control of the regulatory elements (promoter, introns and flanking sequences) of the neurofilament heavy (NFH) gene (Mallucci et al., 2002). The NFH control elements were chosen because of their ability to confer neuron-specific post-natal expression to murine (Julien et al., 1988), rat (Moskowitz and Oblinger, 1995) and human (Lees et al., 1988) NFH genes, and in transgenic mice expressing the human NFH transgene (Cote et al., 1993; Cote et al., 1994).

Indeed, detailed analysis of NFH-Cre/ROSA26 mice and double transgenic NFH-Cre/M*lox*P mice previously showed Cre expression and subsequent recombination occurring in all neuronal cells ~ postnatal week 9-10, as a genuine late activation of the transgene (Mallucci et al., 2002). In addition, early prion disease pathology and cognitive deficits were reversed in the hippocampus of RML infected NFH-Cre/M*lox*P mice upon recombination at 9 wpi (10 weeks of age), and mice that had undergone recombination did not develop clinical prion disease (Mallucci et al., 2003; Mallucci et al., 2007). However, repeat experiments of inoculating NFH-Cre/M*lox*P mice with RML prions, yielded different results, in that NFH-Cre/M*lox*P mice were not fully protected from clinical scrapie.

Moreover, as our data suggested that areas of early prion pathology in the brainstem are likely to correspond to clinical target areas of prion disease, it was essential to further characterise the timing and efficacy of recombination in these areas.

This was done by histological and molecular biological approaches. We first crossed the NFH-Cre line with LacZ ROSA26 reporter mice and studied the spatial characteristics and timing of Cre activation. Both, the β-galactosidase histochemical assay and the immunohistochemical detection of β-galactosidase showed Cre-mediated activation as early as 1 week after birth in the ROSA26 reporter mouse line

in some but not all brain areas. However, at 9 weeks of age, not all the cells in the proposed clinical target areas (the locus coeruleus, the nucleus of the solitary tract and the pre-Bötzinger complex) showed immunoreactivity, indicating that not all cells in each nucleus underwent recombination. The proportion of recombined cells was determined by microscopic observation, but accurate cell counting was not possible given the limited number of sections obtained in this experiment. In addition, we obtained further quantitative data using a molecular approach directly in NFH-Cre/M*lox*P mice.

This analysis confirmed the indication of early recombination; it occurred as early as embryonic day 15 and also demonstrated a change in efficacy of recombination over time. Indeed, we were able to monitor the efficacy of recombination in the hippocampus of NFH-Cre/M*lox*P mice and found that it had taken place with low efficacy at postnatal week 1 but was maximal by postnatal week 5. Since the focus of this thesis is the brainstem, it would have been desirable to have data on this brain area. However, in light of the histology data on ROSA26 reporter mice, qPCR on medulla samples would probably not have been conclusive: not only different brain areas have different timing and efficacy of recombination, but different brainstem nuclei may have had different recombination efficiency at different times.

The data shown here demonstrate that temporal and spatial characteristics of Cre expression in NFH-Cre mice has shifted over time and was now different from published data (Mallucci et al., 2002). However, due to technical limitations of the experiments presented here, we cannot describe unequivocally the recombination in the brainstem nuclei on which we have focussed our attention in the previous chapters. Ideally, one way to circumvent the limits of the analysis presented here would be to combine histological and molecular techniques. More specifically, different brainstem nuclei of NFH-Cre/M*lox*P mice could be dissected by laser-capture microscopy and real time PCR could be performed on the dissected samples. This analysis would be an additional, complementary confirmation of the Cre-mediated recombination.

Based on published data, the observed early recombination was not expected. However, when the NFH-Cre line was generated, premature recombination of the M*lox*P locus had been detected in a single embryo at E15.5. Because transgenes

were generally known to show inconsistencies or variations, and to have alterations in timing of expression when used to drive Cre-mediated recombination (Hoesche et al., 1993; Sauerwald et al., 1990), extensive efforts were made to characterise the recombination and since another such early event was not observed, it was discarded as random. As the Cre-expressing line that has being continually bred within the Prion Unit no longer triggers a late recombination, the original Cre-expressing line was re-derived from mouse embryos frozen at the time of the l experiments. However, in the re-derived line early recombination was observed (Dr Nick Henriquez and Prof. Sebastian Brandner, personal communication) and therefore the line has been terminated.

The change of recombination pattern does not allow a direct comparison with the published data on RML infected NFH-Cre/M*lox*P mice. However, one would intuitively expect that an early recombination would result in a better protection from prion pathology, in that an earlier and more widespread deletion and results in less PrP being available for conversion. In contrast, NFH-Cre/M*lox*P mice are less protected. The detection of partial recombination of the locus coeruleus, the nucleus of the solitary tract and the pre-Bötzinger complex supports our postulate on their critical role in the progression towards a clinical phenotype. Because recombination is not complete in these target areas, prion infected NFH-Cre/M*lox*P mice do survive longer but accumulate abnormal prion protein and hence ultimately develop prion disease.

6.6 Summary

In conclusion, Cre-mediated recombination in NFH-Cre/M*lox*P mice accumulates over time, and not a genuine late activation, as shown previously (Mallucci et al., 2002).

Using a LacZ reporter mouse line, we found recombination occurring as early as postnatal day 2 in the brainstem and the cerebellum. By post-natal week 5, we found recombined cells in the cortex, thalamus, hippocampus and brainstem. With PCR screening, we found evidence of recombination in brains from 15.5 days old embryos and from post-natal week 1 onwards in all the different brain areas analysed (olfactory bulb, hippocampus, caudate nucleus, thalamus, cerebellum, mid brain, pons, medulla, cortex and cerebellum). Specifically, in the hippocampus of NFH-

Cre/M*lox*P mice, low-level recombination is detectable at postnatal week 1 and is maximal by post-natal week 5.

We analysed in greater detail the pattern of recombination in the nuclei identified as clinical target areas (i.e. locus coeruleus, the nucleus of the solitary tract and the pre-Bötzinger complex). We found that recombination is not complete in these nuclei, which explains incomplete protection from prion disease in infected NFH-Cre/M*lox*P mice.

7 Lentiviral mediated RNAi against prion protein

7.1 Introduction

When I started my PhD, I joined the group led by Prof. Giovanna Mallucci. I worked under her supervision on a therapeutic project using lentivirally mediated RNA interference (RNAi) to silence PrP^{C} expression in mice, until she moved to the MRC Toxicology Unit in Leicester.

Mallucci's group had previously shown that recombination-mediated depletion of neuronal PrP^{C} in mice with established prion infection reverses early spongiosis, neuronal loss and cognitive deficits and prevents clinical disease progression (Mallucci et al., 2003; Mallucci et al., 2007). These studies had validated PrP^{C} as a therapeutic target in prion disease, but did not represent a therapeutic possibility, given the recombination-mediated mechanism of PrP^{C} depletion. Potential treatments to achieve the same effect would require reduction of PrP expression through gene silencing. At the time, RNAi had emerged as a powerful tool for gene silencing and gene therapy using viral vectors expressing shRNAs had been successfully used in various neurodegenerative disorders (Xia et al., 2006; Sapru et al., 2006; Gonzalez-Alegre et al., 2005). Moreover, RNAi mediated knockdown of PrP expression had been reported in cell systems (Tilly et al., 2003; Daude et al., 2003; Pfeifer et al., 2006) and in mice (Pfeifer et al., 2006).

Under Mallucci's supervision, Melanie White had prepared and tested shRNA sequences against PrP. In her PhD thesis, siRNA duplexes efficient in reducing PrP^{C} expression *in vitro* and enabling clearance of PrP^{Sc} and infectivity from prion-infected cells were described. Moreover, lentiviruses expressing the interfering sequences were constructed, and effective reduction of PrP^{C} expression both *in vitro* and *in vivo* was demonstrated. Stable expression of the interfering RNA molecules through lentiviral transduction of the hippocampus in prion infected mice reduced local pathology and prolonged animal survival.

These findings were the starting point for the study that resulted in the publication in the Proceedings of the National Academy of Sciences USA "Single treatment with RNAi against prion protein rescues early neuronal dysfunction and prolongs survival in mice with prion disease", attached at the end of this thesis. In the following sections the results presented within the paper are briefly summarised.

7.1.1 Single treatment with RNAi against prion protein rescues early neuronal dysfunction and prolongs survival in mice with prion disease

The MW-1 shRNA sequence was cloned in the Lentiviral vector pLL3.7, expressing also the reporter protein EGFP, to generate the anti PrP-lentivirus LV-MW1. A control virus LV-Empty was also generated, which contained no shRNA sequence. Transduction of neuronal cell lines was tested and it was confirmed that the LV-MW1 virus reduced PrP protein and mRNA (P= 0.0014; Student's t test, two tails) (cf. (White et al., 2008) Fig. 1. (A)), whereas the control LV-Empty virus had no effect. *In vivo,* bilateral hippocampal injections of LV-MW1 in wild-type uninfected mice reduced PrP mRNA by ~80% of normal values, 2 weeks after treatment in whole hippocampi (p< 0.0001; Student's t test, two tails) (cf. (White et al., 2008) Fig. 1. (B)). Lentiviruses were then tested in prion-infected mice. Tg37 mice were intracerebrally injected with RML prions at 1 week of age. Eight weeks later, Michael Farmer stereotaxically injected either LV-MW1 or LV-Empty into the left and right hippocampus. A third group of mice received no lentivirus (n= 20 for each group). All three groups were tested in burrowing and object recognition tasks from 7 wpi. Lentiviral RNAi of PrP prevented the loss of burrowing activity seen in mice treated with LV-Empty or with no virus and also protected against loss of object recognition memory (cf. White et al. 2008 Fig.2).

Effect of focal lentiviral treatment on survival time was assessed: after a localized hippocampal injection, prion-infected mice treated with LV-MW1 survived significantly longer than mice treated with LV-Empty or those that received no virus (respectively 105 ± 4 days; 88 ± 3; 85 ± 3 days) (cf. White et al. 2008 Fig.3). I carried out histopathology on brain slices (cut and stained by the MRC Prion Unit histopathology core facility) from these mice.

7.1.1.1 Neuroprotective effect of lentivirus-mediated PrP knock-down

Blind scoring was performed on up to nine brains from each group of mice, selected at random, and culled when they developed diagnostic clinical signs of terminal prion disease.

Silencing of PrP expression in prion-infected mice was focally neuroprotective in the hippocampus: LV-MW1 treated mice showed protection

against neuronal loss and reduced spongiform degeneration compared to LV-Empty treated mice (Figure 7.1 B and D vs. Figure 7.1 A and C). Moreover, LV-MW1 treatment reduced PrP^{Sc} deposition compared to LV-Empty treatment (Figure 7.1 F vs. Figure 7.1 E). Systematic neuronal counts showed that LV-MW1 treatment preserved CA1 pyramidal cells (852 ± 85 neurons compared with 532 ± 24 neurons in LV-Empty-treated mice (p= 0.029, Student's t-test, two tails) (Figure 7.2 A)). Semiquantitative scoring of spongiosis using a scale of 0–3 [indicating a range of absent (0) to severe (3) spongiosis] showed that hippocampal spongiform degeneration was also significantly less extensive in LV-MW1-treated mice compared to LV-Empty treated mice. Animals with RNAi-mediated PrP knockdown (n = 9) had a mean spongiosis score of 1.3 ± 0.2 in the hippocampus, representing mild spongiosis, compared with a score of 2.7 ± 0.2 (n = 6) in LV-Empty-treated mice, consistent with severe spongiform degeneration (p= 0.0007, Student's t-test, two tails) (Figure 7.2 B). Whole-brain pathology in LV-MW1-treated animals was also evaluated. In the thalamus and the cortex apparent reduction of spongiosis and PrP^{Sc} deposition was distinguishable, compared with LV-Empty treated mice (Figure 7.3). However, the morphological differences seen were statistically significant in the thalamus but not in the cortex (Table 7.1).

As no evidence of lentiviral expression was found in tissues beyond the injected hippocampus using immunohistochemistry for lentiviral EGFP expression, it was reasoned that this reduced pathology could reflect altered prion spread and replication in these areas after knockdown of PrP within the hippocampus by lentiviral injection.

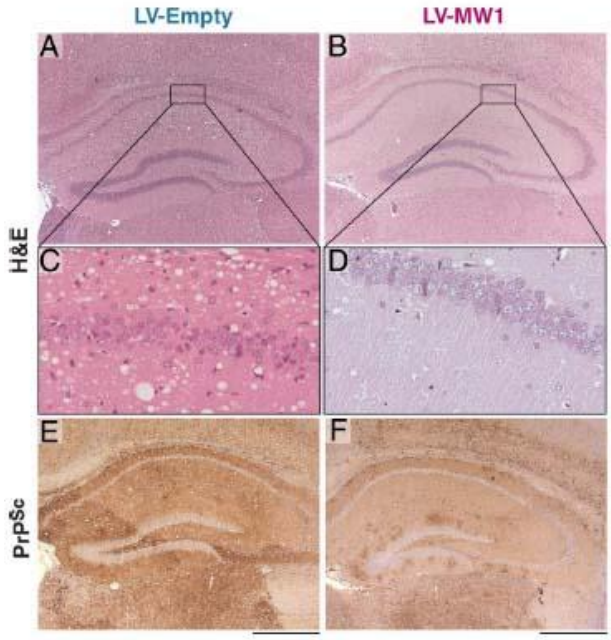

Figure 7.1 Lentivirally mediated RNAi of PrP expression protects against prion mediated neurodegeneration

LV-MW1 treated hippocampus showed protection against neuronal loss, reduced spongiform degeneration (B and D) and PrP^{Sc} deposition (F) compared to LV-Empty treated hippocampus (A and C; E). Scale bar = 500 µm. Adapted from (White et al., 2008)

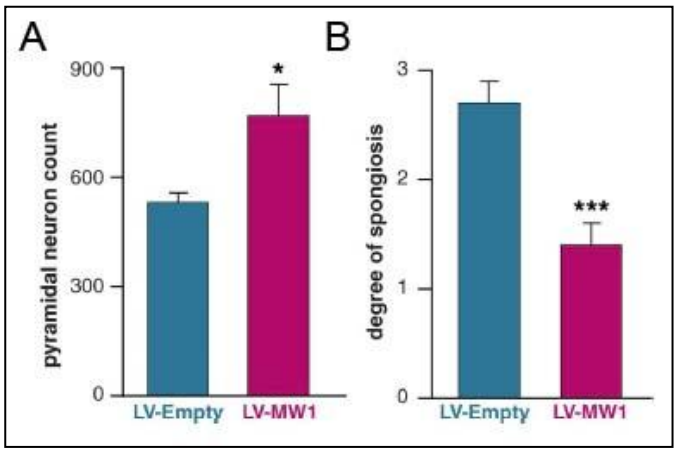

Figure 7.2 Quantitative analysis of LV-MW1 protection against prion mediated neurodegeneration

A. Pyramidal neurons in the CA1 region were systematically counted and confirmed the neuroprotective effect of LV-MW1 (P=0.029, Student's t test, two tails) (n=6).

B. Hippocampi of LV-MW1 and LV-Empty treated prion infected mice were semiquantitatively scored for spongiosis, using a scale of 0–3 [indicating a range of absent (0) to severe (3) spongiosis]. LV-MW1 treated hippocampi showed significantly less spongiosis than LV-Empty treated mice (n=9 and n=6; P=0.0007, Student's t test, two tails). Adapted from (White et al., 2008)

	H&E Spongiosis score (0–3), mean ± SD	Hippocampus	Cortex	Thalamus	Cerebellum
	LV-MW1- treated mice (n = 9)	1.3 ± 0.2	1.8 ± 0.6	1.6 ± 0.5	2.0 ± 0.0
	Student's t test, two tails	$P < 0.001$	$P = 0.10$	$P = 0.03$	$P = 0.51$
	LV-Empty- treated mice (n = 6)	2.7 ± 0.2	2.4 ± 0.5	2.5 ± 0.7	1.8 ± 0.6
PrP (ICSM35) Staining intensity (0–3), mean ± SD mean	LV-MW1- treated mice (n = 9)	2.3 ± 0.3	2.2 ± 0.5	2.3 ± 0.4	2.2 ± 0.5
	Student's t test, two tails	$P = 0.04$	$P = 0.40$	$P = 0.04$	$P = 0.12$
	LV-Empty treated mice (n = 6)	3.0 ± 0.0	2.6 ± 0.4	3.0 ± 0.0	2.8 ± 0.4

Table 7.1 Spongiosis and PrP(ICSM35) scoring in brain of LV-MW1 and LV-Empty treated mice

Significant differences were observed for spongiosis and PrP^{Sc} accumulation in hippocampus and thalamus of LV-MW1 and LV-Empty treated mice, but not in the cortex and cerebellum.

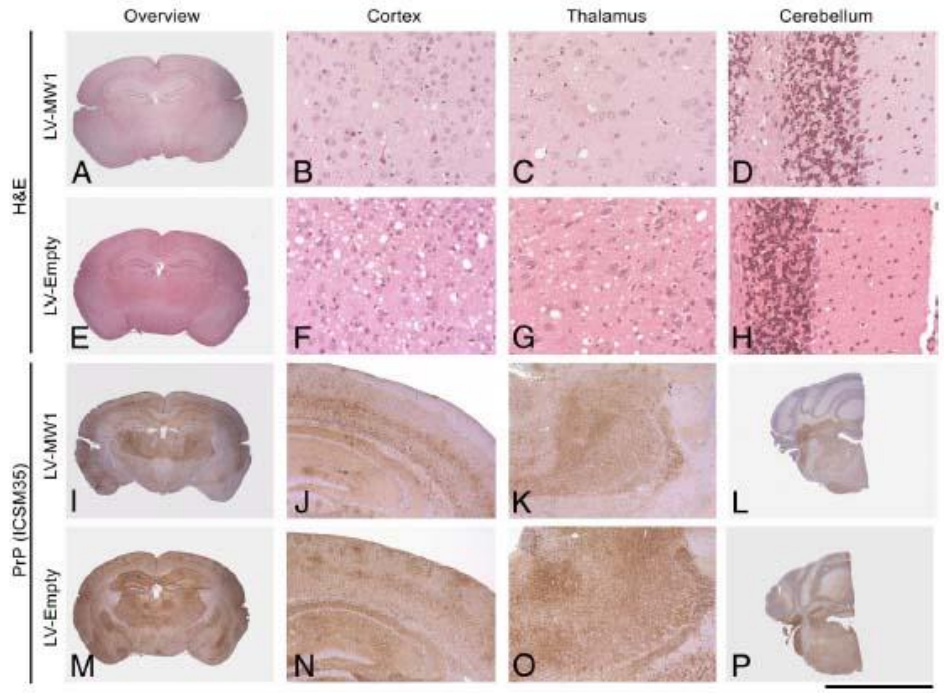

Figure 7.3 Reduced spongiosis and PrP^{Sc} deposition in brain regions outside the hippocampus
Cortex, Thalamus and Cerebellum of mice treated with hippocampal bilateral injection LV-MW1 (A to D and I to L) and LV-Empty (E to H and M to P) were analysed. Sections were stained with H&E for spongiosis (top two rows) and ICSM35 for PrP^{Sc} deposition (bottom two rows). LV-MW1 treatment showed a reduction of spongiosis and PrP^{Sc} deposition in the cortex and in the thalamus. Scale bar = 5 mm (A, E, I, M); 4 mm (L and P); 1.3 mm (J, K, N, O); 170 µm (B to D and F to H). Adapted from (White et al., 2008)

7.1.2 Loss of lentivirus titre

In conclusion, lentivirus-mediated RNAi against PrP was used as treatment of established prion infection in mice. Localized single administration of these viruses to the hippocampus prolonged the lifespan of the infected mice, protected transduced neurons from degenerating, reduced PrP^{Sc} accumulation, and prevented the onset of the first behavioural deficits associated with the disease.

Subsequently, it was planned to use LV-MW1 to knock-down PrP in other areas of the brain. For efficient *in vivo* knock-down, high titres of virus are required. The titre of concentrated virus previously used was estimated to be in the range of 1 - 5 x 10^8 TU/ml. To verify the titre of the remaining lentivirus stocks, HEK293 cells were infected with 15 µl of concentred LV-MW1 virus. To assess the lentivirus titre, the percentage of virus-encoded GFP expressing cells was analysed by flow cytometry at the Institute of Child Health by Dr Annika Alexopoulou. No difference in GFP fluorescence was detected between LV-MW1 infected cells and control cells, treated only with polybrene (Figure 7.4). This analysis suggested that the viral titre had decreased, to levels which were unsuitable for injection experiments. Virus stocks needed to be generated.

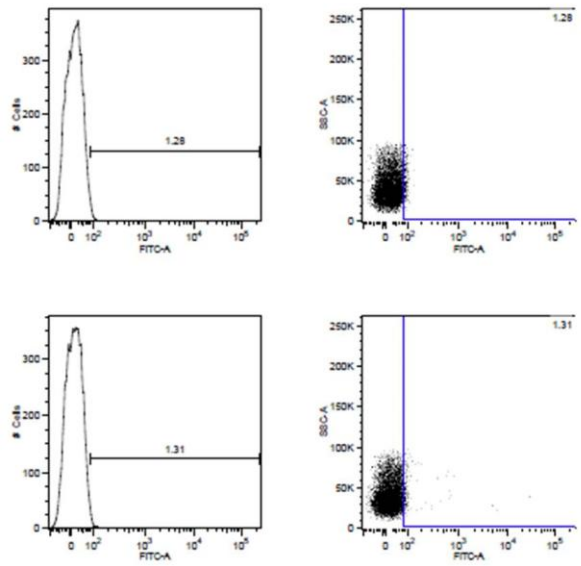

Figure 7.4 LV-MW1 lentivirus stock showed loss of titre

10^5 HEK 293 cells were infected with 15 µl of LV-MW1 in presence of 8 µg/ml of polybrene , or just with polybrene as control. Three days after infection, cells were collected and analysed for EGFP expression with flow cytometry.

No appreciable green fluorescence was observed in LV-MW1 infected cells (bottom row) compared to the polybrene treated control (top row), indicating a significant loss of lentiviral titre.

7.1.3 Production of high titre lentivirus for expression of shRNAs directed against *Prnp*

7.1.3.1 Design of the short hairpin oligonucleotides

In addition to re-producing the LV-MW1 lentivirus used in the previous work, new sequences for short hairpin oligonucleotides against Prnp to be cloned into pLL3.7 were designed. In other work within the Unit, Prof. Parmjit Jat and Parineeta Arora had designed and tested a number of shRNA sequences for silencing PrP expression in PK1 cells and had found that the best candidates for PrP silencing were two short sequences located in the 3' UTR, namely, shRNA clone 4 (bp 2039-2059) and 8 (bp 1512-1530). These sequences were used for production of two new lentiviruses, named LV-Cl4 and LV-Cl8.

The short hairpin oligonucleotide inserts were designed to be directionally cloned into the *Hpa* I and *Xho* I restriction sites of the pLL3.7 lentivector downstream of the U6 promoter. In addition to the new sequences, a new version of

the sh-MW1 was designed, with 5' *Hpa* I restriction site reconstituted. The sequences of the short hairpin inserts were as follows. In blue is the interference sequence, followed by the loop in green and the antisense in red.

shRNA clone 4

sequence: TCTGCATGTACTTCACGTT bp 2039-2059

5′- AACTCTGCATGTACTTCACGTTTTCAAGAGAAACGTGAAGTACATGCAGATTTTTTC-3′

3′- TTGAGACGTACATGAAGTGCAAAAGTTCTCTTTGCACTTCATGTACGTCTAAAAAAGAGCT-5′

shRNA clone 8

sequence: TAGGAGATCTTGACTCTGA bp 1512-1530

5′- AACTAGGAGATCTTGACTCTGATTCAAGAGATCAGAGTCAAGATCTCCTATTTTTTC-3′

3′- TTGATCCTCTAGAACTGAGACTAAGTTCTCTAGTCTCAGTTCTAGAGGATAAAAAAGAGCT-5′

shRNA MW1 new

5′- AACGTACCGCTACCCTAACCAATTCAAGAGATTGGTTAGGGTAGCGGTACTTTTTTC-3′

3′- TTGCATGGCGATGGGATTGGTTAAGTTCTCTAACCAATCCCATCGCCATGAAAAAAGAGCT-5′

7.1.3.2 Cloning of the sh-RNA in the pLL3.7 lentivector

The shRNA oligonucleotides were annealed and cloned into the pLL3.7 lentivector. Ligation reactions were set up using molar ratios of insert DNA: pre-digested pLL3.7 vector DNA ranging from 2:1 to 10:1. Resultant colonies were grown; DNA extracted and sequenced using the primer within the Flap sequence upstream of the U6 promoter in pLL3.7:

Flap sequence primer

5'-CAGTGCAGGGGAAAGAATAGTAGAC-3'

Positive clones were grown to produce high quantity DNA of each shRNA lentiviral construct.

7.1.3.3 Triple transfection in HEK 293 cells to produce lentivirus

To produce lentiviruses, the lentiviral vector plasmid containing the shRNA, was transiently co-transfected with two helper plasmids encoding the genes required for virus production and packaging into HEK293T cells. The helper plasmids were

the packaging vector, p8.91, and the envelope plasmid, pMD2G. The p8.91 plasmid encodes the *gag* and *pol* genes, required for the viral capsid, nucleocapsid and protective matrix and for the enzymatic machinery necessary for replication and integration of the lentivirus. The pMD2G plasmid encodes the VSV-G protein, the coat protein from the Vesicular Stomatitis Virus, to confer broad tropism to the lentivirus.

The viral titre of the produced viruses was tested in HEK293. Cells were infected with serial dilutions of the lentiviruses and the expression of EGFP checked by fluorescent microscopy. An indicative relative titre was calculated, estimating percentage of EGFP positive cells for each virus in each dilution.

7.1.3.4 Pilot experiment on knockdown validation

Equivalent titres of LV-Empty and sh-RNA encoding lentiviruses were tested on the N2A mouse neuroblastoma cell line to assess virus efficacy *in vitro*. Four days after infection, cells were collected and stained with the monoclonal antibody ICSM 18, directed against PrP codons 144–156. Anti mouse PE-conjugated antibody, emitting in the red spectrum, was selected as the secondary antibody to avoid overlap with the "green channel" used for GFP fluorescence. Stained cells were then analysed with flow cytometry by Dr Sara Monteiro: GFP positive cells were gated and mean fluorescence intensity (MFI) in the red channel was used as a measure of PrP knockdown. LV-MW1 and LV-MW1new infected cells did not show any reduction in the red channel MFI compared to LV-Empty treated cells (Figure 7.5 A and B). On the other hand, LV-Cl8 and LV-Cl4 infected cells showed a reduction of ~10% in red MFI compared to LV-Empty treated cells (Figure 7.5 C and D). These data confirmed the two new sequences used to generate LV-Cl8 and LV-Cl4 were better targets for PrP knock-down than previously published sequences.

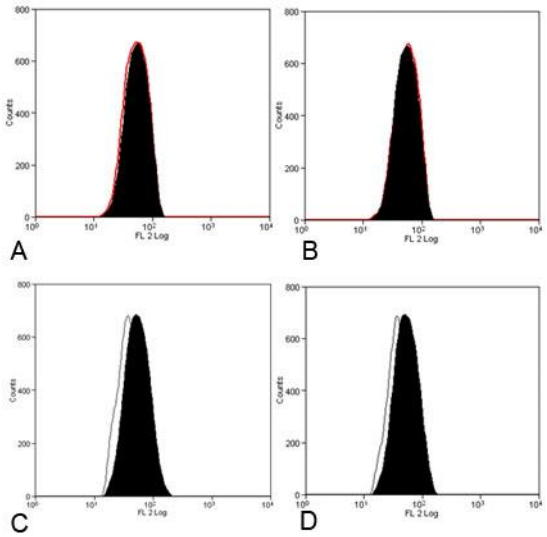

Figure 7.5 LV-Cl4 and LV-Cl8 are more efficient that LV-MW1 in knocking down PrP *in vitro*

In order to test virus efficacy in vitro, equivalent titres of LV-Empty and sh-RNA encoding lentiviruses were tested on the N2A mouse neuroblastoma cell line. Four days after infections cells were collected and stained, with the ICSM 18 antibody, specific for PrP, followed by Goat anti mouse PE-conjugated secondary antibody. GFP positive cells were gated (black area) and mean fluorescence intensity (MFI) in the red channel was used as a measure of PrP knockdown, as reduction red fluorescence intensity implies reduced PrP expression on the cell surface.

A. MFI LV-Empty treated cells= 51%; MFI LV-MW1 treated cells= 51% (grey line);

B. MFI LV-Empty treated cells =51%; MFI LV-MW1new treated cells= 55% (grey line)

C. MFI LV-Empty treated cells =51%; MFI LV-Cl8 treated cells= 42% (red line)

D. MFI LV-Empty treated cells 51%; MFI LV-Cl4 treated cells 42% (red line)

LV-Cl8 and LV-Cl4 successfully knocked -down PrP expression (C and D) but LV-MW1 and LV-MW1new did not.

The flow cytometry was carried out by Dr Sara Monteiro.

7.1.3.5 Titre estimation of produced lentiviruses

In order to produce a stock of lentiviruses for injection into mice, large scale lentivirus production was set up. Before proceeding with lentiviral concentration, the titre was calculated for all the collected viruses. Serial dilutions of virus were added to fresh HEK293 cells. After four days, cells were analysed with flow cytometry for GFP expression by Sara Monteiro and Melania Tangari. The titre was then calculated by correcting for the number of cells plated and the viral dilution factor using the following equation:

Titre = (% GFP-positive) x (virus dilution factor) x (number of cells plated)

Titres in the range of 2-3 x 10^5 TU/ml were achieved for each virus. As lentiviral concentration by ultracentrifugation can improve the titre ~10^3 times, the obtained titres were considered suitable for subsequent concentration. Lentiviruses were concentrated by Michael Farmer in Prof. Greg Tower's laboratory at UCL.

7.1.4 Discussion

Lentiviral-mediated RNAi against PrP has been used as treatment of established prion infection in experimental prion disease. Prion infected mice were treated with localized single administration of these viruses to the hippocampus. RNAi silencing of PrP expression prolonged the lifespan of infected mice, protected transduced neurons from degeneration, reduced PrP^{Sc} accumulation, and prevented the onset of the first behavioural deficits associated with prion disease.

This study is the first step towards the development of a treatment for prion disease. PrP^{C} has been validated as a therapeutic target; however, the physiological function of PrP^{C} is still under debate, and local PrP^{C} knock-down rather than treatments that globally target PrP^{C} seems to be a safer option. In the previous chapters, the locus coeruleus, (LC), the nucleus of the solitary tract and the pre-Bötzinger complex have been described as clinical target areas in experimental prion disease. Reducing PrP expression in these target areas at an early stage of the disease may be an approach to suppress disease progression in these areas.

Although the last two nuclei may represent difficult targets for stereotaxic injection, we envisage the LC to be an easier target for focal delivery of lentivirus encoding shRNAs against PrP. As the lentivirus titre was found to be decreased to unsuitable levels for injection experiments, new virus stocks needed to be generated. In addition to the original LV-MW1, three more lentiviruses were produced: a new version of LV-MW1 and LV-Cl4 and LV-Cl8, whose target interference sequences were based on silencing studies in PK1 cells. Preliminary data showed that LV-CL4 and LV-CL8 give the best knock-down of PrP expression in N2A cells. However, due to time constraints, further validations are needed before proceeding to *in vivo* use of the produced lentivirus.

7.1.5 Summary

It has been shown that hippocampal delivery of anti-PrP shRNA expressing lentivirus effectively prolonged the lifespan of prion infected mice, protected transduced neurons from degenerating, reduced PrP^{Sc} accumulation, and prevented the onset of behavioural deficits.

In order to use this system for focal delivery in clinical target areas outside the hippocampus such as locus coeruleus, new lentiviruses were produced, and shown to elicit a better knockdown PrP expression in N2A cells.

8 Conclusions and future work

8.1 Thesis summary and conclusions

The aims of this thesis were to identify the clinical target areas for prion disease, to define the timing and spatial characteristics of Cre-mediated recombination in the NFH-Cre/M*lox*P mouse model, and to produce new lentiviruses expressing shRNAs against PrP to be used for local PrP knock-down in designated brain areas.

To identify the clinical target areas of prion disease, i.e. areas affected by prion pathology which are responsible for clinical manifestation of the disease, we focussed on the brainstem: this area controls essential body functions such as motor activity, generation of respiratory rhythm and regulation of blood pressure, which are often impaired in mouse models of prion disease. Previous work reported that the first manifestation of prion disease in RML inoculated M*lox*P mice occurs in the thalamus and brainstem (White et al., 2008) and in human prion disease, widespread deposition in the brainstem has been reported as an early pathologic event in sCJD (Iwasaki et al., 2005). However, the authors of this study speculated that a conclusive evaluation of the relationship between clinical signs and brainstem impairment is difficult because the same symptoms could result from overlapping involvement of the basal ganglia or the cortex (Iwasaki et al., 2005).

Using mouse models it is possible to address the variability of human pathology and to directly correlate clinical signs and brainstem involvement. Therefore we set out to investigate clinical target areas of prion disease using the PrP overexpressing M*lox*P and PrP depleted NFH-Cre/M*lox*P transgenic mouse lines (Mallucci et al., 2002). We first characterized the progression of pathology in the brains of PrP overexpressing M*lox*P and PrP depleted NFH-Cre/M*lox*P transgenic mouse lines inoculated with Me7 and Mouse-adapted BSE prions, and confirmed that the brainstem is the first area of prion accumulation for both prion strains, in both genetic backgrounds. Then we focussed on the brainstem and analysed the progression of pathology in the brainstem nuclei of RML and Me7 inoculated M*lox*P and PrP depleted NFH-Cre/M*lox*P mice.

RML infected NFH-Cre/M*lox*P mice were previously shown to be resistant to RML infection (Mallucci et al., 2003). We compared the pathology between pre-

clinical longer surviving RML infected NFH-Cre/M*lox*P mice, and end-stage infected M*lox*P (RML and Me7) and NFH-Cre/M*lox*P (Me7) mice to pinpoint critical areas that once reached by the infection led to the clinical phenotype.

We hypothesized that the clinical target area(s) may be the last one or the first one targeted by prion pathology. In the "last target area scenario", a generalised widespread accumulation of "toxic species" would occur in the CNS during prion disease. This widespread accumulation would not cause clinical impairment, until it localizes to vital areas. These vital areas, which are the last areas to become functionally impaired, would be the "clinical target areas", and their impairment would cause the clinical symptoms. These areas would be relatively sensitive (compared to surrounding structures) to prion accumulation.

We first described the lesion profile in the brainstem nuclei involved in motor and autonomic control at end stage of disease upon RML or Me7 inoculation of M*lox*P mice (12 and 16 wpi) and NFH-Cre/M*lox*P mice (28 and 35wpi). In case clinical target areas were those that were targeted last, we should have been able to see prion affected nuclei in terminal M*lox*P mice that were not affected in prion resistant NFH/Cre-M*lox*P mice. However, in our experiments the NFH-Cre/M*lox*P mice were not resistant to prion infection as previously reported and developed prion disease albeit after a prolonged incubation time. Lesion profiles at intermediate (RML, 12 wpi; Me7, 16 wpi) and end stage of disease (RML, 35 wpi; Me7, 28 wpi) in NFH-Cre/M*lox*P mice were analysed. Since prion pathology was widespread in all the analysed brainstem nuclei at terminal stage, no particular nucleus stood out.

We then explored the hypothesis of clinical target areas being the first target areas. In the "first target area" scenario, the area(s) that first accumulates toxic species would be rate limiting in the disease process. These areas would have to be relatively tolerant of a continuous accumulation of prion toxicity and would cause neurological dysfunction when levels of toxicity exceed a critical threshold. At this point mice would manifest the clinical phenotype.

We focussed on the first areas affected by prion pathology when mice were asymptomatic. The brainstem nuclei of RML and Me7 inoculated M*lox*P and NFH/Cre-M*lox*P mice at early time points (RML, 6 wpi; Me7, 8 wpi) showed that the first areas affected by prion pathology were the locus coeruleus (LC), the nucleus of the solitary tract (NTS) and the pre-Bötzinger complex (PBC). These areas were

then analysed in greater detail in end stage mice. Prion accumulation and spongiosis in these first targeted areas was comparable in M*lox*P and NFH-Cre/M*lox*P mice, although PrP depleted mice survived two (Me7) and three times (RML) longer. Because of the vital role of these areas in control of autonomic functions, we suggest that degeneration of LC, NTS and PBC is the cause of the clinical symptoms and these nuclei may be the clinical target areas of prion disease.

Previous studies had shown that activation of Cre is a late event in NFH-Cre/M*lox*P mice, about 9-10 weeks after birth. NFH-Cre/M*lox*P had been shown to be resistant to prion disease and the effect of PrP depletion in the hippocampal pathology of RML infected mice has been previously studied (Mallucci et al., 2003). However, as our main focus was the brainstem, and NFH-Cre/M*lox*P mice developed clinical signs of prion pathology, even with a prolonged incubation time, we set up a detailed investigation of timing and regional specificity of Cre-mediated recombination in double transgenic NFH-Cre/M*lox*P mice. Cre-mediated recombination in NFH-Cre/M*lox*P mice was found to accumulate over time, and not a genuine late activation; recombination was found in embryos and from postnatal week 1 in different brain areas (olfactory bulb, hippocampus, caudate nucleus, thalamus, cerebellum, mid brain, pons, medulla, cortex and cerebellum). In the hippocampus maximal recombination was reached by post natal week 5. We analysed in greater detail the pattern of recombination in the nuclei we proposed as the clinical target areas in prion disease (LC, NTS and PBC). We found that recombination was not complete in these nuclei and this explains a delayed susceptibility to prion disease in prion infected NFH-Cre/M*lox*P mice.

Finally, new lentiviruses encoding shRNA against PrP were produced. Lentivirus-mediated RNAi against PrP has been shown to be an effective treatment of established prion infection in experimental prion disease. Lentivirus-mediated RNAi of PrP expression in the hippocampus of prion infected mice prolonged their lifespan, protected transduced neurons from degeneration, reduced PrP^{Sc} accumulation, and prevented the onset of the first behavioural deficits associated with the disease (White et al., 2008).

We produced new lentiviruses, using two new interference shRNA sequences and showed that their efficacy in knocking down PrP *in vitro* was higher than the previous published sequences.

8.2 Future directions

8.2.1 Histopathology of MRC2 infected mouse brains and human prion disease.

We have shown that the LC, NTS and PBC are the clinical target areas of prion pathology in an experimental model of RML and Me7 prion disease. In the course of this project, samples of MRC2 inoculated M*lox*P and NFH-Cre/M*lox*P mice were also collected at early and late stage of prion infection, but could not be analysed due to time constraints. It will now be interesting to screen these samples and determine if these areas are targets of prion pathology in MRC2 inoculated M*lox*P and NFH-Cre/M*lox*P mice. MRC2 is a mouse adapted BSE strain: as vCJD is derived from consumption of BSE-contaminated meat, the finding that LC, NTS and PBC are clinical target areas in an experimental model of BSE infection would suggest these areas may also be critical in human prion diseases.

Moreover, a detailed analysis of the brainstem lesions has never been performed in the UK. The Prion Unit, through the Prion Clinic has access to archived brain specimens. Considering the recent localization of PBC in human brains, it would be now be possible to perform a systematic histopathological investigation of LC, NTS and PBC in samples of vCJD, sCJD or inherited prion diseases.

8.2.2 Stereotaxic prion injection in clinical target areas

As a direct consequence of the concept of clinical target areas, the duration of the incubation time is believed to be determined by the complexity of the pathways between the injection site and the clinical target areas (Kimberlin et al., 1987).

The current model of prion infection describes a split between prion infectivity (phase 1) and toxicity (phase 2) (Sandberg et al., 2011). Prion propagation in the brains occurs as a clinically silent exponential phase, not rate-limited by prion protein concentration, which reaches a maximal prion titre. Phase 1 is followed by a distinct switch to an infectivity plateau phase. The pathway switch leads to the production of toxic species, at a rate linearly dependent on PrP^C concentration.

Our data can be integrated into this model: although the LC, NTS and PBC are the first targets of prion replication in both M*lox*P and NFH-Cre/M*lox*P mice, in overexpressing M*lox*P mice the toxicity phase (phase 2) is shorter than in NFH-

Cre/M*lox*P, as in the first mouse line PrP concentration is higher. The shortened toxicity phase gives rise to the shorter incubation time in prion infected M*lox*P mice. However in NFH-Cre/M*lox*P, even though phase 2 is longer, mice become terminally ill when toxic species PrP^{L} reaches the local threshold in these areas.

A further reduction in incubation time could be shown by inoculating the mice stereotaxically in the clinical target areas. The stereotaxic inoculation could be performed in wild type, M*lox*P (overexpressing PrP ~3,4 time) and Tg20 (overexpressing PrP ~7, 8 times) and should show a reduction in the incubation time compared to the incubation times reported in Sandberg's paper (wild type and Tg20 mice) and in our work (M*lox*P mice). This reduction should be proportional to the level of PrP expression in the different mouse lines.

8.2.3 Optimization of PrP knock-out in clinical target areas

We showed that RML and Me7 prion inoculated NFH-Cre/*lox*P mice survived three and two time longer than RML and Me7 inoculated M*lox*P mice, but still developed clinical symptoms (chapter 4). We also showed that in NFH-Cre/*lox*P mice the Cre-mediated recombination in the clinical target areas was not complete (chapter 5). We therefore hypothesize that NFH-Cre/*lox*P mice were not completely protected from prion pathology because of residual PrP expression in the LC, NTS and PBC. To prove this hypothesis, we could knock down PrP locally in these nuclei. Local knockdown could be achieved by germ-line manipulation or by extrinsic tools. Taking advantage of the Cre-lox system, M*lox*P mice could be cross with mice expressing Cre under the control of specific promoters for recombination localized in these areas. For example, M*lox*P mice could be crossed with mice expressing Cre under the TH promoter (Gelman et al., 2003) for specific PrP knockdown in the LC.

An alternative, more direct and technically faster approach, could be to perform stereotaxic injections of lentivirus encoding shRNAi against PrP in these clinical target areas. In chapter 7 we have produced lentiviruses encoding shRNAs that target PrP within the 3'-UTR, and elicit a better PrP knock-down *in vitro* than lentiviruses encoding shRNAs targeting the ORF (White et al., 2008). We could now use these viruses *in vivo*: high titre lentivirus could be injected into the one or more proposed clinical target areas of prion infected NFH-Cre/M*lox*P mice to determine if

the incubation time would be prolonged. We could also set up a study on M*lox*P mice and knockdown PrP locally in the clinical target areas. A prolongation of the incubation time in M*lox*P mice treated with shRNAs against PrP just in the clinical target areas described here would confirm that these areas are fundamental for prion pathogenesis. After a proof of principle experiment, the study could be fine-tuned with multiple injections in the clinical target areas to obtain a more extensive knockdown; also, different time points could be tested: injection could be done during the infective stage to avoid reaching a maximal threshold, or during the toxicity stage, to extend the plateau phase.

8.2.4 Functional impairments in the clinical target areas

The progression of prion pathology described in this thesis identified the LC, the NTS and the PBC as target areas affected early by prion pathology, the degeneration of which correlates with the appearance of clinical signs. It will now be possible to study in more detail the molecular, cellular and functional impairment in these areas after prion inoculation.

For the LC, the first step would be to characterize the extent of neuronal loss. Design-based stereology can be used to quantitatively estimate of the total number of tyrosine hydroxylase (TH) positive neurons in the LC of infected mice compared to uninfected control. For example, the optical fractionator methods (Lockrow et al., 2011) uses thick sections and estimates the total number of cells from the number of cells sampled with a Systematic Randomly Sampled set of unbiased virtual counting spaces for the entire region of interest, with uniform distance between unbiased virtual counting spaces in three dimensional directions. We would expect a significant reduction of TH positive cells in terminally ill prion infected mice, but we cannot exclude some compensatory effect, such as increase in TH mRNA expression in the remaining neurons and sprouting of dendrites into peri-LC dendritic zone, as observed in human post-mortem studies on dementias related to noradrenergic impairments (Szot et al., 2006).

We could also envisage a time course study to determine at which point post inoculation, neuronal loss or increase in TH mRNA occurs in the LC, and how long after these changes an infected animal dies. Then, it will be possible to focus on the effect of impaired noradrenergic transmission on other brain areas, like the

hippocampus. As mentioned in chapter 5, we hypothesized that LC degeneration would affect the hippocampus even before manifestation of prion related pathology in this areas. As the hippocampal related behaviour has been shown to be impaired in prion infected mice and be rescued upon PrP depletion (Mallucci et al., 2007; White et al., 2008), a behavioural study would not answer this question. Alternatively, a histological approach could be taken. To determine whether changes in the cell bodies of LC neurons are linked to changes in hippocampal innervations, monoaminergic terminals in the HC could be stained for VMAT2; also, to examine whether the postsynaptic targets of LC axons in HC are impaired upon LC degeneration, β-adrenergic receptor staining could be performed.

The three clinical target areas identified here are all involved in chemoreception and control of respiration. Their overlapping function requires a multiple technique approach to determine different contribution to impairment in autonomic functions. As a first step, *in vivo* studies should be performed to quantify impairment of chemoreception or alteration of breathing frequency (Li and Nattie, 2006). However, the different contribution of LC, NTS and PBC to these processes should then be investigated with other techniques.

In the prion field, electrophysiological techniques have been used to a limited extent, to investigate PrP function within the hippocampus (Mallucci et al., 2002; Khosravani et al., 2008; Powell et al., 2008; Rangel et al., 2009) or scrapie related hippocampal impairment (Trifilo et al., 2008; Mallucci et al., 2007). Electrophysiological measurements could be performed in preparations from prion infected mice to quantify the effect of prion pathology on excitability and breathing drive in the LC, NTS and PBC. To observe transformation of network behaviour upon prion infection, techniques developed for recording from adult brainstem preparations could be used (Paton, 1996a; Paton, 1996b; Pickering and Paton, 2006). These preparations consist of *in situ* arterially perfused brainstem-spinal cord blocks, with sequential rostral to caudal micro-transection recording cranial and spinal motor outflow and compartmental neuronal population activity. The approach is similar to the one used in neonatal rat brainstem preparation *in vitro* that resulted in the original discovery of the PBC (Smith et al., 1991), but it is applied to a mature nervous system, generating neuronal activity patterns more similar to those *in vivo*.

To study the molecular events underlying prion induced impairments in the clinical target areas, it would be interesting to set up *ex-vivo* organotypic slice cultures from LC and PBC susceptible to prion disease. The *ex-vivo* organotypic slice culture approach has the advantage of allowing an in depth molecular analysis of neuronal tissue in conditions very similar to those *in vivo*. Organotypic cerebellar slice cultures are susceptible to prions (Falsig and Aguzzi, 2008). As viable LC (Hendelman et al., 1982), PBC (Rigatto et al., 2001) and LC and hippocampal co-cultures (Knopfel et al., 1989) can be obtained from neonatal mice, these systems could be used for direct observations of the molecular and network changes in prion pathology, upon development of appropriate protocols for prion infection. Alternatively, if prion infection were not achievable, acute effects of prions in organotypic slice cultures could be studied using recombinant protein mimetics of PrP^{Sc}, like aggregated β PrP.

9 Reference list

Agostinho,P. and Oliveira,C.R. (2003). Involvement of calcineurin in the neurotoxic effects induced by amyloid-beta and prion peptides. Eur. J Neurosci. *17*, 1189-1196.

Alheid,G.F. and McCrimmon,D.R. (2008). The chemical neuroanatomy of breathing. Respir. Physiol Neurobiol. *164*, 3-11.

Alper,T., Cramp,W.A., Haig ,D.A., and Clarke,M.C. (1967). Does the agent of scrapie replicate without nucleic acid? Nature *214*, 764-766.

Alper,T., Haig,D.A., and Clarke,M.C. (1966). The exceptionally small size of the scrapie agent. Biochem. Biophys. Res. Commun. *22*, 278-284.

Alpers,M.P. (1987). Epidemiology and clinical aspects of kuru. In Prions: Novel infectious Pathogens Causing Scrapie and Creutzfeldt-Jakob Disease, S.B.Prusiner and M.P.McKinley, eds. (San Diego: Academic Press), pp. 451-465.

Anderson,R.M., Donnelly,C.A., Ferguson,N.M., Woolhouse,M.E.J., Watt,C.J., Udy,H.J., MaWhinney,S., Dunstan,S.P., Southwood,T.R.E., Wilesmith,J.W., Ryan,J.B.M., Hoinville,L.J., Hillerton,J.E., Austin,A.R., and Wells,G.A.H. (1996). Transmission dynamics and epidemiology of BSE in British cattle. Nature *382*, 779-788.

Andresen,M.C. and Kunze,D.L. (1994). Nucleus tractus solitarius--gateway to neural circulatory control. Annu. Rev. Physiol *56*, 93-116.

Andresen,M.C. and Peters,J.H. (2008). Comparison of baroreceptive to other afferent synaptic transmission to the medial solitary tract nucleus. Am. J. Physiol Heart Circ. Physiol *295*, H2032-H2042.

Asante,E.A., Linehan,J.M., Desbruslais,M., Joiner,S., Gowland,I., Wood,A.L., Welch,J., Hill,A.F., Lloyd,S.E., Wadsworth,J.D., and Collinge,J. (2002). BSE prions propagate as either variant CJD-like or sporadic CJD-like prion strains in transgenic mice expressing human prion protein. EMBO J *21*, 6358-6366.

Aston-Jones,G. and Bloom,F.E. (1981). Activity of norepinephrine-containing locus coeruleus neurons in behaving rats anticipates fluctuations in the sleep-waking cycle. J. Neurosci. *1*, 876-886.

Aston-Jones,G., Chen,S., Zhu,Y., and Oshinsky,M.L. (2001). A neural circuit for circadian regulation of arousal. Nat. Neurosci. *4*, 732-738.

Baeten,L.A., Powers,B.E., Jewell,J.E., Spraker,T.R., and Miller,M.W. (2007). A Natural Case of Chronic Wasting Disease in a Free-ranging Moose (Alces alces shirasi). J Wildl. Dis. *43*, 309-314.

Bailey,T.W., Hermes,S.M., Andresen,M.C., and Aicher,S.A. (2006). Cranial visceral afferent pathways through the nucleus of the solitary tract to caudal ventrolateral

medulla or paraventricular hypothalamus: target-specific synaptic reliability and convergence patterns. J. Neurosci. *26*, 11893-11902.

Balaban,C.D. (1996). Vestibular nucleus projections to the parabrachial nucleus in rabbits: implications for vestibular influences on the autonomic nervous system. Exp. Brain Res. *108*, 367-381.

Balaban,C.D. and Beryozkin,G. (1994). Vestibular nucleus projections to nucleus tractus solitarius and the dorsal motor nucleus of the vagus nerve: potential substrates for vestibulo-autonomic interactions. Exp. Brain Res. *98*, 200-212.

Baloyannis,S.J., Costa,V., and Baloyannis,I.S. (2006). Morphological alterations of the synapses in the locus coeruleus in Parkinson's disease. J. Neurol. Sci. *248*, 35-41.

Barbanti,P., Fabbrini,G., Salvatore,M., Petraroli,R., Cardone,F., Maras,B., Equestre,M., Macchi,G., Lenzi,G.L., and Pocchiari,M. (1996). Polymorphism at codon 129 or codon 219 of *PRNP* and clinical heterogeneity in a previously unreported family with Gerstmann- Straussler-Scheinker disease (PrP-P102L mutation). Neurology *47*, 734-741.

Baron,T., Bencsik,A., Biacabe,A.G., Morignat,E., and Bessen,R.A. (2007). Phenotypic Similarity of Transmissible Mink Encephalopathy in Cattle and L-type Bovine Spongiform Encephalopathy in a Mouse Model. Emerg. Infect. Dis. *13*, 1887-1894.

Bartz,J.C., Kincaid,A.E., and Bessen,R.A. (2002). Retrograde Transport of Transmissible Mink Encephalopathy within Descending Motor Tracts. J. Virol. *76*, 5759-5768.

Basler,K., Oesch,B., Scott,M., Westaway,D., Walchli,M., Groth,D.F., McKinley,M.P., Prusiner,S.B., and Weissmann,C. (1986). Scrapie and cellular PrP isoforms are encoded by the same chromosomal gene. Cell *46*, 417-428.

Bate,C., Boshuizen,R.S., Langeveld,J.P., and Williams,A. (2002). Temporal and spatial relationship between the death of PrP-damaged neurones and microglial activation. Neuroreport *13*, 1695-1700.

Bateman,D., Hilton,D., Love,S., Zeidler,M., Beck J, and Collinge J (1995). Sporadic Creutzfeldt-Jakob disease in a 18-year old in the UK. Lancet *346*, 1155-1156.

Beekes,M., McBride,P.A., and Baldauf,E. (1998). Cerebral targeting indicates vagal spread of infection in hamsters fed with scrapie. J. Gen. Virol. *79*, 601-607.

Benarroch,E.E. (2007). Brainstem respiratory control: substrates of respiratory failure of multiple system atrophy. Mov Disord. *22*, 155-161.

Benarroch,E.E. (2009). The locus ceruleus norepinephrine system: functional organization and potential clinical significance. Neurology *73*, 1699-1704.

Benarroch,E.E., Schmeichel,A.M., Low,P.A., Sandroni,P., and Parisi,J.E. (2008). Loss of A5 noradrenergic neurons in multiple system atrophy. Acta Neuropathol. *115*, 629-634.

Bernoulli,C. (1980). (Creutzfeld-Jakob disease). Schweiz. Med. Wochenschr. *110*, 750-757.

Bernoulli,C., Siegfried,J., Baumgartner,G., Regli,F., Rabinowicz,T., Gajdusek,D.C., and Gibbs,C.J., Jr. (1977). Danger of accidental person-to-person transmission of Creutzfeldt-Jakob disease by surgery. . Lancet *1*, 478-479.

Bessen,R.A., Kocisko,D.A., Raymond,G.J., Nandan,S., Lansbury,P.T., and Caughey,B. (1995). Non-genetic propagation of strain-specific properties of scrapie prion protein. Nature *375*, 698-700.

Bessen,R.A. and Marsh,R.F. (1994). Distinct PrP properties suggest the molecular basis of strain variation in transmissible mink encephalopathy. J Virol *68*, 7859-7868.

Bhaskaran,D. and Freed,C.R. (1988). Changes in neurotransmitter turnover in locus coeruleus produced by changes in arterial blood pressure. Brain Res. Bull. *21*, 191-199.

Biancardi,V., Bicego,K.C., Almeida,M.C., and Gargaglioni,L.H. (2008). Locus coeruleus noradrenergic neurons and CO2 drive to breathing. Pflugers Arch. *455*, 1119-1128.

Bianchi,A.L., Denavit-Saubie,M., and Champagnat,J. (1995). Central control of breathing in mammals: neuronal circuitry, membrane properties, and neurotransmitters. Physiol Rev. *75*, 1-45.

Blomer,U., Naldini,L., Kafri,T., Trono,D., Verma,I.M., and Gage,F.H. (1997). Highly efficient and sustained gene transfer in adult neurons with a lentivirus vector. J. Virol. *71*, 6641-6649.

Bondareff,W., Mountjoy,C.Q., Roth,M., Rossor,M.N., Iversen,L.L., Reynolds,G.P., and Hauser,D.L. (1987). Neuronal degeneration in locus ceruleus and cortical correlates of Alzheimer disease. Alzheimer Dis. Assoc. Disord. *1*, 256-262.

Borchelt,D.R., Scott,M., Taraboulos,A., Stahl,N., and Prusiner,S.B. (1990). Scrapie and cellular prion proteins differ in their kinetics of synthesis and topology in cultured cells. J Cell Biol *110*, 743-752.

Bounhar,Y., Zhang,Y., Goodyer,C.G., and LeBlanc,A. (2001). Prion protein protects human neurons against Bax-mediated apoptosis. Journal of Biological Chemistry *276*, 39145-39149.

Brandner,S., Isenmann,S., Raeber,A., Fischer,M., Sailer,A., Kobayashi,Y., Marino,S., Weissmann,C., and Aguzzi,A. (1996). Normal host prion protein necessary for scrapie-induced neurotoxicity. Nature *379*, 339-343.

Bremer,J., Baumann,F., Tiberi,C., Wessig,C., Fischer,H., Schwarz,P., Steele,A.D., Toyka,K.V., Nave,K.A., Weis,J., and Aguzzi,A. (2010). Axonal prion protein is required for peripheral myelin maintenance. Nat Neurosci.

Britton,T.C., Al-Sarraj,S., Shaw,C., Campbell,T., and Collinge J (1995). Sporadic Creutzfeldt-Jakob disease in a 16-year-old in the UK. Lancet *346*, 1155.

Brodal,A. (1981). Neurology anatomy in in Relation to Clinical Medicine., Oxford University Press, ed.

Brown,D.R. (1999). Prion protein expression aids cellular uptake and veratridine-induced release of copper. J. Neurosci. Res. *58*, 717-725.

Brown,D.R., Qin,K., Herms,J.W., Madlung,A., Manson,J., Strome,R., Fraser,P.E., Kruck,T., von Bohlen,A., Schulz-Schaeffer,W., Giese,A., Westaway,D., and Kretzschmar,H. (1997a). The cellular prion protein binds copper in vivo. Nature *390*, 684-687.

Brown,D.R., Schmidt,B., and Kretzschmar,H.A. (1996). Role of microglia and host prion protein in neurotoxicity of a prion protein fragment. Nature *380*, 345-347.

Brown,D.R., Schulz-Schaeffer,W.J., Schmidt,B., and Kretzschmar,H.A. (1997b). Prion protein-deficient cells show altered response to oxidative stress due to decreased SOD-1 activity. Exp. Neurol *146*, 104-112.

Brown,P. and Bradley,R. (1998). 1755 and all that: a historical primer of transmissible spongiform encephalopathy. BMJ. *317*, 1688-1692.

Brown,P., Cathala,F., Raubertas,R.F., Gajdusek,D.C., and Castaigne,P. (1987). The epidemiology of Creutzfeldt-Jakob disease: conclusion of a 15-year investigation in France and review of the world literature. Neurology *37*, 895-904.

Brown,P., Gibbs,C.J.Jr., Rodgers Johnson,P., Asher,D.M., Sulima,M.P., Bacote,A., Goldfarb,L.G., and Gajdusek,D.C. (1994). Human spongiform encephalopathy: the National Institutes of Health series of 300 cases of experimentally transmitted disease. Ann Neurol *35*, 513-529.

Brown,P., Preece M, Brandel,J.P., Sato,T., McShane,L., Zerr,I., Fletcher,A., Will,R.G., Pocchiari,M., Cashman,N.R., D'Aignaux,J.H., Cervenáková,L., Fradkin,J., Schonberger,L.B., and Collins,S.J. (2000). Iatrogenic Creutzfeldt-Jakob disease at the millennium. Neurology *55*, 1075-1081.

Brown,P., Preece,M.A., and Will,R.G. (1992). "Friendly fire" in medicine: hormones, homografts, and Creutzfeldt-Jakob disease. Lancet *340*, 24-27.

Browning,S.R., Mason,G.L., Seward,T., Green,M., Eliason,G.A., Mathiason,C., Miller,M.W., Williams,E.S., Hoover,E., and Telling,G.C. (2004). Transmission of Prions from Mule Deer and Elk with Chronic Wasting Disease to Transgenic Mice Expressing Cervid PrP. J Virol *78*, 13345-13350.

Bruce,M., Chree,A., McConnell,I., Foster,J., Pearson,G., and Fraser,H. (1994). Transmission of bovine spongiform encephalopathy and scrapie to mice: Strain variation and the species barrier. Philos. Trans. R. Soc. Lond. [Biol.] *343*, 405-411.

Bruce,M.E. (1993). Scrapie strain variation and mutation. Br. Med. Bull. *49*, 822-838.

Bruce,M.E. and Dickinson,A.G. (1985). Genetic control of amyloid plaque production and incubation period in scrapie-infected mice. J Neuropathol. Exp. Neurol *44*, 285-294.

Bruce,M.E., Fraser,H., McBride,P.A., Scott,J.R., and Dickinson,A.G. (1992). The Basis of Strain Variation in Scrapie. In Prion Diseases in Human and Animals, S.B.Prusiner, Collinge J, J.Powell, and B.Anderton, eds. (London: Ellis Horwood).

Bruce,M.E., Will,R.G., Ironside,J.W., McConnell,I., Drummond,D., Suttie,A., McCardle,L., Chree,A., Hope,J., Birkett,C., Cousens,S., Fraser,H., and Bostock,C.J. (1997). Transmissions to mice indicate that 'new variant' CJD is caused by the BSE agent. Nature *389*, 498-501.

Budka,H. (2003). Neuropathology of prion diseases. Br. Med. Bull. *66*, 121-130.

Bueler,H., Aguzzi,A., Sailer,A., Greiner,R.A., Autenried,P., Aguet,M., and Weissmann,C. (1993). Mice devoid of PrP are resistant to scrapie. Cell *73*, 1339-1347.

Bueler,H., Fischer,M., Lang,Y., Bluethmann,H., Lipp,H.-P., DeArmond,S.J., Prusiner,S.B., Aguet,M., and Weissmann,C. (1992). Normal development and behaviour of mice lacking the neuronal cell-surface PrP protein. Nature *356*, 577-582.

Campana,V., Zentilin,L., Mirabile,I., Kranjc,A., Casanova,P., Giacca,M., Prusiner,S.B., Legname,G., and Zurzolo,C. (2009). Development of antibody fragments for immunotherapy of prion diseases. Biochem. J. *418*, 507-515.

Cashman,N.R., Loertscher,R., Nalbantoglu,J., Shaw,I., Kascsak,R.J., Bolton,D.C., and Bendheim,P.E. (1990). Cellular isoform of the scrapie agent protein participates in lymphocyte activation. Cell *61*, 185-192.

Castilla,J., Saa,P., Hetz,C., and Soto,C. (2005). In vitro generation of infectious scrapie prions. Cell *121*, 195-206.

Caughey,B. and Raymond,G.J. (1991). The scrapie-associated form of PrP is made from a cell surface precursor that is both protease- and phospholipase-sensitive. J Biol. Chem. *266 No 27*, 18217-18223.

Caughey,B.W., Dong,A., Bhat,K.S., Ernst,D., Hayes,S.F., and Caughey,W.S. (1991). Secondary structure analysis of the scrapie-associated protein PrP 27-30 in water by infrared spectroscopy. Biochemistry *30*, 7672-7680.

Chandler,R.L. (1961). Encephalopathy in mice produced by inoculation with scrapie brain material. Lancet *1*, 1378-1379.

Chapman,J., Brown,P., Goldfarb,L.G., Arlazoroff,A., Gajdusek,D.C., and Korczyn,A.D. (1993). Clinical heterogeneity and unusual presentations of Creutzfeldt- Jakob disease in Jewish patients with the PRNP codon 200 mutation. J Neurol Neurosurg Psychiatry *56*, 1109-1112.

Chesebro,B., Race,R., Wehrly,K., Nishio,J., Bloom,M., Lechner,D., Bergstrom,S., Robbins,K., Mayer,L., Keith,J.M., and Raeber,A.J. (1985). Identification of scrapie prion protein-specific mRNA in scrapie- infected and uninfected brain. Nature *315*, 331-333.

Coates,E.L., Li,A., and Nattie,E.E. (1993). Widespread sites of brain stem ventilatory chemoreceptors. J. Appl. Physiol *75*, 5-14.

Coddou,C., Bravo,E., and Eugenin,J. (2009). Alterations in cholinergic sensitivity of respiratory neurons induced by pre-natal nicotine: a mechanism for respiratory dysfunction in neonatal mice. Philos. Trans. R. Soc. Lond B Biol. Sci. *364*, 2527-2535.

Cohen,M.I. (1979). Neurogenesis of respiratory rhythm in the mammal. Physiol Rev. *59*, 1105-1173.

Cohen,M.I. and Shaw,C.F. (2004). Role in the inspiratory off-switch of vagal inputs to rostral pontine inspiratory-modulated neurons. Respir. Physiol Neurobiol. *143*, 127-140.

Cole,S. and Kimberlin,R.H. (1985). Pathogenesis of mouse scrapie: dynamics of vacuolation in brain and spinal cord after intraperitoneal infection. Neuropathol & Appl Neurobiol *11*, 213-227.

Colling,S.B., Collinge J, and Jefferys,J.G.R. (1996). Hippocampal slices from prion protein null mice: Disrupted Ca^{2+}-activated K^{+} currents. Neurosci. Lett. *209*, 49-52.

Collinge ,J. (1997). Human prion diseases and bovine spongiform encephalopathy (BSE). Hum Mol Genetics *6*, 1699-1705.

Collinge,J., Beck J, Campbell,T., Estibeiro,K., and Will,R.G. (1996). Prion protein gene analysis in new variant cases of Creutzfeldt-Jakob disease. Lancet *348*, 56.

Collinge,J. (1999). Variant Creutzfeldt-Jakob disease. Lancet *354*, 317-323.

Collinge,J. (2005). Molecular neurology of prion disease. Journal of Neurology Neurosurgery and Psychiatry *76*, 906-919.

Collinge,J. and Clarke,A. (2007). A general model of prion strains and their pathogenicity. Science *318*, 930-936.

Collinge,J., Gorham,M., Hudson,F., Kennedy,A., Keogh,G., Pal,S., Rossor,M., Rudge,P., Siddique,D., Spyer,M., Thomas,D., Walker,S., Webb,T., Wroe,S., and

Darbyshire,J. (2009). Safety and efficacy of quinacrine in human prion disease (PRION-1 study): a patient-preference trial. Lancet Neurol. *8*, 334-344.

Collinge,J., Palmer,M.S., and Dryden,A.J. (1991). Genetic predisposition to iatrogenic Creutzfeldt-Jakob disease. Lancet *337*, 1441-1442.

Collinge,J., Palmer,M.S., Sidle,K.C., Gowland,I., Medori,R., Ironside,J., and Lantos,P. (1995a). Transmission of fatal familial insomnia to laboratory animals. Lancet *346*, 569-570.

Collinge,J., Palmer,M.S., Sidle,K.C.L., Hill,A.F., Gowland,I., Meads,J., Asante,E.A., Bradley,R., Doey,L.J., and Lantos,P.L. (1995b). Unaltered susceptibility to BSE in transgenic mice expressing human prion protein. Nature *378*, 779-783.

Collinge,J. and Rossor,M. (1996). A new variant of prion disease. Lancet *347*, 916-917.

Collinge,J., Sidle,K.C., Meads,J., Ironside,J., and Hill,A.F. (1996). Molecular analysis of prion strain variation and the aetiology of 'new variant' CJD. Nature *383*, 685-690.

Collinge,J., Whitfield,J., McKintosh,E., Beck,J., Mead,S., Thomas,D.J., and Alpers,M.P. (2006). Kuru in the 21st century--an acquired human prion disease with very long incubation periods. Lancet *367*, 2068-2074.

Collinge,J., Whitfield,J., McKintosh,E., Frosh,A., Mead,S., Hill,A.F., Brandner,S., Thomas,D., and Alpers,M.P. (2008). A clinical study of kuru patients with long incubation periods at the end of the epidemic in Papua New Guinea. Philos Trans R Soc Lond B Biol Sci *363*, 3725-3739.

Collinge,J., Whittington,M.A., Sidle,K.C.L., Smith,C.J., Palmer,M.S., Clarke,A.R., and Jefferys,J.G.R. (1994). Prion protein is necessary for normal synaptic function. Nature *370*, 295-297.

Collins,S.J., Lewis,V., Brazier,M., Hill AF, Fletcher,A., and Masters,C.L. (2002). Quinacrine does not prolong survival in a murine Creutzfeldt-Jakob disease model. Ann. Neurol. *52*, 503-506.

Combs,C.K., Johnson,D.E., Cannady,S.B., Lehman,T.M., and Landreth,G.E. (1999). Identification of microglial signal transduction pathways mediating a neurotoxic response to amyloidogenic fragments of β-amyloid and prion proteins. J. Neurosci. *19*, 928-939.

Come,J.H., Fraser,P.E., and Lansbury,P.T.Jr. (1993). A kinetic model for amyloid formation in the prion diseases: importance of seeding. Proc. Natl. Acad. Sci. U. S. A *90*, 5959-5963.

Connelly,C.A., Dobbins,E.G., and Feldman,J.L. (1992). Pre-Botzinger complex in cats: respiratory neuronal discharge patterns. Brain Res. *590*, 337-340.

Cote,F., Collard,J.F., Houle,D., and Julien,J.P. (1994). Copy-dependent and correct developmental expression of the human neurofilament heavy gene in transgenic mice. Brain Res. Mol. Brain Res. *26*, 99-105.

Cote,F., Collard,J.F., and Julien,J.P. (1993). Progressive neuronopathy in transgenic mice expressing the human neurofilament heavy gene: a mouse model of amyotrophic lateral sclerosis. Cell *73*, 35-46.

Coulpier,M., Messiaen,S., Hamel,R., Fernandez,d.M., Lilin,T., and Eloit,M. (2006). Bax deletion does not protect neurons from BSE-induced death. Neurobiol. Dis. *23*, 603-611.

Cuillé,J. and Chelle,P.L. (1936). La maladie dite tremblante du mouton est-elle inocuable? C. R. Acad. Sci. *203*, 1552-1554.

Cunningham,C., Deacon,R., Wells,H., Boche,D., Waters,S., Diniz,C.P., Scott,H., Rawlins,J.N., and Perry,V.H. (2003). Synaptic changes characterize early behavioural signs in the ME7 model of murine prion disease. Eur. J Neurosci. *17*, 2147-2155.

Daude,N., Marella,M., and Chabry,J. (2003). Specific inhibition of pathological prion protein accumulation by small interfering RNAs. J Cell Sci *116*, 2775-2779.

de Marco,M.F., Linehan,J., Gill,O.N., Clewley,J.P., and Brandner,S. (2010). Large-scale immunohistochemical examination for lymphoreticular prion protein in tonsil specimens collected in Britain. J. Pathol. *222*, 380-387.

Dean,J.B., Bayliss,D.A., Erickson,J.T., Lawing,W.L., and Millhorn,D.E. (1990). Depolarization and stimulation of neurons in nucleus tractus solitarii by carbon dioxide does not require chemical synaptic input. Neuroscience *36*, 207-216.

DeArmond,S.J. and Prusiner,S.B. (1997). Prion diseases. In Greenfield's Neuropathology, P.Lantos and D.Graham, eds. (London: Edward Arnold), pp. 235-280.

Doh-ura,K., Ishikawa,K., Murakami-Kubo,I., Sasaki,K., Mohri,S., Race,R., and Iwaki,T. (2004). Treatment of Transmissible Spongiform Encephalopathy by Intraventricular Drug Infusion in Animal Models. J Virol. *78*, 4999-5006.

Dutschmann,M. and Herbert,H. (2006). The Kolliker-Fuse nucleus gates the postinspiratory phase of the respiratory cycle to control inspiratory off-switch and upper airway resistance in rat. Eur. J. Neurosci. *24*, 1071-1084.

Edgeworth,J.A., Farmer,M., Sicilia,A., Tavares,P., Beck,J., Campbell,T., Lowe,J., Mead,S., Rudge,P., Collinge,J., and Jackson,G.S. (2011). Detection of prion infection in variant Creutzfeldt-Jakob disease: a blood-based assay. Lancet *377*, 487-493.

Eghiaian,F., Grosclaude,J., Lesceu,S., Debey,P., Doublet,B., Treguer,E., Rezaei,H., and Knossow,M. (2004). Insight into the PrPC -> PrPSc conversion from the

structures of antibody-bound ovine prion scrapie-susceptibility variants. Proc. Natl. Acad Sci U. S. A *101*, 10254-10259.

Eikelenboom,P., Bate,C., Van Gool,W.A., Hoozemans,J.J., Rozemuller,J.M., Veerhuis,R., and Williams,A. (2002). Neuroinflammation in Alzheimer's disease and prion disease. Glia *40*, 232-239.

Elam,M., Yao,T., Thoren,P., and Svensson,T.H. (1981). Hypercapnia and hypoxia: chemoreceptor-mediated control of locus coeruleus neurons and splanchnic, sympathetic nerves. Brain Res. *222*, 373-381.

Ertmer,A., Gilch,S., Yun,S.W., Flechsig,E., Klebl,B., Stein-Gerlach,M., Klein,M.A., and Schatzl,H.M. (2004). The tyrosine kinase inhibitor STI571 induces cellular clearance of PrPSc in prion-infected cells. J. Biol. Chem. *279*, 41918-41927.

Ezure,K. (2004). Respiration-related afferents to parabrachial pontine regions. Respir. Physiol Neurobiol. *143*, 167-175.

Ezure,K. and Tanaka,I. (2006). Distribution and medullary projection of respiratory neurons in the dorsolateral pons of the rat. Neuroscience *141*, 1011-1023.

Fabris,G., Anselmo-Franci,J.A., and Branco,L.G. (1999). Role of nitric oxide in hypoxia-induced hyperventilation and hypothermia: participation of the locus coeruleus. Braz. J. Med. Biol. Res. *32*, 1389-1398.

Falsig,J. and Aguzzi,A. (2008). The prion organotypic slice culture assay--POSCA. Nat Protoc. *3*, 555-562.

Feldman,J.L. (1986). Neurophysiology of breathing in mammals. In Intrinsic regulatory system of the brain, Bloom FE, ed. (Bethesda, MD: American Physiological Society), pp. 463-524.

Feldman,J.L. and Del Negro,C.A. (2006). Looking for inspiration: new perspectives on respiratory rhythm. Nat. Rev. Neurosci. *7*, 232-242.

Feldman,J.L., Mitchell,G.S., and Nattie,E.E. (2003). Breathing: rhythmicity, plasticity, chemosensitivity. Annu. Rev. Neurosci. *26*, 239-266.

Filosa,J.A., Dean,J.B., and Putnam,R.W. (2002). Role of intracellular and extracellular pH in the chemosensitive response of rat locus coeruleus neurones. J. Physiol *541*, 493-509.

Fischer,M., Rulicke,T., Raeber,A., Sailer,A., Moser,M., Oesch,B., Brandner,S., Aguzzi,A., and Weissmann,C. (1996). Prion protein (PrP) with amino-proximal deletions restoring susceptibility of PrP knockout mice to scrapie. EMBO J. *15*, 1255-1264.

Flechsig,E., Hegyi,I., Leimeroth,R., Zuniga,A., Rossi,D., Cozzio,A., Schwarz,P., Rulicke,T., Gotz,J., Aguzzi,A., and Weissmann,C. (2003). Expression of truncated PrP targeted to Purkinje cells of PrP knockout mice causes Purkinje cell death and ataxia. EMBO J *22*, 3095-3101.

Florio,T., Grimaldi,M., Scorziello,A., Salmona,M., Bugiani,O., Tagliavini,F., Forloni,G., and Schettini,G. (1996). Intracellular calcium rise through L-type calcium channels, as molecular mechanism for prion protein fragment 106-126-induced astroglial proliferation. Biochem. Biophys. Res. Commun. *228*, 397-405.

Ford,M.J., Burton,L.J., Morris,R.J., and Hall,S.M. (2002). Selective expression of prion protein in peripheral tissues of the adult mouse. Neuroscience *113*, 177-192.

Forloni,G., Angeretti,N., Chiesa,R., Monzani,E., Salmona,M., Bugiani,O., and Tagliavini,F. (1993). Neurotoxicity of a prion protein fragment. Nature *362*, 543-546.

Foster,J.D., Parnham,D., Chong,A., Goldmann,W., and Hunter,N. (2001). Clinical signs, histopathology and genetics of experimental transmission of BSE and natural scrapie to sheep and goats. Veterinary Record *148*, 165-171.

Funk,G.D., Smith,J.C., and Feldman,J.L. (1993). Generation and transmission of respiratory oscillations in medullary slices: role of excitatory amino acids. J. Neurophysiol. *70*, 1497-1515.

Gajdusek,D.C., Gibbs,C.J.Jr., and Alpers MP (1967). Transmission and passage of experimental "kuru" to Chimpanzees. Science *155*, 212-214.

Gasset,M., Baldwin,M.A., Fletterick,R.J., and Prusiner,S.B. (1993). Perturbation of the secondary structure of the scrapie prion protein under conditions that alter infectivity. Proc. Natl. Acad. Sci. U. S A. *90*, 1-5.

Gasset,M., Baldwin,M.A., Lloyd,D.H., Gabriel,J.M., Holtzman,D.M., Cohen,F., Fletterick,R., and Prusiner,S.B. (1992). Predicted alpha-helical regions of the prion protein when synthesized as peptides form amyloid. Proc. Natl. Acad. Sci. U. S A. *89*, 10940-10944.

Gelman,D.M., Noain,D., Avale,M.E., Otero,V., Low,M.J., and Rubinstein,M. (2003). Transgenic mice engineered to target Cre/loxP-mediated DNA recombination into catecholaminergic neurons. Genesis *36*, 196-202.

German,D.C., Manaye,K.F., White,C.L., III, Woodward,D.J., McIntire,D.D., Smith,W.K., Kalaria,R.N., and Mann,D.M. (1992). Disease-specific patterns of locus coeruleus cell loss. Ann. Neurol. *32*, 667-676.

Ghani,A.C., Donnelly,C.A., Ferguson,N.M., and Anderson,R.M. (2002). The transmission dynamics of BSE and vCJD. C. R. Acad. Sci. III *325*, 37-47.

Ghani,A.C., Donnelly,C.A., Ferguson,N.M., and Anderson,R.M. (2003). Updated projections of future vCJD deaths in the UK. BMC. Infect. Dis. *3*, 4.

Gibbs,C.J.Jr., Joy,A., Heffner,R., Franko,M., Miyazaki,M., Asher,D.M., Parisi,J.E., Brown,P.W., and Gajdusek,D.C. (1985). Clinical and pathological features and laboratory confirmation of Creutzfeldt-Jakob disease in a recipient of pituitary-derived human growth hormone. N. Engl. J Med. *313*, 734-738.

Glover,K.J., Whiles,J.A., Wood,M.J., Melacini,G., Komives,E.A., and Vold,R.R. (2001). Conformational dimorphism and transmembrane orientation of prion protein residues 110-136 in bicelles. Biochemistry *40*, 13137-13142.

Gonzalez-Alegre,P., Bode,N., Davidson,B.L., and Paulson,H.L. (2005). Silencing primary dystonia: lentiviral-mediated RNA interference therapy for DYT1 dystonia. J. Neurosci. *25*, 10502-10509.

Gordon,W.S. (1946). Advances in veterinary research. Louping-ill, tick-borne fever and scrapie. Veterinary Record *58*, 516-520.

Gray,P.A., Rekling,J.C., Bocchiaro,C.M., and Feldman,J.L. (1999). Modulation of respiratory frequency by peptidergic input to rhythmogenic neurons in the preBotzinger complex. Science *286*, 1566-1568.

Griffith,J.S. (1967). Self Replication and scrapie. Nature *215*, 1043-1044.

Hachiya,N.S., Watanabe,K., Kawabata,M.Y., Jozuka,A., Kozuka,Y., Sakasegawa,Y., and Kaneko,K. (2005). Prion protein with Y145STOP mutation induces mitochondria-mediated apoptosis and PrP-containing deposits in vitro. Biochem. Biophys. Res Commun. *327*, 894-899.

Hadlow,W.J. (1959). Scrapie and kuru. Lancet *ii*, 289-290.

Haire,L.F., Whyte,S.M., Vasisht,N., Gill,A.C., Verma,C., Dodson,E.J., Dodson,G.G., and Bayley,P.M. (2004). The crystal structure of the globular domain of sheep prion protein. J Mol. Biol. *336*, 1175-1183.

Haraguchi,T., Fisher,S., Olofsson,S., Endo,T., Groth,D., Tarentino,A., Borchelt,D.R., Teplow,D., Hood,L.E., Burlingame,A.L., Lycke,E., Kobata,A., and Prusiner,S.B. (1989). Asparagine-linked glycosylation of the Scrapie and cellular prion proteins. Arch Biochem. Biophys. *274*, 1-13.

Harper,S.Q., Staber,P.D., He,X., Eliason,S.L., Martins,I.H., Mao,Q., Yang,L., Kotin,R.M., Paulson,H.L., and Davidson,B.L. (2005). RNA interference improves motor and neuropathological abnormalities in a Huntington's disease mouse model. Proc. Natl. Acad. Sci. U. S. A *102*, 5820-5825.

Hegde,R.S., Mastrianni,J.A., Scott,M.R., DeFea,K.A., Tremblay,P., Torchia,M., DeArmond,S.J., Prusiner,S.B., and Lingappa,V.R. (1998). A transmembrane from of the prion protein in neurodegenerative disease. Science *279*, 827-834.

Hendelman,W.J., Marshall,K.C., Ferguson,R., and Carriere,S. (1982). Catecholamine neurons of the central nervous system in organotypic culture. Dev. Neurosci. *5*, 64-76.

Heneka,M.T., Galea,E., Gavriluyk,V., Dumitrescu-Ozimek,L., Daeschner,J., O'Banion,M.K., Weinberg,G., Klockgether,T., and Feinstein,D.L. (2002). Noradrenergic depletion potentiates beta -amyloid-induced cortical inflammation: implications for Alzheimer's disease. J. Neurosci. *22*, 2434-2442.

Heneka,M.T., Ramanathan,M., Jacobs,A.H., Dumitrescu-Ozimek,L., Bilkei-Gorzo,A., Debeir,T., Sastre,M., Galldiks,N., Zimmer,A., Hoehn,M., Heiss,W.D., Klockgether,T., and Staufenbiel,M. (2006). Locus ceruleus degeneration promotes Alzheimer pathogenesis in amyloid precursor protein 23 transgenic mice. J. Neurosci. *26*, 1343-1354.

Hetz,C., Maundrell,K., and Soto,C. (2003a). Is loss of function of the prion protein the cause of prion disorders? Trends Mol. Med. *9*, 237-243.

Hetz,C., Russelakis-Carneiro,M., Maundrell,K., Castilla,J., and Soto,C. (2003b). Caspase-12 and endoplasmic reticulum stress mediate neurotoxicity of pathological prion protein. EMBO J *22*, 5435-5445.

Hetz,C.A. and Soto,C. (2006). Stressing Out the ER: A Role of the Unfolded Protein Response in Prion-Related Disorders. Curr. Mol Med *6*, 37-43.

Hill,A.F., Antoniou,M., and Collinge,J. (1999). Protease-resistant prion protein produced *in vitro* lacks detectable infectivity. Journal of General Virology *80*, 11-14.

Hill,A.F. and Collinge,J. (2003a). Subclinical prion infection. Trends Microbiol. *11*, 578-584.

Hill,A.F. and Collinge,J. (2003b). Subclinical prion infection in humans and animals. Br. Med. Bull. *66*, 161-170.

Hill,A.F., Desbruslais,M., Joiner,S., Sidle,K.C., Gowland,I., Collinge,J., Doey,L.J., and Lantos,P. (1997). The same prion strain causes vCJD and BSE. Nature *389*, 448-50, 526.

Hill,A.F., Joiner,S., Beck,J.A., Campbell,T.A., Dickinson,A., Poulter,M., Wadsworth,J.D., and Collinge,J. (2006). Distinct glycoform ratios of protease resistant prion protein associated with PRNP point mutations. Brain *129*, 676-685.

Hill,A.F., Joiner,S., Linehan,J., Desbruslais,M., Lantos,P.L., and Collinge,J. (2000). Species-barrier-independent prion replication in apparently resistant species. Proc. Natl. Acad. Sci. U. S. A *97*, 10248-10253.

Hoesche,C., Sauerwald,A., Veh,R.W., Krippl,B., and Kilimann,M.W. (1993). The 5'-flanking region of the rat synapsin I gene directs neuron-specific and developmentally regulated reporter gene expression in transgenic mice. J. Biol. Chem. *268*, 26494-26502.

Hornabrook,R.W. (1968). Kuru--a subacute cerebellar degeneration. The natural history and clinical features. Brain *91*, 53-74.

Hornshaw,M.P., McDermott,J.R., Candy,J.M., and Lakey,J.H. (1995). Copper binding to the N-terminal tandem repeat region of mammalian and avian prion protein: Structural studies using synthetic peptides. Biochem. Biophys. Res. Commun. *214*, 993-999.

Huillard d'Aignaux,J., Costagliola,D., Maccario,J., Billette de Villemeur,T., Brandel,J.P., Deslys,J.P., Hauw,J.J., Chaussain,J.L., Agid,Y., Dormont,D., and Alperovitch,A. (1999). Incubation period of Creutzfeldt-Jakob disease in human growth hormone recipients in France. Neurology *53*, 1197-1201.

Hwang,D., Lee,I.Y., Yoo,H., Gehlenborg,N., Cho,J.H., Petritis,B., Baxter,D., Pitstick,R., Young,R., Spicer,D., Price,N.D., Hohmann,J.G., DeArmond,S.J., Carlson,G.A., and Hood,L.E. (2009). A systems approach to prion disease. Mol Syst. Biol *5*, 252.

Ishikura,N., Clever,J.L., Bouzamondo-Bernstein,E., Samayoa,E., Prusiner,S.B., Huang,E.J., and DeArmond,S.J. (2005). Notch-1 activation and dendritic atrophy in prion disease. Proc. Natl. Acad. Sci. U. S. A *102*, 886-891.

Iversen,L.L., Rossor,M.N., Reynolds,G.P., Hills,R., Roth,M., Mountjoy,C.Q., Foote,S.L., Morrison,J.H., and Bloom,F.E. (1983). Loss of pigmented dopamine-beta-hydroxylase positive cells from locus coeruleus in senile dementia of Alzheimer's type. Neurosci. Lett. *39*, 95-100.

Iwasaki,Y., Hashizume,Y., Yoshida,M., Kitamoto,T., and Sobue,G. (2005). Neuropathologic characteristics of brainstem lesions in sporadic Creutzfeldt-Jakob disease. Acta Neuropathol. *109*, 557-566.

Jackson,G.S. and Clarke,A.R. (2000). Mammalian prion proteins. Curr. Opin. Struct. Biol. *10*, 69-74.

Jackson,G.S., Murray,I., Hosszu,L.L., Gibbs,N., Waltho,J.P., Clarke,A.R., and Collinge,J. (2001). Location and properties of metal-binding sites on the human prion protein. Proc. Natl. Acad. Sci. U. S. A *98*, 8531-8535.

Jardanhazi-Kurutz,D., Kummer,M.P., Terwel,D., Vogel,K., Thiele,A., and Heneka,M.T. (2011). Distinct adrenergic system changes and neuroinflammation in response to induced locus ceruleus degeneration in APP/PS1 transgenic mice. Neuroscience *176*, 396-407.

Jian,B.J., Acernese,A.W., Lorenzo,J., Card,J.P., and Yates,B.J. (2005). Afferent pathways to the region of the vestibular nuclei that participates in cardiovascular and respiratory control. Brain Res. *1044*, 241-250.

Johnson,R.T. (2005). Prion diseases. Lancet Neurol *4*, 635-642.

Johnson,R.T. and Gibbs,C.J., Jr. (1998). Creutzfeldt-Jakob disease and related transmissible spongiform encephalopathies. N. Engl. J. Med. *339*, 1994-2004.

Julien,J.P., Cote,F., Beaudet,L., Sidky,M., Flavell,D., Grosveld,F., and Mushynski,W. (1988). Sequence and structure of the mouse gene coding for the largest neurofilament subunit. Gene *68*, 307-314.

Kanaani,J., Prusiner,S.B., Diacovo,J., Baekkeskov,S., and Legname,G. (2005). Recombinant prion protein induces rapid polarization and development of synapses in embryonic rat hippocampal neurons in vitro. J Neurochem *95*, 1373-1386.

Karapetyan,Y.E., Saa,P., Mahal,S.P., Sferrazza,G.F., Sherman,A., Sales,N., Weissmann,C., and Lasmezas,C.I. (2009). Prion strain discrimination based on rapid in vivo amplification and analysis by the cell panel assay. PLoS One. *4*, e5730.

Kaski,D., Mead,S., Hyare,H., Cooper,S., Jampana,R., Overell,J., Knight,R., Collinge,J., and Rudge,P. (2009). Variant CJD in an individual heterozygous for PRNP codon 129. Lancet *374*, 2128.

Keshet,G.I., Ovadia,H., Taraboulos,A., and Gabizon,R. (1999). Scrapie-infected mice and PrP knockout mice share abnormal localization and activity of neuronal nitric oxide synthase. J. Neurochem. *72*, 1224-1231.

Khosravani,H., Zhang,Y., Tsutsui,S., Hameed,S., Altier,C., Hamid,J., Chen,L., Villemaire,M., Ali,Z., Jirik,F.R., and Zamponi,G.W. (2008). Prion protein attenuates excitotoxicity by inhibiting NMDA receptors. J Cell Biol *181*, 551-565.

Khvorova,A., Reynolds,A., and Jayasena,S.D. (2003). Functional siRNAs and miRNAs exhibit strand bias. Cell *115*, 209-216.

Kim,S.J. and Hegde,R.S. (2002). Cotranslational partitioning of nascent prion protein into multiple populations at the translocation channel. Mol. Biol. Cell *13*, 3775-3786.

Kimberlin,R.H., Cole,S., and Walker,C.A. (1987). Pathogenesis of scrapie is faster when infection is intraspinal instead of intracerebral. Microb. Pathog. *2*, 405-415.

Kimberlin,R.H. and Marsh,R.F. (1975). Comparison of scrapie and transmissible mink encephalopathy in hamsters. I. Biochemical studies of brain during development of disease. J Infect. Dis. *131*, 97-103.

Kimberlin,R.H. and Walker,C.A. (1982). Pathogenesis of mouse scrapie: patterns of agent replication in different parts of the CNS following intraperitoneal infection. J R. Soc. Med. *75*, 618-24.

Kimberlin,R.H. and Walker,C.A. (1983). Invasion of the CNS by scrapie agent and its spread to different parts of the brain. In Virus Non-Conventionnels et Affections du Systéme Nerveux Central, Court LA and Cathala F, eds. (Paris: Masson), pp. 17-33.

Kimberlin,R.H. and Walker,C.A. (1986). Pathogenesis of scrapie (strain 263K) in hamsters infected intracerebrally, intraperitoneally or intraocularly. J Gen. Virol. *67*, 255-263.

Kirkwood,J.K. and Cunningham,A.A. (1994). Epidemiological observations on spongiform encephalopathies in captive wild animals in the British Isles. Vet. Rec. *135*, 296-303.

Kirkwood,J.K., Wells,G.A., Wilesmith,J.W., Cunningham,A.A., and Jackson,S.I. (1990). Spongiform encephalopathy in an arabian oryx (Oryx leucoryx) and a greater kudu (Tragelaphus strepsiceros). Vet. Rec. *127*, 418-420.

Klohn,P., Stoltze,L., Flechsig,E., Enari,M., and Weissmann,C. (2003). A quantitative, highly sensitive cell-based infectivity assay for mouse scrapie prions. Proc. Natl. Acad. Sci U. S. A *100*, 11666-11671.

Knaus,K.J., Morillas,M., Swietnicki,W., Malone,M., Surewicz,W.K., and Yee,V.C. (2001). Crystal structure of the human prion protein reveals a mechanism for oligomerization. Nat Struct. Biol. *8*, 770-774.

Knight,R. (2006). Creutzfeldt-Jakob disease: a rare cause of dementia in elderly persons. Clin. Infect. Dis. *43*, 340-346.

Knopfel,T., Rietschin,L., and Gahwiler,B.H. (1989). Organotypic Co-Cultures of Rat Locus Coeruleus and Hippocampus. Eur. J. Neurosci. *1*, 678-689.

Koch,T.K., Berg,B.O., De Armond,S.J., and Gravina,R.F. (1985). Creutzfeldt-Jakob disease in a young adult with idiopathic hypopituitarism. Possible relation to the administration of cadaveric human growth hormone. N. Engl. J Med. *313*, 731-733.

Kocisko,D.A., Come,J.H., Priola,S.A., Chesebro,B., Raymond,G.J., Lansbury,P.T., and Caughey,B. (1994). Cell-free formation of protease-resistant prion protein. Nature *370*, 471-474.

Kocisko,D.A., Priola,S.A., Raymond,G.J., Chesebro,B., Lansbury,P.T., Jr., and Caughey,B. (1995). Species specificity in the cell-free conversion of prion protein to protease-resistant forms: a model for the scrapie species barrier. Proc. Natl. Acad. Sci. U. S A. *92*, 3923-3927.

Koshiya,N. and Smith,J.C. (1999). Neuronal pacemaker for breathing visualized in vitro. Nature *400*, 360-363.

Kovacs,G.G. and Budka,H. (2008). Prion diseases: from protein to cell pathology. Am. J. Pathol. *172*, 555-565.

Kovacs,G.G. and Budka,H. (2009). Molecular pathology of human prion diseases. Int J Mol Sci *10*, 976-999.

Kretzschmar,H.A., Prusiner,S.B., Stowring,L.E., and DeArmond,S.J. (1986a). Scrapie prion proteins are synthesized in neurons. Am. J Pathol. *122*, 1-5.

Kretzschmar,H.A., Stowring,L.E., Westaway,D., Stubblebine,W.H., Prusiner,S.B., and DeArmond,S.J. (1986b). Molecular cloning of a human prion protein cDNA. DNA *5*, 315-324.

Kristiansen,M., Deriziotis,P., Dimcheff,D.E., Jackson GS, Ovaa,H., Naumann,H., Clarke A, van Leeuwen,F.W., Menendez-Benito,V., Dantuma,N.P., Portis,J.L., Collinge J, and Tabrizi S (2007). Disease-Associated Prion Protein Oligomers Inhibit the 26S Proteasome. Mol. Cell *26*, 175-188.

Kubin,L., Alheid,G.F., Zuperku,E.J., and McCrimmon,D.R. (2006). Central pathways of pulmonary and lower airway vagal afferents. J. Appl. Physiol *101*, 618-627.

Kuczius,T. and Groschup,M.H. (1999). Differences in proteinase K resistance and neuronal deposition of abnormal prion proteins characterize bovine spongiform encephalopathy (BSE) and scrapie strains. Mol. Med. *5*, 406-418.

Kuwahara,C., Kubosaki,A., Nishimura,T., Nasu,Y., Nakamura,Y., Saeki,K., Matsumoto,Y., and Onodera,T. (2000). Enhanced expression of cellular prion protein gene by insulin or nerve growth factor in immortalized mouse neuronal precursor cell lines. Biochemical and Biophysical Research Communications *268*, 763-766.

Kuwahara,C., Takeuchi,A.M., Nishimura,T., Haraguchi,K., Kubosaki,A., Matsumoto,Y., Saeki,K., Yokoyama,T., Itohara,S., and Onodera,T. (1999). Prions prevent neuronal cell-line death. Nature *400*, 225-226.

Kuypers,H.G.J.M. (1981). Anatomy of the descending pathways. In Motor control (Handbook of physiology), Brookhart JM and Mountcastle VB, eds. (Bethesda: American Physiological Society), pp. 597-666.

Lasmézas,C.I., Deslys,J.P., Robain,O., Jaegly,A., Beringue,V., Peyrin,J.M., Fournier,J.G., Hauw,J.J., Rossier,J., and Dormont,D. (1997). Transmission of the BSE agent to mice in the absence of detectable abnormal prion protein. Science *275*, 402-405.

Laszlo,L., Lowe,J., Self,T., Kenward,N., Landon,M., McBride,T., Farquhar,C., McConnell,I., Brown,J., Hope,J., and Mayer,R.J. (1992). Lysosomes as key organelles in the pathogenesis of prion encephalopathies. J. Pathol. *166*, 333-341.

Lauren,J., Gimbel,D.A., Nygaard,H.B., Gilbert,J.W., and Strittmatter,S.M. (2009). Cellular prion protein mediates impairment of synaptic plasticity by amyloid-beta oligomers. Nature *457*, 1128-1132.

Lazarini,F., Deslys,J.-P., and Dormont,D. (1991). Regulation of the glial fibrillary acidic protein, beta actin and prion protein mRNAs during brain development in mouse. Mol. Brain Res. *10*, 343-346.

Lee,H.S., Brown,P., Cervenáková,L., Garruto,R.M., Alpers MP, Gajdusek,D.C., and Goldfarb,L.G. (2001). Increased susceptibility to Kuru of carriers of the *PRNP* 129 methionine/methionine genotype. Journal of Infectious Diseases *183*, 192-196.

Lees,J.F., Shneidman,P.S., Skuntz,S.F., Carden,M.J., and Lazzarini,R.A. (1988). The structure and organization of the human heavy neurofilament subunit (NF-H) and the gene encoding it. EMBO J. *7*, 1947-1955.

Lein,E.S., Hawrylycz,M.J., Ao,N., Ayres,M., Bensinger,A., Bernard,A., Boe,A.F., Boguski,M.S., Brockway,K.S., Byrnes,E.J., Chen,L., Chen,L., Chen,T.M., Chin,M.C., Chong,J., Crook,B.E., Czaplinska,A., Dang,C.N., Datta,S., Dee,N.R., Desaki,A.L., Desta,T., Diep,E., Dolbeare,T.A., Donelan,M.J., Dong,H.W., Dougherty,J.G., Duncan,B.J., Ebbert,A.J., Eichele,G., Estin,L.K., Faber,C., Facer,B.A., Fields,R., Fischer,S.R., Fliss,T.P., Frensley,C., Gates,S.N., Glattfelder,K.J., Halverson,K.R., Hart,M.R., Hohmann,J.G., Howell,M.P., Jeung,D.P., Johnson,R.A., Karr,P.T., Kawal,R., Kidney,J.M., Knapik,R.H.,

Kuan,C.L., Lake,J.H., Laramee,A.R., Larsen,K.D., Lau,C., Lemon,T.A., Liang,A.J., Liu,Y., Luong,L.T., Michaels,J., Morgan,J.J., Morgan,R.J., Mortrud,M.T., Mosqueda,N.F., Ng,L.L., Ng,R., Orta,G.J., Overly,C.C., Pak,T.H., Parry,S.E., Pathak,S.D., Pearson,O.C., Puchalski,R.B., Riley,Z.L., Rockett,H.R., Rowland,S.A., Royall,J.J., Ruiz,M.J., Sarno,N.R., Schaffnit,K., Shapovalova,N.V., Sivisay,T., Slaughterbeck,C.R., Smith,S.C., Smith,K.A., Smith,B.I., Sodt,A.J., Stewart,N.N., Stumpf,K.R., Sunkin,S.M., Sutram,M., Tam,A., Teemer,C.D., Thaller,C., Thompson,C.L., Varnam,L.R., Visel,A., Whitlock,R.M., Wohnoutka,P.E., Wolkey,C.K., Wong,V.Y., Wood,M., Yaylaoglu,M.B., Young,R.C., Youngstrom,B.L., Yuan,X.F., Zhang,B., Zwingman,T.A., and Jones,A.R. (2007). Genome-wide atlas of gene expression in the adult mouse brain. Nature *445*, 168-176.

Li,A., Barmada,S.J., Roth,K.A., and Harris,D.A. (2007). N-terminally deleted forms of the prion protein activate both Bax-dependent and Bax-independent neurotoxic pathways. J Neurosci *27*, 852-859.

Li,A. and Harris,D.A. (2005). Mammalian prion protein suppresses Bax-induced cell death in yeast. J. Biol. Chem. *280*, 17430-17434.

Li,A. and Nattie,E. (2006). Catecholamine neurones in rats modulate sleep, breathing, central chemoreception and breathing variability. J. Physiol *570*, 385-396.

Li,J., Browning,S., Mahal,S.P., Oelschlegel,A.M., and Weissmann,C. (2010). Darwinian evolution of prions in cell culture. Proc-Natl-Acad-Sci-U-S-A. *327*, 869-872.

Liberski,P.P. (2004). Spongiform change--an electron microscopic view. Folia Neuropathol. *42 Suppl B*, 59-70.

Liberski,P.P., Sikorska,B., Bratosiewicz-Wasik,J., Carleton,G.D., and Brown,P. (2004). Neuronal cell death in transmissible spongiform encephalopathies (prion diseases) revisited: from apoptosis to autophagy. Int. J Biochem. Cell Biol *36*, 2473-2490.

Lindgren,P. (1961). Localization and function of the medullary vasomotor center in infracollicularly decerebrated cats. Circ. Res. *9*, 250-255.

Liu,J., Carmell,M.A., Rivas,F.V., Marsden,C.G., Thomson,J.M., Song,J.J., Hammond,S.M., Joshua-Tor,L., and Hannon,G.J. (2004). Argonaute2 is the catalytic engine of mammalian RNAi. Science *305*, 1437-1441.

Livak,K.J. and Schmittgen,T.D. (2001). Analysis of relative gene expression data using real-time quantitative PCR and the 2(-Delta Delta C(T)) Method. Methods *25*, 402-408.

Lloyd,S., Onwuazor,O.N., Beck J, Mallinson,G., Farrall,M., Targonski,P., Collinge J, and Fisher E (2001). Identification of multiple quantitative trait loci linked to prion disease incubation period in mice. Proc. Natl. Acad. Sci. USA *98*, 6279-6283.

Lloyd,S., Uphill,J.B., Targonski,P.V., Fisher E, and Collinge J (2002). Identification of genetic loci affecting mouse-adapted bovine spongiform encephalopathy incubation time in mice. Neurogenetics *4*, 77-81.

Lloyd,S.E., Linehan,J.M., Desbruslais,M., Joiner,S., Buckell,J., Brandner,S., Wadsworth,J.D., and Collinge,J. (2004). Characterization of two distinct prion strains derived from bovine spongiform encephalopathy transmissions to inbred mice. J. Gen. Virol. *85*, 2471-2478.

Lloyd,S.E., Rossor,M., Fox,N., Mead,S., and Collinge,J. (2009). HECTD2, a candidate susceptibility gene for Alzheimer's disease on 10q. BMC Med Genet *10*, 90.

Lockrow,J., Boger,H., Gerhardt,G., Aston-Jones,G., Bachman,D., and Granholm,A.C. (2011). A noradrenergic lesion exacerbates neurodegeneration in a Down syndrome mouse model. J. Alzheimers. Dis. *23*, 471-489.

Loewy,A.D. and Spyer,K.M. (1990). Central regulation of autonomic functions. Oxford University Press, New York).

Lopez,C.D., Yost,C.S., Prusiner,S.B., Myers,R.M., and Lingappa,V.R. (1990). Unusual topogenic sequence directs prion protein biogenesis. Science *248*, 226-229.

Lyness,S.A., Zarow,C., and Chui,H.C. (2003). Neuron loss in key cholinergic and aminergic nuclei in Alzheimer disease: a meta-analysis. Neurobiol. Aging *24*, 1-23.

Ma,J. and Lindquist,S. (2001). Wild-type PrP and a mutant associated with prion disease are subject to retrograde transport and proteasome degradation. Proc. Natl. Acad. Sci. U. S. A *98*, 14955-14960.

Ma,J., Wollmann,R., and Lindquist,S. (2002). Neurotoxicity and neurodegeneration when PrP accumulates in the cytosol. Science *298*, 1781-1785.

Mallucci,G., Dickinson,A., Linehan,J., Klohn,P., Brandner,S., and Collinge,J. (2003). Depleting neuronal PrP in prion infection prevents disease and reverses spongiosis. Science *302*, 871-874.

Mallucci,G.R., Ratte,S., Asante,E.A., Linehan,J., Gowland,I., Jefferys,J.G., and Collinge,J. (2002). Post-natal knockout of prion protein alters hippocampal CA1 properties, but does not result in neurodegeneration. EMBO J. *21*, 202-210.

Mallucci,G.R., White,M.D., Farmer,M., Dickinson,A., Khatun,H., Powell,A.D., Brandner,S., Jefferys,J.G., and Collinge,J. (2007). Targeting cellular prion protein reverses early cognitive deficits and neurophysiological dysfunction in prion-infected mice. Neuron *53*, 325-335.

Manson,J., West,J.D., Thomson,V., McBride,P., Kaufman,M.H., and Hope,J. (1992). The prion protein gene: a role in mouse embryogenesis? Development *115*, 117-122.

Manson,J.C., Clarke A, Hooper,M.L., Aitchison,L., McConnell,I., and Hope,J. (1994). 129/Ola mice carrying a null mutation in PrP that abolishes mRNA production are developmentally normal. Mol. Neurobiol. *8*, 121-127.

Manson,J.C., Hope,J., Clarke A, Johnston,A., Black,C., and MacLeod,N. (1995). PrP gene dosage and long term potentiation. Neurodegen. *4*, 113-114.

Marien,M.R., Colpaert,F.C., and Rosenquist,A.C. (2004). Noradrenergic mechanisms in neurodegenerative diseases: a theory. Brain Res. Brain Res. Rev. *45*, 38-78.

Marsh,R.F. (1992). Transmissible Mink Encephalopathy. In Prion Diseases of Humans and Animals, S.B.Prusiner, Collinge J, J.Powell, and B.Anderton, eds. (London: Ellis Horwood).

Marsh,R.F., Sipe,J.C., Morse,S.S., and Hanson,R.P. (1976). Transmissible mink encephalopathy. Reduced spongiform degeneration in aged mink of the Chediak-Higashi genotype. Lab Invest *34*, 381-386.

Martinez,J., Patkaniowska,A., Urlaub,H., Luhrmann,R., and Tuschl,T. (2002). Single-stranded antisense siRNAs guide target RNA cleavage in RNAi. Cell *110*, 563-574.

Masters,C.L., Harris,J.O., Gajdusek,D.C., Gibbs,C.J.Jr., Bernoulli,C., and Asher,D.M. (1979). Creutzfeldt-Jakob disease: patterns of worldwide occurrence and the significance of familial and sporadic clustering. Ann Neurol *5*, 177-188.

Masters,C.L. and Richardson,E.P.Jr. (1978). Subacute spongiform encephalopathy (Creutzfeldt-Jakob disease). The nature and progression of spongiform change. Brain *101*, 333-344.

Matranga,C., Tomari,Y., Shin,C., Bartel,D.P., and Zamore,P.D. (2005). Passenger-strand cleavage facilitates assembly of siRNA into Ago2-containing RNAi enzyme complexes. Cell *123*, 607-620.

McBride,P.A., Eikelenboom,P., Kraal,G., Fraser,H., and Bruce,M.E. (1992). PrP protein is associated with follicular dendritic cells of spleens and lymph nodes in uninfected and scrapie-infected mice. J Pathol *168*, 413-418.

McHattie,S.J., Brown,D.R., and Bird,M.M. (1999). Cellular uptake of the prion protein fragment PrP106-126 *in vitro*. J. Neurocytol. *28*, 149-159.

McKay,B.E., Engbers,J.D., Mehaffey,W.H., Gordon,G.R., Molineux,M.L., Bains,J.S., and Turner,R.W. (2007). Climbing fiber discharge regulates cerebellar functions by controlling the intrinsic characteristics of purkinje cell output. J. Neurophysiol. *97*, 2590-2604.

McKinley,M.P., Bolton,D.C., and Prusiner,S.B. (1983). A protease-resistant protein is a structural component of the scrapie prion. Cell *35*, 57-62.

McKinley,M.P., Lingappa,V.R., and Prusiner,S.B. (1988). Developmental regulation of prion protein mRNA in brain. Ciba. Found. Symp. *135*, 101-116.

Mead,S., Stumpf,M.P., Whitfield,J., Beck J, Poulter,M., Campbell,T., Uphill,J., Goldstein,D., Alpers MP, Fisher E, and Collinge J (2003). Balancing selection at the prion protein gene consistent with prehistoric kuru-like epidemics. Science *300*, 640-643.

Mead,S. (2006). Prion disease genetics. European Journal of Human Genetics *14*, 273-281.

Mead,S., Poulter,M., Beck,J., Webb,T.E., Campbell,T.A., Linehan,J.M., Desbruslais,M., Joiner,S., Wadsworth,J.D., King,A., Lantos,P., and Collinge,J. (2006). Inherited prion disease with six octapeptide repeat insertional mutation--molecular analysis of phenotypic heterogeneity. Brain *129*, 2297-2317.

Mead,S., Poulter,M., Uphill,J., Beck,J., Whitfield,J., Webb,T.E., Campbell,T., Adamson,G., Deriziotis,P., Tabrizi,S.J., Hummerich,H., Verzilli,C., Alpers,M.P., Whittaker,J.C., and Collinge,J. (2009a). Genetic risk factors for variant Creutzfeldt-Jakob disease: a genome-wide association study. Lancet Neurol *8*, 57-66.

Mead,S., Whitfield,J., Poulter,M., Shah,P., Uphill,J., Campbell,T., Al Dujaily,H., Hummerich,H., Beck,J., Mein,C.A., Verzilli,C., Whittaker,J., Alpers,M.P., and Collinge,J. (2009b). A Novel Protective Prion Protein Variant that Colocalizes with Kuru Exposure. N Engl J Med *361*, 2056-2065.

Meister,G. and Tuschl,T. (2004). Mechanisms of gene silencing by double-stranded RNA. Nature *431*, 343-349.

Mifflin,S.W. (1992). Arterial chemoreceptor input to nucleus tractus solitarius. Am. J. Physiol *263*, R368-R375.

Mifflin,S.W. (1993). Absence of respiration modulation of carotid sinus nerve inputs to nucleus tractus solitarius neurons receiving arterial chemoreceptor inputs. J. Auton. Nerv. Syst. *42*, 191-199.

Miller,M.W. and Williams,E.S. (2003). Prion disease: horizontal prion transmission in mule deer. Nature *425*, 35-36.

Mironov,S.L., Skorova,E., Hartelt,N., Mironova,L.A., Hasan,M.T., and Kugler,S. (2009). Remodelling of the respiratory network in a mouse model of Rett syndrome depends on brain-derived neurotrophic factor regulated slow calcium buffering. J. Physiol *587*, 2473-2485.

Mobley,W.C., Neve,R.L., Prusiner,S.B., and McKinley,M.P. (1988). Nerve growth factor increases mRNA levels for the prion protein and the beta-amyloid protein precursor in developing hamster brain. Proc. Natl. Acad. Sci. U. S. A. *85*, 9811-9815.

Moore,R.C., Lee,I.Y., Silverman,G.L., Harrison,P.M., Strome,R., Heinrich,C., Karunaratne,A., Pasternak,S.H., Chishti,M.A., Liang,Y., Mastrangelo,P., Wang,K.,

Smit,A.F.A., Katamine,S., Carlson,G.A., Cohen,F.E., Prusiner,S.B., Melton,D.W., Tremblay,P., Hood,L.E., and Westaway,D. (1999). Ataxia in prion protein (PrP)-deficient mice is associated with upregulation of the novel PrP-like protein Doppel. Journal of Molecular Biology *292*, 797-817.

Moreau,K., Luo,S., and Rubinsztein,D.C. (2010). Cytoprotective roles for autophagy. Curr. Opin. Cell Biol. *22*, 206-211.

Morris,R.J., Parkyn,C.J., and Jen,A. (2006). Traffic of prion protein between different compartments on the neuronal surface, and the propagation of prion disease. FEBS Lett. *580*, 5565-5571.

Moser,M., Colello,R.J., Pott,U., and Oesch,B. (1995). Developmental expression of the prion protein gene in glial cells. Neuron *14*, 509-517.

Moskowitz,P.F. and Oblinger,M.M. (1995). Transcriptional and post-transcriptional mechanisms regulating neurofilament and tubulin gene expression during normal development of the rat brain. Brain Res. Mol. Brain Res. *30*, 211-222.

Mouillet-Richard,S., Ermonval,M., Chebassier,C., Laplanche,J.L., Lehmann,S., Launay,J.M., and Kellermann,O. (2000). Signal transduction through prion protein. Science *289*, 1925-1928.

Mukherjee,A., Morales-Scheihing,D., Gonzalez-Romero,D., Green,K., Taglialatela,G., and Soto,C. (2010). Calcineurin inhibition at the clinical phase of prion disease reduces neurodegeneration, improves behavioral alterations and increases animal survival. PLoS Pathog. *6*, e1001138.

Nagy,A. (2000). Cre recombinase: the universal reagent for genome tailoring. Genesis *26*, 99-109.

Naldini,L., Blomer,U., Gallay,P., Ory,D., Mulligan,R., Gage,F.H., Verma,I.M., and Trono,D. (1996). In vivo gene delivery and stable transduction of nondividing cells by a lentiviral vector. Science *272*, 263-267.

Nattie,E. and Li,A. (2009). Central chemoreception is a complex system function that involves multiple brain stem sites. J. Appl. Physiol *106*, 1464-1466.

Neubauer,J.A. and Sunderram,J. (2004). Oxygen-sensing neurons in the central nervous system. J. Appl. Physiol *96*, 367-374.

Nicholls,J.G. and Paton,J.F. (2009). Brainstem: neural networks vital for life. Philos. Trans. R. Soc. Lond B Biol. Sci. *364*, 2447-2451.

Nicoll,A.J. and Collinge,J. (2009). Preventing prion pathogenicity by targeting the cellular prion protein. Infect Disord Drug Targets *9*, 48-57.

Nieznanski,K. (2010). Interactions of prion protein with intracellular proteins: so many partners and no consequences? Cell Mol. Neurobiol. *30*, 653-666.

O'Donovan,C.N., Tobin,D., and Cotter,T.G. (2001). Prion protein fragment PrP-(106-126) induces apoptosis via mitochondrial disruption in human neuronal SH-SY5Y cells. Journal of Biological Chemistry *276*, 43516-43523.

Oesch,B., Westaway,D., Walchli,M., McKinley,M.P., Kent,S.B.H., Aebersold,R., Barry,R.A., Tempst,P., Teplow,D.B., Hood,L.E., Prusiner,S.B., and Weissmann,C. (1985). A Cellular Gene Encodes Scrapie Prp 27-30 Protein. Cell *40*, 735-746.

Okazaki,M., Takeda,R., Yamazaki,H., and Haji,A. (2002). Synaptic mechanisms of inspiratory off-switching evoked by pontine pneumotaxic stimulation in cats. Neurosci. Res. *44*, 101-110.

Onimaru,H., Arata,A., and Homma,I. (1995). Intrinsic burst generation of preinspiratory neurons in the medulla of brainstem-spinal cord preparations isolated from newborn rats. Exp. Brain Res. *106*, 57-68.

Oyamada,Y., Ballantyne,D., Muckenhoff,K., and Scheid,P. (1998). Respiration-modulated membrane potential and chemosensitivity of locus coeruleus neurones in the in vitro brainstem-spinal cord of the neonatal rat. J. Physiol *513 (Pt 2)*, 381-398.

Palmer,M.S., Dryden,A.J., Hughes,J.T., and Collinge J (1991). Homozygous prion protein genotype predisposes to sporadic Creutzfeldt-Jakob disease. Nature *352*, 340-342.

Pan,K.-M., Baldwin,M.A., Nguyen,J., Gasset,M., Serban,A., Groth,D., Mehlhorn,I., Huang,Z., Fletterick,R.J., Cohen,F.E., and Prusiner,S.B. (1993). Conversion of α-helices into β-sheets features in the formation of the scrapie prion proteins. Proc Natl Acad Sci USA *90*, 10962-10966.

Paton,J.F. (1996a). A working heart-brainstem preparation of the mouse. J. Neurosci. Methods *65*, 63-68.

Paton,J.F. (1996b). The ventral medullary respiratory network of the mature mouse studied in a working heart-brainstem preparation. J. Physiol *493 (Pt 3)*, 819-831.

Paton,J.F. (1998). Pattern of cardiorespiratory afferent convergence to solitary tract neurons driven by pulmonary vagal C-fiber stimulation in the mouse. J. Neurophysiol. *79*, 2365-2373.

Paton,J.F. (1999). The Sharpey-Schafer prize lecture: nucleus tractus solitarii: integrating structures. Exp. Physiol *84*, 815-833.

Paton,J.F., Deuchars,J., Li,Y.W., and Kasparov,S. (2001). Properties of solitary tract neurones responding to peripheral arterial chemoreceptors. Neuroscience *105*, 231-248.

Pauly,P.C. and Harris,D.A. (1998). Copper stimulates endocytosis of the prion protein. Journal of Biological Chemistry *273*, 33107-33110.

Paxinos,G. and Franklin,K.B.J. (2004). The Mouse Brain in Stereotaxic Coordinates, Second Edition. Elsevier Academic Press).

Peden,A.H., Ritchie,D.L., Head,M.W., and Ironside,J.W. (2006). Detection and Localization of PrPSc in the Skeletal Muscle of Patients with Variant, Iatrogenic, and Sporadic Forms of Creutzfeldt-Jakob Disease. Am J Pathol. *168*, 927-935.

Peden,A.H., Ritchie,D.L., and Ironside,J.W. (2005). Risks of transmission of variant Creutzfeldt-Jakob disease by blood transfusion. Folia Neuropathol. *43*, 271-278.

Pena,F. (2010). PACAP modulates the respiratory rhythm generated in the brainstem slice preparation. Adv. Exp. Med. Biol. *669*, 119-122.

Pennington,B.F., Moon,J., Edgin,J., Stedron,J., and Nadel,L. (2003). The neuropsychology of Down syndrome: evidence for hippocampal dysfunction. Child Dev. *74*, 75-93.

Peretz,D., Scott,M.R., Groth,D., Williamson,R.A., Burton,D.R., Cohen,F.E., and Prusiner,S.B. (2001). Strain-specified relative conformational stability of the scrapie prion protein. Prot. Sci. *10*, 854-863.

Perry,V.H., Cunningham,C., and Boche,D. (2002). Atypical inflammation in the central nervous system in prion disease. Curr. Opin. Neurol. *15*, 349-354.

Peters,P.J., Mironov,A., Jr., Peretz,D., Van Donselaar,E., Leclerc,E., Erpel,S., DeArmond,S.J., Burton,D.R., Williamson,R.A., Vey,M., and Prusiner,S.B. (2003). Trafficking of prion proteins through a caveolae-mediated endosomal pathway. J Cell Biol. *162*, 703-717.

Pfeifer,A., Eigenbrod,S., Al Khadra,S., Hofmann,A., Mitteregger,G., Moser,M., Bertsch,U., and Kretzschmar,H. (2006). Lentivector-mediated RNAi efficiently suppresses prion protein and prolongs survival of scrapie-infected mice. J Clin. Invest *116*, 3204-3210.

Piccardo,P., Manson,J.C., King,D., Ghetti,B., and Barron,R.M. (2007). Accumulation of prion protein in the brain that is not associated with transmissible disease. Proc. Natl. Acad. Sci U. S A *104*, 4712-4717.

Pickering,A.E. and Paton,J.F. (2006). A decerebrate, artificially-perfused in situ preparation of rat: utility for the study of autonomic and nociceptive processing. J. Neurosci. Methods *155*, 260-271.

Pilowsky,P.M., Lung,M.S., Spirovski,D., and McMullan,S. (2009). Differential regulation of the central neural cardiorespiratory system by metabotropic neurotransmitters. Philos. Trans. R. Soc. Lond B Biol. Sci. *364*, 2537-2552.

Polak,M.P. and Zmudzinski,J.F. (2011). Distribution of a pathological form of prion protein in the brainstem and cerebellum in classical and atypical cases of bovine spongiform encephalopathy. Vet. J. in press.

Porter,J.D. and Balaban,C.D. (1997). Connections between the vestibular nuclei and brain stem regions that mediate autonomic function in the rat. J. Vestib. Res. *7*, 63-76.

Powell,A.D., Toescu,E.C., Collinge,J., and Jefferys,J.G. (2008). Alterations in Ca2+-buffering in prion-null mice: association with reduced afterhyperpolarizations in CA1 hippocampal neurons. J. Neurosci. *28*, 3877-3886.

Powell-Jackson,J., Weller,R.O., Kennedy,P., Preece,M.A., Whitcombe,E.M., and Newsom-Davis,J. (1985). Creutzfeldt-Jakob disease after administration of human growth hormone. Lancet *3 August*, 244-245.

Prusiner,S.B. (1982). Novel proteinaceous infectious particles cause scrapie. Science *216*, 136-144.

Prusiner,S.B. (1989). Scrapie Prions. Annu. Rev. Microbiol. *43*, 345-374.

Prusiner,S.B. (1991). Molecular Biology of Prion Diseases. Science *252*, 1515-1522.

Prusiner,S.B., McKinley,M.P., Bowman,K., Bolton,D.C., Bendheim,P.E., Groth,D.F., and Glenner,G.G. (1983). Scrapie prions aggregate to form amyloid-like birefringent rods. Cell *35*, 349-358.

Prusiner,S.B., Scott,M., Foster,D., Pan,K.M., Groth,D., Mirenda,C., Torchia,M., Yang,S.L., Serban,D., Carlson,G.A., and Raeber,A.J. (1990). Transgenetic studies implicate interactions between homologous PrP isoforms in scrapie prion replication. Cell *63*, 673-686.

Puckett,C., Concannon,P., Casey,C., and Hood,L. (1991). Genomic Structure of the Human Prion Protein Gene. Am. J Hum. Genet. *49*, 320-329.

Pugh,P.L., Vidgeon-Hart,M.P., Ashmeade,T., Culbert,A.A., Seymour,Z., Perren,M.J., Joyce,F., Bate,S.T., Babin,A., Virley,D.J., Richardson,J.C., Upton,N., and Sunter,D. (2007). Repeated administration of the noradrenergic neurotoxin N-(2-chloroethyl)-N-ethyl-2-bromobenzylamine (DSP-4) modulates neuroinflammation and amyloid plaque load in mice bearing amyloid precursor protein and presenilin-1 mutant transgenes. J. Neuroinflammation. *4*, 8.

Rambold,A.S., Muller,V., Ron,U., Ben Tal,N., Winklhofer,K.F., and Tatzelt,J. (2008). Stress-protective signalling of prion protein is corrupted by scrapie prions. EMBO J. *27*, 1974-1984.

Ramirez,J.M. and Richter,D.W. (1996). The neuronal mechanisms of respiratory rhythm generation. Curr. Opin. Neurobiol. *6*, 817-825.

Rand,T.A., Petersen,S., Du,F., and Wang,X. (2005). Argonaute2 cleaves the anti-guide strand of siRNA during RISC activation. Cell *123*, 621-629.

Rangel,A., Madronal,N., Masso,A., Gavin,R., Llorens,F., Sumoy,L., Torres,J.M., Delgado-Garcia,J.M., and Del Rio,J.A. (2009). Regulation of GABA(A) and glutamate receptor expression, synaptic facilitation and long-term potentiation in the hippocampus of prion mutant mice. PLoS ONE *4*, e7592.

Raoul,C., Abbas-Terki,T., Bensadoun,J.C., Guillot,S., Haase,G., Szulc,J., Henderson,C.E., and Aebischer,P. (2005). Lentiviral-mediated silencing of SOD1

through RNA interference retards disease onset and progression in a mouse model of ALS. Nature Medicine *11*, 423-428.

Reiniger,L., Lukic,A., Linehan,J., Rudge,P., Collinge,J., Mead,S., and Brandner,S. (2011). Tau, prions and Abeta: the triad of neurodegeneration. Acta Neuropathol. *121*, 5-20.

Rekling,J.C. and Feldman,J.L. (1998). PreBotzinger complex and pacemaker neurons: hypothesized site and kernel for respiratory rhythm generation. Annu. Rev. Physiol *60*, 385-405.

Remy,P., Doder,M., Lees,A., Turjanski,N., and Turjanski,N. (2005). Depression in Parkinson's disease: loss of dopamine and noradrenaline innervation in the limbic system. Brain *128*, 1314-1322.

Richter,D.W. and Spyer,K.M. (2001). Studying rhythmogenesis of breathing: comparison of in vivo and in vitro models. Trends Neurosci. *24*, 464-472.

Riek,R., Hornemann,S., Wider,G., Billeter,M., Glockshuber,R., and Wuthrich,K. (1996). NMR structure of the mouse prion protein domain PrP (121-231). Nature *382*, 180-182.

Riek,R., Wider,G., Billeter,M., Hornemann,S., Glockshuber,R., and Wuthrich,K. (1998). Prion protein NMR structure and familial human spongiform encephalopathies. Proc Natl Acad Sci U. S. A. *95*, 11667-11672.

Rigatto,H., Wilson,C.G., Koshiya,N., House,S., and Smith,J.C. (2001). Stationary organotypic culture of the pre-Botzinger complex from the newborn rat. Adv. Exp. Med. Biol. *499*, 139-145.

Rodriguez-Lebron,E., Denovan-Wright,E.M., Nash,K., Lewin,A.S., and Mandel,R.J. (2005). Intrastriatal rAAV-mediated delivery of anti-huntingtin shRNAs induces partial reversal of disease progression in R6/1 Huntington's disease transgenic mice. Mol. Ther. *12*, 618-633.

Rogers,R.F., Paton,J.F., and Schwaber,J.S. (1993). NTS neuronal responses to arterial pressure and pressure changes in the rat. Am. J. Physiol *265*, R1355-R1368.

Rommelfanger,K.S. and Weinshenker,D. (2007). Norepinephrine: The redheaded stepchild of Parkinson's disease. Biochem. Pharmacol. *74*, 177-190.

Rossi,D., Cozzio,A., Flechsig,E., Klein,M.A., Rülicke,T., Aguzzi,A., and Weissmann,C. (2001). Onset of ataxia and Purkinje cell loss in PrP null mice inversely correlated with Dpl level in brain. EMBO J. *20*, 694-702.

Roucou,X., Giannopoulos,P.N., Zhang,Y., Jodoin,J., Goodyer,C.G., and LeBlanc,A. (2005). Cellular prion protein inhibits proapoptotic Bax conformational change in human neurons and in breast carcinoma MCF-7 cells. Cell Death. Differ. *12*, 783-795.

Russelakis-Carneiro,M., Hetz,C., Maundrell,K., and Soto,C. (2004). Prion replication alters the distribution of synaptophysin and caveolin 1 in neuronal lipid rafts. Am J Pathol. *165*, 1839-1848.

Rutz,S. and Scheffold,A. (2004). Towards in vivo application of RNA interference - new toys, old problems. Arthritis Res. Ther. *6*, 78-85.

Safar,J., Cohen,F.E., and Prusiner,S.B. (2000). Quantitative traits of prion strains are enciphered in the conformation of the prion protein. Arch. Virol. 227-235.

Safar,J., Wille,H., Itri,V., Groth,D., Serban,H., Torchia,M., Cohen,F.E., and Prusiner,S.B. (1998). Eight prion strains PrP^{Sc} molecules with different conformations. Nat. Med. *4*, 1157-1165.

Sakaguchi,S., Katamine,S., Nishida,N., Moriuchi,R., Shigematsu,K., Sugimoto,T., Nakatani,A., Kataoka,Y., Houtani,T., Shirabe,S., Okada,H., Hasegawa,S., Miyamoto,T., and Noda,T. (1996). Loss of cerebellar Purkinje cells in aged mice homozygous for a disrupted PrP gene. Nature *380*, 528-531.

Saladin,K.S. (2004). Anatomy and Physiology: The Unit of Form and Function, Third Edition. The McGraw-Hill Companies).

Salehi,A., Faizi,M., Colas,D., Valletta,J., Laguna,J., Takimoto-Kimura,R., Kleschevnikov,A., Wagner,S.L., Aisen,P., Shamloo,M., and Mobley,W.C. (2009). Restoration of norepinephrine-modulated contextual memory in a mouse model of Down syndrome. Sci. Transl. Med. *1*, 7ra17.

Sales,N., Rodolfo,K., Hassig,R., Faucheux,B., Di-Giamberardino,L., and Moya,K.L. (1998). Cellular prion protein localization in rodent and primate brain. Eur. J Neurosci. *10*, 2464-2471.

Sandberg,M.K., Al Doujaily,H., Sharps,B., Clarke,A.R., and Collinge,J. (2011). Prion propagation and toxicity in vivo occur in two distinct mechanistic phases. Nature *470*, 540-542.

Sapru,M.K., Yates,J.W., Hogan,S., Jiang,L., Halter,J., and Bohn,M.C. (2006). Silencing of human alpha-synuclein in vitro and in rat brain using lentiviral-mediated RNAi. Exp. Neurol. *198*, 382-390.

Sauerwald,A., Hoesche,C., Oschwald,R., and Kilimann,M.W. (1990). The 5'-flanking region of the synapsin I gene. A G+C-rich. J. Biol. Chem. *265*, 14932-14937.

Schmitt-Ulms,G., Legname,G., Baldwin,M.A., Ball,H.L., Bradon,N., Bosque,P.J., Crossin,K.L., Edelman,G.M., DeArmond,S.J., Cohen,F.E., and Prusiner,S.B. (2001). Binding of neural cell adhesion molecules (N-CAMs) to the cellular prion protein. Journal of Molecular Biology *314*, 1209-1225.

Schwarz,A., Kratke,O., Burwinkel,M., Riemer,C., Schultz,J., Henklein,P., Bamme,T., and Baier,M. (2003). Immunisation with a synthetic prion protein-

derived peptide prolongs survival times of mice orally exposed to the scrapie agent. Neurosci. Lett. *350*, 187-189.

Schwarzacher,S.W., Rub,U., and Deller,T. (2011). Neuroanatomical characteristics of the human pre-Botzinger complex and its involvement in neurodegenerative brainstem diseases. Brain *134*, 24-35.

Schwarzacher,S.W., Smith,J.C., and Richter,D.W. (1995). Pre-Botzinger complex in the cat. J. Neurophysiol. *73*, 1452-1461.

Seo,S.W., Shin,H.Y., Kim,S.H., Han,S.W., Lee,K.Y., Kim,S.M., and Heo,J.H. (2004). Vestibular imbalance associated with a lesion in the nucleus prepositus hypoglossi area. Arch. Neurol. *61*, 1440-1443.

Shmerling,D., Hegyi,I., Fischer,M., Blättler,T., Brandner S, Götz,J., Rülicke,T., Flechsig,E., Cozzio,A., von Mering,C., Hangartner,C., Aguzzi,A., and Weissmann,C. (1998). Expression of amino-terminally truncated PrP in the mouse leading to ataxia and specific cerebellar lesions. Cell *93*, 203-214.

Shyng,S.-L., Huber,M.T., and Harris,D.A. (1993). A prion protein cycles between the cell surface and an endocytic compartment in cultured neuroblastoma cells. J Biol. Chem. *268 (21)*, 15922-15928.

Shyng,S.-L., Heuser,J.E., and Harris,D.A. (1994). A glycolipid-anchored prion protein is endocytosed via clathrin- coated pits. J. Cell Biol. *125*, 1239-1250.

Sigurdsson,E.M., Brown,D.R., Daniels,M., Kascsak,R.J., Kascsak,R., Carp,R., Meeker,H.C., Frangione,B., and Wisniewski,T. (2002). Immunization delays the onset of prion disease in mice. Am. J. Pathol. *161*, 13-17.

Simons,K. and Ikonen,E. (1997). Functional rafts in cell membranes. Nature *387*, 569-572.

Singer,O., Marr,R.A., Rockenstein,E., Crews,L., Coufal,N.G., Gage,F.H., Verma,I.M., and Masliah,E. (2005). Targeting BACE1 with siRNAs ameliorates Alzheimer disease neuropathology in a transgenic model. Nat Neurosci. *8*, 1343-1349.

Smith,J.C., Abdala,A.P., Koizumi,H., Rybak,I.A., and Paton,J.F. (2007). Spatial and functional architecture of the mammalian brain stem respiratory network: a hierarchy of three oscillatory mechanisms. J. Neurophysiol. *98*, 3370-3387.

Smith,J.C., Ellenberger,H.H., Ballanyi,K., Richter,D.W., and Feldman,J.L. (1991). Pre-Botzinger complex: a brainstem region that may generate respiratory rhythm in mammals. Science *254*, 726-729.

Smith,P.G. and Bradley,R. (2003). Bovine spongiform encephalopathy (BSE) and its epidemiology. Br. Med. Bull. *66*, 185-198.

Solforosi,L., Criado,J.R., McGavern,D.B., Wirz,S., Sanchez-Alavez,M., Sugama,S., DeGiorgio,L.A., Volpe,B.T., Wiseman,E., Abalos,G., Masliah,E., Gilden,D.,

Oldstone,M.B., Conti,B., and Williamson,R.A. (2004). Cross-linking cellular prion protein triggers neuronal apoptosis in vivo. Science *303*, 1514-1516.

Song,J.J., Smith,S.K., Hannon,G.J., and Joshua-Tor,L. (2004). Crystal structure of Argonaute and its implications for RISC slicer activity. Science *305*, 1434-1437.

Soriano,P. (1999). Generalized lacZ expression with the ROSA26 Cre reporter strain. Nat. Genet. *21*, 70-71.

Sparkes,R.S., Simon,M., Cohn,V.H., Fournier,R.E., Lem,J., Klisak,I., Heinzmann,C., Blatt,C., Lucero,M., Mohandas,T., and Raeber,A.J. (1986). Assignment of the human and mouse prion protein genes to homologous chromosomes. Proc. Natl. Acad. Sci. U. S. A. *83*, 7358-7362.

Spencer,M.D., Knight,R.S., and Will,R.G. (2002). First hundred cases of variant Creutzfeldt-Jakob disease: retrospective case note review of early psychiatric and neurological features. BMJ *324*, 1479-1482.

Spielhaupter,C. and Schatzl,H.M. (2001). PrPC directly interacts with proteins involved in signaling pathways. J. Biol. Chem. *276*, 44604-44612.

Spyer,K.M. and Gourine,A.V. (2009). Chemosensory pathways in the brainstem controlling cardiorespiratory activity. Philos. Trans. R. Soc. Lond B Biol. Sci. *364*, 2603-2610.

Stahl,N., Borchelt,D.R., Hsiao,K., and Prusiner,S.B. (1987). Scrapie prion protein contains a phosphatidylinositol glycolipid. Cell *51*, 229-240.

Stahl,N., Borchelt,D.R., and Prusiner,S.B. (1990). Differential release of cellular and scrapie prion proteins from cellular membranes by phosphatidylinositol-specific phospholipase. Biochemistry *29*, 5405-5412.

Steele,A.D., King,O.D., Jackson,W.S., Hetz,C.A., Borkowski,A.W., Thielen,P., Wollmann,R., and Lindquist,S. (2007). Diminishing Apoptosis by Deletion of Bax or Overexpression of Bcl-2 Does Not Protect against Infectious Prion Toxicity In Vivo. J Neurosci *27*, 13022-13027.

Steinhoff,B.J., Zerr,I., Glatting,M., Schulz-Schaeffer,W., Poser,S., and Kretzschmar,H.A. (2004). Diagnostic value of periodic complexes in Creutzfeldt-Jakob disease. Ann. Neurol. *56*, 702-708.

Stephenson,D.A., Chiotti,K., Ebeling,C., Groth,D., DeArmond,S.J., Prusiner,S.B., and Carlson,G.A. (2000). Quantitative trait loci affecting prion incubation time in mice. Genomics *69*, 47-53.

Stocker,S.D., Steinbacher,B.C., Jr., Balaban,C.D., and Yates,B.J. (1997). Connections of the caudal ventrolateral medullary reticular formation in the cat brainstem. Exp. Brain Res. *116*, 270-282.

Sun,Q.J., Goodchild,A.K., Chalmers,J.P., and Pilowsky,P.M. (1998). The pre-Botzinger complex and phase-spanning neurons in the adult rat. Brain Res. *809*, 204-213.

Sunyach,C., Jen,A., Deng,J., Fitzgerald,K.T., Frobert,Y., Grassi,J., McCaffrey,M.W., and Morris,R. (2003). The mechanism of internalization of glycosylphosphatidylinositol-anchored prion protein. EMBO J *22*, 3591-3601.

Supattapone,S. (2004). Prion protein conversion in vitro. J. Mol. Med. (Berl) *82*, 348-356.

Supattapone,S., Nguyen,H.O.B., Cohen,F.E., Prusiner,S.B., and Scott,M.R. (1999). Elimination of prions by branched polyamines and implications for therapeutics. Proc. Natl. Acad. Sci. USA *96*, 14529-14534.

Sved,A.F. and Felsten,G. (1987). Stimulation of the locus coeruleus decreases arterial pressure. Brain Res. *414*, 119-132.

Svensson,T.H. and Thoren,P. (1979). Brain noradrenergic neurons in the locus coeruleus: inhibition by blood volume load through vagal afferents. Brain Res. *172*, 174-178.

Swietnicki,W., Petersen,R.B., Gambetti,P., and Surewicz,W.K. (1998). Familial mutations and the thermodynamic stability of the recombinant human prion protein. Journal of Biological Chemistry *273*, 31048-31052.

Szot,P., White,S.S., Greenup,J.L., Leverenz,J.B., Peskind,E.R., and Raskind,M.A. (2006). Compensatory changes in the noradrenergic nervous system in the locus ceruleus and hippocampus of postmortem subjects with Alzheimer's disease and dementia with Lewy bodies. J. Neurosci. *26*, 467-478.

Tabrizi,S., Scaravilli,F., Howard,R.S., Collinge,J., and Rossor,M.N. (1996). Creutzfeldt-Jakob disease in a young woman. Report of a Meeting of Physicians and Scientists, St. Thomas' Hospital, London. Lancet *347*, 945-948.

Tahiri-Alaoui,A., Gill,A.C., Disterer,P., and James,W. (2004). Methionine 129 variant of human prion protein oligomerizes more rapidly than the valine 129 variant: implications for disease susceptibility to Creutzfeldt-Jakob disease. J. Biol. Chem. *279*, 31390-31397.

Taneja,P., Ogier,M., Brooks-Harris,G., Schmid,D.A., Katz,D.M., and Nelson,S.B. (2009). Pathophysiology of locus ceruleus neurons in a mouse model of Rett syndrome. J. Neurosci. *29*, 12187-12195.

Tilly,G., Chapuis,J., Vilette,D., Laude,H., and Vilotte,J.L. (2003). Efficient and specific down-regulation of prion protein expression by RNAi. Biochem. Biophys. Res. Commun. *305*, 548-551.

Tobler,I., Gaus,S.E., Deboer,T., Achermann,P., Fischer,M., Rulicke,T., Moser,M., Oesch,B., McBride,P.A., and Manson,J.C. (1996). Altered circadian activity rhythms and sleep in mice devoid of prion protein. Nature *380*, 639-642.

Trevitt,C.R. and Collinge,J. (2006). A systematic review of prion therapeutics in experimental models. Brain *129*, 2241-2265.

Trifilo,M.J., Sanchez-Alavez,M., Solforosi,L., Bernard-Trifilo,J., Kunz,S., McGavern,D., and Oldstone,M.B. (2008). Scrapie-induced defects in learning and memory of transgenic mice expressing anchorless prion protein are associated with alterations in the gamma aminobutyric acid-ergic pathway. J. Virol. *82*, 9890-9899.

Tschampa,H.J., Kallenberg,K., Urbach,H., Meissner,B., Nicolay,C., Kretzschmar,H.A., Knauth,M., and Zerr,I. (2005). MRI in the diagnosis of sporadic Creutzfeldt-Jakob disease: a study on inter-observer agreement. Brain *128*, 2026-2033.

Turk,E., Teplow,D.B., Hood,L.E., and Prusiner,S.B. (1988). Purification and properties of the cellular and scrapie hamster prion proteins. Eur. J Biochem. *176*, 21-30.

Turlo,K.A., Gallaher,S.D., Vora,R., Laski,F.A., and Iruela-Arispe,M.L. (2010). When Cre-mediated recombination in mice does not result in protein loss. Genetics *186*, 959-967.

Vassallo,N. and Herms,J. (2003). Cellular prion protein function in copper homeostasis and redox signalling at the synapse. J Neurochem. *86*, 538-544.

Verghese-Nikolakaki,S., Michaloudi,H., Polymenidou,M., Groschup,M.H., Papadopoulos,G.C., and Sklaviadis,T. (1999). Expression of the prion protein in the rat forebrain - an immunohistochemical study. Neuroscience Letters *272*, 9-12.

Vey,M., Pilkuhn,S., Wille,H., Nixon,R., DeArmond,S.J., Smart,E.J., Anderson,R.G.W., Taraboulos,A., and Prusiner,S.B. (1996). Subcellular colocalization of the cellular and scrapie prion proteins in caveolae-like membranous domains. Proc. Natl. Acad. Sci. USA *93*, 14945-14949.

Vidal,C., Herzog,C., Haeberle,A.M., Bombarde,C., Miquel,M.C., Carimalo,J., Launay,J.M., Mouillet-Richard,S., Lasmezas,C., Dormont,D., Kellermann,O., and Bailly,Y. (2009). Early dysfunction of central 5-HT system in a murine model of bovine spongiform encephalopathy. Neuroscience *160*, 731-743.

Vogtherr,M., Grimme,S., Elshorst,B., Jacobs,D.M., Fiebig,K., Griesinger,C., and Zahn,R. (2003). Antimalarial drug quinacrine binds to C-terminal helix of cellular prion protein. J Med. Chem *46*, 3563-3564.

Wadsworth,J.D. and Collinge,J. (2007). Update on human prion disease. Biochimica et Biophysica Acta *1772*, 598-609.

Wadsworth,J.D., Hill,A.F., Joiner,S., Jackson,G.S., Clarke,A., and Collinge,J. (1999). Strain-specific prion-protein conformation determined by metal ions. Nature Cell Biology *1*, 55-59.

Wadsworth,J.D., Joiner,S., Fox,K., Linehan,J., Desbruslais,M., Brandner,S., Asante,E.A., and Collinge,J. (2007). Prion infectivity in variant Creutzfeldt-Jakob disease rectum. Gut *56*, 90-94.

Wadsworth,J.D., Joiner,S., Hill,A.F., Campbell,T.A., Desbruslais,M., Luthert,P.J., and Collinge,J. (2001). Tissue distribution of protease resistant prion protein in variant CJD using a highly sensitive immuno-blotting assay. Lancet *358*, 171-180.

Wadsworth,J.D., Joiner,S., Linehan,J., Cooper,S., Powell,C., Mallinson,G., Buckell,J., Gowland,I., Asante,E.A., Budka,H., Brandner,S., and Collinge,J. (2006). Phenotypic heterogeneity in inherited prion disease (P102L) is associated with differential propagation of protease-resistant wild-type and mutant prion protein. Brain *129*, 1557-1569.

Weissmann,C. and Aguzzi,A. (1997). Bovine spongiform encephalopathy and early onset variant Creutzfeldt-Jakob disease. Curr Opin Neurobiol. *7*, 695-700.

Westaway,D., Cooper,C., Turner,S., Da Costa,M., Carlson,G.A., and Prusiner,S.B. (1994). Structure and polymorphism of the mouse prion protein gene. Proc. Natl. Acad. Sci. USA *91*, 6418-6422.

Westergard,L., Christensen,H.M., and Harris,D.A. (2007). The cellular prion protein (PrP(C)): Its physiological function and role in disease. Biochim. Biophys Acta *1772*, 629-644.

Weston,M., Wang,H., Stornetta,R.L., Sevigny,C.P., and Guyenet,P.G. (2003). Fos expression by glutamatergic neurons of the solitary tract nucleus after phenylephrine-induced hypertension in rats. J. Comp Neurol. *460*, 525-541.

White,A.R., Enever,P., Tayebi,M., Mushens,R., Linehan,J., Brandner,S., Anstee,D., Collinge,J., and Hawke,S. (2003). Monoclonal antibodies inhibit prion replication and delay the development of prion disease. Nature *422*, 80-83.

White,M.D., Farmer,M., Mirabile,I., Brandner,S., Collinge,J., and Mallucci,G.R. (2008). Single treatment with RNAi against prion protein rescues early neuronal dysfunction and prolongs survival in mice with prion disease. Proc Natl Acad Sci U S A *105*, 10238-10243.

White,M.D. and Mallucci,G.R. (2009). Therapy for prion diseases: Insights from the use of RNA interference. Prion *3*, 121-128.

Wilesmith,J.W., Ryan,J.B., and Atkinson,M.J. (1991). Bovine spongiform encephalopathy: epidemiological studies on the origin. Vet. Rec. *128*, 199-203.

Wilesmith,J.W., Wells,G.A., Cranwell,M.P., and Ryan,J.B. (1988). Bovine spongiform encephalopathy: epidemiological studies. Vet. Rec. *123*, 638-644.

Will,R.G. (2003). Acquired prion disease: iatrogenic CJD, variant CJD, kuru. Br. Med. Bull. *66*, 255-265.

Will,R.G., Ironside,J.W., Zeidler,M., Cousens,S.N., Estibeiro,K., Alperovitch,A., Poser,S., Pocchiari,M., Hofman,A., and Smith,P.G. (1996). A new variant of Creutzfeldt-Jakob disease in the UK. Lancet *347*, 921-925.

Williams,A.E., Lawson,L.J., Perry,V.H., and Fraser,H. (1994). Characterization of the microglial response in murine scrapie. Neuropathol & Appl Neurobiol *20*, 47-55.

Williams,E.S. and Young,S. (1980). Chronic wasting disease of captive mule deer: a spongiform encephalopathy. J Wildl. Dis. *16*, 89-98.

Williams,E.S. and Young,S. (1982). Spongiform encephalopathy of Rocky Mountain elk. J Wildl. Dis. *18*, 465-471.

Wyatt,J.M., Pearson,G.R., Smerdon,T.N., Gruffydd-Jones,T.J., Wells,G.A.H., and Wilesmith,J.W. (1991). Naturally occurring scrapie-like spongiform encephalopathy in five domestic cats. Vet. Rec. *129*, 233-236.

Xia,H., Mao,Q., Eliason,S.L., Harper,S.Q., Martins,I.H., Orr,H.T., Paulson,H.L., Yang,L., Kotin,R.M., and Davidson,B.L. (2004). RNAi suppresses polyglutamine-induced neurodegeneration in a model of spinocerebellar ataxia. Nature Medicine *10*, 816-820.

Xia,X., Zhou,H., Huang,Y., and Xu,Z. (2006). Allele-specific RNAi selectively silences mutant SOD1 and achieves significant therapeutic benefit in vivo. Neurobiol. Dis. *23*, 578-586.

Yates,B.J., Balaban,C.D., Miller,A.D., Endo,K., and Yamaguchi,Y. (1995). Vestibular inputs to the lateral tegmental field of the cat: potential role in autonomic control. Brain Res. *689*, 197-206.

Yates,B.J., Billig,I., Cotter,L.A., Mori,R.L., and Card,J.P. (2002). Role of the vestibular system in regulating respiratory muscle activity during movement. Clin. Exp. Pharmacol. Physiol *29*, 112-117.

Yates,B.J., Grelot,L., Kerman,I.A., Balaban,C.D., Jakus,J., and Miller,A.D. (1994). Organization of vestibular inputs to nucleus tractus solitarius and adjacent structures in cat brain stem. Am. J. Physiol *267*, R974-R983.

Yates,B.J., Holmes,M.J., and Jian,B.J. (2003). Plastic changes in processing of graviceptive signals during spaceflight potentially contribute to postflight orthostatic intolerance. J. Vestib. Res. *13*, 395-404.

Yates,B.J. and Stocker,S.D. (1998). Integration of somatic and visceral inputs by the brainstem - Functional considerations. Experimental Brain Research *119*, 269-275.

Zamore,P.D., Tuschl,T., Sharp,P.A., and Bartel,D.P. (2000). RNAi: double-stranded RNA directs the ATP-dependent cleavage of mRNA at 21 to 23 nucleotide intervals. Cell *101*, 25-33.

Zanata,S.M., Lopes,M.H., Mercadante,A.F., Hajj,G.N., Chiarini,L.B., Nomizo,R., Freitas,A.R., Cabral,A.L., Lee,K.S., Juliano,M.A., de Oliveira,E., Jachieri,S.G.,

Burlingame,A., Huang,L., Linden,R., Brentani,R.R., and Martins,V.R. (2002). Stress-inducible protein 1 is a cell surface ligand for cellular prion that triggers neuroprotection. EMBO J. *21*, 3307-3316.

Zarow,C., Lyness,S.A., Mortimer,J.A., and Chui,H.C. (2003). Neuronal loss is greater in the locus coeruleus than nucleus basalis and substantia nigra in Alzheimer and Parkinson diseases. Arch Neurol. *60*, 337-341.

Zhang,J. and Mifflin,S.W. (2000). Responses of aortic depressor nerve-evoked neurones in rat nucleus of the solitary tract to changes in blood pressure. J. Physiol *529 Pt 2*, 431-443.

Zigas,V. and Gajdusek,D.C. (1957). Kuru: clinical study of a new syndrome resembling paralysis agitans in natives of the Eastern Highlands of Australian New Guinea. Med J Aust *2*, 745-754.

10 Publication related to this thesis

White,M.D., Farmer,M., **Mirabile,I**., Brandner,S., Collinge,J., and Mallucci,G.R. (2008). Single treatment with RNAi against prion protein rescues early neuronal dysfunction and prolongs survival in mice with prion disease. Proc Natl Acad Sci U S A *105*, 10238-10243